

**PORPHYRIN AND METALLOPORPHYRIN AGENTS FOR THE
PERSONALISED TREATMENT AND IMAGING OF CANCERS**



**being a Thesis submitted for the Degree of
Doctor of Philosophy at the University of Hull**

**Jordon Sandland
MChem (Hons) PGDip AMRSC**

**University of Hull
September 2019**

Abstract

The improvement of cancer medicine by utilizing the approach of personalised medicine has been investigated, principally, through the combination of diagnostic imaging (PET imaging) with treatment modalities (radiotherapy). Radiotherapy is key to both curative and palliative care and can be administered as adjuvant or neoadjuvant therapy, with or without combination therapies. Over the last few decades, research has been carried out into “radiosensitizers” – molecules which enhance the effects of ionizing radiation. To date, the mechanism of action of porphyrin-based radiosensitizers is still disputed. In this thesis the mechanism of action has been probed by investigating the synthesis and biological evaluation of a small library of trans-A₂-diphenylporphyrin-based radiosensitizers with the aims of improving the therapeutic effects of radiotherapy. A lead structure has been identified which contains the core motif of a porphine ring chelated to Cu(II) in the pyrrolic cavity, nitro groups in the 5- and 15-*meso* positions and hydrophilic aryl rings in the 10- and 20-*meso* positions of the porphine unit. This hydrophilic compound has been evaluated through clonogenic assays, FACS assays, comet assays, and immunofluorescence microscopy assays on HT-29 (p53 null) and HCT-116 (p53 WT) colorectal cancer cell lines. This porphyrin has been found to not only enhance the effects of ionizing radiation by a substantial margin, but also enhance the proportion of cells undergoing radiation-induced cell cycle arrest and increases the proportion of cells undergoing apoptosis as their mechanism of death. Using “click” chemistry, the radiosensitizer was conferred with a powerful imaging modality (PET imaging). The successful radiochemical synthesis of a conjugatable [¹⁸F] radiolabelled heterobifunctional prosthetic was optimised, and the “hot” conjugation procedure to yield the [¹⁸F] radiolabelled radiosensitizer was carried out.

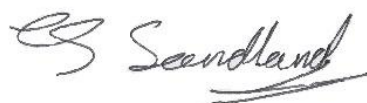
Additionally, the field of dual-therapeutics has been investigated. The Ru(II) arene 1,3,5-triaza-7-phosphaadamantane (RAPTA) family of chemotherapeutics has recently emerged with several key advantages over the use of traditional Pt(II) therapeutics, including fewer off-target side effects and fewer mechanisms of resistance. To date, only a few examples of dual-therapeutic porphyrin-Ru(II) conjugates exist. A water-soluble cationic porphyrin-[Ru(η^6 -arene)(C₂O₄)PTA] conjugate which retains its exquisite photochemical properties has been successfully synthesised. This novel conjugate was found to be readily internalized by HT-29 (p53 null) cancer cells, and MTT assays found that this unique conjugate is 2.5 times more cytotoxic in the “dark” when compared to the RAPTA species alone, while still acting as a photodynamic sensitizer when irradiated with white light. We attribute the extra decrease in cell viability to the natural ability of the cationic porphyrin to be internalised by the cancer cells. Herein, this thesis focuses on the synthesis of porphyrins as theranostic radiosensitizers, and porphyrins as theranostic dual-therapeutics with *in vitro* biological evaluation carried out to determine their efficacy and mechanism of action.

Authors Declaration

The work presented herein was conducted in the Department of Chemistry and Biochemistry at the University of Hull from September 2016 to September 2019. The research conducted was under the supervision of Prof. Ross W. Boyle as primary investigator and Prof. Stephen Archibald as secondary supervisor.

All experiments were carried out after completing respective risk assessments and COSHH forms which were assessed and signed by the principal investigator (Prof. R. W. Boyle) and the local departmental safety officer (Dr Rob Lewis).

All of the work presented is my own, except where stated otherwise, and has not been submitted for any other degree at this or any other university.

A handwritten signature in black ink, appearing to read 'E Sandland', with a horizontal line underneath the name.

September 2019

Acknowledgements

Firstly, I would like to extend the greatest of thanks to my project supervisor Prof. R. W. Boyle for the opportunities he has afforded me throughout this PhD project. Ross has encouraged me to be the best researcher that I could be. I thank my second supervisor, Prof. S. J. Archibald, for allowing me to use the PET centre and its facilities as well as the collaborations it has afforded me. I thank Dr Juozas Domarkas and my fellow radiochemistry companions for their support and patient guidance during my radiochemistry training, without which my project would not have been possible. And of course, I need to thank Dr Dave Allen for the operation of the cyclotron. I'd like to thank all my fantastic project students, I am fortunate to have had a wonderful bunch over the years (Alicia, Anthony, Antonia, Harry, Hifza, Jacob, Lauren, Matt, Ming, Natalia, Nathaniel, Selina, Tom C, and Tom P) whose contributions to my research have always been appreciated.

Thank you to Carol Kennedy for CHN analysis. Alice, thank you for letting me steal ice from your lab, and for the memorable moments during teaching labs. I thank the EPSRC national mass spectrometry service at Swansea for carrying out MS analyses and providing technical expertise. I thank Ellie Beeby for providing training in fluorescent microscopy, plate reading and staining, and Western blotting. A big thank you goes out to Huguette Savoie for carrying out cell culture and training, as well as the delicious cakes on Friday mornings. Huguette has always been a supporting ear to listen to my problems and give me gardening advice. I extend my thanks to Dr Isabel Pires who has supported me throughout my time as a PhD student, pushing me forwards to learn and carry out a wide array of biological experiments, without her help my project wouldn't have been the same. I'd like to thank Dr Ben Murray for collaborating with me on multiple projects, thank you Ben for believing in my crazy ideas.

Thank you to all the present and past members of lab C120 (Aimie Rendle, Guy Entact, Dr Steven Yap, Dr Miffy Cheng, Dr Lauren Turner, Dr Cinzia Spagnul, and Dr Joao Rodriguez) for the amazing times I have had throughout my PhD, for encouraging me, providing me with friendship, love, and laughter. Thank you to my partner Calum for his continued love, support, and encouragement throughout my time as a postgraduate student. Thank you for putting up with me when everything went wrong and thank you for picking me back up again and celebrating with me when things went well. Finally, I would like to give the greatest thanks to my mother for her loving support and encouragement throughout my life, and of course during my time at the University of Hull to whom I am extremely grateful. This thesis is dedicated to my father who passed away from lung cancer in 2013.

Table of Contents

Abstract	i
Authors Declaration	i
Acknowledgements	iii
Table of Contents	iv
Table of Figures, Tables and Schemes.....	vi
Figures	vi
Tables	x
Schemes.....	xi
Abbreviations	xiii
Chapter 1	1
Introduction.....	1
1.0 Cancer and Personalised Medicine	2
1.1 Tumour Biology	3
1.1.1 Angiogenesis and the EPR Effect.....	3
1.1.2 Warburg Effect	4
1.1.3 Tumour Hypoxia	5
1.1.4 Tumour Suppressor Protein p53.....	5
1.1.5 Cell Cycle	7
1.2 Approaches to Cancer Therapy	8
1.2.1 Radiotherapy	8
1.2.2 Chemotherapy	22
1.2.3 Photodynamic Therapy.....	26
1.3 Cancer Imaging	31
1.3.1 Positron Emission Tomography	32
1.4 Theranostic Medicine.....	35
1.5 Dual-Therapy	38
1.6 Literature Conclusions	40
1.7 Research Aims	41
Chapter 2.....	43
Synthesis and Biological Evaluation of Diphenylporphyrin Radiosensitizers.....	43
2.1 Introduction	44
2.2 Synthesis of Trans-A ₂ -Diphenylporphyrins	44
2.3 Synthesis of Metalloporphyrins	46
2.4 Synthetic Strategy	46

2.5 Synthesis of Hydrophilic Trans-A ₂ -Diphenylporphyrins.....	54
2.5.1 Synthesis of Hydrophilic Carboxylic Acid Trans-A ₂ -Diphenylporphyrins.....	54
2.5.2 Synthesis of Facially Hindered Hydrophilic Trans-A ₂ Diphenylporphyrins.....	64
2.5.3 Synthesis of Super-Hydroxylated Diphenylporphyrin	66
2.6 Radiobiological Evaluation of Hydrophilic Metalloporphyrins.....	68
2.6.1 Pre-Clinical Drug Formulation.....	72
2.6.2 Dose-Response Curves of HT-29 and HCT-116.....	73
2.6.3 Quantification of Drug Internalisation by ICP-OES	74
2.6.4 MTT Assays for Cell Number/Viability.....	75
2.6.5 5,15-Dinitro-10,20-diphenylporphyrins Cause Sensitization of Colorectal Cancers to Ionizing Radiation	76
2.6.6 5,15-Carboxy-10,20-diphenylporphyrins Do Not Cause Sensitization of Colorectal Cancers to Ionizing Radiation	79
2.6.7 Evaluation of the Impact on Cell Cycle Progression after Treatment with Ionizing Radiation	79
2.6.8 Evaluation of the Impact on DNA Damage/Repair after Treatment with Ionizing Radiation	83
2.6.9 Determination of the Mode of Cell Death.....	85
2.7 Chapter Conclusion.....	89
Chapter 3.....	90
Synthesis and Validation of a Theranostic Radiosensitizer	90
3.1 Introduction.....	91
3.2 <i>Meso</i> -Modification.....	92
3.2.1 Formylation	92
3.2.2 Diazotisation.....	95
3.2.3 Sonogashira Coupling	97
3.3 <i>Meso</i> -phenyl Modification.....	99
3.3.1 Synthesis of Bifunctional Linkers	99
3.3.2 Conjugation of Diphenylporphyrins to Heterobifunctional Linkers	101
3.4 Synthesis of a Novel [¹⁸ F]F Fluorinated Diphenylporphyrin.....	102
3.4.1 Synthesis of the ‘Cold’ Standard PEG Prosthetic	102
3.4.2 Radiochemical Synthesis of [¹⁸ F]F PEG Prosthetics.....	104
3.4.3 Synthesis of the ‘Cold’ Standard Conjugates.....	106
3.4.4 Synthesis of a ‘Hot’ [¹⁸ F]F Radiolabelled Diphenylporphyrin.....	108
3.5 Chapter Conclusion.....	110
Chapter 4.....	112
Synthesis and Biological Evaluation of a Novel Porphyrin-RAPTA Conjugate.....	112

4.0 Introduction	113
4.1 Synthesis of a Conjugatable Porphyrin	114
4.2 Synthesis of an Amide-capped Porphyrin	116
4.3 Synthesis of a Porphyrin-RAPTA Conjugate.....	116
4.4 Photochemical Studies	117
4.5 <i>In Vitro</i> Phototoxicity Studies	121
4.6 Cell Uptake by ICP-MS	124
4.7 Chapter Conclusion	124
Chapter 5	126
Conclusion, Contributions to the Field, and Future Work	126
5.0 Conclusion and Contributions to the Field.....	127
5.1 Future Work	129
Chapter 6.....	131
Experimental.....	131
6.0 Experimental	132
6.1 Methods and Materials	132
6.2 Biological Methodology.....	134
6.3 Synthetic Protocols.....	138
Chapter 7.....	222
References.....	222
7.0 References	223

Table of Figures, Tables and Schemes

Figures

Figure 1. Schematic showing normal blood flow and blood flow of tumour vasculature; gaps can be opened hydrodynamically by AT-II induced hypotension leading to enhanced tumour selective delivery. ¹³	4
Figure 2. Representation of hypoxia induction with increasing distance from the capillary network.	5
Figure 3. p53 pathway in cancer and aging.	6
Figure 4. p53 pathway leading to the expression of genes.	7
Figure 5. Schematic of the process of X-ray fluorescence occurring in an atom.	11
Figure 6. Schematic of the processes of photoabsorption, photoionization and Auger electron emission.	12
Figure 7. Schematic diagram of the breaking of DNA strands by the action of ionizing radiation.	14
Figure 8. 3D model PARP-1 enzyme.....	15
Figure 9. Structure of a substituted nitroimidazole with known radiosensitizing abilities.	18

Figure 10. Nimorazole, a known radiosensitiser used clinically.	19
Figure 11. Gemcitabine (left), and gefitinib (right).	19
Figure 12. Reaction scheme showing the one electron reduction of a nitro substituent on an aromatic ring; nitro group to nitro radical anion. ²⁵	20
Figure 13. Tetraarylporphyrins and diarylporphyrins displaying positions for modification with electron withdrawing groups.....	21
Figure 14. The skeletal structure of Gd–Tex, a known radiosensitizer.....	21
Figure 15. Chemical structure of MTL-005 a radiosensitizer in human clinical trials in the NHS, UK.....	22
Figure 16. Paclitaxel, a taxane which is a potent anti-mitotic compound.....	23
Figure 17. Doxorubicin, a fluorescent cytotoxic anti-tumoural compound.	24
Figure 18. Camptothecin, a lipophilic topoisomerase inhibitor.	24
Figure 19. Cis-platin, a platinum(II) based chemotherapeutic.....	24
Figure 20. RAPTA-C, a known anti-metastatic ruthenium(II) agent.....	25
Figure 21. Simplified Jablonski diagram outlining the photosensitisation processes.	26
Figure 22. Molecular orbital diagrams of singlet oxygen (¹ O ₂) and triplet oxygen (³ O ₂).	27
Figure 23. 5-Aminolaevulinic acid.	29
Figure 24. Benzoporphyrin monoacid ring A (BDP-MA).	30
Figure 25. Temoporfin, an example of a chlorin photosensitiser.....	31
Figure 26. Chlorin 6e, a hydrophilic chlorin photosensitiser	31
Figure 27. Diagrammatic representation of the emission of a positron, following annihilation and subsequent detection. ¹⁴⁹	33
Figure 28. ¹⁸ O (p,n) [¹⁸ F]F nuclear reaction schematic detailing the synthesis of [¹⁸ F]F, positron emission, and [¹⁸ F]F decay.....	35
Figure 29. An amphiphilic porphyrin appended to a lipophilic [¹⁸ F] radiolabelled chain.	36
Figure 30. A cationic water-soluble Zn(II) porphyrin appended to a [¹⁸ F] radiolabelled prosthetic. ¹⁵⁴	37
Figure 31. Alkylated nitroimidazole labelled with [¹⁸ F].	37
Figure 32. Al- ¹⁸ F radiolabelled DODA conjugated to 2-nitroimidazole.	38
Figure 33. Dual-therapeutic platinum-porphyrin conjugate.....	39
Figure 34. Tetranuclear Ru(II)-porphyrin conjugate.	39
Figure 35. A cationic tetranuclear Ru(II)-porphyrin conjugate.	40
Figure 36. Mechanism of acidolysis of 5-phenyldipyromethane. ¹⁷⁸	45
Figure 37. UV-Vis spectrum of compound 2 in DCM.....	49
Figure 38. UV-Vis spectrum of 3 obtained in DCM.....	50
Figure 39. Absorption spectra of 2 (left) obtained in DCM and 6 (right) obtained in DCM.	52
Figure 40. Absorption spectra of 10 (left) obtained in DCM and 11 (right) obtained in DCM. .	55
Figure 41. UV-Vis absorption spectrum for compound 22 (left) and 23 (right), exhibiting four and two Q bands respectively.	64
Figure 42. UV-Vis absorption spectrum for compound 37 (left) and 38 (right), exhibiting four and two Q bands respectively.	67
Figure 43. A pictorial representation of the three potential compounds in order of increasing polarity.	68
Figure 44. Brightfield optical micrographs of HT-29 (p53 null) cells (top) grown on glass coverslips, brightfield optical micrographs of HCT-116 (p53 WT) cells (bottom) grown on glass coverslips.	70
Figure 45. Screening of the delivery vehicle for incubation of the drug candidates with the cells. The graph shows the mean percentage of the surviving fraction of cells incubated with media	

alone versus media supplemented with 1% DMSO. Bars represent $x \pm SD$ (n=3). Statistical analysis was performed using the double-sided unpaired Student's t-test. ns; $p > 0.05$, *; $p < 0.05$, **; $p < 0.01$, ***; $p < 0.001$, ****; $p < 0.0001$	73
Figure 46. Dose-response curve for the interaction of HT-29 (p53 null) cells (left) and HCT-116 (p53 WT) (right) with non-collimated ionising radiation (0-8 Gy) under oxic conditions. Data plotted represent mean values $x \pm SD$ (n=3).....	73
Figure 47. ICP-OES data for compounds 18 and 23 incubated into HT-29 (p53 null) (left) and HCT-116 (p53 WT) (right) for 1 hr followed by centrifugation and washing. Bars represent $x \pm SD$ (n=3). Statistical analysis was performed using multiple double-sided unpaired Student's t-test. ns; $p > 0.05$, *; $p < 0.05$, **; $p < 0.01$, ***; $p < 0.001$, ****; $p < 0.0001$	74
Figure 48. MTT cell number surviving fraction data for 18 in HT-29 (p53 null) measured every 24 hr for 2 hrs. Bars represent $x \pm SD$ (n=3). Statistical analysis was performed using multiple double-sided unpaired Student's t-test. ns; $p > 0.05$, *; $p < 0.05$, **; $p < 0.01$, ***; $p < 0.001$, ****; $p < 0.0001$	75
Figure 49. MTT cell number surviving fraction data for 23 in HT-29 (p53 null) measured every 24 hr for 2 hrs. Bars represent $x \pm SD$ (n=3). Statistical analysis was performed using multiple double-sided unpaired Student's t-test. ns; $p > 0.05$, *; $p < 0.05$, **; $p < 0.01$, ***; $p < 0.001$, ****; $p < 0.0001$	76
Figure 50. Dose-response curves of HT-29 (p53 null): A; cell only, B; 25 μ M, C; 50 μ M. Dose-response curved of HCT-116 (p53 WT): D; cell only, E; 25 μ M, F; 50 μ M. IRR = Irradiated. Data points represent $x \pm SD$ (n=3). Statistical analysis was performed using a two-factor ANOVA with Bonferroni's multiple comparisons <i>post-hoc</i> significance testing. ns; $p > 0.05$, *; $p < 0.05$, **; $p < 0.01$, ***; $p < 0.001$, ****; $p < 0.0001$	77
Figure 51. Surviving fraction of HT-29 (p53 null) cells, with various doses of ionising radiation and concentration of 23 after 1 hour incubation.	79
Figure 52. Stacked-columns representing the cell cycle proportions observed by FACS for given treatments at two different time points. IRR = Irradiated. Data points represent $x \pm SD$ (n=3). 10 Gy control data points represent $x \pm SD$ (n=6).....	80
Figure 53. The fraction of the G2/M population (%) observed by FACS for given treatments. IRR = Irradiated. Data points represent $x \pm SD$ (n=3). 10 Gy control data points represent $x \pm SD$ (n=6). Statistical analysis was performed using three-factor ANOVA with Bonferroni's multiple comparisons <i>post-hoc</i> significance testing. ns; $p > 0.05$, *; $p < 0.05$, **; $p < 0.01$, ***; $p < 0.001$, ****; $p < 0.0001$	81
Figure 54. The fraction of Sub-G1 cells (%) observed by FACS for given treatments. IRR = Irradiated. Data points represent $x \pm SD$ (n=3). 10 Gy control data points represent $x \pm SD$ (n=6).....	82
Figure 55. The fraction of Sub-G1 cells (%) observed by FACS for given treatments. IRR = Irradiated. Data points represent $x \pm SD$ (n=3). 10 Gy control data points represent $x \pm SD$ (n=6). Statistical analysis was performed using three-factor ANOVA with Bonferroni's multiple comparisons <i>post-hoc</i> significance testing. ns; $p > 0.05$, *; $p < 0.05$, **; $p < 0.01$, ***; $p < 0.001$, ****; $p < 0.0001$	83
Figure 56. Fluorescence micrographs of treated and untreated HT-29 (p53 null) and HCT-116 (p53 WT) cells seeded into agarose gel stained with propidium iodide after being lysed in alkaline buffer and electrophoretically separated.	84
Figure 57. DNA in comet tails observed through the alkaline comet assay for HT-29 (p53 null) (left) an HCT-116 (p53 WT) (right) cells after a given treatment. Data points represent $x \pm SD$ (n=3). Statistical analysis was performed using two-factor ANOVA with Bonferroni's multiple	

comparisons <i>post-hoc</i> significance testing. ns; p>0.05, *, p<0.05, **, p<0.01, ***, p<0.001, ****, p<0.0001.	85
Figure 58. Fluorescence micrographs of the nuclear morphology of HT-29 (p53 null) and HCT-116 (p53 WT) cells with and without ionizing radiation treatment.	86
Figure 59. Fluorescence micrographs examples of healthy colorectal cancer cells, and colorectal cells treated with 10 Gy of ionizing radiation displaying typical examples of arrested cells, blebbing cells, canonical apoptotic cells and cells undergoing mitotic catastrophe.	87
Figure 60. Figures displaying stacked columns of the fraction of cell morphologies observed <i>via</i> immunofluorescence microscopy of colorectal cells stained with DAPI. MC; mitotic catastrophe, Ap; canonical apoptosis, CCA; cell cycle arrest, Healthy; cells expressing normal nuclear morphology. Data points represent $x \pm SD$ (n=3). Statistical analysis was performed using two-factor ANOVA with Bonferroni's multiple comparisons <i>post-hoc</i> significance testing. ns; p>0.05, *, p<0.05, **, p<0.01, ***, p<0.001, ****, p<0.0001.	88
Figure 61. Pictorial representation of the available three sites on the existing scaffold of molecule 18 to append an [¹⁸ F]F prosthetic.	91
Figure 62. UV-Vis spectrum of compounds 42 (left) and 43 (right), each showing a Soret band and two Q bands.	94
Figure 63. Retrosynthetic breakdown of a porphyrin bearing a <i>meso</i> -alkyne functionality.	97
Figure 64. (A) Radio-TLC of the reaction mixture, denoting free unbound [¹⁸ F]F ⁻ and the [¹⁸ F]F radiolabelled prosthetic ([¹⁸F]62). (B) Radio-TLC of the reaction mixture, denoting free unbound [¹⁸ F]F ⁻ and the [¹⁸ F]F radiolabelled prosthetic ([¹⁸F]67).	105
Figure 65. (A) QC radio-TLC of [¹⁸F]62 . (B) QC radio-TLC of [¹⁸F]67 . (C) QC radio-HPLC (C-18 silica, method 1) of [¹⁸F]62 . (D) QC radio-HPLC (C-18 silica, method 1) of [¹⁸F]67	106
Figure 66. Radio-TLC chromatograms of the reaction optimisation of the radiochemical conjugation of [¹⁸F]62 to 69 yielding [¹⁸F]70	109
Figure 67. HPLC of 72 , Rt = 18.7 mins (left). Radio-HPLC of [¹⁸F]72 , Rt = 18.1 mins (right).	110
Figure 68. UV-Vis absorption spectra of 78 (left) and 80 (right) determined in d(H ₂ O).	118
Figure 69. UV-Vis absorbance spectra of ABDA irradiated with red light (617 - 651 nm) with and without photosensitizer (PS). Curves are averages of three independent experiments (n=3). A; ABDA (100 μM), B: ABDA (100 μM) irradiated in the presence of 4.75 μM of TMePyP , C: ABDA (100 μM) irradiated in the presence of 4.75 μM of 80 , C: ABDA (100 μM) irradiated in the presence of 4.75 μM of 78	119
Figure 70. (A) Photostability studies of compounds 78 , 80 and TMePyP irradiated continuously with red light (617 - 651 nm, 1035.8 W m ⁻²). (B) Photostability studies of compounds 78 , 80 and Rose Bengal irradiated continuously with white light. Data are presented as $x \pm SD$ (n=3).	120
Figure 71. ³¹ P-NMR of 14 after receiving 0, 20, 40, or 60 J cm ⁻² of white light revealing the evolution of PTA phosphine oxide through photoinduced electron transfer. Chemical shifts (δ) measured in ppm.	121
Figure 72. Temporal MTT assay of 78 , 79 and 80 displaying time-dependent and concentration-dependent cell viabilities with 0 J cm ⁻² and 20 J cm ⁻² light doses. NI; non-irradiated, IRR; irradiated. Data are presented as $x \pm SD$ (n=3). ANOVA statistical analysis was carried out with Bonferroni's <i>post-hoc</i> significance testing.	122
Figure 73. Dose-response cytotoxicity curves of 78 and 80 measured over two incubation periods (24 hour and 48 hour). Data are presented as $x \pm SD$ (n=3).	123
Figure 74. ICP-MS data highlighting the concentration of ¹⁰¹ Ru (ppb) in HT-29 cells incubated with 10 μM for 48 hour. Data are presented as $x \pm SD$ (n=3). An ordinary ANOVA statistical	

analysis was carried out with Dunnett's post-hoc multiple comparisons significance testing, ns; (p>0.05), *, (p<0.05), **, (p<0.01)..... 124

Tables

Table 1. Comparison of ionizing power and penetration depth of ionizing radiation and electromagnetic radiation.....	8
Table 2. Common radioactive transformations and the processes that occur, with charge, nucleon, and lepton numbers been conserved.....	8
Table 3. The four main delivery techniques of radiotherapy.....	13
Table 4. Table of the five Rs of radiotherapy and the impact they have after a given dose.....	16
Table 5. Tabulated idealized properties of radiosensitizer.....	17
Table 6. Ideal properties of a chemotherapy agent.....	23
Table 7. Ideal properties of a photodynamic sensitizer.....	29
Table 8. Common particles and their corresponding antiparticles.....	32
Table 9. Common radioisotopes used for PET imaging. ¹⁴⁷	34
Table 10. Table showing key principles an ideal PET tracer should obey.....	35
Table 11. Screening of metal salts used in one-pot porphyrin condensation reactions. ^a Yields reported are from isolated compounds after purification by column chromatography.....	49
Table 12. Table of attempted saponification reactions for route A. ^a Yields reported are from isolated compounds after purification by column chromatography.....	57
Table 13. Table of attempted nitration reactions for route A. ^a Yields reported are from isolated compounds after purification by column chromatography.....	57
Table 14. Table of attempted nitration reactions for route B. ^a Yields reported are from isolated compounds after purification by column chromatography.....	58
Table 15. Table of attempted saponification reactions for route B. ^a Yields reported are from isolated compounds after purification by column chromatography.....	58
Table 16. Table of attempted bromination reactions of 10 . ^a Yields reported are from isolated compounds after purification by column chromatography. RT; room temperature.....	59
Table 17. Table of attempted nitration reactions of 15 . ^a Yields reported are from isolated compounds after purification by column chromatography.....	59
Table 18. Table of attempted saponification reactions. ^a Yields reported are from isolated compounds after purification by column chromatography.....	63
Table 19. Key hydrophilic copper(II) chelated trans-A ₂ -diphenylporphyrins for <i>in vitro</i> evaluation of the porphyrin macrocycle.....	72
Table 20. Schedule 1 ionising radiation therapy routine.....	76
Table 21. Tabulated data representing the RER and DMR factors calculated using equations 17 and 18. RER; radiation enhancement ratio, DMR; dose-modifying ratio.....	78
Table 22. Tabulated conditions investigated in the optimisation of the alkaline comet assay....	84
Table 23. Tabulated conditions attempted to synthesise a dithiolated diarylporphyrin.....	95
Table 24. Table of results from optimisation studies of a Sonogashira coupling reaction to a trans-A ₂ -diarylporphyrin. ^a Yields given are isolated yields obtained after column chromatography and precipitation.....	99
Table 25. Table of attempted conditions for the formation of peptide linkages. ^a Yields given are isolated yields obtained after column chromatography and precipitation.....	101
Table 26. Table of conditions for copper (I) catalysed alkyne-azide cycloaddition reaction. ^a Yield is reported after purification by column chromatography.....	107

Table 27. Tabulated experimental conditions investigated for the radiochemical conjugation of [¹⁸ F]62 to 69. ^a Radiochemical purity (RCP) determined by radio-TLC. ^b Radiochemical purity (RCP) determined by radio-HPLC.....	109
Table 28. UV-Vis absorption maxima and molar absorptivity coefficients determined in d(H ₂ O). Molar absorptivity coefficients are given as log ₁₀ values in brackets.	118
Table 29. Data for the relative singlet oxygen quantum yields (Φ _Δ) for given compounds obtained by photochemical studies by time-course UV-Vis spectroscopy with the presence of a singlet oxygen radical trap (ABDA). Data presented are averages of three independent experiments (n=3).	119

Schemes

Scheme 1. Synthesis of 5-phenyldipyrromethane. Conditions used; i) neat degassed pyrrole, freshly distilled benzaldehyde, indium(III) trichloride, Ar, RT, stir 4 hr.	47
Scheme 2. Synthesis of 5,15-diphenylporphyrin. Conditions used; i) degassed DCM, 5-phenyldipyrromethane, trimethyl orthoformate, trichloroacetic acid in DCM, Ar, RT, stir 17 hr. ii) degassed DCM, 5-phenyldipyrromethane, paraformaldehyde, trifluoroacetic acid, Ar, RT, stir 4 hr, DDQ, stir 30 mins. iii) degassed DCM, 5-phenyldipyrromethane, trimethyl orthoformate, trichloroacetic acid in DCM, Zn(OAc) ₂ dihydrate, Ar, RT, stir 17 hr.	48
Scheme 3. <i>Meso</i> -bromination of 5,15-diphenylporphyrin. Conditions used; i) NBS, chloroform, Ar, 0 °C, stir 10 mins, acetone, stir 30 mins.....	51
Scheme 4. Nitration of 5,15-diphenylporphyrin. Conditions used; i) NaNO ₂ , TFA, Ar, 0 °C, stir 30 mins.....	51
Scheme 5. Metallation of 5,15-diphenylporphyrin. Conditions used; i) Cu(OAc) ₂ monohydrate, DMF, MW heating 90 °C 1 hr.....	52
Scheme 6. Microwave-assisted metallation of 4 with Cu(OAc) ₂ monohydrate. Conditions used; i) Cu(OAc) ₂ monohydrate, DMF, MW heating 90 °C, 1 hour.....	53
Scheme 7. Microwave-assisted metallation of 5 with Cu(OAc) ₂ monohydrate. i) Cu(OAc) ₂ monohydrate, DMF, MW heating 90 °C, 1 hour.....	53
Scheme 8. Synthesis of a metalloporphyrin bearing two ester groups. Conditions used; i) neat degassed pyrrole, methyl 4-formylbenzoate, indium(III) trichloride, Ar, RT, stir 4 hr. ii) degassed DCM, 5-(methylbenzoate)dipyrromethane, trimethyl orthoformate, trichloroacetic acid in DCM, Ar, RT, stir 17 hr.....	55
Scheme 9. Two possible synthetic routes to yield the desired 5,15-dinitro-10,20-diphenylporphyrin.....	56
Scheme 10. Synthesis of a <i>meso</i> -brominated metalloporphyrin. Conditions used; i) NBS, CHCl ₃ , 0 °C, 10 mins. ii) TFA/NaNO ₂ , 0 °C, 3 hr. iii) KOH, THF/MeOH, 80 °C, 17 hr.	59
Scheme 11. Synthesis of a <i>meso</i> -brominated metalloporphyrin. Conditions used; i) NBS, CHCl ₃ , 0 °C, 3 hr. ii) KOH, THF/MeOH, 80 °C, 17 hr.....	60
Scheme 12. Synthesis of a hydrophilic metalloporphyrin. Conditions used; i) Cu(OAc) ₂ monohydrate, DMF, MW heating 90 °C 1 hr.....	60
Scheme 13. Synthesis of a hydrophilic metalloporphyrin. Conditions used; i) Cu(OAc) ₂ monohydrate, DMF, MW heating 90 °C 1 hr.....	61
Scheme 14. Synthesis of a hydrophilic metalloporphyrin. Conditions used; i) Cu(OAc) ₂ monohydrate, DMF, MW heating 90 °C 1 hr.....	61
Scheme 15. Synthesis of a tetraesterporphyrin. Conditions used; i) degassed DCM, 5-(methylbenzoate)dipyrromethane, ethyl glyoxalate, BF ₃ , Ar, RT, stir 4 hr, DDQ.	62
Scheme 16. Saponification reaction i) KOH, THF/MeOH, 50 °C, 72 hr. i) Cu(OAc) ₂ monohydrate, DMF, MW heating 90 °C 1 hr.....	63

Scheme 17. Synthesis of a library of ‘masked’ aldehydes. Conditions used; i) ‘Aldehyde’, K ₂ CO ₃ , DMF, 80 °C 17 hr. ii) neat degassed pyrrole, aldehyde 24 , 25 or 26 , indium(III) trichloride, Ar, RT, stir 4 hr.	64
Scheme 18. Synthesis of a hydrophilic porphyrin. Conditions used; i) degassed DCM, dipyrromethane 27 , 28 , or 29 trimethyl orthoformate, trichloroacetic acid in DCM, Ar, RT, stir 17 hr.	65
Scheme 19. Synthesis of a facially-hindered hydrophilic porphyrin. Conditions used; i) NaNO ₂ , TFA, Ar, 0 °C, stir 30 mins. ii) Cu(OAc) ₂ monohydrate, DMF, MW heating 90 °C 1 hr.	66
Scheme 20. Synthesis of a hydrophilic metalloporphyrin. Conditions used; i) degassed DCM, dipyrromethane 27 , trimethyl orthoformate, trichloroacetic acid in DCM, Ar, RT, stir 17 hr. ..	67
Scheme 21. Synthesis of a hydrophilic metalloporphyrin. Conditions used; i) BBr ₃ 1M in DCM, RT, overnight.	68
Scheme 22. Formylation of diphenylporphyrin. Conditions used: i) Cu(OAc) ₂ monohydrate, MW heating, 80 °C, 1 hr. ii) Ni(OAc) ₂ , MW, 160 °C, 1 hr. iii) DMF/POCl ₃ , 60 °C, Ar, 16 hr, . iv) H ₂ SO ₄ , RT, stir 30 mins.	93
Scheme 23. Formylation of diphenylporphyrin. Conditions used: i) Dithiane, n-BuLi, 12, -78 °C warming to -40 °C, 2 hr, Ar.	95
Scheme 24. Synthesis of an aromatic heterobifunctional linker. Conditions used: i) Boc ₂ O, MeOH, Ar, stir RT 17 hrs. ii) Propargyl bromide, K ₂ CO ₃ , DMF, Ar, stir 17 hrs. iii) TFA, stir RT, 30 mins. iv) TFA, NaNO ₂ , HPF ₆ , H ₂ O, Ar, -10 °C, 1.5 hr.	96
Scheme 25. Formylation of diphenylporphyrin. Conditions used: i) 47 , THF, Ar, RT stir, 17 hr.	96
Scheme 26. Formylation of diphenylporphyrin. Conditions used: i) TFA, NaNO ₂ , HPF ₆ , H ₂ O, Ar, -10 °C, 1.5 hr.	97
Scheme 27. Formylation of diphenylporphyrin. Conditions used: i) 48 , THF, Ar, RT stir, 17 hr.	97
Scheme 28. Formylation of a heterobifunctional linker for Sonogashira coupling. Conditions used: i) Propargyl bromide, NaI, TBAI, KOH, THF, Ar, -10 °C warming to RT, 17 hr. ii) TosCl, TEA, DCM, Ar, RT, 17 hr. iii) NaN ₃ , MeCN, reflux, 48 hr.	98
Scheme 29. Synthesis of an alkyl ether alkyne-amine heterobifunctional linker. Conditions used; i) Boc ₂ O, TEA, DCM, Ar, 0 °C, 17 hr, RT. ii) TBAI, NaI, KOH, propargyl bromide, Ar, THF, 17 hr, RT. iii) 4 N HCl in dioxane, ethyl acetate, 17 hr, RT.	100
Scheme 30. Synthesis of an alkyl ether azide-amine bifunctional linker. Conditions used; i) Boc ₂ O, TEA, DCM, Ar, 0 °C, 17 hr, RT. ii) TBAI, NaI, KOH, propargyl bromide, Ar, 17 hr, RT. iii) 4 N HCl in dioxane, ethyl acetate, 17 hr, RT.	101
Scheme 31. Synthesis of a clickable porphyrin. Conditions used; i) PEG chain (54 or 57), TBTU, DIPEA, DMF, 80 °C, 17 hr, RT.	102
Scheme 32. Zinc(II) protection of 58 and 59 . Conditions used; i) 58 or 59 , Zn(OAc) ₂ dihydrate, DMF, MW heating 80 °C, 1 hr.	102
Scheme 33. Synthesis of clickable alkyne-fluorine alkyl ether PEG chain. Conditions used; i) TBAF, THF, Ar, reflux, 17 hr.	103
Scheme 34. Synthesis of clickable azide-fluorine alkyl ether PEG chain. Conditions used; i) PBr ₃ , DCM, Ar, -10 °C warming to RT, 17 hr. ii) NaN ₃ , MeCN, reflux, 48 hr. iii) TosCl, Et ₃ N, DCM, Ar, 0 °C warming to RT, 17 hr. iv) TBAF, THF, reflux, 17 hr.	104
Scheme 35. Trapping of [¹⁸ F]F ⁻ . Conditions used; i) K ₂₂₂ , MeCN, RT, 20 mins.	104
Scheme 36. Radiofluorination of 50 and 66 . Conditions used; i) [¹⁸ F]K ₂₂₂ , acetonitrile, 90 °C, 20 mins.	105

Scheme 37. Click reaction yielding mono- and bis-adducts. Conditions used; i) 61 , Cu(OAc) ₂ monohydrate, sodium ascorbate, TBTA, THF/MeOH (8:2), MW heating, 80 °C, 20 mins.	107
Scheme 38. Metallation of 59 with Cu(OAc) ₂ monohydrate under microwave heating, and subsequent CuAAC conjugation to 62 . Conditions used; i) 62 , Cu(OAc) ₂ monohydrate, DMF, MW heating, 80 °C, 1 hr. ii) 69 , Cu(OAc) ₂ monohydrate, sodium ascorbate, TBTA, THF/MeOH (8:2), MW heating, 80 °C, 20 mins.	108
Scheme 39. Synthesis of a carboxylic acid reactive porphyrin. Conditions used; i) propionic acid, reflux 180 °C, 2 hr. ii) KOH, THF/MeOH (4:1), Ar, 60 °C, stir 17 hr. iii) TBTU, DIPEA, DMF, Ar, 40 °C, stir 17 hr. iv) MeI, DMF, DIPEA, Ar, 40 °C, stir 17 hr. v) TFA/DCM (1:1), RT, stir 1 hr.	116
Scheme 40. Synthesis of an amide capped porphyrin. Conditions used; i) TFA/DCM (1:1), RT, stir 1 hr. ii) Ac ₂ O, DIPEA, DMF, Ar, 40 °C, stir 17 hr. iii) MeI, DMF, DIPEA, Ar, 40 °C, stir 17 hr.	116
Scheme 41. Synthesis of a porphyrin-RAPTA conjugate. Conditions used; i) TBTU, DIPEA, DMSO, Ar, stir 3 hr.	117

Abbreviations

(aq)	Aqueous
5-ALA	5-Aminolevulinic acid
ABDA	9,10-Anthracenediyl-bis(methylene)dimalonic acid
ADC	Antibody-drug-conjugate
ANOVA	Analysis of variance
Ap	Apoptosis
ASAP	Atmospheric solids analysis probe
ATP	Adenosine triphosphate
ATR	Attenuated total reflection
Ar	Argon
BDP-MA	Benzoporphyrin derivative monoacid a
Boc ₂ O	Di-tert-butyl dicarbonate
Bq	Becquerel
CCA	Cell cycle arrest
CT	Computerised tomography
CuAAC	Copper catalysed azide-alkyne click
Cys	Cysteine
DAPI	4',6-Diamidino-2-phenylindole
DCC	N,N'-Dicyclohexylcarbodiimide
DCBT	Trans-2-[3-(4-tert-Butylphenyl)-2-methyl-2propenylidene]malononitrile
DCM	Dichloromethane
DDQ	2,3-Dichloro-5,6-dicyano-1,4-benzoquinone
DIPEA	N,N-diisopropylethylamine

DME	Dimethoxyethane
DMF	Dimethyl formamide
DMR	Dose modifying ratio
DMSO	Dimethyl sulfoxide
DNA	Deoxyribonucleic acid
DPM	Dipyrromethane
DPP	5,15-Diphenylporphyrin
DSB	Double strand break
EDC	N-(3-Dimethylaminopropyl)-N'-ethylcarbodiimide
EDG	Electron donating group
EM	Electromagnetic
EPR	Enhanced permeation and retention
ESI	Electrospray ionization
EU	European Union
EWG	Electron withdrawing group
FACS	Fluorescence-assisted cell sorting
FDA	Food and Drug Administration
FDG	Fluorodeoxyglucose
[¹⁸ F]FDG	2-Deoxy-2-[¹⁸ F]fluoro-D-glucose
FI	Fluorescence imaging
FT	Fourrier-transform
Gy	Gray
HATU	1-[Bis(dimethylamino)methylene]-1H-1,2,3-triazolo[4,5-b]pyridinium3-oxid hexafluorophosphate
HCl	Hydrogen chloride
HER+	Human epidermal growth factor 2
His	Histine
HOBt	1-Hydroxybenzotriazole
HOMO	Highest occupied molecular orbital
HPLC	Higher performance liquid chromatography
HRMS	High resolution mass spectrometry
ICP	Inductively coupled plasma
IR	Infrared
IRR	Irradiated
ISA	Imidazole-1-sulfonyl azide hydrogen sulfate
LET	Linear energy transfer
LINAC	Linear accelerator

LQM	Linear-quadratic model
LQ	Linear-quadratic
LUMO	Lowest unoccupied molecular orbital
K ₂₂₂	Kryptofix [®]
MALDI	Matrix-assisted laser desorption ionization
MC	Mitotic catastrophe
MRI	Magnetic resonance imaging
MeOH	Methanol
Met	Methionine
MeV	Mega electronvolt
Mp	Melting point
MS	Mass spectrometry
MTT	3-(4,5-dimethylthiazole-2-yl)-2,5-diphenyltetrazolium bromide
MW	Microwave
NBS	N-Hydroxysuccinimide
NHS	National health service
NI	Not irradiated
NIR	Near infrared
NMR	Nuclear magnetic resonance
PBS	Phosphate buffered saline
PDT	Photodynamic therapy
PEG	Polyethylene glycol
PET	Positron emission tomography
PI	Propidium iodide
PS	Photosensitizer
PTA	1,3,5-Triaza-7-phosphaadamantane
PPIX	Protoporphyrin IX
Py	Pyridine
QC	Quality control
RAPTA	Ruthenium(II) 1,3,5-Triaza-7-phosphaadamantane
RCP	Radiochemical purity
RCY	Radiochemical yield
RE	Radio enhancer
RER	Radiation enhancement ratio
Rf	Retention factor
RF	Radiofrequency
ROS	Reactive oxygen species

RP	Reverse phase
RS	Radiosensitizer
Rt	Retention time
RT	Room temperature
SER	Sensitisation enhancement ratio
SSB	Single strand break
SPECT	Single photon emission computerised tomography
SUV _{max}	Standardised uptake value (maximum)
TBAF	Tetrabutylammonium fluoride
TBTA	Tris(benzyltriazolymethyl)amine
TBTU	2-(1H-Benzotriazole-1-yl)-1,1,3,3-tetramethylammonium tetrafluoroborate
TCA	Trichloroacetic acid
TEA	Triethylamine
TEG	Tetraethylene glycol
TFA	Trifluoroacetic acid
TLC	Thin-layer chromatography
THF	Tetrahydrofuran
TMS	Tetramethylsilane
TOF	Time-of-flight
Trp	Tryptophan
TsCl	p-Toluenesulfonyl chloride
TPP	5,15,20,25-Tetraphenylporphyrin
Tyr	Tyrosine
UK	United Kingdom
US	Ultrasound
UV	Ultraviolet
VEGF	Vascular endothelial growth factor
Vis	Visible
WT	Wild-type

Chapter 1
Introduction

1.0 Cancer and Personalised Medicine

The term cancer is used to describe a collection of diseases that are linked by two main characteristics: cancerous cells divide uncontrollably, and they can invade other parts of the body through a process called metastasis. Cancers are divided into six main groups: carcinomas, leukaemia, lymphoma, myeloma, sarcoma, and finally mesothelioma. According to Cancer Research UK, a leading cancer charity, there were 359,960 new cases of cancer diagnosed in 2015; with 163,444 deaths from cancer being registered in 2016. More than half of new diagnoses were breast, prostate, lung and bowel/colon cancers. Cancer is a particular problem for developed nations with an ageing population. As the life expectancy of a population increases so does the complication of medical afflictions such as cancer, cardiovascular diseases, neurological diseases, and diabetes. This is echoed by the 85-89 age group in the UK having the highest incident rates of cancer. Although the survival rates of cancer have doubled in the past 40 years, the incident rates of cancer in the UK are predicted to increase by 2% until 2035. The strain felt by healthcare systems is ever increasing, as is the financial burden, thus new techniques, methods and technologies are being developed to alleviate these pressures.

Traditional well-established cancer therapy techniques include: surgery, chemotherapy, and radiotherapy. New and emerging techniques include: photodynamic therapy (PDT), hormone therapy, and immunotherapy. It is believed that a more personalised approach to cancer diagnosis and therapy would confer great benefits on the clinical outcomes for patients. As of January 2015, the UK government pledged an almost £14 million investment in personalised medicine.¹ The Head of the Medical Research Council Oxford Institute for Radiation Oncology has suggested that the future of cancer treatment is personalised medicine.¹ He then went onto to say that 40% of patients with local advanced colorectal cancer do not currently respond to radiotherapy.¹ Personalised medicine is the application of bespoke treatment tailored to the individual and the individual's needs, not "one treatment cures all" as is commonly employed. This is important clinically as not all patients respond in the same manner and understanding the disease and how to combat it improves the efficacy of the treatment regime. One way in which treatment of cancer can be personalised is by the combination of therapy and imaging into a single scaffold (theranostics) or by combining two therapeutic modalities into a single construct (dual-therapy). Both theranostics and dual-therapy are investigated in this thesis.

1.1 Tumour Biology

In a healthy body, the maintenance of tissue size and tissue function depends on the existence of a small number of primitive stem cells.² These cells have the ability for unlimited proliferation which is the base of the hierarchy of cells that make up epithelial and haemopoietic tissues in the body.² Cancer can begin through the exposure of biological tissues to several key stressors: ionizing radiation, chemical agents, and time. Ionizing radiation and exposure to certain chemicals can trigger DNA damage which causes genetic mutations in the cells. Telomeres are specialised nucleoprotein structures which protect chromosome ends.³ These structures maintain the genetic integrity of normal cells, however, they sequentially shorten each time a parent cell divides into daughter cells inducing chromosomal instability.⁴ When cells with critically short telomeres divide, the DNA of the cell can mistakenly be “chopped”.^{5,6} During this process, a loss of genetic information can occur which leads to the generation of a cancerous cell.⁵ Healthy cells have fixed lifespans, when a cell is damaged or has outlived its time then it undergoes a programmed death.^{5,7} Cells which have mechanisms that resist this pre-programmed cell death are said to be cancerous. The cancerous cells continue to divide uncontrollably using vital oxygen and nutrients which can lead to further health complications. Additionally, cancer cells can spread to other parts of the body *via* a process called metastasis *via* the lymph nodes which can lead to secondary cancers. It follows that not all the cells in a tumour are neoplastic stem cells; some have embarked on an irreversible process of differentiation.⁸ In addition, carcinomas contain many normal host cells that make up the stroma (fibroblasts, endothelial cells, macrophages, etc.).⁸ Some cancers can result in visible growths called tumours, while other types of cancer such as leukaemia do not. Most of the cells that make up the volume of many tumour types are not malignant.² If these non-malignant cells were the only cells left intact at the end of therapy, then the tumour would not regrow.² Tumour growth is driven by the neoplastic stem cells, and it is these that must be eradicated.² When a tumour regrows after non-curative treatment, it does so because some stem cells were not killed.² Biologists have recognised that the key to understanding tumour response is to determine how many tumour stem cells are left.²

1.1.1 Angiogenesis and the EPR Effect

One of the major flaws of tumour morphology is that they develop abnormal vasculature (neovasculature) and lymphatic vessels in order to supply themselves with an adequate supply of oxygen, nutrients, and to remove waste products.⁹ These processes are called angiogenesis and lymphangiogenesis respectively.⁹ Briefly, the process of angiogenesis is schematically simple to understand; first, basement membrane tissues are injured, second, endothelial cells are activated by angiogenic factors, third, endothelial cells proliferate, and finally angiogenic factors continue to influence the angiogenic process.^{9,10} Consequently, the newly developed neovasculature is malformed and “leaky” which leads to the existence of the enhanced permeation and retention

(EPR) effect (Figure 1). This effect is mediated by the overexpression of one of the most potent angiogenic cytokines, vascular endothelial growth factor (VEGF), this enhances the permeability of neoplastic tissues.¹¹ This remarkable feat of biology can, however, be the downfall of cancer cells due to their selectivity towards large molecular structures which allows for increased selective uptake of the molecule.^{12,13} However, despite this there are two other factors in play: surface charge and hydrophobicity.¹³ Hydrophobic molecules will have increased affinity for cell membranes, however membranes made of phospholipids are charged, so some charged character may be required of the drug molecule. Macrocyclic molecules and nanoparticles can accumulate in the stroma through the enhanced permeability and retention EPR effect.^{12,13}

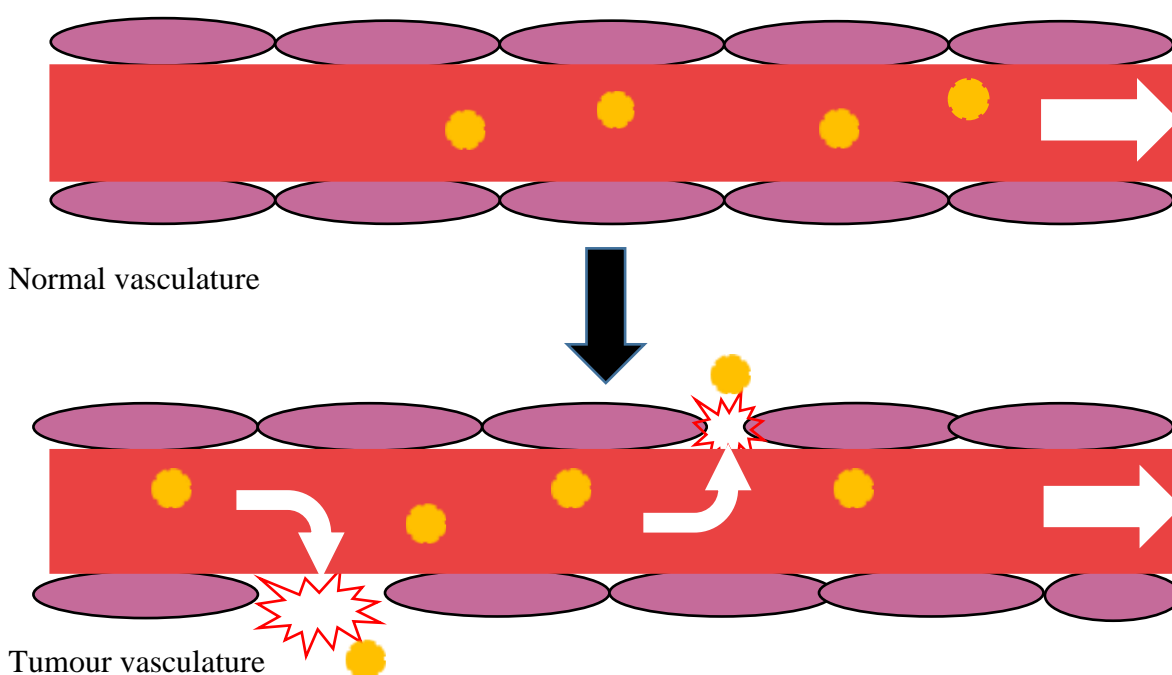


Figure 1. Schematic showing normal blood flow and blood flow of tumour vasculature; gaps can be opened hydrodynamically by AT-II induced hypotension leading to enhanced tumour selective delivery.¹³

1.1.2 Warburg Effect

Briefly, it is well understood that cells devour carbohydrates in a respiration process in order to produce adenosine triphosphate (ATP). Cancer's "sweet tooth" has been well documented, the cause of this is the change in the metabolism of the tumour cells and is well described by the Warburg hypothesis.^{14,15} Popular opinion is that cancer cells can ferment and metabolise glucose (glycolysis), even when in an oxygen deficient environment (anaerobically), at a surprisingly enhanced rate.¹⁵ The three main oncogenes required for the Warburg effect to be expressed are the RAS, SRC and MYC genes which enhance glycolytic enzymes and glucose transporters.^{16,17} This effect has been exploited through the conjugation of imaging agents, radioisotopes or therapeutic agents to sugars to enhance the selectivity of cancer treatment and imaging.^{18,19}

1.1.3 Tumour Hypoxia

The effectiveness of some cancer therapy techniques can be diminished by an abnormal lack of oxygen in a tumour (hypoxia) (Figure 2). Normally, hypoxia leads to increased production of hypoxia-inducible transcription factor (HIF-1).²⁰ HIF-1 is a heterodimer of HIF-1 α and HIF-1 β subunits. It is a key transcription factor responsible for adaptive cellular changes.²¹ HIF-1 up-regulates the expression of genes that control a range of physiological parameters.²² The expression of HIF-1 can be used to determine whether a cell is hypoxic, which determines its sensitivity towards ionizing radiation.²² The detection of HIF-1 can be routinely carried out by electrophoretic blotting techniques. Other markers include carbonic anhydrase IX (CAIX), the glucose transporters GLUT-1 and GLUT-3, and osteopontin (OPN). Various approaches have been investigated for eliminating the hypoxic population, these include: increasing oxygen availability, directly sensitizing or killing the hypoxic cells, indirectly affecting them by targeting the tumour vascular supply and targeted knockout of the mitochondria.²³ Hypoxia can lead to the proliferation of the neoplastic tissue by a tumour adopting a more aggressive phenotype.²⁴ Additionally, the cancer cells exhibit changes in gene expression that suppress apoptosis, making them markedly harder to eliminate.²⁵ Due to these factors, tumour hypoxia is a significant obstacle in cancer therapy as it severely reduces the effectiveness of treatments such as radiotherapy and PDT which are mediated by the presence of oxygen.^{26,27}

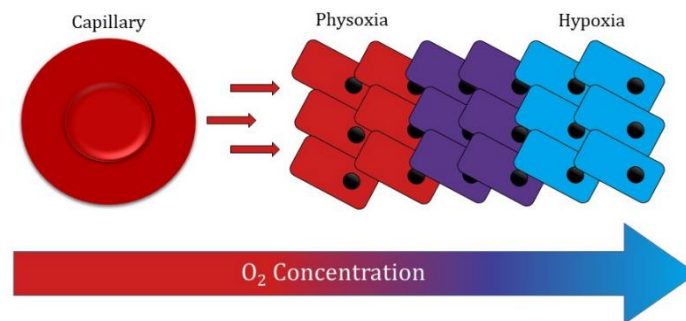


Figure 2. Representation of hypoxia induction with increasing distance from the capillary network.

1.1.4 Tumour Suppressor Protein p53

The Cancer Genome Atlas Research Network demonstrates that high-grade serous cancer is characterized by TP53 mutations in up to 96% of the cases.²⁸ p53 is the tumour suppressor phosphoprotein, which consists of 393 amino acid residues, the protein is encoded by the *TP53* gene expressed on the 17th chromosome in humans.²⁹ This homolog gene is also expressed in other mammals such as mice (*Trp53*).²⁹ The presence of these proteins can be detected by electrophoretic techniques.³⁰ The protein has been widely dubbed the “guardian of the genome” due to its impressive ability to prevent genome mutations.³¹ p53 functions as a transcription factor by binding to specific DNA sequences and by transactivating or repressing a large group of target

genes.³² Mutant p53 acts as a dominant-negative inhibitor toward wild-type (WT) p53. With regards to cancers, 50% of human tumours carry p53 mutations where the protein is either present but defunct or the protein isn't correctly transcribed by RNA at all. Mutations in the p53 protein allow for the initiation and progression of tumours. The downstream effects that p53 regulates include: the pathways of cell cycle arrest, apoptosis, hypoxia, and DNA repair.³² The restoration of (WT) p53 activity has long been sought after as a goal for successful tumour therapy.³² Clinically, the function of p53 has been associated with the prognosis, progression, and therapeutic response of tumours (Figure 3).³²

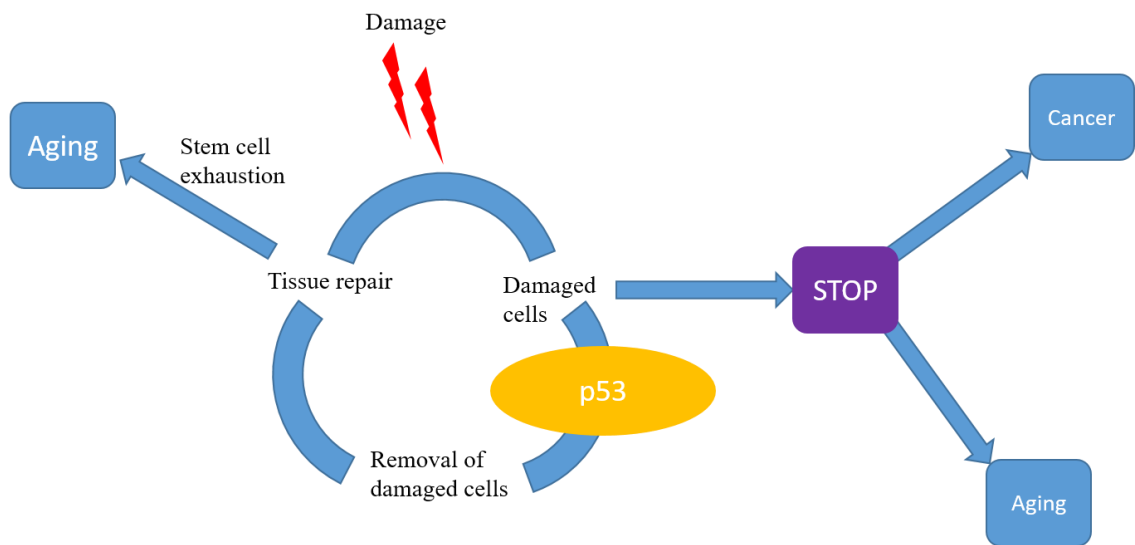


Figure 3. p53 pathway in cancer and aging.

Tumour cells containing mutant p53 have been found to be less responsive to radiotherapy and chemotherapy due to exhibiting a radio- and chemo-resistant phenotype.^{32,33} In response to endogenous or exogenous cellular stresses p53 is induced to accumulate in the cell nucleus to exert its pro-apoptotic function, the activated protein promotes cell cycle arrest to allow for DNA repair or apoptosis to prevent the propagation of cells with a damaged genome (Figure 4).^{33,34} The tetrameric transcription factor is activated upon cellular stress, depending on the stress, the activation results in upregulation or repression of multiple genes.³⁴ In unstressed cells, p53 protein levels are tightly regulated *via* a negative-feedback loop, whereby p53 induces the transcription of its own negative regulator, MDM2.³⁴ In conjunction with its homolog MDMX, MDM2 ubiquitinates p53, resulting in nuclear export and proteasomal degradation of p53.³⁴ The literature is replete with publications highlighting efforts to target these overexpressed or repressed genes in order to understand cancers further and better treat them.^{35,36,37,38} It is clear, that any new or emerging cancer therapy must be able to destroy tumours with or without p53.

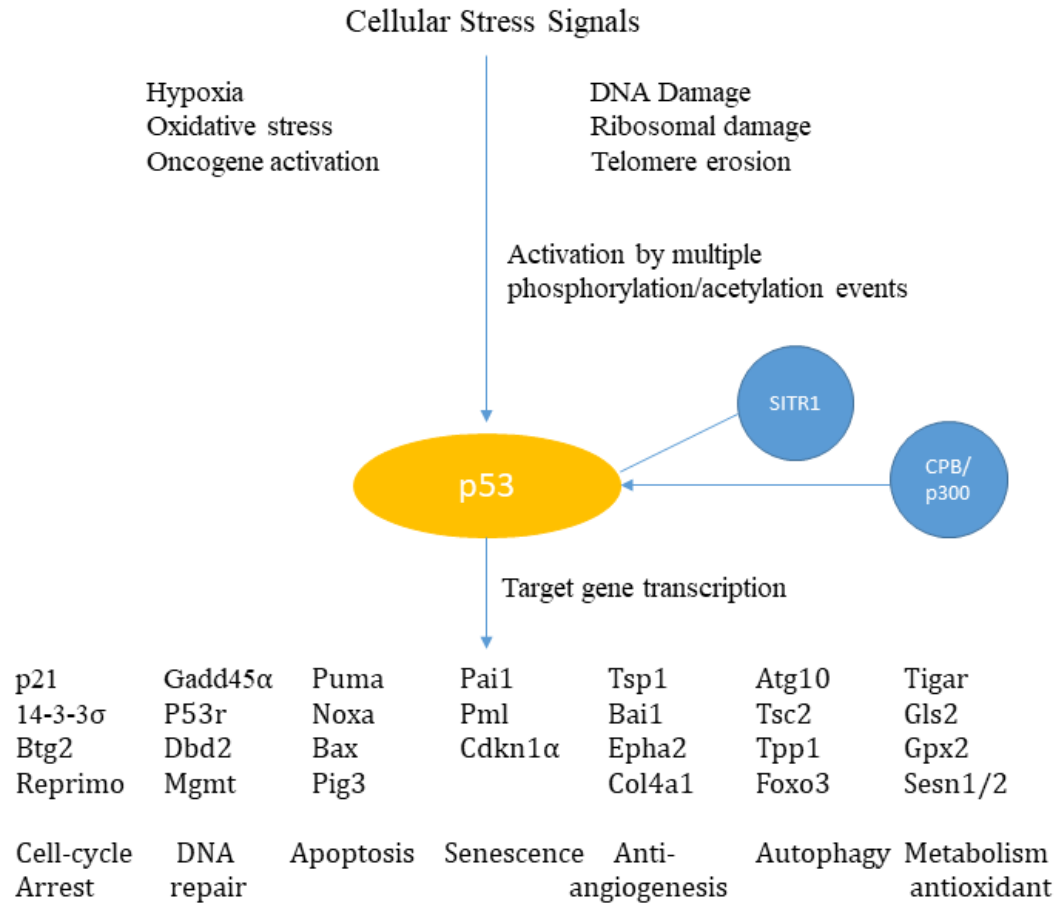


Figure 4. p53 pathway leading to the expression of genes.

1.1.5 Cell Cycle

The mechanism by which cells proliferate is well understood, but it has implications on the effectiveness of cancer therapy. Briefly, cells enter the cell cycle from a quiescent phase where they are not metabolically active, they then enter the G1 phase in which cellular contents excluding chromosomes are duplicated.³⁹ Following this, they enter the S phase in which each of the 46 chromosomes is duplicated by the cell.³⁹ The cell progresses into the G2 phase where mechanisms take place to check the chromosomes for damage, once successfully carried out the cell enters the M phase where cell mitosis occurs and the cell proliferates.³⁹ The cells can continue in this cycle again, or enter the quiescent phase.³⁹ The cell cycle and the proportion of cells in each phase of the cycle has a subtle effect on the therapeutic outcome of an adjuvant, neoadjuvant or palliative cancer treatment. For example, mitotic cells are hyper sensitive to ionizing radiation, thus ideally, a treatment regime will take this into account and target the cells when they will be most affected by the treatment.⁴⁰

1.2 Approaches to Cancer Therapy

1.2.1 Radiotherapy

1.2.1.1 X-ray Production

The two main methods of administering radiotherapy include external beam therapy and brachytherapy. For the purpose of this thesis, only external beam therapy will be discussed as it is the most abundantly used form of radiotherapy.⁴¹ External beam therapy requires a linear accelerator or ‘LINAC’ to generate either X-ray or gamma photons. Ion beams can also be used to high effect. The main difference between photon beams such as gamma and X-ray and charged particles such as electrons, protons, and heavy ions is the depth profile of the incident radiation.⁴² The patient is then bombarded with ionizing radiation to destroy a tumour.⁴³ In comparison, brachytherapy uses a small localised source in the body, which typically is an alpha particle emitter. The key difference between the two is that external beam therapy uses highly penetrating (Table 1), but weakly ionizing, gamma or X-rays, while brachytherapy uses highly ionizing alpha particles to deliver a high dose within close proximity, but with poor penetration depth.

Ionizing Radiation	Ionizing Power	Penetration Depth
Gamma	Weakest	Largest
X-rays	↓ Strongest	↑ Smallest
β - beta		
α - alpha		

Table 1. Comparison of ionizing power and penetration depth of ionizing radiation and electromagnetic radiation.

Gamma rays can be generated from the decay of unstable nuclei *via* several nuclear decay processes (Table 2). The most common process being the interaction of an antiparticle with its corresponding natural particle.

Radioactive Transformation	Schematic Nuclear Process
Alpha decay	${}^Z_A X \longrightarrow {}^{Z-4}_{A-4} Y + {}^4_2 He$
Beta negative decay	${}^Z_A X \longrightarrow {}^{Z}_{A+1} Y + \beta^- + \bar{\nu}_e$
Beta positive decay	${}^Z_A X \longrightarrow {}^{Z}_{A-1} Y + \beta^+ + \nu_e$
Electron capture	${}^Z_A X + e^- \longrightarrow {}^{Z}_{A-1} Y + \nu_e$
Nuclear isomerism	${}^Z_A X^* \longrightarrow {}^Z_A X + \gamma$

Table 2. Common radioactive transformations and the processes that occur, with charge, nucleon, and lepton numbers been conserved.

In general terms, gamma rays are less ionizing than electrons and positrons, and they are in turn less ionizing than alpha particles. It is the ionizing power of radioactive emissions that are used in cancer therapy to destroy neoplastic tissue. In terms of the medical application of radiative transformations for tumour therapy, the radioactivity and radioactive decay is random. But radioactive elements are used with known decay pathways that typically emit gamma and beta ionizing radiation which are directed in controlled bursts at the patient's tumour site in a controlled environment.

The energy deposited on the tumour site is measured in Gray (Gy), which can be defined as the absorption of one joule of radiation energy per kilogram of matter. For particles, the energy deposited can be understood by firstly understanding the first principles of electromagnetic (EM) radiation in a vacuum. The principle of relativity states that the mass of an object is not constant; such that it varies with its velocity (Equation 1).²

$$m = \frac{m_o}{\sqrt{1-\frac{v^2}{c^2}}} \quad (1)$$

Where: m: mass (kg); m_o: rest mass (kg); v: velocity (ms⁻¹); c: the speed of light *in vacuo* (ms⁻¹).

The energy of the object with mass, m, is given by the Einstein energy-mass equivalence equation.² When a particle is moving its total energy corresponds to the rest mass of the object and the translational kinetic energy (Equation 2).² When a particle's velocity becomes small the energy mass equivalence equation is such that the energy is similar to that obtained by the classical value given by equation 3.²

$$E_k = \frac{1}{2}mv^2 \quad (2)$$

Where: E_k: kinetic energy (J); m: mass (kg); v: velocity (ms⁻¹).

Theory predicts that the energy range of electrons used for medical radiology and their very small rest mass can allow for large kinetic energies obtained at high velocities,² thus delivering large amounts of energy capable of ionizing atoms in biological tissues.

X-ray photon beams are produced as electron Bremsstrahlung radiation in clinical linear accelerators.⁴⁴ LINACs use an electron gun to generate electrons from a heated wire which are then accelerated in the presence of an electric field towards a uniform metal plate.⁴⁵ Upon interaction with the metal plate, the Coulomb fields of the bombarded nuclei decelerate the charged electron particle, which causes a loss of kinetic energy of which a small fraction is converted to X-rays. This type of radiation is called Bremsstrahlung radiation, or 'braking radiation'. In terms of the mechanical operation of the LINAC, the metal target is usually a copper sheet which serves to generate X-rays, and acts as an efficient heatsink. The relative intensity of the radiation can be increased by increasing the kinetic energy of the electrons, typically in the

region of keV of potential. Generally, this type of radiation can be split into two categories, orthovoltage radiation which has a range of 100-500 kV, while megavoltage radiation is generated from LINACs above 1000 kV. X-rays used in radiotherapy are considered to be low linear energy transfer (LET) radiation, whereas particle beam based radiotherapy is high LET.^{46,47} Electromagnetic radiation (EM) consists of a propagating transverse wave of an electric field vector perpendicular to a propagating transverse wave of a magnetic field vector.² The key parameters of an electromagnetic wave are the wavelength, λ , and the frequency, ν . When a photon propagates through a vacuum its speed is equal to the speed of light, c , which is expressed by equation 3. Electromagnetic radiation is only ionizing when at sufficiently high enough energies to cause the loss of an electron from a species. Each photon carries energy which is a function of Planck's constant and the frequency which is expressed by equation 4.

$$c = f\lambda \quad (3)$$

$$E = h\nu \quad (4)$$

Where: c : the speed of light *in vacuo* (ms^{-1}); f : frequency (Hz); λ : wavelength (m); E : energy (J); h : Planck's constant (Js^{-1}); ν : velocity (ms^{-1}).

1.2.1.2 Physical Interactions of X-rays

X-rays can interact with matter through a variety of processes. The interaction that takes place is typically either absorption (transfer of energy from the X-ray photon to the absorbing material) or scattering (in which the X-ray photon is “redirected” by interaction with the scattering material). Theoretically, there are twelve processes that can occur during these interactions; the main three types of interactions that occur are the: photoelectric effect, Compton scattering and pair-production. The dominating process is a factor of the atomic weight of the nuclei and the energy of the X-rays. Two main energy transfer mechanisms that can occur when X-rays interact with matter. The first being ionization where the incoming radiation causes the removal of an electron from an atom or molecule producing a positively charged species and a dissociated electron. The second mechanism is excitations wherein some of the X-rays energy is transferred to the target leaving it in a higher energetic state.

Photoelectric Effect:

At its core, the photoelectric effect is simple to understand. X-rays interact with core-shell electrons in atoms, the transfer of energy to the electron causes the electron to be promoted to a higher energy level (Figure 5). This energy is emitted as a photon when the electron relaxes back to its original shell. The presence of a core hole means that the atom is in a highly excited state and a process of X-ray fluorescence occurs. The excited state decays by the core hole filling with

an electron from a valence orbital followed by the quantised emission of a photon of energy equal to the energy gap of the electron transition.

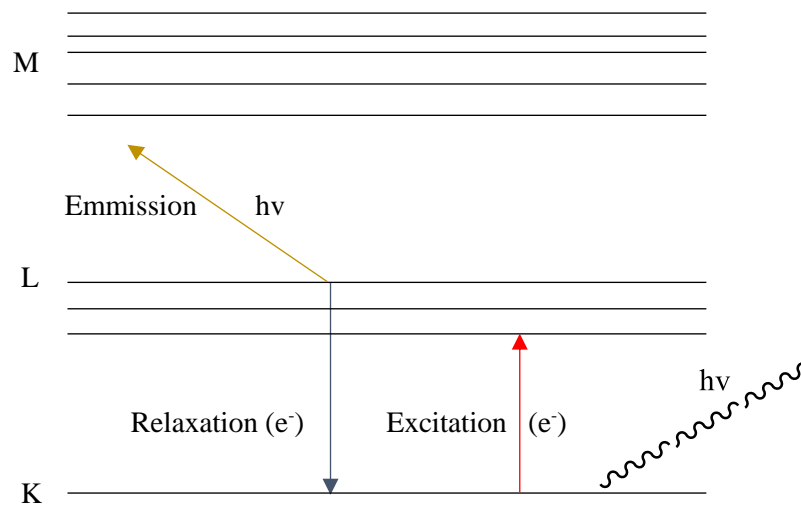


Figure 5. Schematic of the process of X-ray fluorescence occurring in an atom.

If sufficient energy is deposited on a core-shell electron the photoelectric effect dominates and not X-ray fluorescence. A core-shell electron is given sufficient energy to be promoted to the highest energy levels where it dissociates from the atom causing photoionization resulting in a core-hole. For this process to occur the energy deposited on the atom or molecule needs to be greater than the work-function (ϕ) of the material. Excess energy is converted into the kinetic energy of the escaping electron. This relationship can be described by a mathematic relationship (Equation 5).

$$E_{k \max} = h\nu - \phi \quad (5)$$

Where: $E_{k \max}$: maximum kinetic energy (J); h : Planck's constant (Js^{-1}); ν : frequency (Hz); ϕ : work-function (J).

If the newly liberated electron interacts with an outer-shell electron in an atom or molecule, and the energy transfer is sufficient to cause ionization of that species, then an Auger electron is produced (Figure 6). The statistical probability of this occurring is directly proportional to the kinetic energy of the photoelectron.

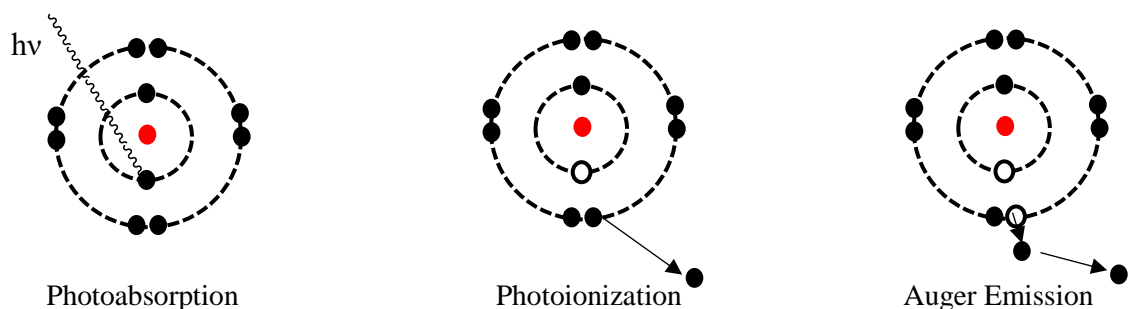


Figure 6. Schematic of the processes of photoabsorption, photoionization and Auger electron emission.

The X-ray spectrum for a copper target gives a characteristic spectrum containing $K\alpha_1$, $K\alpha_2$, and $K\beta$ peaks. The origin of the $K\alpha_2$ (1.54439 Å) is the relaxation of the free unpaired electron in the 2p-orbitals of the copper atom, while the $K\alpha_1$ (1.54056 Å) is a feature of overcoming the spin-orbit coupling energy from a pair of electrons in the d-orbital. The $K\beta$ (1.39222 Å) peak is characteristic of transitions from the 3d-orbital to the 1s-orbital.

Compton Scattering:

Compton scattering is an incoherent scattering effect when X-ray photons cause photoionization of an atom or molecule and an X-ray photon of lower energy is scattered from the atom. In the Compton scattering process, relativistic energy and momentum are conserved. Compton scattering is dominated by low atomic weight species. Briefly, the incident X-ray photon is scattered by electrons in atoms or molecules. During scattering processes, the direction of the X-ray photon changes, and the energy lost is imparted to an electron in the atom or molecule (Equation 6).

$$E = \frac{E_x}{1+4E_x} \quad (6)$$

Where: E: maximum energy of Compton electron (J); E_x : energy of the incident photon (J).

Pair-Production:

Pair production occurs at high X-ray energy levels (>1 MeV). During this process, a particle and an antiparticle are created by the annihilation of the X-ray photon. This rare quantum mechanical phenomenon occurs followed by the positron annihilation which evolves two co-incident photons of lower energy than the original X-ray photon. The pair production processes occur when high energy X-rays pass through materials with high atomic masses.

In general, the three processes discussed above dominate the interactions of X-rays with matter during radiotherapy. Rayleigh scattering (coherent) and photodisintegration effects can be observed but have minimal effect. With these effects in mind, it is clear to see that X-rays can significantly damage atoms and molecules through these interaction processes.

1.2.1.3 Radiotherapy Administration Techniques

Clinically, external body radiotherapy can be administered *via* several main techniques (Table 3). Radiotherapy can be administered for both curative and palliative treatments. It can also be administered to shrink tumours before resection (neoadjuvant) and after resection (adjuvant).

Administration Technique	Overview of Technique	Ref
Image Guided Radiotherapy (IGRT)	Uses images to guide the delivery of the ionising radiation dose.	48
Intensity Modulated Radiotherapy (IMRT)	Modulates the intensity of the ionising radiation and shapes the beam to fit a tumour using a multileaf collimator.	48, 49
Volumetric Modulated Arc Therapy (VMAT)	Highly conformal dose distribution with improved target volume coverage.	50
Stereotactic Ablative Radiotherapy (SABR)	Fewer doses in the fractionation schedule are used to deliver a large amount of Gy over a short period.	51

Table 3. The four main delivery techniques of radiotherapy.

Each of the techniques has their own advantages and disadvantages. Clinicians carefully plan which technique is likely to damage the most neoplastic tissue while sparing as much healthy tissue as possible. In general, radiotherapy administered to patients for both curative and palliative treatment has reached a golden age. The ionising radiation beams spare almost all of the healthy tissues, and patients suffer from limited side effects. Little has been done over the past decade in terms of linear accelerator technology in order to improve radiotherapy, apart from coupling to molecular imaging techniques.

While doses of ionizing radiation administered to patients can be in the range of 10-40 Gy, the whole dose is not administered as a single treatment. Typically, ionizing radiation is fractionated, this method allows the patient to receive small therapeutic doses that maximise damage to the tumour, while minimising damage to healthy tissues. In human astrocytoma, fractionated doses were found to increase the induction of apoptosis by capsase-3 activation compared to single dose treatments.⁵² However, cell cultures do have different intrinsic radiosensitivities depending on cell type, and respond differently to ionizing radiation depending on genes or receptors which are overexpressed or underexpressed.⁵² Transcriptome profiling studies report that different genes are involved in responses to low doses (10 cGy) of radiation when compared to higher doses (2 Gy), a finding which has been confirmed *in vivo* murine models.^{5,53}

1.2.1.4 Interaction of Biological Matter with X-rays

As discussed, the key desired outcome of radiotherapy is the eradication of the tumour tissue. This section discusses the interaction of ionizing radiation with biological matter and the resulting biological responses. There are two main modes of action for the damage of cells by ionising radiation. The first is the direct mechanism caused by the interaction of ionising radiation with cellular DNA.⁵⁴ The second mechanism is the indirect mechanism, which is due to radiolysis of water and other biological molecules generating radicals which indirectly damage the cell.⁵⁴

Direct Mechanism:

Exposure of biological tissues to ionizing radiation immediately leads to excitation and ionization of their constituent atoms. DNA is the most vulnerable constituent of a cell when acted upon by ionizing radiation.² When DNA is ionized, the atoms become more energetic and the physical processes that occur cause bonds to break. Briefly, the three main effects occurring are double-strand breaks,^{55,56} single strand breaks and DNA adducts.^{57,58,59} The prevailing mechanisms of action are double and single-strand breaks (Figure 7).⁶⁰

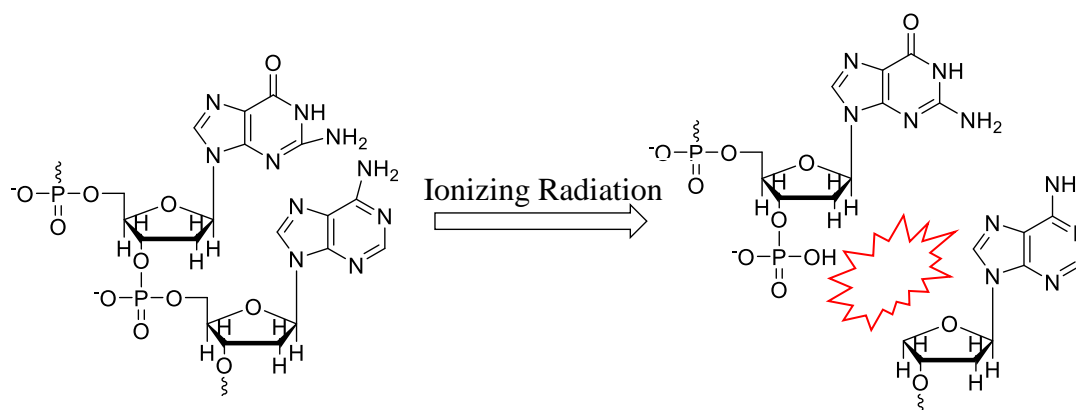


Figure 7. Schematic diagram of the breaking of DNA strands by the action of ionizing radiation.

Indirect Mechanism:

Constitutionally, water makes up a significant proportion of the matter inside biological cells, so the largest fraction of free radicals created are hydroxyl radicals.⁶¹ Hydroxyl radicals react with neighbouring molecules and damage proteins, enzymes and membranes.² Most crucially hydroxyl radicals damage the DNA.⁶² However, the complexity and resilience of the human body is such that a dose of 1 Gy in every cell nucleus yields typically 2×10^5 ionisations,⁵⁷ leading to around 1000 single strand breaks and up to 40 hybridizations of DNA, but cell repair mechanisms can instruct enzymes to repair the DNA.² The eradication of every viable tumour cell will lead to tumour cure, however in reality if a single cancer cell is left then the tumour may return and this is often the cause of the local recurrence of tumours after radiotherapy. One gram of a tumour can contain 10^9 cells, human tumours typically have a mass of 10–100 g, meaning they can contain up to 10^9 clonogenic cells.² Radiotherapy techniques focus the radiation and reduce the number of normal tissues that are in the high-dose volume.² If each radiation dose is assumed to result in a surviving fraction of 0.5 then the relationship will develop an exponential population decay for the number of clonogenic cells decreasing over time, assuming a constant effect per dose fraction.

Incomplete treatment of a tumour leads to a temporary phase of tumour regression which is followed by tumour recurrence.² Regression is due to the death and eradication of cells killed by radiation, cells of limited lifespan which would have been produced by the killed stem cells.² Naturally, tumours can react differently where some will shrink during the course of radiation

therapy while others will regress very slowly.² Regrowth is due to a population of surviving clonogenic cells, and the speed of regrowth depends on the individual tumour.²

Through the indirect mechanism, the efficacy of radiotherapy is a function of the concentration of oxygen in the tumour site. Oxygen is a dose-modifying factor; the effective dose required to give a biological response is reduced in regions of high oxygen concentration.^{63,64} Oxygen can react with radicals becoming a cytotoxic reactive oxygen species (ROS) during radiotherapy, thus a decrease in oxygen concentration hinders damage to the cell.⁶⁵ The growth and survival of cells in solid tumours is dependent on the oxygen supply,^{66,67} as well as the nutrients available.^{24,68} In order to meet their needs the neoplastic cells develop their own neovasculature which is morphologically and functionally abnormal, leading to tissue hypoxia.^{69,70,71} Tumour hypoxia typically occurs at a distance of 100-200 μm from the blood vessels that are not capable of delivering sufficient supplies to the local cells.²⁵

Under the action of ionizing radiation, molecular oxygen reacts rapidly with free radicals.⁷² The cascade of reactions that occurs can irreversibly damage DNA which ultimately leads to programmed cell death if repair mechanisms cannot take place (Figure 8).⁷² The lack of oxygen greatly reduces the radiosensitivity of the neoplastic tissues, thus giving origin to the difficulty of eradicating hypoxic tumours *via* the action of ionizing radiation.²⁵ This is supported by clinical and preclinical assays that have shown that the number of double-strand breaks in anoxic conditions is decreased by 2-3 fold.⁷³ When fatally damaged by radiation most cells do not immediately die, after a given dose of ionizing radiation the cells progress to mitosis.² Damaged cells fail to undergo mitosis, and may have to undergo many cell phases to reach mitosis, lymphocytes can, however, undergo apoptosis before reaching the mitosis phase.² The two main forms of cell death after irradiation with ionizing radiation are proliferative cell death and programmed cell death, or commonly called apoptosis.²

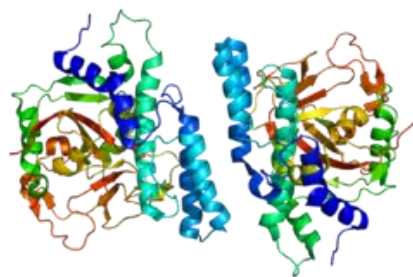


Figure 8. 3D model PARP-1 enzyme.

The damage caused by radiotherapy to normal tissues of the body varies widely, in type and severity.² Many patients testify that the morbidity associated with cancer therapy is distressing and detracts from therapeutic effects.² Tissues such as lung, intestine and bone marrow are vital to life and severe radiation damage to these areas can prove fatal.² Whereas damage to skin, limbs and genitalia may not be life-threatening but can impair quality of life.² Contrary to popular belief

the application of radiation therapy is not indiscriminate in its therapeutic effect, by focusing the radiation the amount of damage to healthy cells can be significantly reduced.²

The speed of cellular recovery has been measured in many cell and tissue types, there is evidence from DNA repair studies that recovery is a multi-exponential process with one or more time components.² The clinical implications of this are that when treatment is given with multiple fractions per day it is important to allow full recovery between doses.²

Within the process of radiotherapy, one has to consider the four Rs of radiotherapy as stated by Schaffer *et al.* repair of sub-lethal injury, regeneration, redistribution within cell cycle and re-oxygenation in tumours,^{74,75,76} Mayles added a 5th R to this; radiosensitivity (Table 4).² Repair is the cell's mechanism used to repair damaged DNA and is a function of the enzymes present.² Assortment/redistribution occurs when cells survive a dose of radiation and they are in a resistant phase of their cell cycle.² Regeneration occurs over a four to six week period of radiotherapy; tumour cells that survive irradiation can proliferate, increasing the number of cells that need to be irradiated to destroy a tumour.² Radiosensitivity is considered after a given dose of radiation, the haemopoietic system shows a greater response than the kidney, allowing for different timings of responses, some tumours are more radioresponsive than others to a particular fractionation schedule.^{2,55} Reoxygenation is one of the most important factors of radiotherapy. Hypoxic tumour cells are markedly more resistant and will selectively survive after a dose fraction, but if the oxygen concentration increases in the environment so does the radiosensitivity.²

Considerations	Impact
Repair	Cancer cell repairs after sub-lethal damage.
Regeneration	Cancer cell repairs after sub-lethal damage.
Redistribution	Over a period of time, the cancer cells can move within a tumour or redistribute in the body.
Re-oxygenation	Effect of radiotherapy is a function of the concentration of oxygen.
Radiosensitivity	Different regions of anatomy will respond differently to the given dose, additionally, radiosensitivity of cells depends on the cell phase.

Table 4. Table of the five Rs of radiotherapy and the impact they have after a given dose.

The Steel paradigm defines the interaction of radiation and chemotherapy^{77,78} which is well documented. The Steel paradigm states that the spatial configuration defines the concept that different therapeutic approaches affect distinct anatomical sites of disease.⁷⁸ Furthermore, it states that the translation of experimental data to the clinic is not easily done due to the diverse and complex pharmacokinetics and diverse genetic alterations in tumours affecting biological pathways, leading to resistance.^{77,79}

1.2.1.5 Radiosensitisers

Radiosensitizers are a class of compound that sensitize biological cells and tissues to the effects of ionizing radiation with the end goal of increasing the efficacy of the treatment overall. Firstly, as with many drugs, it is important to understand the key characteristics that they should possess so that they can be translated to the clinic (Table 5).

Radiosensitizer Properties
High uptake by neoplastic tissues
Low uptake by non-neoplastic tissues
Low systemic toxicity
Rapid clearance from the blood
Long half-life within neoplastic tissues
Not cytotoxic
High sensitization ratios
Known and constant chemical formula and structure
Hydrophilic for IV administration

Table 5. Tabulated idealized properties of radiosensitizer.

Radiosensitizers and drugs, in general, can be divided into several sub-classes: small molecules,^{80,81} biologics,⁸² and nanoparticle materials.^{83,84,85} Each of these offer significant advantages and disadvantages over the others. For the purpose of this thesis, only small molecule radiosensitizers will be discussed. Small molecules are typically characterised by having a molecular mass <1 kDa. Controversially, some mechanisms of actions have been implied but there is no definitive mechanism of action of radiosensitizers and no definitive structure-activity relationships have been determined for radiosensitizers as a whole. Wilson *et al.* discussed how drugs sensitize through a diverse mechanism involving the modification of DNA damage, interference with DNA repair, cytokinetic cooperation caused by cell cycle redistribution, inhibition of proliferation and enhancement of apoptosis.^{77,86} Wilson *et al.* agreed with the current literature that the mechanism of radiosensitization with drugs is not fully understood.⁷⁷

Nitroimidazoles:

Wardman *et al.* discussed how electron-affinic chemicals are able to react with DNA free radicals as produced in the mechanisms discussed by Moyles and co-workers that have potential for universal activity to combat hypoxia-associated radio-resistance; nitroimidazoles and nimorazole are particularly good at this.⁷⁹ Several small molecule pharmacophores have been identified with the most prevalent being the aforementioned nitroimidazole moiety. The general relationship between sensitizing efficiency and electron affinity has been supported by various pulse radiolysis studies on one-electron transfer reactions between known sensitizers.^{87,88} The biological activity of these molecules has been linked to their electron affinity; either the vertical or adiabatic electron affinities. Vertical electron affinity is the energy difference between the neutral molecule and the negative anion at its initial geometry.⁸⁷ The adiabatic electron affinity is the energy

difference between the neutral molecule and anion when both are in their most stable state.⁸⁷ Another approach has been the correlation of sensitization efficiency with the Hammett constants for a range of substituted nitrobenzenes.⁸⁸ Some nitroimidazole based drugs such as misonidazole (Figure 9) were successful in their ability to control local tumours, delay regrowth and caused negligible sensitization to normal cells.^{79,89} Remarkably, their toxicity *in vitro* paralleled the radiosensitization efficacy because the electron reduction potential dominated the structure-activity relationship.⁷⁹ Furthermore, the electron reduction potential showed that there was evidence for the redox dependence of radiosensitization efficiency with electron affinity.⁷⁹ Nitroimidazoles are capable of undergoing radiation-induced redox reactions which can stabilise the DNA radicals produced in hypoxic tumours, increasing the likelihood of cell death.^{90,91} Crucially, this class of molecules causes radiosensitization by replacing the need for molecular oxygen in oxic and especially hypoxic tumours for ionizing radiation-induced DNA radicals to generate cytotoxic DNA strand breaks.^{25,67,84}

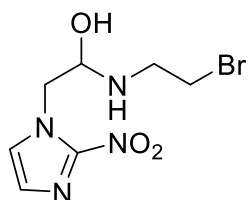


Figure 9. Structure of a substituted nitroimidazole with known radiosensitizing abilities.

As of 2018, only nimorazole is used clinically as a radiosensitizer (Figure 10). Studies have been carried out to determine whether 2-nitro or 5-nitro moieties confer the best sensitization enhancement ratios.⁹² Further studies have been carried out on reducing the cytotoxicity of the compound by substituting the imidazole ring with functional alkyl groups.⁹³ A clinical study in cancer patients with head and neck squamous cell carcinoma in Denmark between 1990 and 2013 found that only 58% of patients could receive the full dose of the compound during their radiotherapy treatment.⁹⁴ Female patients were more likely to be adversely affected by the latent toxicity of the compound. Patients over the age of 70 were highly likely to suffer from nausea and vomiting.⁹⁴ These data highlight that while these compounds do confer significant benefits the dose required for the pharmacological benefit was found to reduce the quality of life of the patients and cause side effects.⁹⁴ Recently, sulfonamide analogues of these compounds have been synthesised and good sensitisation enhancement ratios have been observed in HCT-116 human colorectal carcinoma cells under both hypoxic and oxic conditions albeit with clinically undesirable radiation doses of 15 Gy.⁹²

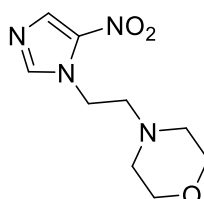


Figure 10. Nimorazole, a known radiosensitiser used clinically.

Nucleosides:

Several analogues of heterocyclic nucleoside bases (purines and pyrimidines) have been investigated as radiosensitizers (Figure 11). Chief among these is the fluorinated cytosine heterocyclic base, gemcitabine (Gemzar™), which is a chemotherapy agent in its own right.⁹⁵ The mechanism of action of this compound is still disputed with sources citing that it may affect cycle distribution, induction of apoptosis, the role of p53, modulation of metabolic deoxynucleosides, and interference with homologous repair pathways.⁹⁵ A schedule-dependency study was carried out with human bladder cells (ECV304) and human lung cancer cells (H292) to determine its role in the perturbation of the cell cycle.⁹⁵ Excellent sensitization enhancement ratios were observed with a dependency on incubation times and dosing schedules with an S-phase arrest. 5-Selenocyanatouracil has been investigated and found to generate a selenium centred radical, stabilising the hydrated electrons formed during radiolysis⁸⁴. The differences in radiosensitivity might reflect variations in the levels of activity of proteins involved in the repair of damage to DNA.⁷⁹

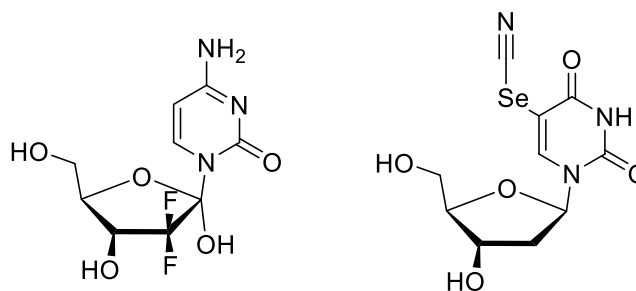


Figure 11. Gemcitabine (left), and gefitinib (right).

Bio-reductive drugs:

It has been noted that the electron-affinic nature of nitroimidazoles can be reduced by cellular enzymes; donating an electron to form a radical anion (Figure 12).^{59,79} These species can cause substantial damage to surrounding DNA as discussed previously. Wardman *et al.* elucidated that nitroimidazoles and similar molecules can act as bio-reductive compounds by being readily reduced selectively in hypoxic environments by the ‘trigger effect’.⁷⁹ Interestingly, the use of nitro moieties on bio-reductive molecules has been shown to produce radical nitro species by Wilson *et al.*²⁵ Crucially, molecules bearing nitro groups can undergo one-electron reductions to become radicals and radical anions that are cytotoxic or undergo further reactions to damage DNA or stabilise DNA radicals.^{25,96} One study identified through mass spectrometry that NO radical species can be released from nitroimidazoles with relative ease.⁹⁷

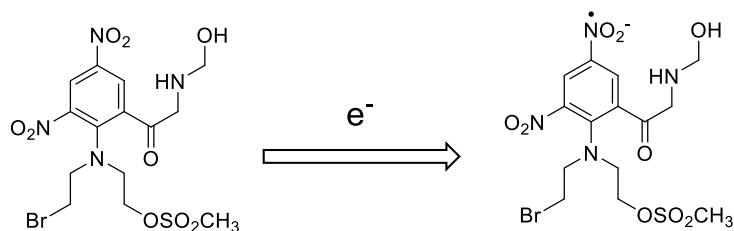


Figure 12. Reaction scheme showing the one electron reduction of a nitro substituent on an aromatic ring; nitro group to nitro radical anion.²⁵

Porphyrins and related macrocycles:

Porphyrins are an interesting class of molecule for use in medicine; they are nitrogen-containing tetrapyrrolic macrocycles that obey Hückel's rules for aromaticity with absorption wavelengths of *ca.* 400 nm for the high extinction coefficient Soret band, and weaker Q bands in the region of 500–700 nm.^{98,99,100} They represent an interesting potential class of radiosensitizers due to several factors: they are non-toxic in the 'dark', have high chemical stability, have affinity for serum proteins, have favourable pharmacokinetic and pharmacodynamic properties, they can be passively retained in tumours by utilizing the EPR effect, they are fluorescent and absorb strongly in the UV-Vis region, they can chelate metals and can be subjected to a diverse range of chemistries to functionalised them.¹⁰¹ Again, no structure-activity-relationships have been definitively proven, but there are some working theories. Tagliatesta *et al.* stated that for the introduction of electron withdrawing groups to the *meso* phenyl rings, the redox relationship increases linearly with the number of bromides.¹⁰² This was not the case for bromination in the beta position of pyrroles due to the distortion of the porphyrin macrocycle which in turn altered redox potentials, and this was confirmed by X-ray crystallography.¹⁰² Furthermore, they elucidated that HOMO-LUMO calculations corroborate this by shifting the energy of the HOMO relative to the LUMO.^{102,103} In addition, the distortion effect on metalloporphyrins greatly changes the electronic properties by altering the HOMO-LUMO gap and by changing the distance of bonding atomic orbitals and overlap into molecular orbitals as well as relative orientation.¹⁰⁴ Shelnutt *et al.* showed through molecular orbital calculations and crystallographic studies that octaethylporphyrins when metallated would undergo a distortion of planarity,¹⁰⁴ which increased with an increase in cation radii.¹⁰⁵ Other factors which affect the redox properties of porphyrins include axial ligands and planarity of the macrocycle.¹⁰⁶ Other electron withdrawing groups have been studied computationally on Ni(II) porphyrins. The study found that the electron affinity increases by replacing inductive donor groups (alkyl), with inductive electron acceptors (CF₃) and resonance enabled acceptors (NO₂). They also elucidated that these substituents have a greater effect on distorting the planarity of the macrocycle in the *meso* positions of the macrocycle, as opposed to the β positions (Figure 13).¹⁰⁷

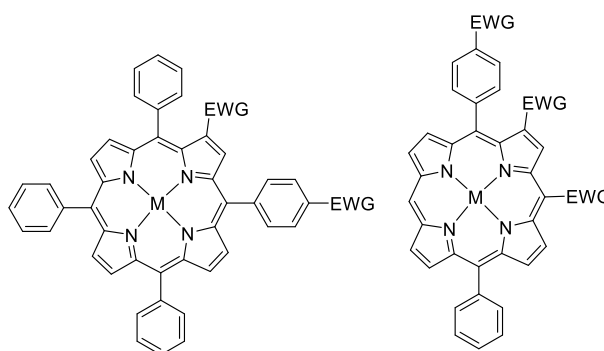


Figure 13. Tetraarylporphyrins and diarylporphyrins displaying positions for modification with electron withdrawing groups.

Texaphyrins are expanded porphyrins, large and planar, capable of complexing with large cations including paramagnetic gadolinium (Figure 14).⁵⁹ Gadolinium texaphyrin (Gd-Tex) is a complex which is stable and easily reduced with a reduction potential of 0.08 V relative to the standard hydrogen electrode.⁵⁹ They can readily form long-lived π -radical anions upon exposure to hydrated electrons.⁵⁹ Gd-Tex, which is a gadolinium(III) based texaphyrin, has shown great potential as a clinical radiosensitizer due to its efficacy *in vitro* and *in vivo*.^{75,108} Furthermore, research has been undertaken to yield water soluble and *meso* substituted metalloporphyrins similar to Gd-Tex for use as a radiosensitizer.⁷⁵ Some of these have been reported to be selectively retained and taken up by tumour tissues, demonstrating their utilisation of the EPR effect.⁷⁵ Gd-Tex is the benchmark for macrocyclic radiosensitizers and is currently the only drug of its class available on the medical markets. However, it's clear to see that the Gd-Tex doesn't have any nitro groups, but does have a paramagnetic metal, sources also cite the mechanism of radiosensitizers to involve either reduction potential, paramagnetism, or solvation of electrons, or a combination of these characteristics. Furthermore, copper(II) chelates of modified nitroimidazoles had enhanced radiosensitizing properties, again, showing that paramagnetic metals can increase the efficacy of a radiosensitizer. It has been reported that Cu(II) porphyrins can be reduced to their π -radical anions indicating that metal chelation could affect redox potentials.¹⁰⁹

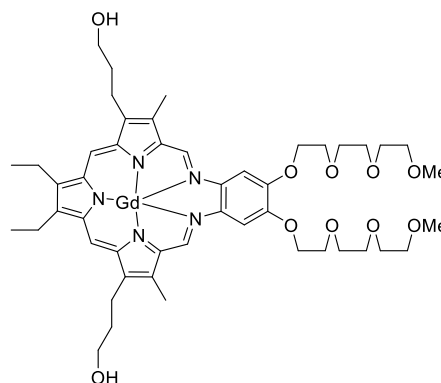


Figure 14. The skeletal structure of Gd-Tex, a known radiosensitizer.

Finally, another predominant mechanism explaining the action of radiosensitizers is the value of the reduction potential, and the ability of the molecule to abstract an electron becoming reduced to a cytotoxic π -radical.¹¹⁰

The UK National Health Service (NHS) does not currently employ any chemical radiosensitizing agents to enhance the therapeutic effects of radiation therapy, but a metalloporphyrin is currently being investigated in stage II human clinical trials (MorEx Development Partners; MLT-005).

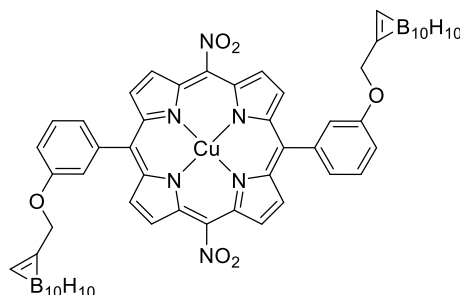


Figure 15. Chemical structure of MTL-005 a radiosensitizer in human clinical trials in the NHS, UK.

MLT-005 (Figure 15) has poor water solubility, no active targeting ability, only passive targeting from the EPR effect. Diphenylporphyrins have been found to be useful for other medical applications such as being potent photosensitizers in photodynamic therapy (PDT).¹¹¹ However, this molecule can be improved upon by incorporating features into the structure which would inevitably increase the effectiveness of the radiosensitizer by increasing its ability to partition through the phospholipid bilayer of cells. Again, the mechanism of action of this compound isn't known, but some sources cite that it could be mediated through the production of Auger electrons through the photoelectric effect *via* the interaction of X-rays with high Z number elements.⁴⁰

1.2.2 Chemotherapy

Chemical therapy or “chemotherapy” as it's more commonly known, in terms of cancer therapy is far simpler to understand than radiotherapy, in essence, it is the introduction of a cytotoxic compound to the body to destroy the cancer cells. Chemotherapy began to make traction in the 1940s as a cancer therapy technique. Again, chemotherapy agents can be divided into small molecule agents, biologics, and nanoparticles. In fact, biologics are the fastest growing medicine and the top 10 selling medicines in the world are biologics, however, biologics are not being considered in this thesis. Small molecule agents can be divided neatly into organic and inorganic-based (metal-based) agents. Biologics such as antibody-drug conjugates (ADCs) are highly targeted agents with exquisite selectivity and specificity towards antigen receptors, and patients typically receive fewer off-target side effects. However, with regards to small molecules, the vast majority of these pharmaceutical compounds do not lend themselves to personalised medicine, this is because they are devoid of active or passive targeting of tumours, which is where the myriad of side-effects occur. Side effects include nausea, vomiting, hair loss, loss of appetite, diarrhoea

etc. Clearly, there is room for further improvement in terms of increasing selectivity and specificity towards tumour tissues and reducing off-target side effects. Ideally, chemotherapy agents will satisfy several key criteria (Table 6).

Chemotherapy Agent Properties
High uptake by neoplastic tissues
Low uptake by non-neoplastic tissues
Low systemic toxicity
Rapid clearance from the blood
Long half-life within neoplastic tissues
Excellent cytotoxicity in neoplastic tissues
Known and constant chemical formula and structure
Hydrophilic for IV administration

Table 6. Ideal properties of a chemotherapy agent.

1.2.2.1 Chemotherapy Agents

Organic agents:

Paclitaxel (Figure 16), sold under the brand name of Taxol® is a compound that was first extracted from the bark of the Pacific yew tree (*Taxus brevifolia*).¹¹² This compound is a cytoskeletal drug that is typically administered *via* intravenous infusion that targets tubulin. Cells treated with paclitaxel have defects in mitotic spindle assembly, chromosome segregation, and cell division.¹¹² The chromosomes in these cells are unable to undergo mitosis and prolonged activation of the mitotic checkpoint initiates apoptosis or causes the cell to become quiescent.¹¹² This highly potent compound achieved an LD₉₀ in the 5-50 nM range when investigated against human brain tumour cell lines by colony forming assays *in vitro*.¹¹³

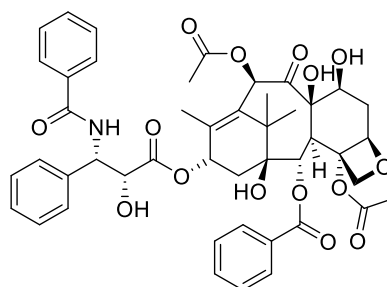


Figure 16. Paclitaxel, a taxane which is a potent anti-mitotic compound.

Doxorubicin, sold under the brand name Adriamycin® is another common chemotherapy agents (Figure 17). Again, the side effects of this compound from being administered are typical of chemotherapy: hair loss, nausea, vomiting, inflammation, etc. This compound interacts with DNA by intercalating between the major grooves of the heterocyclic bases where it inhibits the biosynthesis of topoisomerase II which is an enzyme responsible for the relaxation of supercoils in DNA transcription.¹¹⁴ Cell death occurs due to the stable topoisomerase II complex preventing the “unzipped” DNA duplex from reforming.¹¹⁴

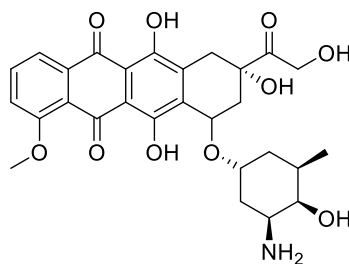


Figure 17. Doxorubicin, a fluorescent cytotoxic anti-tumoural compound.

Camptothecin, again, is a topoisomerase inhibitor compound, like doxorubicin, it requires administration in Cremophor EL (Kolliphor EL) or can be administered *via* liposomal formulation (Figure 18). This non-polar compound binds to topoisomerase I and DNA resulting in a ternary complex. This ternary complex is unable to re-ligate which initiates apoptosis. Interestingly, the lactone ring can readily hydrolyse in physiological conditions which yields a pharmacologically inactive open-ring form.

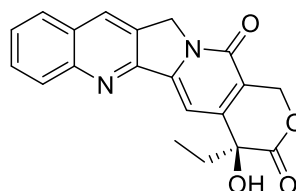


Figure 18. Camptothecin, a lipophilic topoisomerase inhibitor.

Metal-based agents:

Metals can exhibit cytotoxic properties when biological tissues are exposed to them.¹¹⁵ In 1965 Rosenberg *et al.* serendipitously discovered that traces of platinum inhibit the growth of *Escherichia coli* (*E. coli*) bacteria, which led the way to discovery of the platinum-based cis-platin complex (Figure 19).¹¹⁵ Typically, platinum-based chemotherapy agents are poorly soluble in polar-media, thus required liposomal administration, or the use of organic solvents like DMSO and DME, or Cremophor EL.¹¹⁶ Following administration of the compound, the chloride ligands are exchanged for aqua ligands through aquation.¹¹⁷ This process is favoured in the intracellular environment where the concentration of chloride ions is approximately 1-20 mM compared to the extracellular environmental fluid (90-110 mM). The aqua ligand is readily displaced and the active platinum(II) can bind to the heterocyclic bases of the DNA double helix.¹¹⁷ Three variations of this process can occur: the first being by forming a mono DNA adduct, the second is by forming a dual DNA adduct, and the last being inter-strand cross-linking.¹¹⁷ The platinum-guanine adduct is the most favourable adduct with the GpG adduct accounting for the vast majority of adducts. The three types of adducts inhibit cell mitosis thus initiating apoptosis.

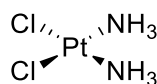


Figure 19. Cis-platin, a platinum(II) based chemotherapeutic.

The administration of platinum(II) based agents is synonymous with horrific side effects, in reality, a patient can suffer from any combination of 40 specific adverse side effects.¹¹⁶ Much research has been carried out to increase the solubility, efficacy, stability, selectivity, and specificity of these platinum(II) agents. LD_{90S} of these compounds are in the low nM to mid μM range when examined *in vitro*. However, the major drawback in the use of platinum as a chemotherapy agent is platinum resistance in tumours. The expression of the MUC1 glycoprotein and localisation of its C-terminal subunit to the mitochondria affects resistance.¹¹⁸ This glycoprotein blocks apoptosis by reducing cytochrome *c* release from the mitochondria and reduced caspase-3 activation.¹¹⁸ Over half of the women with ovarian cancers were found to be intrinsically resistant to platinum chemotherapy.¹¹⁸ Cells expressing copper-transporting P-type adenosine triphosphatase ATP7B are more resistant to platinum.¹¹⁸ The main mechanisms include: decline in adduct levels, reaction with intracellular reducing agents, binding to transporters, reduced endocytosis, and cross-linking repair.¹¹⁹ To overcome this, research is now focusing on Pt(VI) pro-drugs which undergo intercellular reduction to eliminate the axial ligands before undergoing the aquation process.¹²⁰

An emerging class of metal-based chemotherapy agents are the ruthenium(II) arene 1,3,5-triazaphosphaadamantane (PTA) compounds, known as RAPTA complexes (Figure 20).¹²¹ These compounds are not strictly cytotoxic, rather, they are anti-metastatic compounds. Although the mechanism of action for these ruthenium (II)-based agents isn't fully understood, it's believed to be similar to that of platinum(II), the exchange of ligands with water yielding a highly reactive metal centre in the intracellular environment.¹²¹ These complexes generally have a low systemic toxicity profile, while showing marked efficacy against metastases. Another major advantage of using these ruthenium(II)-based compounds over platinum(II)-based compounds is that there are far fewer associated off-target side-effects. Due to their greater steric bulk, they are also markedly more soluble in polar-media than cis-platin and other related platinum(II)-based compounds.

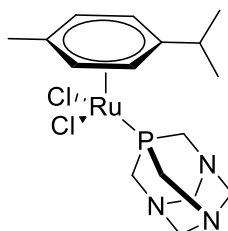


Figure 20. RAPTA-C, a known anti-metastatic ruthenium(II) agent.

Interestingly, cytotoxicity assays require incubation periods of at least 72 hr to observe cytotoxic/cytostatic effects with the best reported anti-metastatic behaviour being observed in the highly invasive MDA-MB-231 (HER+) breast cancer cell line with RAPTA-T *in vitro*.¹²² *In vivo* evaluation in murine models were found to exhibit a 35% reduction in the weight of lung

metastases while exerting a good degree of selectivity towards cancer cells.¹²² Covalent linkage of two ruthenium(II) complexes together with aliphatic and chiral alicyclic linkers were found to significantly enhance the cytotoxicity LD₅₀ value observed in three cell lines, including a platinum(II) resistant cell line from >400 μM for the mononuclear complexes to <100 μM for the dinuclear tethered complexes.¹²³ Mononuclear RAPTA complexes with a pH-dependant intramolecular chelate were found to not only increase the solubility of the compound in polar media but also give rise to a pH –dependent chemotherapy agent which became active towards substitution with 5'-GMP.¹²⁴

1.2.3 Photodynamic Therapy

Photodynamic therapy (PDT) is an emerging cancer therapy technique in modern medicine. However, it is a powerful technique and has been utilized since antiquity where ancient civilisations in Egypt and India utilised dye molecules to alleviate dermatological conditions such as vitiligo and psoriasis, notably, with the use of psoralen.¹²⁵ PDT was re-discovered by modern Western civilisation at the beginning of the 20th century through the efforts of Niels Finzen, Oscar Raab and Herman von Tappeiner.¹²⁵ Principally, photodynamic therapy requires three ingredients: light, a photosensitiser (PS), and molecular oxygen.

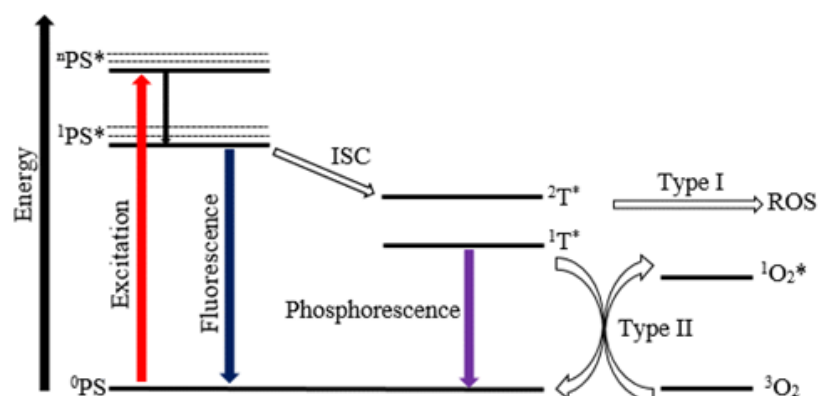


Figure 21. Simplified Jablonski diagram outlining the photosensitisation processes.

The process of photosensitization, best described by the simplified Jablonski diagram (Figure 21), is the use of light energy, input into the system in the form of quantised energy packets (photons), by a photosensitizer to generate highly reactive species. Briefly, a photosensitizer absorbs light of an appropriate wavelength and is promoted to an excited singlet state from a singlet ground state. Naturally, internal conversion and vibrational relaxation can occur within the excited states. These excited singlet states can decay through an energy emissive process in the form of fluorescence but can also undergo inter-system crossing *via* the Laporte forbidden inversion of the spin of an electron to give an excited triply degenerate state. In this state two processes can occur; either emission of a photon by phosphorescence, or generation of cytotoxic species, usually by electron or energy transfer to molecular oxygen (Figure 22). The lifetime of the excited singlet

state is short, typically $10^{-12} - 10^{-9}$ s,¹²⁶ however, the excited triplet state is much more long-lived, 10^{-3} - 10^1 s. This limits the photochemistry available *via* the singlet excited state, but photochemical reactions *via* the excited triplet state are more versatile.

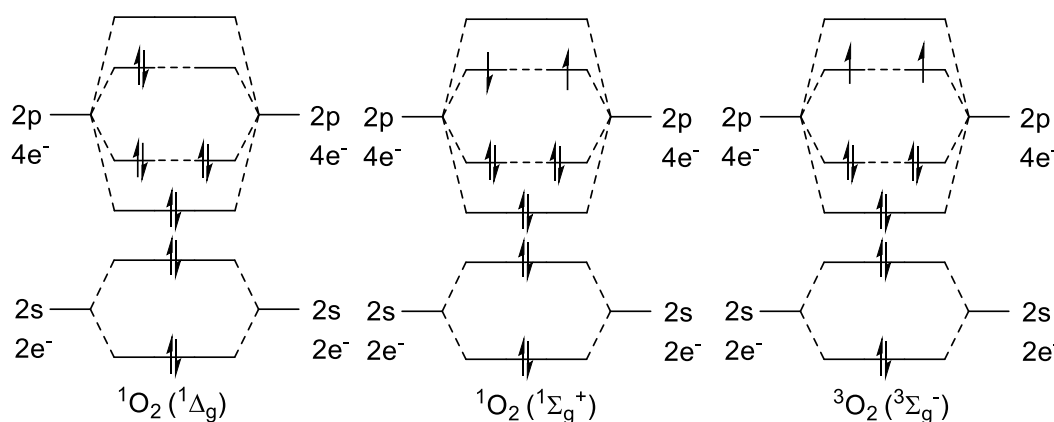


Figure 22. Molecular orbital diagrams of singlet oxygen ($^1\text{O}_2$) and triplet oxygen ($^3\text{O}_2$).

Two relevant mechanisms are possible *via* the excited triplet state: Type I - this mechanism occurs through electron transfer to species in close proximity to the photosensitizer and can generate, among other species, hydroxyl radicals, superoxide radicals and peroxy radicals;¹²⁷ Type II - through this mechanism, molecular oxygen in its triplet ground state is converted to singlet oxygen by energy transfer, singlet oxygen is a highly reactive species and is widely reported to be the dominant cytotoxic species in PDT.¹²⁸ Cell death occurring due to PDT can be by apoptosis, necrosis, or in some cases autophagy.¹²⁹ However, in tumour tissues, the concentration of molecular oxygen is often depleted due to an inadequate network of vasculature supplying the growing tumour. This leads to hypoxia which can result in a treatment such as PDT or radiotherapy being rendered ineffective. The generation of singlet oxygen, *via* photosensitization, has also been used to destroy Gram-negative bacteria.^{130, 131} As previously mentioned, for PDT activity to occur a spin-forbidden transition from an excited singlet state to the excited triplet state must occur,¹³² and this process can be enhanced by the introduction of an atom with high atomic weight, known as the heavy atom effect.¹³² Heavy-metal cations that the porphyrin tetradentate macrocycle can ligate include palladium,¹³³ silver,¹³⁴ and gold.¹³⁵ This can result in a bathochromic shift, enhancing tissue transmission of light.¹³² Furthermore, they can increase the excited state lifetimes which can increase the phototoxicity of the system. For this to occur, a spin-orbital perturbation must occur, which is enhanced by the presence of the heavy-atom.¹³⁶

Once singlet oxygen and other ROS are produced, these cytotoxic species can react with many components of the cancer cell, including unsaturated lipids, amino acid residues and nucleic acids.¹³⁷ Sufficient oxidative remodelling of cellular structures leads to cell death that can be programmed (apoptosis) or unprogrammed (necrosis).¹³⁷ The singlet oxygen produced by irradiation of porphyrins interacts with the cell components through a number of defined chemical

reactions.¹³⁷ Proteins and DNA are important biological macromolecules within the cell responsible for cellular function, and even moderate modification of these systems can lead to apoptosis, the details of which are discussed below.¹³⁷ Amino acid residues such as cysteine (Cys), methionine (Met), tyrosine (Tyr), histidine (His) and tryptophan (Trp) are particularly sensitive to oxidation by singlet oxygen.¹³⁷ Cys and Met are oxidised to sulfoxides, His gives endoperoxides, and Tyr gives a product of phenolic oxidative coupling.¹³⁷ The DNA double-stranded helix can be oxidatively damaged at both the nucleic acid bases and the deoxyribose parts that link the bases to the strand.¹³⁷ Oxidation of DNA mostly takes place at deoxyguanosine via Diels-Alder cycloaddition with singlet oxygen, which yields 8-oxo-2'-deoxyguanosine.¹³⁷ The oxidation of lipids, on the other hand, usually gives hydroperoxides and mostly with E configuration.¹³⁷ As a result of damaging the proteins, DNA and lipids in a cell and its membranes, regular functioning will be disrupted and apoptosis, or other cell death modes, can begin.¹³⁷

Naturally, the human body responds differently to PDT and singlet oxygen depending on the cells being damaged.¹³⁷ An ideal photosensitizer would have a high cellular uptake in the cancer cells, but low uptake in healthy tissues. The amount of cellular damage that occurs will depend on the localization of the photosensitizer within the cell or tissue.¹³⁷ Mitochondria, lysosomes, plasma membrane, and nuclei of tumour cells have all been evaluated as potential PDT targets, along with the tumour vasculature.¹³⁷ Due to limited migration of singlet oxygen *in vivo* the damage is, however, highly localized.¹³⁷ Most photosensitizers will not accumulate in the cell nuclei, so there is little chance of PDT causing mutations.¹³⁷ Lysosomes, endosomes, mitochondria and plasma membranes, are all sensitive targets for singlet oxygen.¹³⁷ Cell death by PDT induced apoptosis has been reported *in vivo* and *in vitro* but is unlikely to be the sole mechanism of cell death, as mechanisms such as necrosis and autophagy are also possible.¹³⁷ PDT is considered to be a highly spatially controlled cancer therapy, where the high reactivity of singlet oxygen means that the therapeutic action is localised to molecules and biological structures proximal to the PS.¹³⁷ In order to efficiently generate singlet oxygen *in situ* the optical transparency of the human body needs to be taken into consideration.¹³⁷ Light used to activate the PS must be able to sufficiently penetrate the body with high enough intensity in order to generate sufficient singlet oxygen to mediate the therapeutic effect.¹³⁷ Biological tissues are highly heterogeneous, and the transmission of light is affected by scattering and absorption by biological macromolecules and chromophores.¹³⁷ Major absorption occurs due to haemoglobin, myoglobin and cytochromes, all of which are composed of, or incorporate, porphyrin-based molecules.¹³⁷ A natural pigment in the skin, melanin, is another dominant absorber, especially in the 500–600 nm region.¹³⁷ Therefore, an optical window exists where maximum penetration depth by light will occur.¹³⁷ Another important optical parameter is the anisotropy, which is a measure of the direction of scattered light.¹³⁷ Monte Carlo modelling can be employed to predict how the light will travel through biological tissues, giving information on optical properties such as fluence, fluence rate,

wavelength and angle of incidence at specific locations.¹³⁷ In terms of PDT, these factors result in an average effective penetration depth of around 1–3mm at 630 nm.¹³⁷ Increased transmission occurs at longer wavelength allowing for enhanced penetration depths.¹³⁷ Taking these parameters into account it is clear that PDT is a useful modality for tumours close to the surface, although surgically implanting fibre optics can allow for deeper-seated tumours to be effectively treated.¹³⁷

1.2.3.1 Photosensitisers

Structurally, photosensitisers all contain extended aromatic systems with excessive π -conjugation. The main classes of photosensitisers include: cyanine dyes, methylene blue, and tetrapyrroles and other related macrocycles. For the purposes of this thesis, only porphyrins and related macrocycles are considered. Many porphyrin-based photosensitisers have been synthesised, evaluated and approved for biomedical applications by health administration bodies. Ideally, a photosensitiser will satisfy several criteria (Table 7).

Photosensitiser Properties
High uptake by neoplastic tissues
Low uptake by non-neoplastic tissues
Low systemic toxicity
Rapid clearance from the blood
Long half-life within neoplastic tissues
Known and constant chemical formula and structure
Hydrophilic for IV administration
Low photobleaching
High quantum yield
High triplet state lifetimes
Strong absorption in the 400-800 nm region.

Table 7. Ideal properties of a photodynamic sensitiser.

5-Aminolaevulinic acid (5-ALA), Gliolan®, which has been approved for human use in the EU, Asia, and Australia, is an aliphatic pro-drug which is typically administered to patients by topical formulation applied to the stratum corneum (Figure 23).^{138, 139} 5-ALA is a key precursor in the biosynthetic pathway of haem production, which is the porphyrin co-factor at the centre of haemoglobin. The precursor to haem in its synthesis is the metal-free free-base porphyrin, protoporphyrin IX (PPIX), which is itself is a powerful photosensitizer. Previous studies have shown that exogenous 5-ALA is preferentially uptaken by malignant central nervous system neoplasms.¹³⁸ The Soret band of PPIX occurs at 405 nm, and the Q-bands in the 450-700 nm region. However, the issue with the application of 5-ALA to the skin is that it can only be used for surface cancers arising from poor penetration depth of light matching the absorption bands of PPIX.

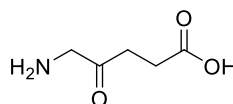


Figure 23. 5-Aminolaevulinic acid.

Benzoporphyrin monoacid ring A (BDP-MA) is sold under the brand name of Visudyne® (Figure 24) which is an FDA approved PS chromophore related to PPIX.¹⁴⁰ This porphyrin has been approved for biomedical applications in the field of ophthalmology and age-related macular degeneration.¹⁴¹ The presence of the exocyclic ring induces a red-shift of the absorption spectrum to a more favourable absorption maxima of 690 nm, bordering the NIR region.¹⁴⁰ The main failing of this PS is the lack of solubility in polar media, albeit, it is significantly higher than that of PPIX which is only soluble in alkaline buffered solutions. This porphyrin has been conjugated to nanoparticles and antibodies in an attempt to increase specificity and selectivity towards tumours, and as a delivery agent for multiple PSs.

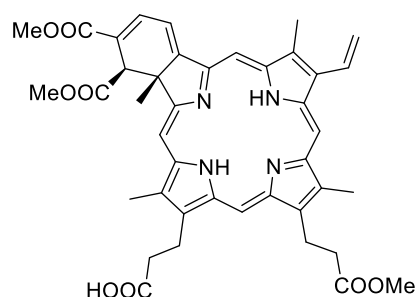


Figure 24. Benzoporphyrin monoacid ring A (BDP-MA).

Temoporfin is sold under the brand name Foscan® within the EU and is approved by the FDA (Figure 25). This chlorin structure is similar to that of a porphyrin, however, it contains a reduced exocyclic pyrrolic double bond. This causes a significant red-shift of the Soret band absorption maxima and causes an increase in the molar absorptivity of the final Q-band (652 nm) allowing for good absorption at a higher wavelength for enhanced tissue penetration. It is important to note that while all porphyrins are 22 π electron conjugated systems all chlorins are 20 π electron systems. Another significant difference of this compound compared to the previous examples is that it is not β -functionalised, but rather it is *meso*-substituted. The presence of *meta* alcohol groups on *meso*-phenyl rings confers some hydrophilicity to the compound. *In vivo*, this compound has been shown to control the growth of tumours in Balb C nude mice bearing human mesothelioma xenografts (H-MESO I) when irradiated with several fractionated light doses of 30 J cm⁻¹ at a fluence rate of 100 mW cm⁻².¹⁴²

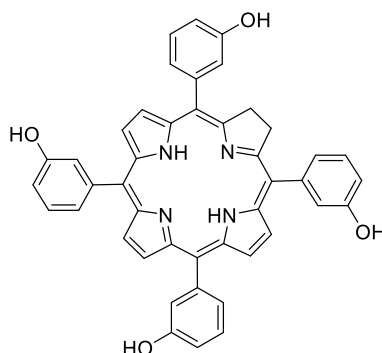


Figure 25. Temoporfin, an example of a chlorin photosensitizer.

Chlorin e6 is, as the name suggests, a chlorin-based photosensitizer (Figure 26). This chlorin structure is reminiscent of that of PPIX, however, it only has a 20 π -electron conjugated system and is hydrophilic due to the presence of three acidic carboxylic acid functional groups.¹⁴³ This chlorin, unlike Foscan®, doesn't contain any *meso*-functional groups. Its absorption spectrum reveals a high absorptivity Soret band at 405 nm, and high absorptivity Q-band at 662 nm of $64612 \text{ cm}^{-1} \text{ M}^{-1}$ in ethanol.^{144,145} Similarly, this compound has been conjugated to antibodies and polymer substrates to enhance its selectivity and specificity towards tumours.¹⁴⁶

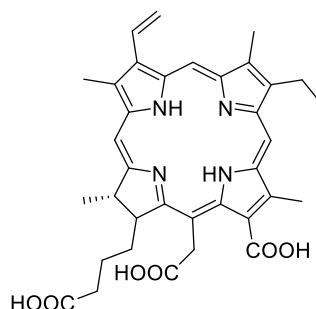


Figure 26. Chlorin 6e, a hydrophilic chlorin photosensitizer.

1.3 Cancer Imaging

In the field of oncology, medical imaging is used to determine the morphology, physiology, location, metabolism and function of tumours.¹⁴⁷ Typically, a patient requires a diagnostic scan to obtain the maximum amount of accurate information about a tumour. Only by obtaining accurate information about cancer can the clinician prescribe a suitable treatment for the patient. The main techniques used in cancer diagnosis include: single-photon emission computed tomography (SPECT), positron emission tomography (PET), magnetic resonance imaging (MRI), computerised tomography (CT), X-ray radiology, ultrasound (US), and fluorescence imaging (FI). Each technique has different associated physics and will offer its own associated advantages and disadvantages for real-time monitoring of human biology without destruction of the tissues and loss of information.¹⁴⁷

Imaging techniques can vary in their function and how they image tumours and the sensitivity of the technique too. Positron emission tomography can be highly accurate with concentrations of the imaging agent in the picomolar to the nanomolar range, while MRI requires micromolar concentrations.¹⁴⁷ Some techniques can be coupled together to offer enhanced information recoveries, such as PET-CT, utilizing the sensitivity of PET and the spatial resolution of CT.¹⁴⁷

For the purposes of this project, the main imaging techniques that can lend themselves to radiotherapy, chemotherapy, and PDT are PET imaging and fluorescence imaging. Naturally, theranostic fluorescent-PDT porphyrins have been synthesised and biologically evaluated.

However little investigation has been carried out on combining radiosensitizing molecules with an imaging modality.

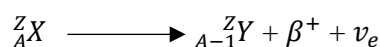
1.3.1 Positron Emission Tomography

Paul Dirac in 1928 theorised that the standard model of fundamental particles was incomplete with solely matter, he theorised the presence of anti-matter in the universe.¹⁴⁸ The properties of anti-matter are that they are characterised by having exactly the same rest mass as their matter counterparts, and if they are charged then they will have the opposite charge. When matter and antimatter interact they annihilate by converting their combined rest masses into heat and two quantised gamma photons.¹⁴⁸ Dirac also went on to propose pair production where a single photon can disintegrate to create a particle and antiparticle. The table of anti-matter particles is given below (Table 8).

Matter	Anti-matter
Proton	Antiproton
Neutron	Antineutron
Electron (Negatron)	Positron
Neutrino	Antineutrino
Muon	Antimuon
Muon neutrino	Anti-muon neutrino

Table 8. Common particles and their corresponding antiparticles.

The annihilation process can be considered to be analogous to a chemical reaction but instead of conservation of atoms taking place, several other fundamental properties must be conserved. The fundamental properties that are always conserved are energy, momentum, charge, lepton number and strangeness. Below is an example of the radiative process for the emission of a positron from an atom, undergoing spontaneous nuclear radioactive decay. Once the positron particle has been emitted from a nucleus then it may readily interact with neighbouring electrons.¹⁴⁸



Scheme 1. Spontaneous emission of positron antiparticle from a nucleus.

When the annihilation process occurs the particle's rest masses are converted to pure energy, in this case, particles with zero mass travelling at the speed of light, photons.¹⁴⁸ The diagrammatic representation of annihilation (below) shows that two photons are produced, which are then detected by a ring detector. Two photons are created by the conservation of the law of momentum. In order to understand how to use the annihilation of antimatter particles in medical imaging one should first understand the final concept of relativity. The annihilation process occurs as discussed and two photons co-incident are produced at 180° to each other (Figure 27).¹⁴⁸ The energy of a single gamma photon is equal to the rest mass energy and the momentum contribution of the interacting particles as expressed by Einstein's energy mass equivalency (Equation 7).

$$E^2 = (mc)^2 + p^2 \quad (7)$$

Where: E: energy (J); m: mass (kg); c: the speed of light *in vacuo* ($m s^{-2}$); p: momentum ($kg m s^{-1}$).

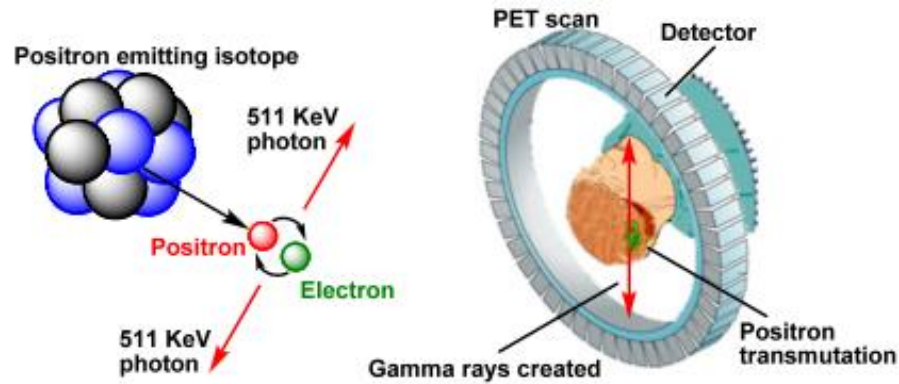


Figure 27. Diagrammatic representation of the emission of a positron, following annihilation and subsequent detection.¹⁴⁹

When high energy photons interact with matter, their energy can be transferred to the material.¹⁴⁸ Commonly photoionization, scattering or excitation through adsorption when an atom interacts with incident EM radiation.¹⁴⁸ Through a Compton scattering process, the photon loses energy and is scattered (Equation 8).

$$I_x = I_0 e^{-kx} \quad (8)$$

Attenuation is a function of the photon energy and the electron density.¹⁴⁸ The attenuation coefficient is a measure of the probability that a photon will be attenuated by a unit length through a medium.¹⁴⁸ When dealing with annihilations *in vivo* the resultant gamma photons are not well-collimated but will be emitted in all directions.¹⁴⁸ Therefore broad-beam conditions exist, photons which may have been taken out of the angle of acceptance for the detector will have been observed.¹⁴⁸ In the narrow beam case scattered photons are precluded and thus the measurement considers the bulk attenuation properties of the object alone.¹⁴⁸ Considering the source where coincident gamma photons are detected the count rate will be given by Equation 9.¹⁴⁸

$$C = C_0 e^{-kD} \quad (9)$$

Therefore the count rate depends on the total thickness of the object and is independent of the position of the object, thus attenuation of coincidence detection from annihilation, the attenuation path length is the only parameter required.¹⁴⁸ Radiation detectors typically convert the total energy deposited by the gamma photons into an electrical signal to which the integral of the signal is proportional to the energy deposited.¹⁴⁸ In PET the energy of the photons is in the gamma region of 511 keV.¹⁴⁸ Accurate measurements of this energy is therefore paramount to the accuracy of the PET imaging technique to accurately map cancer. Typically, the detectors used include gas

chambers, semiconductor solid-state detectors and scintillators. But in all cases, the interaction of gamma photons with the matter in the detector creates an electrical signal which is processed to give the image.

In order to make use of the physics above, a viable molecule incorporating a radioisotope needs to be delivered to a tumour, then detection can begin. Commonly there are several main radioisotopes that are used in PET imaging and have positron emission as part of their decay path (Table 9). The two main considerations when choosing a PET isotope are the maximum positron energy in MeV and the relative percentage of positron decay. The higher the maximum energy the further the positron will travel before it annihilates, therefore resulting in a lower resolution image.

Radioisotope	Half-life $t_{1/2}$ / min	Maximum energy / MeV	Decay Product	Range In Water / mm (max)
^{11}C	20.40	0.96	^{11}B	4.12
^{15}N	9.97	1.19	^{13}C	5.39
^{15}O	2.04	1.72	^{15}N	8.20
^{18}F	109.8	0.64	^{18}O	2.39
^{64}Cu	762.0	0.65	^{64}Ni	2.50
^{89}Zr	4704.6	0.90	^{89}Y	1.18
^{44}Sc	238.2	1.45	^{44}Ca	N/A
^{68}Ga	67.7	1.89	^{68}Zn	8.20

Table 9. Common radioisotopes used for PET imaging.¹⁴⁷

Apart from the discomfort of the injection of the radioactive tracer, PET imaging is a painless process and can be used for highly accurate diagnosis with very sensitive drugs requiring concentrations as little as picomolar concentrations. Disadvantages are that the process involves ionizing radiation which patients are typically sceptical of, and the confinement from being in the ring detector can be distressing to patients.

The main PET radiopharmaceutical used worldwide is 2-deoxy-2- (^{18}F) fluoro-D-glucose commonly known as $[^{18}\text{F}]\text{FDG}$.¹⁵⁰ While several other PET tracers have been approved and are under development this thesis concentrates on the application of $[^{18}\text{F}]\text{F}$. $[^{18}\text{F}]\text{F}$ is an excellent radionuclide for PET imaging due to its decay path progressing mostly through positron emission (96.9%) and only 3.14% decay by electron capture. $[^{18}\text{F}]\text{FDG}$ utilises the Warburg effect as previously described to passively target cancers by its enhanced uptake by tumour tissues. Firstly, the $[^{18}\text{F}]\text{F}$ needs to be synthesised by a nuclear reaction by the bombardment of ^{18}O -enriched water by protons in a cyclotron *via* a (p,n) reaction (Figure 28).

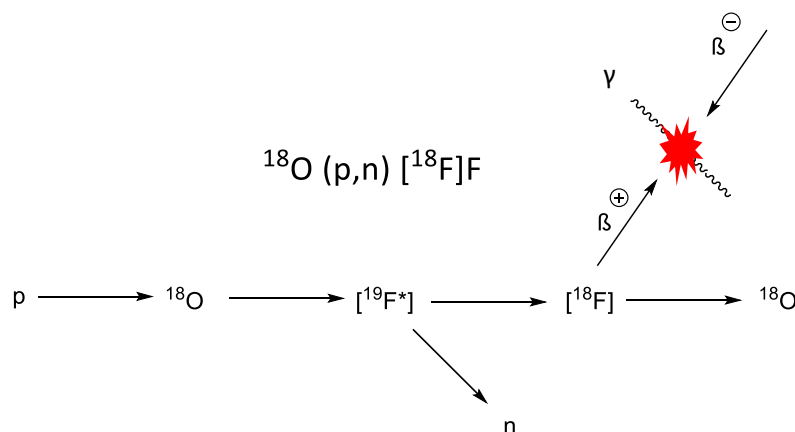


Figure 28. $^{18}\text{O} (p,n) [^{18}\text{F}]\text{F}$ nuclear reaction schematic detailing the synthesis of $[^{18}\text{F}]\text{F}$, positron emission, and $[^{18}\text{F}]\text{F}$ decay.

This yields “carrier-free” $[^{18}\text{F}]\text{F}^-$ ions in water. The fluoride ions can be trapped by a cryptand and potassium carbonate. The highly nucleophilic $[^{18}\text{F}]\text{F}^-$ then can undergo an $\text{S}_{\text{N}}2$ reaction with acetyl protected mannose triflate. Aqueous work up gives the fully deprotected radiolabelled $[^{18}\text{F}]\text{FDG}$. Importantly, the decay product of a radiopharmaceutical is an important factor, with regards to $[^{18}\text{F}]\text{F}$, it decays to ^{18}O which is not radioactive, this heavy-isotope of oxygen will exist as an $^{18}\text{O}^-$ anion which can readily abstract a proton from H_3O^+ forming a hydroxyl group. $[^{18}\text{F}]\text{F}$ represents an interesting radioisotope to produce novel radiopharmaceuticals and has potential to be attached to therapeutic molecules giving so-called theranostic molecules. When synthesising new radiopharmaceuticals one must consider the three principles of radiochemistry: tracer principle, stability, and targeting (Table 10).

Principle	Explanation
Tracer principle	Specific activity should not be so low that no radiolabelled molecules enter the site, and so high that radioactivity perturbs the system.
Stability	The molecule should be stable enough such that the body does not metabolise the molecule or release the radioactive component before it reaches the active site.
Targeting	The radiolabelled drug should be targeted to accumulate in the site under investigation and not in another part of the anatomy.

Table 10. Table showing key principles an ideal PET tracer should obey.

1.4 Theranostic Medicine

The idea of theranostic medicine is a simple one, its aim is to combine together imaging modalities with therapeutic molecules or materials. The advantages of this are clear. Firstly, a clinician can clinically validate whether a therapeutic molecule can research a tumour site by observing it through imaging modalities such as PET and fluorescence imaging. Secondly, dynamic image acquisition allows for determination of the ideal time point at which to administer a therapy such as radiotherapy or PDT based on the maximum uptake of the compound. Thirdly, the degradation

path of the compound can be elucidated by the observation of its location in the body, typically, pharmaceuticals are eliminated either renally or hepatically. However, one needs to be aware that there is a sensitivity difference between therapy and imaging using different techniques. With regards to PET imaging, trace amounts of radiopharmaceuticals are administered in accordance with the tracer principle, while for MRI up to 2 grams of Gd(III) is administered to a patient for imaging to take place. Fluorescence imaging can be acquired with μM doses of compound. Chemotherapy and PDT typically requires administration of nM to μM concentrations to observe a therapeutic effect.

It will be demonstrated in this thesis that throughout cancer medicine porphyrins represent an interesting class of pharmaceutical. They are fluorescent and can generate cytotoxic ROS and singlet oxygen. Additionally, they have been investigated for use as radiosensitizers and have been found to cause good sensitization of cancers *in vitro* and *in vivo*. The development of combined therapeutic PET imaging agents is a novel combination of two powerful modalities in the treatment of cancer.^{151,152} Therefore all further discussion will take place with respect to porphyrins for medical applications for the personalised treatment and imaging of cancers.

PET-PDT:

To the best of our knowledge, the first known example of a [^{18}F] radiolabelled porphyrin was reported in 2013 (Figure 29).¹⁵³ A zinc(II) ligated porphyrin was appended with an aliphatic bifunctional hydroxyl-alkyne chain by a Sonogashira coupling reaction.¹⁵³ The hydroxyl was exchanged for a tosyl functional group.¹⁵³ Tetrabutylammonium hydroxide was azeotropically distilled with [^{18}F]F $^-$ in ^{18}O -enriched water to yield [^{18}F]-TBAF.¹⁵³ Nucleophilic substitution was then carried out with this reagent to give the radiolabelled porphyrin species, however, no biological evaluation either *in vitro* or *in vivo* was carried out to determine the therapeutic or imaging efficacy of the radiopharmaceutical.¹⁵³

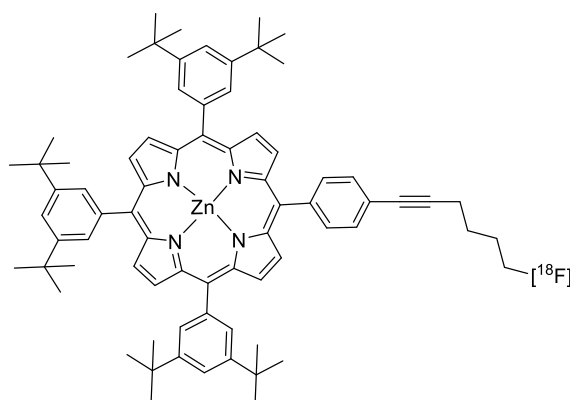


Figure 29. An amphiphilic porphyrin appended to a lipophilic [^{18}F] radiolabelled chain.

More recently, Entract *et al.* reported the synthesis of the first ever cationic water-soluble porphyrins appended to a [^{18}F] radiolabelled prosthetic (Figure 30).¹⁵⁴ This theranostic agent

integrated the therapeutic selectivity of PDT with the efficacy and unparalleled sensitivity of PET imaging.¹⁵⁴ The ‘cold’ product was evaluated in human adenocarcinoma (HT-29) cells with a filter to remove light below 550 nm.¹⁵⁴ The LD₉₀ was found to be approximately 1×10^{-4} M, although ‘dark’ toxicity was approximately 75%.¹⁵⁴ A two-step radiolabelling procedure was carried out where a tosyl group was exchanged with the [¹⁸F] as described previously.¹⁵⁴ The prosthetic was conjugated to the porphyrin macrocycle *via* a copper(I) catalysed alkyne-azide cycloaddition (CuAAC) reaction followed by purification by RP-HPLC resulting in a radiochemical yield (RCY) of 77%, and a radiochemical purity (RCP) of >99%.¹⁵⁴ The radiopharmaceutical was evaluated *in vivo* in HT-29 and U87 xenograft models, as expected for a porphyrin, the majority of the compound localised in the liver, while a good tumour to muscle ratio of 2.4:1 (SUV_{max}) was achieved.¹⁵⁴

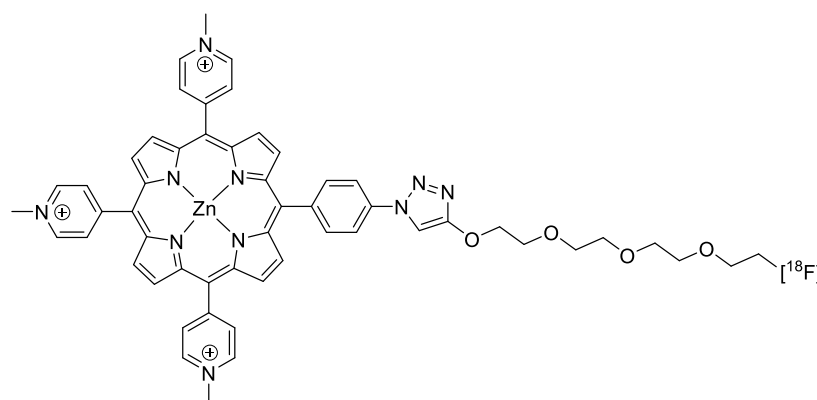


Figure 30. A cationic water-soluble Zn(II) porphyrin appended to a [¹⁸F] radiolabelled prosthetic.¹⁵⁴

PET-RS:

1-Fluoro-3-(2-nitroimidazole-1-yl)-propan-2-ol ([¹⁸F]FMISO) became the first PET probe used clinically to image hypoxia (Figure 31).¹⁵⁵ The chiral compound is administered as a racemic mixture to patients.¹⁵⁵ Over the years RCYs have increased from 7% to 38% with the use of microfluidic chips with activities from 7 to 55 GBq been reported.¹⁵⁵ However, SUV_{max} metrics have been found to be far lower for [¹⁸F]FMISO compared to [¹⁸F]FDG.¹⁵⁶

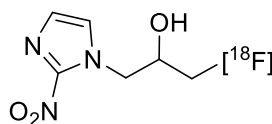


Figure 31. Alkylated nitroimidazole labelled with [¹⁸F].

In order to overcome the two-step radiochemical labelling of nitroimidazoles, the facile Al-F technology was utilised by the complexation of Al(III) by a modified 1,4,7-triaza-1,4-diacetic acid (NODA) macrocycle, since this doesn't require azeotropic distillation which is difficult to automate using cassette-based systems (Figure 32).¹⁵⁷ The study found that the [¹⁸F] complexes had good stabilities, efficiencies, and specific uptakes in several hypoxic tumour cell lines. RCYs

of >99% were achieved and the complexes demonstrated good serum stability >90%.¹⁵⁷ While their investigations were focused around PET imaging of hypoxia, it is reasonable to assume that this pharmacologically active radiosensitizing molecule has the potential to be a theranostic agent for the combined imaging and therapy of cancers.¹⁵⁷

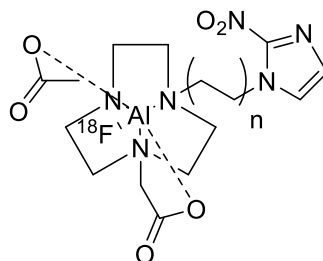


Figure 32. Al-[¹⁸F] radiolabelled DODA conjugated to 2-nitroimidazole.

It has been recognised that the combination of a radiosensitizing molecule with a radioisotope represents a powerful medicinal tool to personalise diagnosis and treatment of cancers. While there are several examples of [¹⁸F] labelled porphyrin photosensitisers, there is no literature focusing on the synthesis and biological evaluation of porphyrin-based radiosensitizers combined with [¹⁸F] radioisotopes.

1.5 Dual-Therapy

As previously discussed, over time tumours can become resistant to platinum-based chemotherapies. One strategy to overcome this is to combine two therapeutic techniques together. Simply, the rationale behind this is that two therapies are better than one, as the cancer cells don't have mechanisms to repair multiple types of damage. Furthermore, it reduces the likelihood of cancers building resistance to the two therapies combined. Strategies that have been utilised include the combination of two therapeutic molecules giving a single dual-therapeutic agent, or the conjugation of two separate therapeutic molecules to a single carrier such as an antibody, protein, or polymer surface.

PDT-Chemotherapy:

The combination of a PS with a chemotherapy agent represents a unique opportunity to create a dual-therapeutic molecule with two different mechanisms of action. Strategies include the chelation of Pt(II) complexes to porphyrin macrocycles (Figure 33). TCC-SUP cells were incubated with various concentrations of novel dual PS-chemotherapeutic agents which were found to induce a phototoxic effect at 1 μM concentrations with a light dose of 24 J cm^{-1} .¹⁵⁸

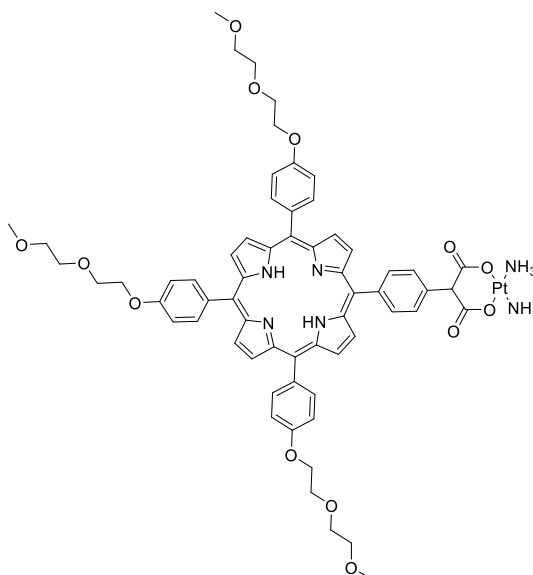


Figure 33. Dual-therapeutic platinum-porphyrin conjugate.

The literature is replete with examples where Pt(II) and Pt(IV) have been conjugated to porphyrins, however, there are only two examples of dual-therapeutic ruthenium(II)-porphyrin conjugates. To the best of our knowledge, the first known example of a cytotoxic Ru(II)-porphyrin complex was reported by Therrien *et al.* in a collaboration with Paul J. Dyson (Figure 34).¹⁵⁹ The nitrogen atoms on *meso*-pyridyl functional groups were chelated to Ru(II) centres giving a tetranuclear ruthenium-porphyrin complex.¹⁵⁹ It is important to note that the Ru(II) complex is not a true RAPTA complex. These complexes fared well in MTT cytotoxicity assays against Me300 human melanoma cells with cytotoxicity values of around 30% cell survival after 24 hr incubation with 100 μ M concentrations of the conjugates.¹⁵⁹

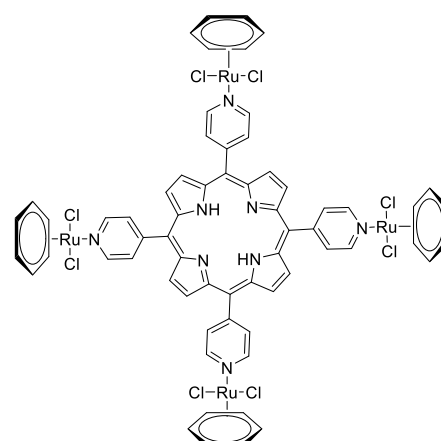


Figure 34. Tetranuclear Ru(II)-porphyrin conjugate.

The second known cytotoxic Ru(II)-porphyrin conjugate was synthesised and biologically evaluated by Gianferrara *et al.* In this case, the cationic conjugate was synthesised by conjugation of a 2,2'-bipyridine ligand to the tetraarylporphyrin followed by chelation to the Ru(II) metal complex.¹⁶⁰ Cytotoxicity evaluation was carried out in triple negative MDA-MB-231 breast

cancer cells with an exposure period of 72 hr at concentrations up to 100 μM .¹⁶⁰ IC_{50} s of 4/5 μM were obtained for the structure below (Figure 35) with the absence of light irradiation. An analogue using alkyl spacers was found to give a similar response.¹⁶⁰ A light dose-dependent relationship was observed with an incubation period of 24 hour.¹⁶⁰

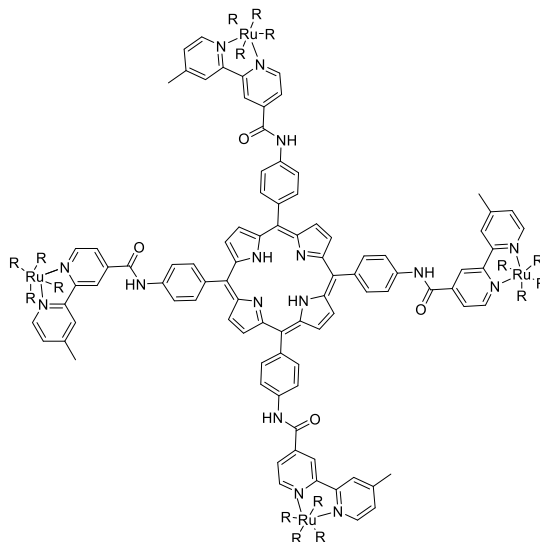


Figure 35. A cationic tetranuclear Ru(II)-porphyrin conjugate.

Clearly, there is a president set for further research into the synthesis and biological evaluation of these novel Ru(II)-porphyrin conjugates. The literature is lacking in research conducted with RAPTA-porphyrins conjugates, and so far all the Ru(II)-porphyrin conjugates are tetranuclear analogues. As ruthenium is a rare and expensive resource clearly a reduction in the number of ruthenium atoms per porphyrin would be commercially beneficial.

1.6 Literature Conclusions

Healthcare systems are facing increasing financial strains, due to the incident rates of cancer and other diseases such as cardiac diseases and diabetes increasing. Furthermore, due to an aging population, more people are suffering from ever more complicated diseases. While cancer therapies have evolved over time, and new emerging techniques are promising, some of these therapies become quite ineffective in highly aggressive tumours, tumours with a p53 mutant, or tumours deficient in oxygen. Personalised medicine clearly is a way forward to alleviate these pressures while providing enhanced healthcare solutions to patients who would otherwise die from highly aggressive metastatic tumours and hypoxic tumours where therapies mediated by oxygen partial pressures become ineffective. Porphyrins are highly versatile molecules with exquisite properties that lend themselves to biomedical applications.

A thorough review of the literature has found that these privileged structures can be used as radiosensitizers, photosensitisers, and molecular imaging agents. Furthermore, theranostic porphyrin-based PET/PDT agents have been synthesised and biologically evaluated, while there are no known examples of theranostic RS/PET porphyrin-based agents in the literature. The use of [^{18}F]F $^-$ is advantageous due to its versatility and ideal half-life and decay product, additionally, hospitals already have the facilities and infrastructure to utilize [^{18}F]F $^-$ in the form of [^{18}F]FDG, therefore through this project it is the isotope of choice. These theranostic RS/PET porphyrins theoretically should be able to sensitise tumours to ionizing radiation regardless of the expression of p53 and tissue hypoxia.

Furthermore, porphyrins have been proven to be effective dual-therapy agents for the combined treatment of cancers. Examples in the literature include porphyrins conjugated to Pt(II) and Ru(II) cytotoxic agents. The use of RAPTA complexes is emerging in the literature, but large excesses of Ru(II) are required in order to obtain any cytotoxic or anti-metastatic behaviour, therefore there is scope for improvement in the number of ruthenium complexes per porphyrin, and the possibility to decorate a scaffold with both molecules to deliver an anti-cancer payload to the tumour site. These conjugates have excellent applications in personalised medicine as they would be able to destroy cancer cells *via* the generation of singlet oxygen, and then the retained compound would further damage the cancer cells due to the cytotoxic ruthenium complex mitigating the effects of tissue hypoxia. Additionally, the fluorescent porphyrin-RAPTA conjugates can be validated as theranostic molecular imaging agents through fluorescence microscopy.

1.7 Research Aims

The aims of the research project can be summarised in several important points which will be examined through experimentation:

- Investigate the synthesis of trans- A_2 -diarylporphyrins and develop a route to obtain potential radiosensitising structures.
- Biologically evaluate potential candidates to determine their efficacy at sensitising cancer cells to ionizing radiation and determine their mode of action.
- Investigate the synthesis of ‘cold’ prosthetics and their covalent attachment to the biologically evaluated molecules.
- Investigate the synthesis of ‘cold’ standards and determine QC RP-HPLC purification protocols.
- Investigate the radiolabelling of radiosensitisers for the combined PET imaging and therapy of cancers.
- Re-evaluate ‘cold’ radiosensitisers through biological experimentation.

- Investigate the synthesis and use of chemo- phototherapeutic conjugates for the dual-treatment of cancers.
- Evaluate the photochemical properties of the novel conjugate.
- Biologically evaluate the phototherapeutic and chemotherapeutic efficacy against cancers.

Chapter 2
Synthesis and Biological Evaluation of Diphenylporphyrin
Radiosensitizers

2.1 Introduction

This chapter discusses the synthesis of porphyrins, and in particular, the synthesis of trans-A₂ porphyrins and trans-A₂-metalloporphyrins *via* the condensation of dipyrromethanes. Our approach is to develop a target lead compound with a structure similar to that of the MLT-005 radiosensitizing trans-A₂-diarylporphyrin. Development of the methodology required for incorporating electron withdrawing groups in the *meso*-positions and inducing water-solubility has been carried out on multiple porphyrin scaffolds with the aim of synthesising an electron-affinic water-soluble trans-A₂-diphenylporphyrin. This chapter discusses the synthesis of numerous dipyrromethanes with various functionalities which are used in the MacDonald [2+2] approach to diarylporphyrin synthesis. The use of Zn(II) has been investigated for use as a templating agent in the synthesis of diarylporphyrins from dipyrromethanes in an attempt to create a one-pot synthesis of metalloporphyrins with the added function of increasing the obtained yield of the compound. These functionalised diarylporphyrins have been ligated to M²⁺ cations by microwave irradiation to give the corresponding metalloporphyrins. Biological assays of selected successful candidates have been carried out to determine their effectiveness as photosensitizers and radiosensitizers.

2.2 Synthesis of Trans-A₂-Diphenylporphyrins

5,15-Diarylporphyrins represent an interesting sub-class of tetrapyrroles, the reduction to two *meso*-aryl groups when compared to their tetraaryl cousins, means that these porphyrins can be subjected to interesting chemical modifications, not possible with the more common 5,10,15,20-tetraarylporphyrins. These modifications include *meso*-nitration, alkylation, alkynylation, halogenation, and subsequent palladium catalyzed cross-coupling reactions.^{161,162,163,164} Specifically, it has been reported that bromination and nitration of trans-A₂-diarylporphyrins yields a distorted porphyrin macrocycle giving either domed (A_{2u}), waded (E_g), ruffled (B_{1u}), or saddled (B_{2u}) conformations depending on the specific porphyrin.^{165,166,167,168} This greatly distorts the electron density of the macrocycle by introducing these electron withdrawing groups, which should increase the reduction potential as previously discussed in Chapter 1, Section 1.2.1.5.

Using retrosynthetic analysis, there are many routes to yield a desired diphenylporphyrin; the synthesis of 5,15-diarylporphyrins typically takes place *via* the MacDonald [2+2] condensation which was utilized by Nobel Laureate Woodward to synthesize chlorophyll.^{169,170} This involves the condensation of a dicarbinoldipyrromethane or diformyldipyrromethane with a dipyrromethane using acid catalysis yielding a porphyrinogen, which is oxidised to the corresponding porphyrin.¹⁷⁰ Condensation under Baldwin's conditions requires the implementation of an orthoester and a dipyrromethane which yields the desired 5,15-diphenylporphyrin.^{171,172} The corresponding trans-A₂-porphyrinogen is then oxidised to the

porphyrin *via* either a mild oxidising agent such as compressed air, or a chemical oxidising agent such as 2,3-dichloro-5,6-dicyano-1,4-benzoquinone (DDQ) or tetrachloro-1,4-benzoquinone (p-chloranil), which typically require exhaustive column chromatography to remove. Dipyrromethanes can be synthesised *via* a number of routes, typically condensation of an aldehyde with excess pyrrole is employed,¹⁷³ catalysed with either a Brønsted-Lowry acid or a Lewis acid. These acid catalysts include but are not limited to: aqueous hydrogen chloride ($\text{HCl}_{(\text{aq})}$), trifluoroacetic acid (TFA), indium(III) chloride, and *para*-toluenesulphonic acid.¹⁷⁴ Condensation of aldehyde and pyrrole has even been performed in a biphasic mixture of organic and aqueous media with $\text{HCl}_{(\text{aq})}$ catalyst.¹⁷⁵

Synthesis of trans- A_2 -porphyrins is typically carried out *via* a condensation reaction of dipyrromethanes under dilute conditions, in either DCM, toluene, or ethanol, assisted by an acid catalyst. The nature of the dipyrromethane (DPM) in terms of its substituents, governs its polarity, which determines whether the synthesis of the corresponding porphyrin is viable. Unfortunately, under acidic conditions, the DPMs can undergo cleavage *via* a competing back-reaction. The nature of the R groups on the phenyl ring are known to determine the rate of acidolysis.¹⁷⁶ Acidolysis can lead to “scrambling”, or the synthesis of N-confused dipyrromethanes.^{176,177} Several sets of kinetics govern the formation of porphyrins through a [2+2] condensation reaction. Electron withdrawing groups can accelerate the rate of hydrolysis such that the rate of porphyrin formation becomes relatively insignificant. Therefore, it is reasonable to assume that several dipyrromethanes and diphenyl porphyrins are inaccessible through this route, therefore functional group interconversions must be employed as a synthetic tool.

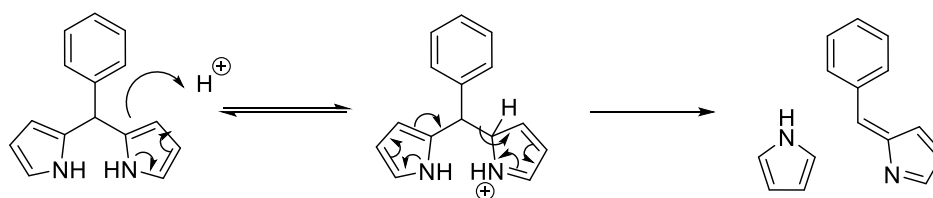


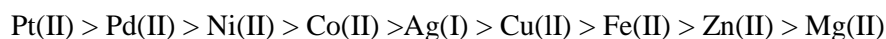
Figure 36. Mechanism of acidolysis of 5-phenyldipyrromethane.¹⁷⁸

The condensation of dipyrromethanes into a diphenylporphyrin with trans- A_2 structure requires a molecule to become the bridging *meso*-positions. Two main restrictions limit the versatility of dipyrromethane condensation: the orthoester, and the substituents on the phenyl ring. More sterically hindered orthoesters such as trimethyl orthoacetate and trimethyl orthobenzoate decrease the rate of reaction for condensation so that the rate of acidolysis becomes more significant, which leads to a significantly reduced yield after isolation by silica-gel column chromatography.¹⁷⁹ Therefore, throughout this thesis, trimethyl orthoformate was used as the orthoester for all [2+2] condensation reactions.

2.3 Synthesis of Metalloporphyrins

Metalloporphyrins represent an interesting series of tetrapyrrolic compounds. They have vastly altered photochemical and electrochemical properties when compared to free-base tetrapyrroles. In order to produce a metalloporphyrin, the metal species must form an outer sphere complex with the deformed conformer of the porphyrin.¹⁸⁰ The mechanism described in the literature reports that metallation occurs by a dissociative ligand interchange.¹⁸⁰ The metal centre can influence the optoelectronic properties of the porphyrin, and in particular, the spectroscopic properties by dictating the symmetry. For example, a tetraarylporphyrin changes from a D_{2h} to a D_{4h} point group upon complexation to $M(II)$ due to the vibrational components of x and y becoming equal.^{181,100} Porphyrins readily chelate to $Zn(II)$ and $Cu(II)$, even without the use of heat, however, $Ni(II)$, $Ga(III)$, and $Pt(II)$ require harsher conditions to introduce the metal into the cavity, usually by refluxing in DMF with an organic base. With regards to larger metals such as $Ln(III)$ cations, sitting-atop and sandwich complexes are favoured as the cation is too large to fit into the plane of the tetradentate macrocyclic ligand.¹⁸² Metal insertion into the cavity usually requires the organic soluble acetate salts, $M(OAc)_2$, but it is possible for the insertion of metals from salts of chloride and sulphate. In the case of $Pt(II)$, the affinity of the Pt^{2+} cation to acetate or chloride ligands is greater than that of the Pt^{2+} to the porphyrin tetradentate ligand. Ligand exchange of acetate to the more labile DMSO ligands or acetoacetate ligands has been employed.¹⁸³ Indeed, various metals have been inserted into the cavity of porphyrins, and sandwich complexes have been isolated and studied. In the case of M^{3+} cations, the tetradentate Por^{2-} ligand is not enough to stabilise the complex alone, therefore axial ligands are almost always required to balance the charge.

The ease of removal of a metal cation from a metalloporphyrin depends on the nature of the macrocycle as well as the metal centre.¹⁸⁴ Alkali and rare earth metals such as: Li, Na, K, Ca, and Ba can be removed by treatment with water.¹⁸⁴ Mg and Zn require dilute acid. Fe, Cu, Co, and Ni require concentrated mineral acids such as hydrochloric acid or sulfuric acid.¹⁸⁴ The reactivity series for the demetallation of metalloporphyrins is given below.

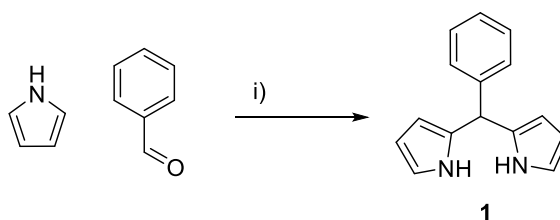


2.4 Synthetic Strategy

The main obstacle in the use of porphyrins for biomedical applications is overcoming the unusual solubilities of these planar tetrapyrrolic macrocycles. Initially, synthetic porphyrins are only soluble in organic solvents, however, they can be derivatized to give porphyrins which are hydrophilic for solubilisation in polar media for ideal drug formulation and administration. In order to improve upon the structure of MLT-005, firstly, a hydrophilic porphyrin needs to be synthesised in order to facilitate radiolabelling and biological evaluation. The aldehyde used to

synthesise the corresponding dipyrromethane had to ideally contain an electron donating group (EDG) to facilitate a high yield of the dipyrromethane and be able to undergo functional group interconversion or derivatisation to give reactive handles or solubilising groups. One strategy is to use a “masked” hydrophilic group, which can undergo functional group interconversion to ‘unmask’ the group and allow it to be used as a solubilisation group or as a handle for bioconjugation or for use in radiochemistry. This synthetic strategy has been employed by Muresan *et al.* in the synthesis of hydrophilic trans-AB-diphenylporphyrins.¹⁸⁵ As Sahin *et al.* outlined, anionic groups are preferred over cationic to reduce non-specific binding to cellular structures.¹⁸⁶ The solubilisation group must be able to be unmasked in a facile single step and must not interfere with any other functional groups present. The challenge presented is the lack of sites for modification on diphenylporphyrins while incorporating solubilising groups and potential handles for bioconjugation in a single small molecule compact motif while still emulating the structure of MLT-005.

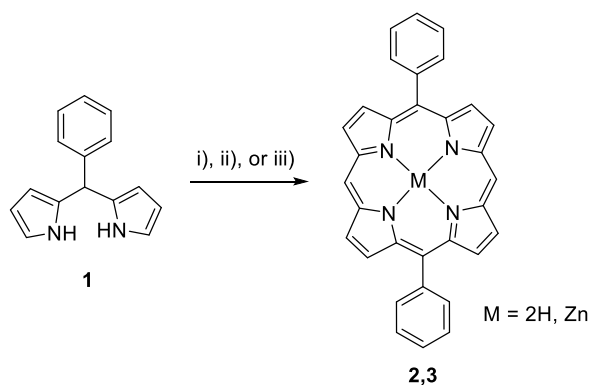
The synthesis of 5-phenyldipyrromethane (**1**) was carried out in neat pyrrole according to the procedure of Brückner *et al.* the acid catalysed reaction proceeded by protonation of the carbonyl group.¹⁷¹ The solution was quenched with weak base and the product was worked-up as a dark brown oil which was purified by flash column chromatography to yield a dark beige solid. For comparison, **1** was synthesised according to the procedure developed by Laha *et al.*¹⁷³ who reported building upon the method of Brückner *et al.* by comparing the use of Lewis acid and Brønsted-Lowry acid catalysis.¹⁷³ The results of which showed that a mild Lewis acid catalyst (InCl₃) gave excellent results, as using TFA led to a higher proportion of oligomers and N-confused dipyrromethanes.¹⁷³ Furthermore, the improvements implemented by Lindsey *et al.* do not require the use of column chromatography for purification. Thus, this method was adopted, obtaining a product which had excellent yield (87%) and purity as shown by CHN analysis (CHN Anal. Calcd for C₁₅H₁₄N₂: C, 81.05; H, 6.35; N, 12.60. Found C, 80.1; H 6.11; N, 12.89.) ¹H- and ¹³C-NMR gave excellent results to confirm the structure of the molecule alongside HRMS. The protons of the pyrrolic nitrogen are very de-shielded so appear at a relatively high chemical shift of 8 ppm, but this can change depending on the electron withdrawing groups (EWG) or electron donating groups (EDG) on the phenyl ring.



Scheme 1. Synthesis of 5-phenyldipyrromethane. Conditions used; i) neat degassed pyrrole, freshly distilled benzaldehyde, indium(III) trichloride, Ar, RT, stir 4 hr.

5,15-Diphenylporphyrin (**2**), DPP, was synthesised according to the method of Brückner *et al.* by the Baldwin modified MacDonald [2+2] condensation reaction.¹⁷¹ Following the procedure, compressed air was used as a mild oxidising agent. Thus, the reaction mixture was purged with compressed air for approximately 4 hrs or until no chlorin could be observed by thin layer chromatography (TLC). Compressed air was used as a mild oxidising agent rather than p-chloranil or DDQ, both of which require exhaustive chromatography in order to remove them. To facilitate good separation and facile purification by flash column chromatography a mobile phase of 1% MeOH in DCM was used. The structure of the purified product was confirmed by ¹H- and ¹³C-NMR by the presence of the *meso*-porphyrin protons present at 10.32 ppm, and the splitting pattern and integration values of the aromatic phenyl and *beta* protons. HRMS and UV-Vis were also used as complementary techniques to confirm the structure. The UV-Vis spectrum revealed that the Soret band was found at 407 nm (Figure 37), compared to 5,10,15,20-tetraphenylporphyrin (TPP) whose Soret band is present at 417 nm. The condensation reaction could be scaled up by a factor of four with a nearly linear response for the yield obtained; *ca.* 14% to give a crystalline purple solid.

A second synthesis route was attempted utilizing paraformaldehyde as a source of formaldehyde and 5-phenyldipyrromethane, catalysed by a few drops of TFA (30 μ L), which led to increased degradation of the DPM. However, the reaction was far more facile, taking only 5 hours compared to over 24 hours. The porphyrin was oxidised from the porphyrinogen by using DDQ and vigorously stirring for 30 mins with an instant darkening of the solution. However, the yield obtained was 6% as opposed to the 17% yield reported by Brückner *et al.* this could be attributed to the poor solubility and reactivity of paraformaldehyde compared to trimethyl orthoformate. Additionally, in terms of health and safety, the use of trimethyl orthoformate is preferred over paraformaldehyde. The use of TFA may have also encouraged acidolysis of the dipyrromethane species and increased the rate of reaction for scrambling of the dipyrromethanes.



Scheme 2. Synthesis of 5,15-diphenylporphyrin. Conditions used; i) degassed DCM, 5-phenyldipyrromethane, trimethyl orthoformate, trichloroacetic acid in DCM, Ar, RT, stir 17 hr. ii) degassed DCM, 5-phenyldipyrromethane, paraformaldehyde, trifluoroacetic acid, Ar, RT, stir 4 hr, DDQ, stir 30

mins. iii) degassed DCM, 5-phenyldipyrromethane, trimethyl orthoformate, trichloroacetic acid in DCM, Zn(OAc)₂ dihydrate, Ar, RT, stir 17 hr.

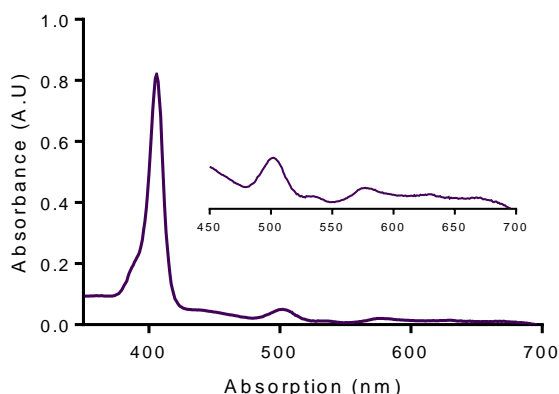


Figure 37. UV-Vis spectrum of compound **2** in DCM.

Clarke *et al.* reported that the condensation of 5-phenyldipyrromethanes with 1,9-diformyl-5-phenyldipyrromethanes produces intermediates which undergo significant twisting of the pyrrole rings.¹⁸⁷ The increase in steric strain may account for the decrease in yield, which may vary with substituents on the 5-phenyl ring. Clarke *et al.* showed that the yield increased by as much as 19%.¹⁸⁷ A test reaction of the [2+2] condensation of two unformylated-dipyrromethanes was carried out in the presence of three M(II) acetates. Zinc(II) acetate dihydrate, nickel(II) acetate tetrahydrate and copper(II) acetate monohydrate were all investigated to provide a *dication* to the reaction mixture, the first two being diamagnetic and the last being a paramagnetic metal when chelated to the porphyrin macrocycle (Table 11). As previously discussed, copper(II) forms thermodynamically and kinetically stable chelates with porphyrins that require concentrated mineral acids to expunge from the centre of the macrocycle. The acetate salts were chosen as the acetate counter ion enhances solubility in the DCM-based reaction mixture. A model one-pot condensation-metallation reaction was carried out with 5-phenyldipyrromethane which showed a significant improvement of the yield obtained, by approximately 20%, upon inclusion of zinc(II).

Dipyrromethane	M(OAc) ₂	% Yield ^a
5-Phenyldipyrromethane	none	9
5-Phenyldipyrromethane	Zn	29
5-Phenyldipyrromethane	Ni	0
5-Phenyldipyrromethane	Cu	0

Table 11. Screening of metal salts used in one-pot porphyrin condensation reactions. ^a Yields reported are from isolated compounds after purification by column chromatography.

Clearly, the use of zinc(II) was advantageous, both increasing the yield obtained, and giving direct access to the synthetically desired and versatile zinc(II) chelate. The use of nickel(II) and copper(II) were found to have deleterious effects on the yield obtained, reducing it to zero. We believe that $\text{Zn}(\text{OAc})_2$ dihydrate dissociates to give Zn^{2+} ions which two dipyrromethane units can chelate around forming a zinc complex. In theory, this would potentially lock the conformation of the dipyrromethanes increasing the rate of formation. The underlying mechanism we propose involves stabilization of the sensitive and sterically ruffled porphyrinogen intermediate by its chelation with zinc. The presence of a Ni(II) template was found to be crucial when forming 5,10,15,20-tetramethylporphyrinogen, and an enhancement in yield was also obtained, compared to the analogous metal-free reaction.^{188,189} We propose that during air oxidation only partial oxidation of the porphyrinogen intermediates occur, with the majority degrading into polypyrrolic materials, but in the case of the metalloporphyrinogen, a greater proportion is oxidized, thus increasing the yield obtained. This reaction gave 29% yield, with an average increase in yield of 13%. As the Zn^{2+} metal is diamagnetic, $^1\text{H-NMR}$ and $^{13}\text{C-NMR}$ could still be easily performed to confirm the structure. The key difference being observed through the use of $^1\text{H-NMR}$ by the loss of the internal protons and, the change in the number of Q bands from four to two in the absorption spectrum (Figure 38).

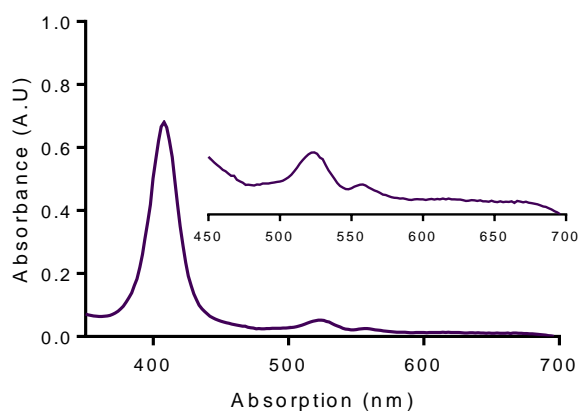
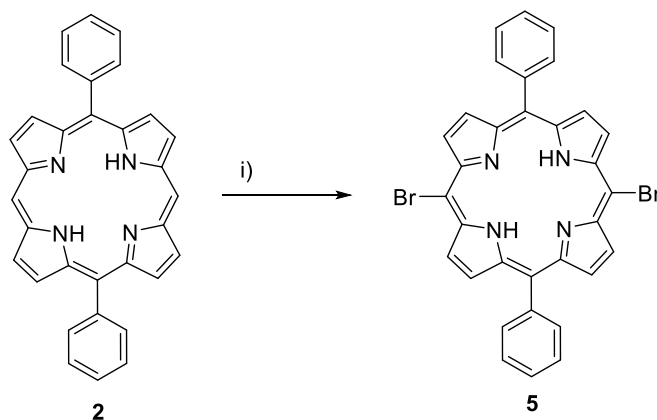


Figure 38. UV-Vis spectrum of **3** obtained in DCM.

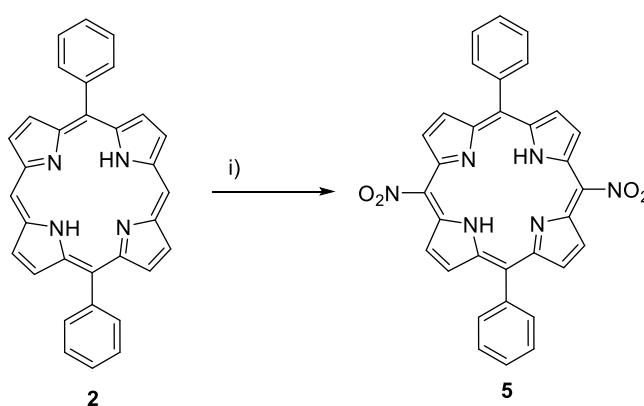
Next, **2** was treated with N-bromosuccinimide in chloroform as a source of bromide anions which could perform aromatic substitution with the reactive *meso*-protons to give **4** in excellent yield (71%), which agreed with the literature.¹⁹⁰ Reportedly, if the temperature was allowed to rise higher than 0 °C then bromination of the *meso*-phenyl rings could occur rapidly, which could be observed by the change of aromatic phenyl substitution patterns from an integration ratio of 3:2 turning to 1:1 with a double doublet splitting pattern. The reaction was thermodynamically controlled, as shown by the rapid process, taking no longer than 10 mins for the complete consumption of the starting material when followed qualitatively by TLC. The $^1\text{H-NMR}$ showed a loss of the proton signals at 10.5 ppm for the *meso* protons indicating the substitution with

bromine had taken place. No splitting or signal changes occurred in the aromatic region, indication bromination of the phenyl ring did not take place. HRMS confirmed the structure with the correct isotope pattern for the presence of two bromines.



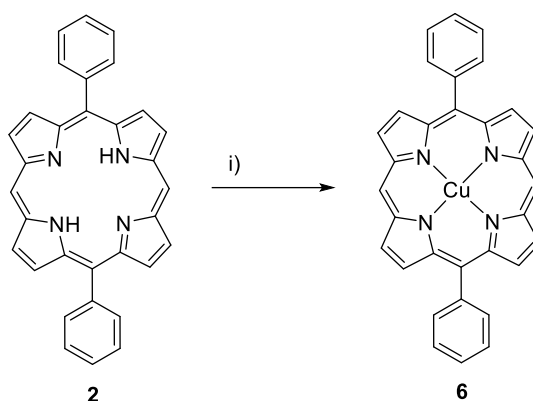
Scheme 3. *Meso*-bromination of 5,15-diphenylporphyrin. Conditions used; i) NBS, chloroform, Ar, 0 °C, stir 10 mins, acetone, stir 30 mins.

Nitration of porphyrins has been achieved by several methods by subjecting them to AgNO_2/I_2 , TFA/ NaNO_2 , and nitronium tetrafluoroborate.^{191,192,193} **1** was treated with sodium nitrite in neat TFA following the protocol of Banfi *et al.*¹⁹⁴. In the case of AgNO_2/I_2 , treatment of the porphyrin with excess iodine oxidises the porphyrin yielding a π -cation radical, treatment of this species with NO_2^- followed by the loss of an electron to a second mole of oxidant and loss of a proton gives the desired product. The dinitro product was formed in good yield and purified by flash column chromatography Both brominating and nitrating in the *meso*-position resulted in the loss of a singlet around 10.30 ppm as shown by $^1\text{H-NMR}$. The structure of the compound was confirmed by HRMS: (ESI+) m/z $[\text{M}+\text{H}]^+$ 553.1613.



Scheme 4. Nitration of 5,15-diphenylporphyrin. Conditions used; i) NaNO_2 , TFA, Ar, 0 °C, stir 30 mins.

The next step was to perform the metallation of the free-base porphyrin to yield the corresponding metalloporphyrin, this was carried out at 90 °C in DMF with $\text{Cu}(\text{OAc})_2$ monohydrate by microwave-assisted heating. Microwave synthesis gave **6** in good yield (64%).



Scheme 5. Metallation of 5,15-diphenylporphyrin. Conditions used; i) $\text{Cu}(\text{OAc})_2$ monohydrate, DMF, MW heating $90\text{ }^\circ\text{C}$ 1 hr.

Unfortunately, ^1H - and ^{13}C -NMR couldn't be carried out as a structural determination technique due to the paramagnetic shift emanating from the metal centre which caused a broadening of the signals. However, UV-Vis spectroscopy confirmed the presence of the metal, and HRMS supported this structure by the presence of the molecular ion and the correct isotope pattern. UV-Vis absorption spectroscopy was most informative as this sensitive technique gave four Q bands for the free base porphyrin, while the metalloporphyrins gave only two Q bands indicating the reaction had gone to completion (Figure 39).

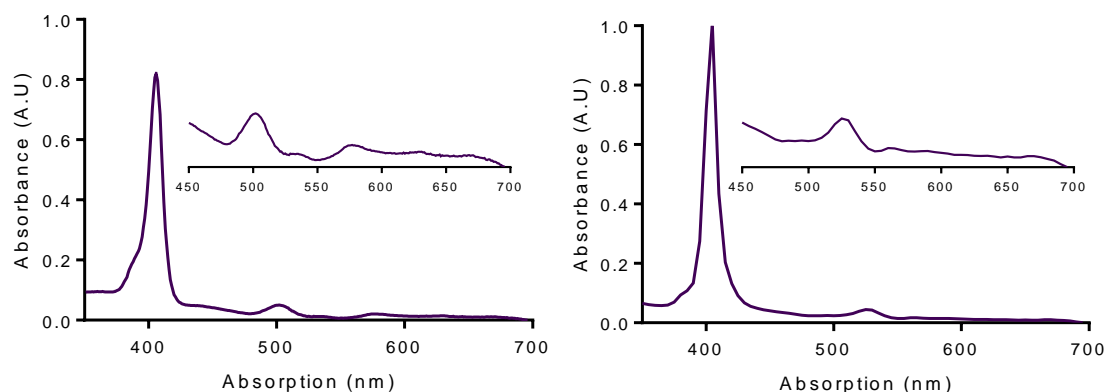
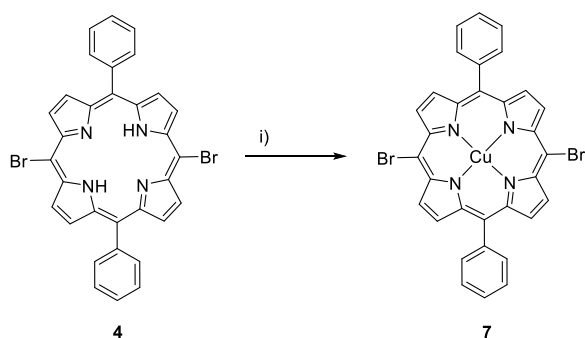
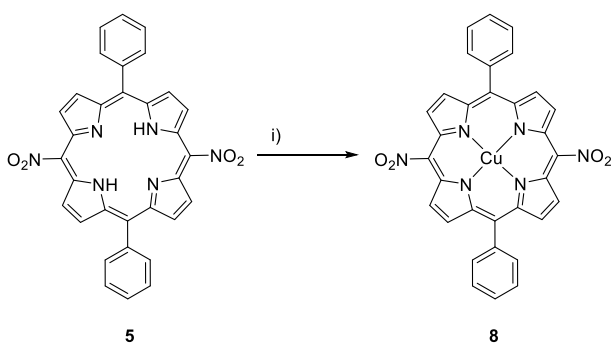


Figure 39. Absorption spectra of **2** (left) obtained in DCM and **6** (right) obtained in DCM.

The next and final step was to carry out the microwave assisted metallation of the 5,15-dibromo-10,20-diphenylporphyrin (**4**) and 5,15-dinitro-10,20-diphenylporphyrin (**5**) with copper(II) acetate monohydrate. Due to the poor solubility of these compounds in common organics solvents, highly dilute reaction conditions were required, therefore, performing this reaction at scale (>30 mg in 30 mL of solvent) required conventional thermal heating at reflux in chloroform for 1 hour. Therefore, porphyrin **7** was synthesised by thermal heating at reflux in chloroform followed by purification by column chromatography to give the metalloporphyrins in excellent yield (96%) respectively. The chelate was characterised by UV-Vis spectroscopy and HRMS.



Scheme 6. Microwave-assisted metallation of **4** with $\text{Cu}(\text{OAc})_2$ monohydrate. Conditions used; i) $\text{Cu}(\text{OAc})_2$ monohydrate, DMF, MW heating 90°C , 1 hour.



Scheme 7. Microwave-assisted metallation of **5** with $\text{Cu}(\text{OAc})_2$ monohydrate. i) $\text{Cu}(\text{OAc})_2$ monohydrate, DMF, MW heating 90°C , 1 hour.

To summarise, the utilization of $\text{Zn}(\text{II})$ as a transition metal scaffold to give direct access to synthetically useful zinc(II) metalloporphyrins has been investigated, not only was this achieved, but we observed an enhancement of the yield obtained after purification by column chromatography. 5,15-Diphenylporphyrin has been derivatised with bromine or nitro electron withdrawing groups in the free meso positions in order to emulate the structure of MLT-005. The free-bases have been chelated to $\text{Cu}(\text{II})$ *via* the use of a microwave reaction giving access to the metalloporphyrins in high yields with minimal reaction times. The main drawback in the use of trans- A_2 -diarylporphyrins is the low yields obtained, the high number of multi-step reactions, and the requirement of column chromatography for purification. For subsequent reactions, the use of $\text{Zn}(\text{OAc})_2$ dihydrate was employed to increase the yield. The obvious next step was to develop a hydrophilic version of this model lipophilic scaffold so that administration to cells in polar media could be carried out. While Smith *et al.* demonstrated that cationic unsymmetrical trans-AB-diarylporphyrins can be effective photosensitizers,¹⁹⁵ they are synthetically difficult to produce at scale and suffer from even lower yields after isolation by column chromatography, and thus the symmetrical trans- A_2 -diphenylporphyrins are the preferred option. In the following sections, the discussion of more hydrophilic porphyrins takes place so that *in vitro* clonogenic assays may take place.

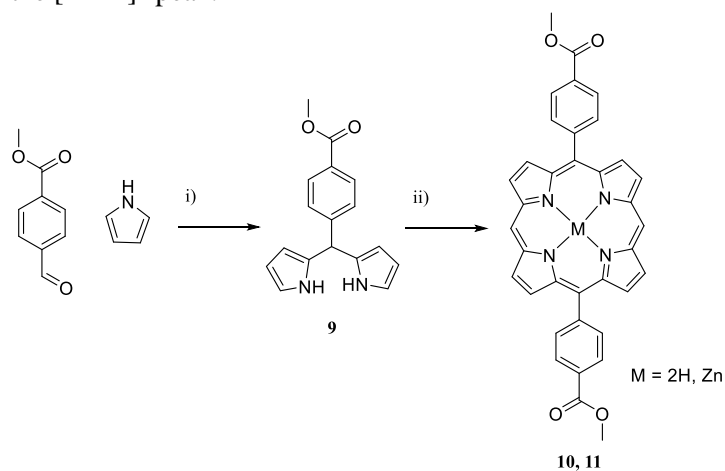
2.5 Synthesis of Hydrophilic Trans-A₂-Diphenylporphyrins

2.5.1 Synthesis of Hydrophilic Carboxylic Acid Trans-A₂-Diphenylporphyrins

Carboxylic acids are important polar functional groups which have been utilized to increase the solubility of organic molecules in polar media. They are capable of hydrogen bonding at the carbonyl oxygen with the lone pairs of electrons, as well as dissociating their proton to become negative carboxylate anions. Muresan *et al.* demonstrated that carboxylate appended diphenylporphyrins can confer some degree of hydrophilicity to the molecule.¹⁸⁵ Lindsey and co-workers also demonstrated that phosphonic acid appended ‘swallow-tail’ alkyl chains are useful solubilizing groups for A₂-porphyrins.^{196,197,198} However, these motifs require complicated advanced multi-step syntheses, air-sensitive reagents, and expensive starting materials.

The dipyrromethane **9** was synthesised from commercially available methyl-4-formylbenzoate according to the method of Laha *et al.* The methyl ester aldehyde was selected over that of the carboxylic acid aldehyde to facilitate column chromatography purification, as the ester is less attracted to silica than the carboxylic acid. Furthermore, the electron withdrawing nature of the carboxylic acid aldehyde would give a low yield of both DPM and trans-A₂-diarylporphyrin. Laha *et al.* reported synthesising 5-(4-carbomethylphenyl)dipyrromethane as yellow crystals, however, in our hands, performing the same solventless synthesis method in neat pyrrole with InCl₃ gave an off-white crude powder. Purification by trituration with hexane followed by overnight recrystallization from ethanol/water (4:1) gave an off-white solid. However, the crude could be purified by precipitation from ethyl acetate over hexane to yield a white crystalline powder. **9** was analysed and gave excellent NMR and near perfect CHN values. CHN Anal. Calcd for C₁₇H₁₆N₂O₂: C, 72.84; H, 5.75; N, 9.99. Found C, 72.94; H 5.92; N, 10.13. HRMS found the m/z [M-H]⁺ 279.1136 indicating the correct molecule was isolated. This DPM was synthesised without the need for column chromatography, and the product was used without further purification in the synthesis of the corresponding porphyrin.

9 was obtained in good yield for a 5,15-diphenylporphyrin, *ca.* 17% after purification by column chromatography and the structures confirmed by $^1\text{H-NMR}$, $^{13}\text{C-NMR}$, HRMS and UV-Vis. This reaction was repeated but with the addition of a methanolic solution of Zn(OAc)_2 dihydrate, as with **2**, gave **10** in a higher yield of 24%. The presence of Zn(II) in the central cavity was confirmed by UV-Vis spectroscopy with the characteristic two Q bands (Figure 40). $^1\text{H-NMR}$ spectroscopy confirmed the structure by the presence of the aromatic double doublet, *meso* protons and *beta* protons, but could not confirm the loss of the internal protons as the sample was insoluble in all common deuterated NMR solvents, so deuterated-TFA was used as last resort to obtain spectroscopic data. HRMS confirmed the presence of the Zn(II) by the expected isotope pattern as well as the $[\text{M}+\text{H}]^+$ peak.



Scheme 8. Synthesis of a metalloporphyrin bearing two ester groups. Conditions used; i) neat degassed pyrrole, methyl 4-formylbenzoate, indium(III) trichloride, Ar, RT, stir 4 hr. ii) degassed DCM, 5-(methylbenzoate)dipyromethane, trimethyl orthoformate, trichloroacetic acid in DCM, Ar, RT, stir 17 hr.

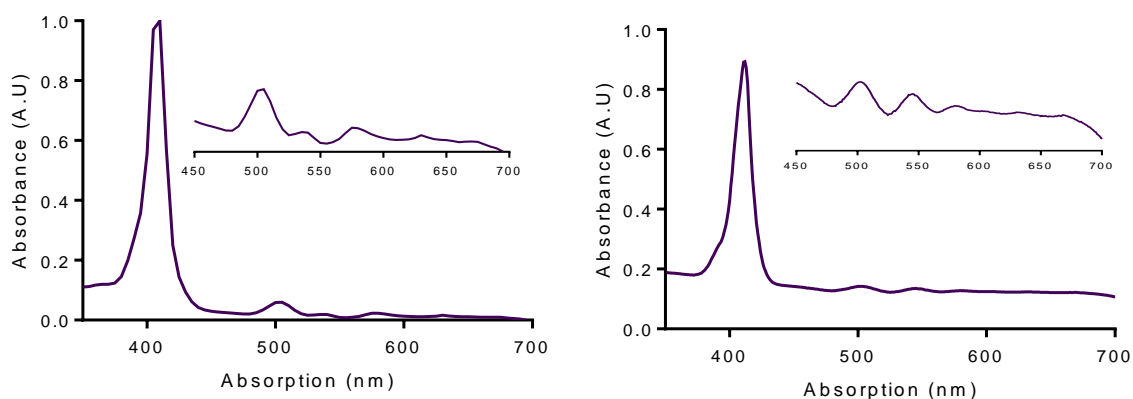
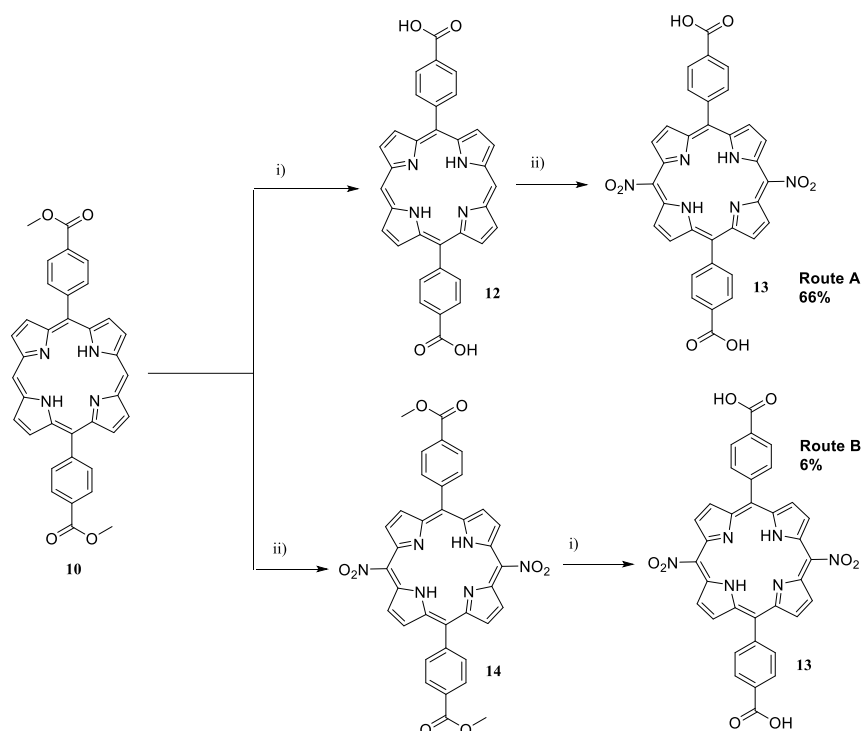


Figure 40. Absorption spectra of **10** (left) obtained in DCM and **11** (right) obtained in DCM.

Interestingly, it was found that once porphyrins **10** and **11** were dried under reduced pressure from DCM they became poorly soluble in DCM. We predict that this is due to π - π stacking of the porphyrins forming hydrophobic aggregates in the semi-polar organic solvent. The next phase in

the synthesis was to determine in which order the subsequent derivatisation reactions should be performed to yield the target 5,15-dinitro-10,20-diarylporphyrin. The two options are nitration followed by saponification or saponification followed by nitration as shown by Scheme 9.



Scheme 9. Two possible synthetic routes to yield the desired 5,15-dinitro-10,20-diphenylporphyrin.

Saponification – Nitration:

Esters can be hydrolysed in concentrated aqueous basic solutions by nucleophilic attack on the carbonyl carbon followed by elimination of the methoxide anion to give the corresponding carboxylic acid after acidic work-up. Saponification of the ester functionality in basic conditions was attempted in numerous solvents due to poor solubility of the compound. DMF/H₂O or DMF/MeOH gave poor results with little to none of the carboxylic acid porphyrin being isolated due to poor solubility of the starting material in the solvent system, even when warming to 50 °C. Attempted saponification in THF/MeOH in basic conditions at 80 °C gave optimal conditions for the hydrolysis of the ester (Table 12). The acidic work-up caused the carboxylic acid porphyrin to precipitate which could be filtered and washed with excess methanol to give the desired porphyrin **12** in virtually quantitative yield (98%).

Entry	Solvent	Base	Temperature (°C)	Time (hr)	Yield (%) ^a
10	DMF / H ₂ O	KOH	RT	24	-
10	DMF/MeOH	KOH	RT	24	-
10	DMF/MeOH	KOH	50	24	73
10	THF/H ₂ O	KOH	50	24	-
10	THF/MeOH	KOH	50	24	94
10	THF/MeOH	KOH	80	24	96

Table 12. Table of attempted saponification reactions for route A. ^aYields reported are from isolated compounds after purification by column chromatography.

Optimal conditions for the saponification of the methyl ester to the carboxylic acid have been determined, with exceptional purity and almost quantitative yield for the THF/MeOH (4:1) solvent system to give compound **12**. Method development with varying base was not undertaken. The structure was confirmed by ¹H-NMR by the loss of the methyl singlet at 4.13 ppm, previously with an integration value of 6H. Neither the carboxylic acid protons nor the internal protons were observed in the CF₃COOD protic solvent. Further reactions employed the THF/MeOH solvent system, which proved to be reproducible.

Compound **12** was nitrated in good yield to give **13** as a purple solid. The nitrating mixture used in this procedure was a mixture of sodium nitrite and TFA, which has been previously reported in the literature (Table 13).^{191,199} The work-up for this porphyrin was simplified due to the porphyrin precipitating out of the acidic solution when diluted and neutralised with saturated aqueous NaHCO_{3(aq)}. The structure was confirmed by the loss of the *meso* protons at 10.40 ppm indicating that nitration had occurred. The porphyrin was DMSO soluble, which has a relatively high dielectric constant when compared to water ($\epsilon_{\text{DMSO}} = 46.7$, $\epsilon_{\text{water}} = 80.1$), indicating that the porphyrin was becoming more hydrophilic. UV-Vis spectroscopy was performed in DMSO which gave an unusually high extinction coefficient for a diphenyl porphyrin with a value of $\log \epsilon = 5.62$.

Entry	Solvent	Reagents	Temperature (°C)	Time (hr)	Yield (%) ^a
12	TFA	TFA/NaNO ₂	0	3	67

Table 13. Table of attempted nitration reactions for route A. ^aYields reported are from isolated compounds after purification by column chromatography.

Nitration-Saponification:

The second route of nitration followed by saponification was attempted. Nitration under conditions used for compound **10** was found to be less than favourable. Two sets of conditions for nitration were attempted using I₂/AgNO₂ in refluxing C₂H₂Cl₂/MeCN according to the method

of Arnold *et al.* (Table 14).²⁰⁰ The reaction proceeds as an oxidative addition of the iodine perpendicular to the plane of the macrocycle in the free *meso*-positions followed by the substitution by the nitrate anion.

Entry	Solvent	Reagents	Temperature (°C)	Time (hr)	Yield (%) ^a
10	TFA	TFA/NaNO ₂	0	3	6
10	C ₂ H ₂ Cl ₂ /MeCN	I ₂ /AgNO ₂	90	17	32

Table 14. Table of attempted nitration reactions for route B. ^a Yields reported are from isolated compounds after purification by column chromatography.

Compound **14** was saponified using concentrated KOH_(aq) in DCM/MeOH, THF/MeOH and DMF/MeOH at 80 °C. The poor solubility of the compound meant different solvents were used to find a method to obtain the maximum possible yield. The bulk solvent was removed under reduced pressure, the solid residue dissolved in water and precipitated from water by the dropwise addition of 1M HCl to give the carboxylic acid from the sodium salt. The resulting data are presented in Table 15.

Entry	Solvent	Base	Temperature (°C)	Time (hr)	Yield (%) ^a
14	DCM/MeOH	KOH	80	17	-
14	DMF/MeOH	KOH	80	17	4
14	THF/MeOH	KOH	80	17	79

Table 15. Table of attempted saponification reactions for route B. ^a Yields reported are from isolated compounds after purification by column chromatography.

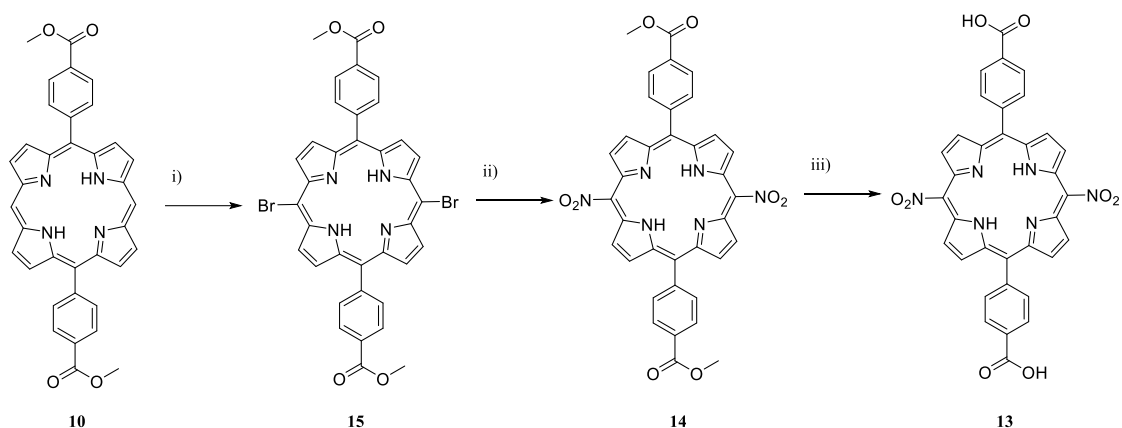
Nitro-debromination:

The synthesis of **10** was repeated. Again, due to the poor solubility of this compound, the reaction conditions had to be optimised through small-scale reactions. The porphyrin was subjected to temperatures of 0 °C with pyridine and N-bromosuccinimide (NBS) and stirred under an inert atmosphere. The reaction was monitored by TLC until all of the starting material had been consumed. The optimal conditions were found to be room temperature in CHCl₃/Py (Table 16).

Entry	Solvent	Reagent	Temperature (°C)	Time (mins)	Yield (%) ^a
10	DCM/Py	NBS	0	10	5
10	CHCl ₃ /Py	NBS	0	10	56
10	CHCl ₃ /Py	NBS	RT	10	81
10	THF/Py	NBS	0	10	36
10	DMF/Py	NBS	0	10	29

Table 16. Table of attempted bromination reactions of **10**.^a Yields reported are from isolated compounds after purification by column chromatography. RT; room temperature.

The reaction was then quenched with acetone and worked-up to yield the 5,15-dibromo product in good yield (81%). The presence of the bromo groups was confirmed by ¹H-NMR by the removal of the *meso* protons at 10.50 ppm. HRMS was obtained and also confirmed the structure as the [M+H]⁺ species. The dibromo species obtained was extremely soluble in DMSO.



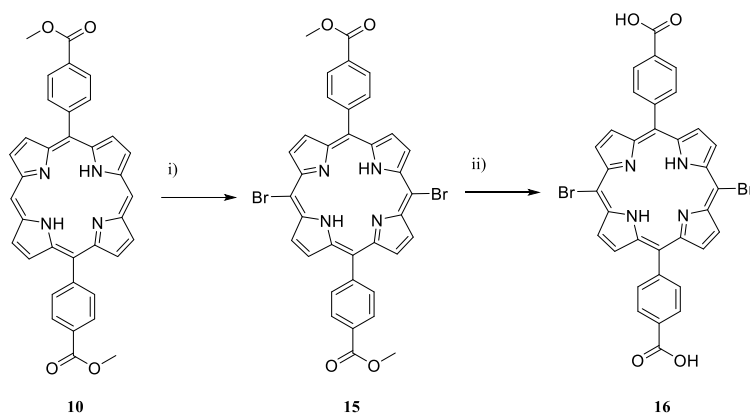
Scheme 10. Synthesis of a meso-brominated metalloporphyrin. Conditions used; i) NBS, CHCl₃, 0 °C, 10 mins. ii) TFA/NaNO₂, 0 °C, 3 hr. iii) KOH, THF/MeOH, 80 °C, 17 hr.

The subsequent nitration reaction was performed under the two conditions given in Table 17. Unfortunately, neither of these two conditions gave acceptable yields, therefore this route was abandoned.

Sample Entry	Solvent	Reagent	Temperature (°C)	Time (hr)	Yield (%) ^a
15	TFA	TFA/NaNO ₂	0	3	9
15	C ₂ H ₂ Cl ₂ / MeCN	AgNO ₂ /I ₂	80	17	-

Table 17. Table of attempted nitration reactions of **15**.^a Yields reported are from isolated compounds after purification by column chromatography.

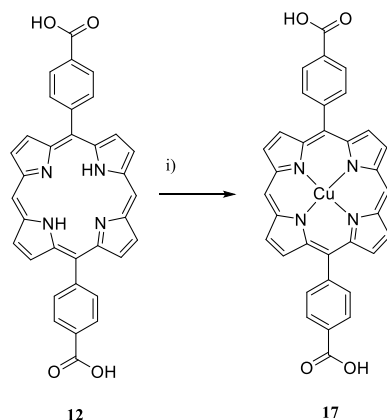
The brominated porphyrin (**15**) was taken and saponified using previously discussed conditions to yield the corresponding carboxylic acid porphyrin (**16**) in good yield (74%). The structure was confirmed by the loss of the characteristic singlet emanating for the methyl group.



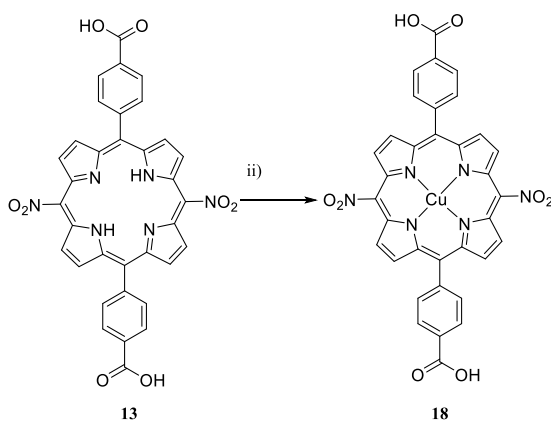
Scheme 11. Synthesis of a *meso*-brominated metalloporphyrin. Conditions used; i) NBS, CHCl_3 , 0°C , 3 hr. ii) KOH, THF/MeOH, 80°C , 17 hr.

Metallation:

Compound **12** was metallated to give the copper(II) chelate of the porphyrin, **17**, under microwave conditions with copper(II) acetate monohydrate. The UV-Vis spectrum revealed that the Soret band had a wavelength of 410 nm and the wavelength of the Q bands were 520 and 555 nm respectively. The porphyrin was slightly soluble in DMSO and very soluble in MeOH. Unfortunately, due to the lack of hydrophilicity of this molecule, it was not investigated as a radiosensitizer.



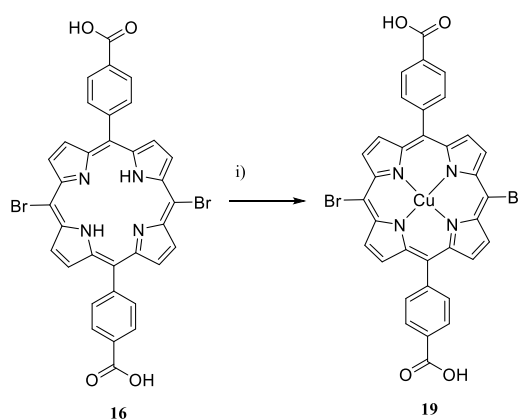
Scheme 12. Synthesis of a hydrophilic metalloporphyrin. Conditions used; i) $\text{Cu}(\text{OAc})_2$ monohydrate, DMF, MW heating 90°C 1 hr.



Scheme 13. Synthesis of a hydrophilic metalloporphyrin. Conditions used; i) $\text{Cu}(\text{OAc})_2$ monohydrate, DMF, MW heating 90 °C 1 hr.

Compound **13** was dissolved in DMF with excess copper(II) acetate monohydrate and heated under microwave irradiation at 90 °C for 1 hour. For compound **18**, the reaction gave a pinky-red solid suspended in the DMF solution. The bulk solvent was removed under reduced pressure and the solids triturated with distilled water. **18** was soluble in DMSO and could be diluted into 1% DMSO in water (~1 mg/mL) with no visible precipitation after 1 hr upon standard at room temperature. The UV-Vis spectrum showed a sharp Soret band at 408 nm with a high extinction coefficient of $\log \epsilon = 5.20$. Compound **18** was selected as a viable candidate for *in vitro* biological evaluation. In terms of structural determination, only HRMS and UV-Vis spectroscopy can be routinely and reliably used for paramagnetic porphyrins. The overall yield of the product after a highly optimized five-step route was 8.5%.

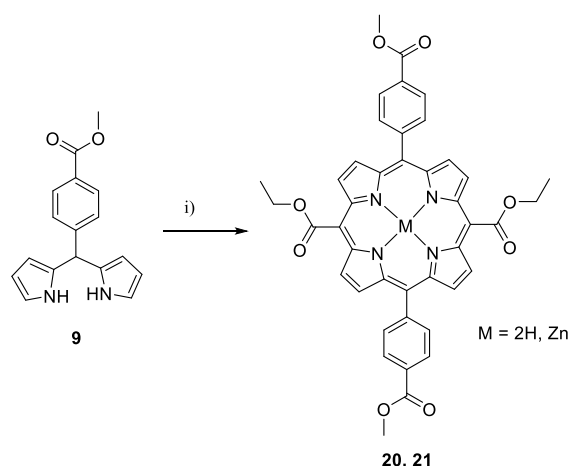
Porphyrin **16** was then metallated as discussed previously with copper(II) acetate monohydrate in DMF to give the corresponding copper metalloporphyrin (**19**) which was confirmed HRMS, however, the porphyrin was found to be insoluble in all common deuterated solvents for NMR studies and did not give optically transparent solutions for photospectroscopic analysis. The porphyrin wasn't soluble in polar solvents such as ethanol, methanol, PBS, media or DMSO. The reduced solubility in polar media could be attributed to the bromo groups on the macrocycle and the removal of the pyrrolic hydrogens which increased the planarity of the ring, causing aggregation in the form of J or H dimers. This porphyrin was an unsuitable candidate for *in vitro* biological evaluation.



Scheme 14. Synthesis of a hydrophilic metalloporphyrin. Conditions used; i) $\text{Cu}(\text{OAc})_2$ monohydrate, DMF, MW heating 90 °C 1 hr.

A synthetic strategy was developed to further increase the solubility of the core motif. Condensation of dipyrromethane **9** was performed with ethyl glyoxylate 50% in toluene rather than trimethyl orthoformate. The oxidation was followed by TLC to reveal no porphyrin had been formed. Instead, condensation of the dipyrromethane under Lindsey conditions with ethyl

glyoxylate in anhydrous DCM with boron trifluoride diethyl etherate as a Lewis acid catalyst was performed.^{201, 202} DDQ was used as a chemical oxidant, rather than using compressed air. The reaction yielded the porphyrin in excellent yield (28%) after successive flash column chromatography, however, these yields were not consistent. Synthesis of the analogous zinc metalloporphyrin was attempted with the addition of zinc(II) acetate dihydrate in excess, but no increase in the yield was observed. Unlike previous conditions, the Lindsey reaction conditions were not amenable to scale up. The structure of the freebase porphyrin was confirmed by the presence of the ethyl groups with a triplet and quartet at 4.18 ppm and 5.09 ppm respectively. As predicted no *meso* protons were observed. The freebase porphyrin showed the two pyrrolic hydrogens at -3.07 ppm and the zinc metalloporphyrin didn't show any pyrrolic hydrogens. Two environments in the ¹³C-NMR spectra were observed for the two different carbonyl carbons. HRMS confirmed the presence of the molecular ion for both compounds. UV-Vis spectroscopy was attempted with four Q bands for the freebase at 509, 550, 590 and 644 nm. The zinc metalloporphyrin only gave two Q bands at 550 and 585 nm.



Scheme 15. Synthesis of a tetraesterporphyrin. Conditions used; i) degassed DCM, 5-(methylbenzoate)dipyrromethane, ethyl glyoxalate, BF₃, Ar, RT, stir 4 hr, DDQ.

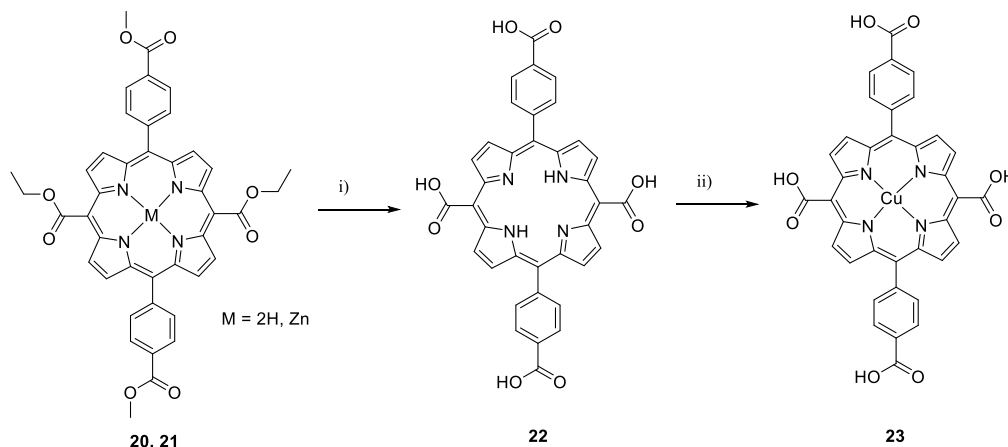
Again, as with the previous ester protected porphyrins, **20** and **21** were saponified in concentrated aqueous basic solutions. This time the reaction proceeded with the loss of methoxide and ethoxide. Saponification of the ester in basic conditions was attempted in numerous solvents due to poor solubility at high concentrations. Attempted saponification in a polar organic solvent with water to dissolve the KOH resulted in the porphyrin precipitating out of solution. DMF/H₂O or DMF/MeOH gave poor results with little to none of the carboxylic acid porphyrin being synthesised due to poor solubility in the media and the porphyrin precipitating. Attempted saponification in THF/MeOH in basic conditions at 80 °C gave optimal conditions for the hydrolysis to the carboxylic acid functional group (Table 18). The work-up for these porphyrins involved the solution being acidified to pH 2 followed by extraction into DCM/THF (1:1) to give the protonated carboxylic acid porphyrin. Work up with zinc metalloporphyrin gave the freebase

porphyrin due to acidification of the pyrrolic nitrogens to give the N-H bonds. This procedure resulted in a facile one-pot saponification/demetallation reaction.

Entry	Solvent	Base	Temperature (°C)	Time (hr)	Yield (%) ^a
20	DMF/MeOH	KOH	80	24	74
21	THF/MeOH	KOH	80	24	88

Table 18. Table of attempted saponification reactions. ^a Yields reported are from isolated compounds after purification by column chromatography.

Once the esters had been fully unmasked the highly hydrophilic 5,15-dicarboxy-10,20-di-(4 carboxyphenyl)porphyrin was revealed. ¹H-NMR showed the loss of the methyl protons at 5.09 ppm and the ethyl protons at 1.74 ppm and 4.08 ppm protons respectively. However, this methodology meant that no nitro groups could be introduced onto the macrocycle. Biological evaluation of these compound would allow for a comparison of whether or not the nitro groups were having a positive effect on the efficacy of the drug compared to the carboxylic acids. Compound **22** was dissolved in DMF with excess copper(II) acetate monohydrate and heated under microwave irradiation at 90 °C for 1.5 hr. The reaction gave a pinky-red solid suspended in the DMF solution. The bulk solvent was removed under reduced pressure and the solids triturated with distilled water. HRMS and UV-Vis spectroscopy were used in tandem to confirm the presence of the metal centre (Figure 41).



Scheme 16. Saponification reaction i) KOH, THF/MeOH, 50 °C, 72 hr. ii) Cu(OAc)₂ monohydrate, DMF, MW heating 90 °C 1 hr.

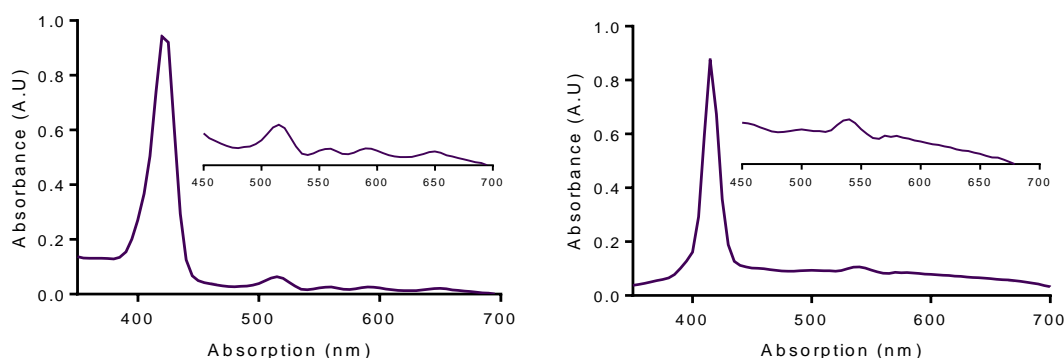
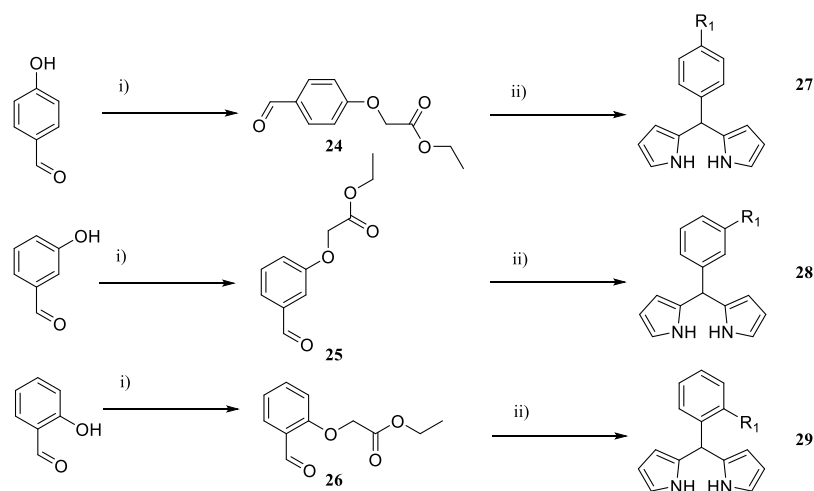


Figure 41. UV-Vis absorption spectrum for compound **22** (left) and **23** (right), exhibiting four and two Q bands respectively.

23 was highly soluble in DMSO and DMSO/PBS 0.1 M. The UV-Vis spectrum showed a sharp slightly red-shifted Soret band at 415 nm with a high extinction coefficient of $\log \epsilon = 5.19$ and two Q bands at 500 and 545 nm indicating complete metallation had been carried out. This compound was selected for *in vitro* biological evaluation.

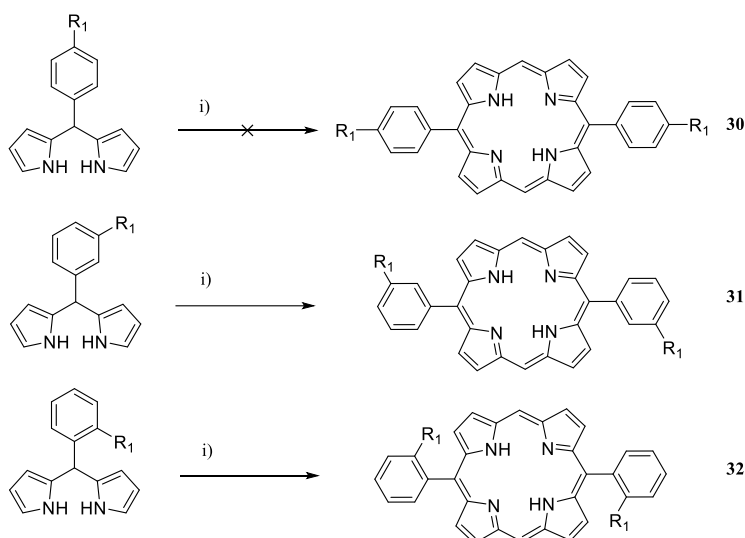
2.5.2 Synthesis of Facially Hindered Hydrophilic Trans-A₂ Diphenylporphyrins

As Tanaka *et al.* demonstrated, diphenylporphyrins have a propensity to aggregate, and this modulates their solubility.²⁰³ Lindsey *et al.* recognised this when developing hydrophilic trans-AB-diphenylporphyrins; Lindsay *et al.* stated that the projection of polar substituents above and below the plane of the macrocycle is expected to suppress co-facial aggregation. In order to further increase the solubility of these molecules while keeping to the MLT-005 motif, a route was developed to yield a diphenylporphyrin which would incorporate a pendant chain which could be unmasked to give a hydrophilic ionisable group to both allow for water solubility and reduced co-facial aggregation. As it was unknown where the chain should be located in 3D space in order to decrease co-facial aggregation and increase the maximum amount of steric hindrance three different aldehydes with the phenolic hydroxyl groups positioned in the *ortho*, *meta* and *para* positions were selected (Scheme 17). The aldehydes were functionalised by reacting regioisomers of salicylic acid with excess ethyl bromoacetate and anhydrous potassium carbonate in anhydrous DMF. Through the Williamson ether synthesis, the three aldehydes were successfully synthesised after purification by column chromatography. The mechanism is dominated by the following process; the phenolic hydroxyl was deprotonated by the carbonate anion to give the phenolate, which attacks the ethyl bromoacetate in an S_N2 reaction followed by the simultaneous elimination of a bromide anion.



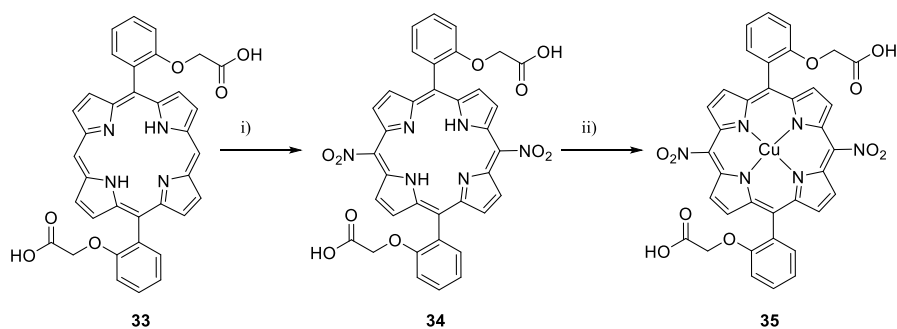
Scheme 17. Synthesis of a library of 'masked' aldehydes. Conditions used; i) 'Aldehyde', K₂CO₃, DMF, 80 °C 17 hr. ii) neat degassed pyrrole, aldehyde **24**, **25** or **26**, indium(III) trichloride, Ar, RT, stir 4 hr.

The structure of the compounds was confirmed by $^1\text{H-NMR}$, $^{13}\text{C-NMR}$, FT-IR, and HRMS as well as CHN for solid samples. The NMR spectra showed the loss of the phenolic hydroxyl proton which was replaced by a singlet at the ether bridge, followed by the acetate group. $^{13}\text{C-NMR}$ indicated the presence of the carbonyl bond in all of the structures. The yields obtained for **27**, **28**, and **29** were found to be 81%, 94%, and 59% respectively. These novel aldehydes were then used to make the corresponding dipyrromethanes by the method described previously. All three of the novel dipyrromethanes were condensed to give the corresponding porphyrins. Porphyrin **30** was isolated in such low yield after successive column chromatography that it was discarded and no longer investigated. Porphyrins **31** and **32** were produced with acceptable yields of 6% and 9% respectively. The splitting patterns of the porphyrins corresponded with the splitting patterns of the corresponding dipyrromethane species shown by $^1\text{H-NMR}$.



Scheme 18. Synthesis of a hydrophilic porphyrin. Conditions used; i) degassed DCM, dipyrromethane **27**, **28**, or **29** trimethyl orthoformate, trichloroacetic acid in DCM, Ar, RT, stir 17 hr.

Attempted saponification of the remaining two porphyrins gave porphyrin **33** in low yield due to poor workup, while porphyrin **35** was isolated in 88% yield. Saponification took place in THF/MeOH (4:1) with potassium hydroxide. The structure of the porphyrin was confirmed by the loss of the ethyl group at 1.05 and 4.04 ppm respectively with no cleavage of the aryl ether bond. Successive nitration was performed, and the product purified by column chromatography in THF to give the saponified “unmasked” porphyrin. The free-base porphyrin was soluble in MeOH, DMSO and sparingly soluble in 0.1 M PBS solution.



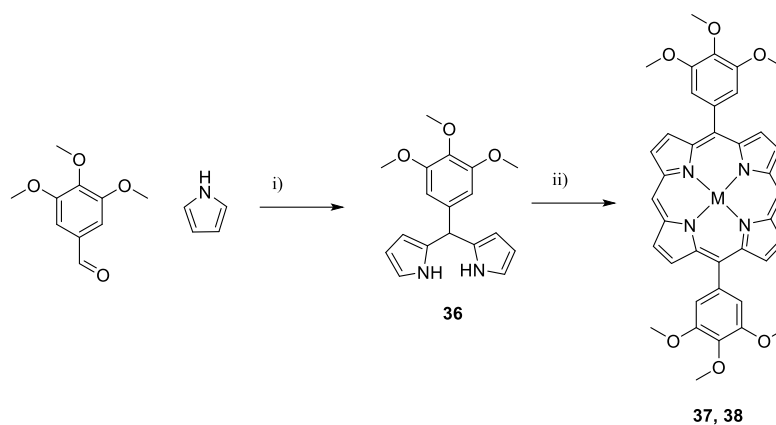
Scheme 19. Synthesis of a facially-hindered hydrophilic porphyrin. Conditions used; i) NaNO_2 , TFA, Ar, 0 °C, stir 30 mins. ii) $\text{Cu}(\text{OAc})_2$ monohydrate, DMF, MW heating 90 °C 1 hr.

Copper(II) was inserted under previously discussed conditions under microwave irradiation. The product was worked up to give a 98% yield (**35**). Unfortunately, this porphyrin was poorly soluble in DMSO and not soluble in 0.1 M PBS, or 1% DMSO in $\text{d}(\text{H}_2\text{O})$. This difference in solubility could be due to the potential coordination of the carboxylate or carboxylic acid functional groups to the copper(II) cation in the porphyrin cavity and the lower pKa of the acidic group. This porphyrin was not selected for investigation as a radiosensitizer.

2.5.3 Synthesis of Super-Hydroxylated Diphenylporphyrin

Hydroxyl groups allow for points of hydrogen bonding and can give a molecule latent hydrophilicity. Phenolic hydroxyl groups are acidic and can be deprotonated in basic solution. In solutions of pH 7.4 which is the pH used in biological experiments, the hydroxyl groups will not readily deprotonate but will still possess latent hydrophilicity and are capable of hydrogen bonding. Hydroxyl groups have been used to render porphyrins water-soluble for biomedical applications. However, highly electron withdrawing hydroxyl groups increase the rate of hydrolysis during the condensation reaction. To overcome this, aryl ethers were used which can be eventually de-protected to give the desired phenolic hydroxyl groups.

36 was synthesised using conditions previously described to give the dipyrromethane in high yield (87%) and excellent purity by CHN: $\text{C}_{18}\text{H}_{20}\text{N}_2\text{O}_3$: C, 69.21; H, 6.45. Found C, 69.29; H 6.39. ^1H -NMR gave the peaks characteristic for a dipyrromethane including the methylene bridge proton as a singlet at 5.29 ppm. The methyl singlets appeared at 3.63 ppm and 3.69 ppm by ^{13}C -NMR respectively. Dipyrromethane **36** was condensed to give **37**, and **38** when the flask was charged with a methanolic solution of zinc(II) acetate dihydrate. The introduction of zinc into the central cavity increased the yield from 13% to a good yield of 26% after successive chromatography. The product gave characteristic peaks of 4.36 ppm and 4.38 ppm for the aryl methyl ethers with integration values of 3H and 6H respectively, the internal protons for the free base porphyrin were at - 3.02 ppm. UV-Vis of the freebase gave peaks at 405, 505, 545, 585 and 635 nm while the zinc analogue gave 415, 550 and 590 nm (Figure 42). For following repeat syntheses the zinc metalloporphyrin was synthesised.



Scheme 20. Synthesis of a hydrophilic metalloporphyrin. Conditions used; i) degassed DCM, dipyrromethane 27, trimethyl orthoformate, trichloroacetic acid in DCM, Ar, RT, stir 17 hr.

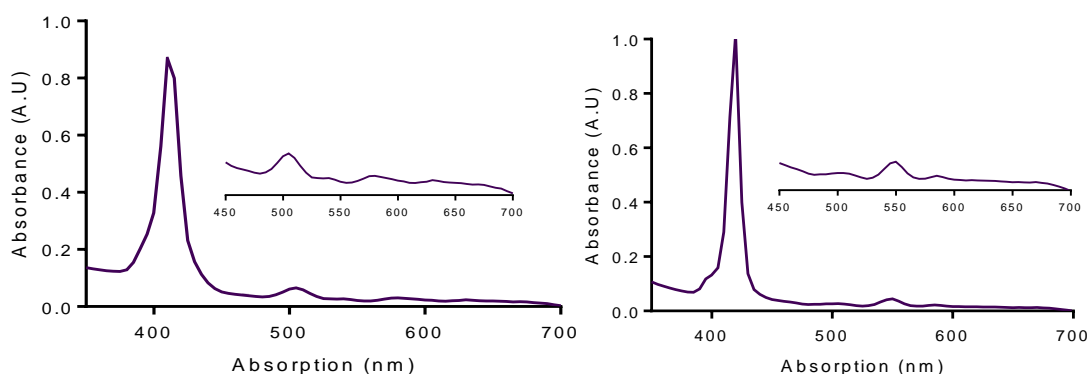
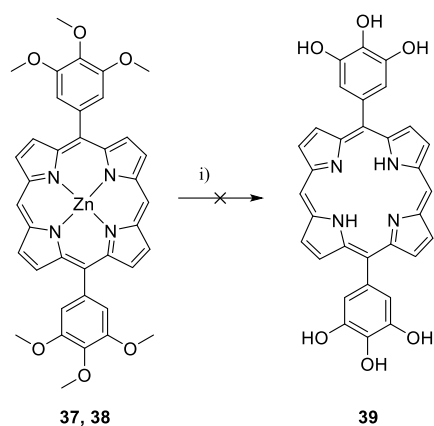


Figure 42. UV-Vis absorption spectrum for compound **37** (left) and **38** (right), exhibiting four and two Q bands respectively.

The products **37** and **38** were treated with BBr_3 (1 M in DCM), which is a powerful Lewis acid which coordinates to the oxygen, by losing a bromide anion which in turn demethylates the aryl methyl ether to evolve methyl bromide. Water or methanol can be used to hydrolyse the intermediate which gives the corresponding alcohol product. The reaction proceeds with the evolution of hydrogen bromide which is a strong acid and demetalates the porphyrin to give the free-base analogue. This procedure served as a one-pot demethylation-demetalation reaction. The product was worked up as a purple crystalline solid. In order to achieve full demethylation, the flask was charged several times with boron tribromide over several days in order to push the reaction to completion. Unfortunately, the sample was worked up and found to be highly insoluble in common solvents used for NMR and UV-Vis spectroscopy, it was also found to be very pH sensitive, dissolving only sparingly in basic solution but not in pH 7.4 PBS. Qualitative UV-Vis photospectrometry showed that the porphyrin had been de-metallated by the HBr by-product, as indicated by the presence of four Q bands. Attempted accurate mass of the sample only yielded background ions. Further investigation with this set of compounds was discontinued.



Scheme 21. Synthesis of a hydrophilic metalloporphyrin. Conditions used; i) BBr_3 1M in DCM, RT, overnight.

Overview of Synthesis:

Briefly, a small library of functional hydrophilic diphenylporphyrins has been synthesised and fully characterised where possible. Unfortunately, only a few members of the library possessed the relevant hydrophilic properties in order to be hydrophilic enough for formulation in media. Selected candidates (Figure 43) were carried forwards for *in vitro* biological evaluation to determine their efficacy as photosensitizers or radiosensitizers.

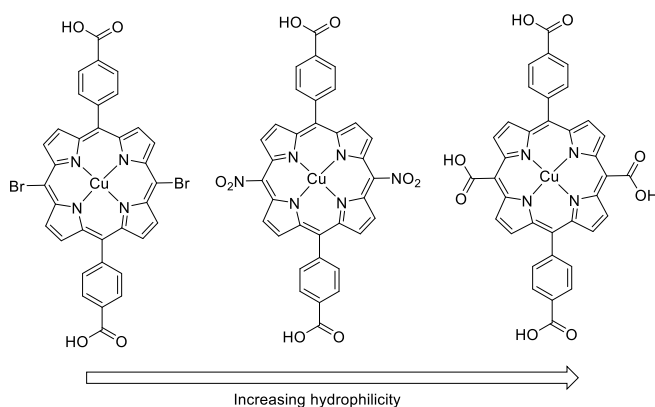


Figure 43. A pictorial representation of the three potential compounds in order of increasing polarity.

2.6 Radiobiological Evaluation of Hydrophilic Metalloporphyrins

Pre-clinical evaluation of potential radiosensitizers can generally be performed by two main biological assays for the determination of cell-viability through *in vitro* experiments:²⁰⁴ the first method is the colony forming assay, the second method is the MTT/MTS assay.^{205,206} Both methods are well known for their use in studying the effects of ionizing radiation on a given cell line.^{205,207} The MTT assay is based upon the reduction of a yellow water-soluble tetrazolium salt to form a purple insoluble formazan dye by metabolically active cells.²⁰⁵ The reduction process occurs in the mitochondria and the cytoplasm by redox active cytochromes.^{208,209} Therefore, the absorbance of the samples can be related to the number of viable cells.²⁰⁵ Typically, in the field

of radiobiology, there are two plating methods, plating before treatment with ionizing irradiation or plating after treatment with ionizing radiation.²⁰⁵ The colony forming assay is an *in vitro* cell number/viability assay based on the ability of the single cell to grow into a colony.^{210,211} The definition of a colony in this context is the agglomeration of 50 cells.²¹⁰ According to the literature, the clonogenic assay is the gold-standard for radiation sensitization experiments.²¹⁰ The procedure used through the *in vitro* experiments was adapted from that of Miller *et al.* and Franken *et al.*²¹² The most commonly used histological dye to visualize cells and colonies for clonogenic assays is a cationic phenylmethane salt, crystal violet. Typically, cell membranes are permeabilised and fixed using an aqueous solution of the dye in methanol to fix and stain the cells. The dye is a DNA intercalator which sits in the major groove in the DNA helix.²¹³

The aim of both of the assays is to determine the relative changes of cell number/viability after cells are exposed to a given stressor. However, the assays do not determine the amount of cell death *per se*, rather they measure the ability of cells to reduce MTT into formazan or, in the case of clonogenic assays, a reduction in colony numbers. In the case of clonogenic assays, the crystal violet dye cannot distinguish between dead cells or cells which have entered cell cycle arrest, neither of which can proliferate into colonies. The surviving fraction is determined by the following equation (Equation 11).²¹⁴

$$\text{Plate efficiency (PE)} = [\text{colonies counted} / \text{cells seeded (non-irradiated)}] \times 100 \quad (10)$$

$$\text{Surviving fraction (SF)} = [\text{colonies counted} / (\text{cells seeded} \times \text{plating efficiency})] \quad (11)$$

The influence of chemical agents on radiation dose survival curves can be analysed using the clinically relevant linear-quadratic model (LQM, Equation 12).²¹⁵ The LQ model is a mechanistic model derived from cell death.²¹⁶ The underlying application of the LQ model is the use of fractionation, which effects the misrepair of primary lesions such as double-strand breaks or damage to heterocyclic bases.²¹⁶ The linear parameter α , represents the lethal damage from single particle events and describes the low dose area.²¹⁵ The quadratic parameter, β , indicates sublethal damage and dominates at higher doses of ionising radiation. By comparing the ratios of these α and β values we can determine whether the drugs are having an effect on the linear or the quadratic aspect of the radiotherapy.²¹⁵ Typically, low doses of ionizing radiation (0-4 Gy) lie within the linear section of the curve, while higher doses (>4 Gy) lie within the quadratic region.

$$\frac{S_D}{S_0} = \text{Exp}^{-(\alpha D + \beta D^2)} \quad (12)$$

Clonogenic experiments are highly dependent on the scheduling as it plays a vital role in the biological response. For example, experimentation with the concentration of the drug, cell number, ionizing radiation dose, time of delivery, multiple doses of the drug and ionizing radiation, oxygen concentration and temperature are all variables that have been studied in the

literature. The overall scheduling used was developed to mimic what would take place in the clinic to obtain the most clinically relevant results. As discussed in Chapter 1, ideally, a clinically viable radiosensitizer would operate within a dose range of 0-4 Gy. Irradiation of the cells was carried out using a BioRad RS-2000 X-ray biological irradiator which was previously been calibrated as according to the literature.²⁰²

In order to obtain clinically relevant results, a robust cell line which is noted for being radioresistant and stems from a cancer type for which radiotherapy is used as a curative or palliative technique to control the cancer was chosen. To satisfy this, we selected the adherent human colorectal cancer (HT-29) which is an epithelial adenocarcinoma originating from the lining of colorectal glands from a 44-year-old Caucasian woman.^{217,218,219,220} This cancer cell line is p53 null, p53 is a fundamental factor in preserving genome stability and in the DNA damage response. p53 expression and function are lost in the majority of solid tumours, and this loss is associated with tumour progression and therapy resistance. In order to determine the drug candidate's efficacy effectively, a p53 WT cell line was also selected, we opted for the adherent human colorectal cancer (HCT-116), this epithelial carcinoma has a mutation in codon 13 of the ras proto-oncogene. Below, the typical epithelial morphology of these two adherent colorectal cancers can be seen by bright field micrographs of the cancers grown on coverslips with a confluence of 60-70% (Figure 44). Incident rates and mortality rates of colorectal cancers are high worldwide, and 50% of patients with colorectal cancers have a localized return and suffer from metastases.^{221,222}

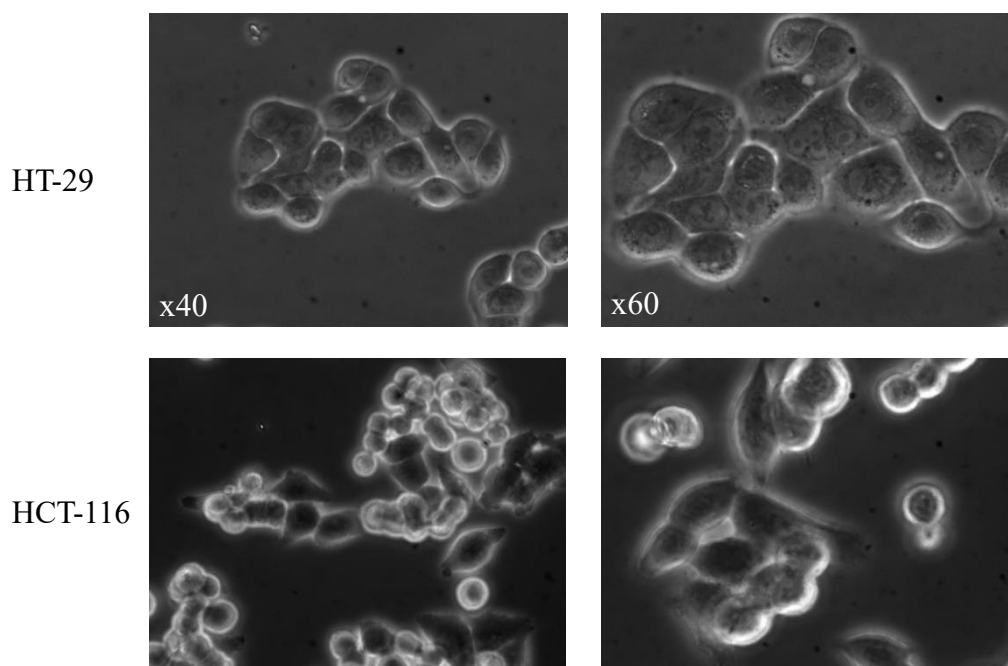


Figure 44. Brightfield optical micrographs of HT-29 (p53 null) cells (top) grown on glass coverslips, brightfield optical micrographs of HCT-116 (p53 WT) cells (bottom) grown on glass coverslips.

Both of these cell cultures morphologically form monolayers when confluent and were found to be consistent with the morphologies published in the literature.²²⁰ HT-29 (p53 null) has been tested for radiosensitization using various drugs at concentrations in the order of micromolar to millimolar levels.²²³ Adenocolorectal cancers have a high mortality rate of around 50%, of which 30% of patients have advanced diseased states at presentation.²²⁴ Cells being deficient in p53 protein limits their ability to undergo apoptosis when exposed to a stressor and cell cycle arrest is hindered.^{225,226} Therefore, any death occurring in HT-29 (p53 null) is predominantly not mediated by p53 pathways when compared to wild type (WT) p53 cells.^{225,227} In a study of 56 colorectal cell lines over 75% were found to be TP53 mutants and demonstrated their resistance to irradiation.²²⁸

The scheduling of these experiments consisted of incubating the cells for 1 hour followed by replenishing the media then irradiating the cells under normoxic conditions to minimise any downstream effects from the drug post-irradiation. Any effects occurring during the experiments could then be attributed to the porphyrins either binding to the membrane of the cells or being internalised and not effects from the unbound drug in the media. Radiobiological experiments herein are broken down into their administration schedules.

The selected drug candidates are given below (Table 19). In terms of translation to the clinic, the product could be supplied as a reddish-purple powder and has a shelf life of several years when correctly stored in the freezer in a sealed glass silicate vial under argon. The appropriate amount of the drug could be weighted and constituted in the delivery vehicle ready for intravenous infusion/injection. The cells were incubated with the drug candidates at three concentrations: 1 μM , 25 μM , and 50 μM . Ionising radiation doses of 0, 2, 4, 6 and 8 Gy were chosen as it is a common range of doses used for the investigation of radiosensitizers by *in vitro* examination.⁸² A viable candidate could be moved onto development to be a targeted theranostic radiosensitizer provided that it had desirable enhancement parameters.

Entry	Structure	Delivery Vehicle
18		1% DMSO in Media
23		<1% DMSO in Media

Table 19. Key hydrophilic copper(II) chelated trans-A₂-diphenylporphyrins for *in vitro* evaluation of the porphyrin macrocycle.

2.6.1 Pre-Clinical Drug Formulation

The reddish-purple crystalline solids, **18** and **23**, were taken up in sterile DMSO (Sigma Aldrich; Hybri-Max™ >99.7%.) to give a concentrated intermediate stock solution followed by dilution into McCoy's 5A modified media (Life Science Productions) and the concentration adjusted by UV-Vis photospectrometry. The stock was filtered through a 0.22 μm filter (Starlab; PES membrane, diameter = 33 mm) and sequentially diluted into McCoy's 5A modified media (Life Science Productions) to give 50 μM, 25 μM and 1 μM solutions of the compound with a final DMSO concentration of <0.1 %. The delivery vehicle used for biological assays was 1% DMSO in media which is known to be a non-toxic delivery vehicle for use in clinical applications. Higher concentrations of **23** could be obtained due to its significantly higher solubility in the vehicle. 1% DMSO was used as a control versus cell-only samples. After 7 days of incubation, the delivery vehicle was not statistically different and didn't cause any acute toxicity. Furthermore, we observed that the presence of 1% DMSO does not cause any statistical difference in cell death by the inhibition or quenching of cytotoxic radicals formed *via* radiolysis (Figure 45).

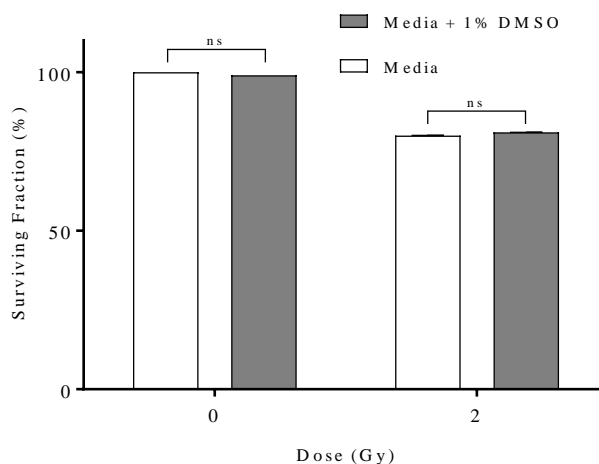


Figure 45. Screening of the delivery vehicle for incubation of the drug candidates with the cells. The graph shows the mean percentage of the surviving fraction of cells incubated with media alone versus media supplemented with 1% DMSO. Bars represent $\bar{x} \pm SD$ ($n=3$). Statistical analysis was performed using the double-sided unpaired Student's t-test. ns; $p>0.05$, *; $p<0.05$, **; $p<0.01$, ***; $p<0.001$, ****; $p<0.0001$.

2.6.2 Dose-Response Curves of HT-29 and HCT-116

In order to begin clonogenic assays, first, the response of the HT-29 (p53 null) and HCT-116 (p53 WT) cell lines to ionizing radiation had to be measured. The dose-response curve shows what dose of ionising radiation is required in order to yield a given biological response. The dose-response curves (Figure 46) highlight that the ionizing radiation dose to cause 50% growth inhibition (ID_{50}) for a non-collimated source of low LET X-rays were found to be 3.13 Gy and 2.79 Gy for HT-29 (p53 null) and HCT-116 (p53 WT) respectively. These data agree with the predicted curve for cells treated with low LET ionizing radiation. Furthermore, these agree with the hypothesis that the cancer cells with WT p53 will be more susceptible to ionizing radiation.

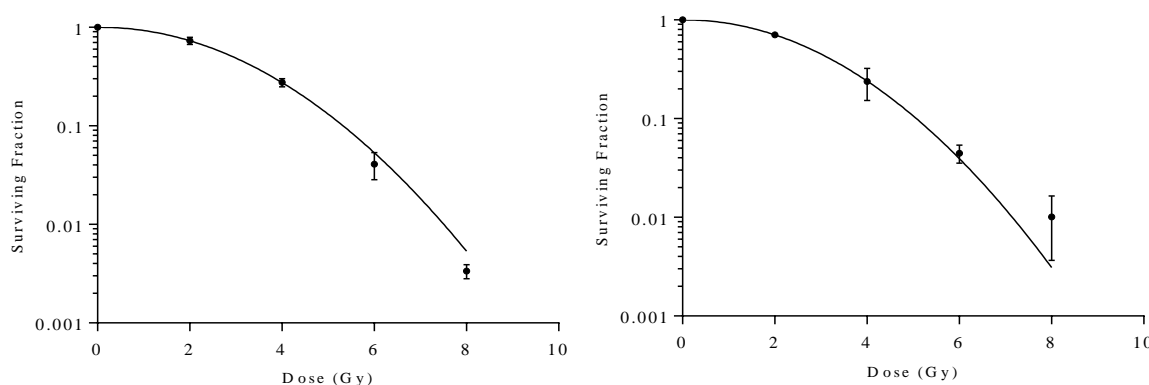


Figure 46. Dose-response curve for the interaction of HT-29 (p53 null) cells (left) and HCT-116 (p53 WT) (right) with non-collimated ionising radiation (0-8 Gy) under oxyc conditions. Data plotted represent mean values $\bar{x} \pm SD$ ($n=3$).

2.6.3 Quantification of Drug Internalisation by ICP-OES

Typically, porphyrins used in biomedical applications are highly fluorescent which means that *in vitro* live cell fluorescence microscopy can be used for intracellular bio-distribution determination, however, copper(II) porphyrins have their excited state lifetimes diminished by the paramagnetic metal.²²⁹ Thus, in order to determine whether or not the two compounds could be internalised by the cells or whether they would attach to the membranes a simple incubation experiment was carried out. 6-Well plates were seeded with a fixed concentration and number of cells and allowed to attach overnight. In the following day the compounds were administered to the cells in triplicate. The cells were incubated with the compounds for 1 hour, followed by washing the wells with PBS. The cells were trypsinized from the plates and were collected by centrifugation. The cells were re-suspended in fresh PBS and pelleted again by centrifugation. The PBS was decanted and the pellets washed with d(H₂O) followed by removing traces of the water by lyophilisation. The pellets were digested in *aqua regia* and analysed by inductively coupled plasma optical emission spectroscopy (ICP-OES). The data are presented in the figure below (Figure 47).

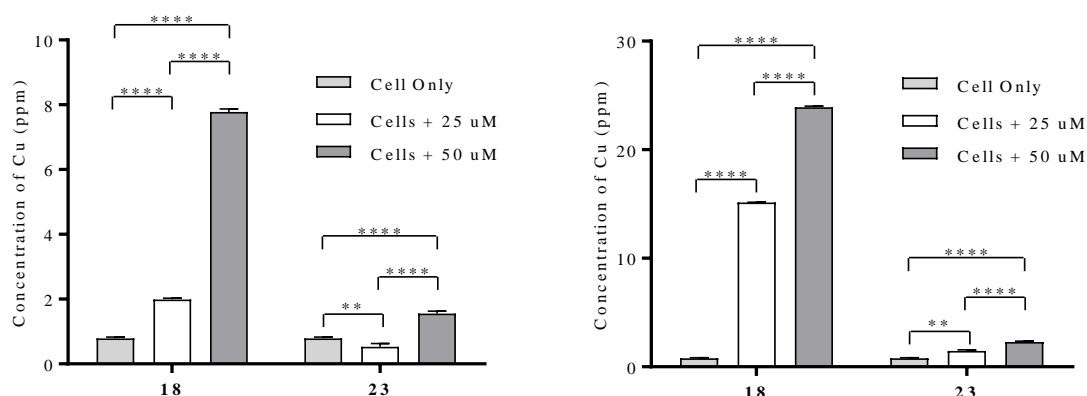


Figure 47. ICP-OES data for compounds **18** and **23** incubated into HT-29 (p53 null) (left) and HCT-116 (p53 WT) (right) for 1 hr followed by centrifugation and washing. Bars represent $\bar{x} \pm SD$ (n=3). Statistical analysis was performed using multiple double-sided unpaired Student's t-test. ns; p>0.05, *, p<0.05, **, p<0.01, ***, p<0.001, ****, p<0.0001.

Clearly, a concentration-dependent response was observed with **18**. **23** also had a concentration dependency, but to a lesser effect. The relative observed levels of Cu from **18** were far higher than **23** in both of the cell lines. Interestingly, the magnitude of the observed levels of Cu from **18** was significantly higher in HCT-116 (p53 WT) than HT-29 (p53 null). From this data, it would not be surprising if the desired radiosensitizing effect of **18** was higher than **23** due to the levels of internalization alone. The differences could be due to the **23** possessing two extra carboxylic acids which may inhibit internalization.

2.6.4 MTT Assays for Cell Number/Viability

In order to determine whether the compounds possessed any intrinsic cytotoxic effects which would affect the cell number/viability of HT-29 (p53 null). A time-course MTT assay was performed to determine the ‘dark’ cytotoxicity of the two porphyrins. When the HT-29 (p53 null) cells were incubated with various concentrations for up to 72 hour a time-dependent toxicity was observed. The data for **18** are shown in Figure 48 and data for **23** by Figure 49. The results from the MTT assay are clear, administration of 1-50 μM concentrations of compound **18** caused no significant cytotoxic/cytostatic effects over a course of 24 hour ($p>0.05$). However, after 48 hr there were statistically significant variations in cell number/viability observed. Therefore, an incubation period of <24 hour should be used for clonogenic assays or the compound would be expected to have deleterious effects on cell number.

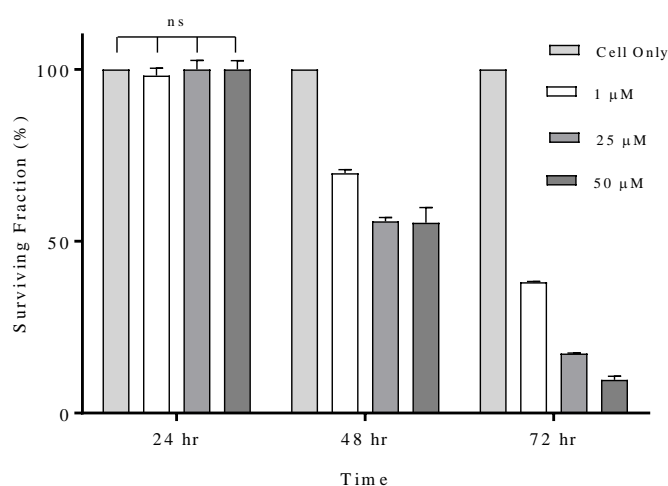


Figure 48. MTT cell number surviving fraction data for **18** in HT-29 (p53 null) measured every 24 hr for 2 hrs. Bars represent $\bar{x} \pm \text{SD}$ ($n=3$). Statistical analysis was performed using multiple double-sided unpaired Student's t-test. ns; $p>0.05$, *; $p<0.05$, **; $p<0.01$, ***; $p<0.001$, ****; $p<0.0001$.

23 was found to have a statistically significant ($p<0.001$) negative effect on the cell number when incubated with 25 μM or 50 μM concentrations at the 24 hour time point, which is surprising considering the ICP-OES results suggest there is a far lower concentration of this compound being internalised by the HT-29 (p53 null) cells.

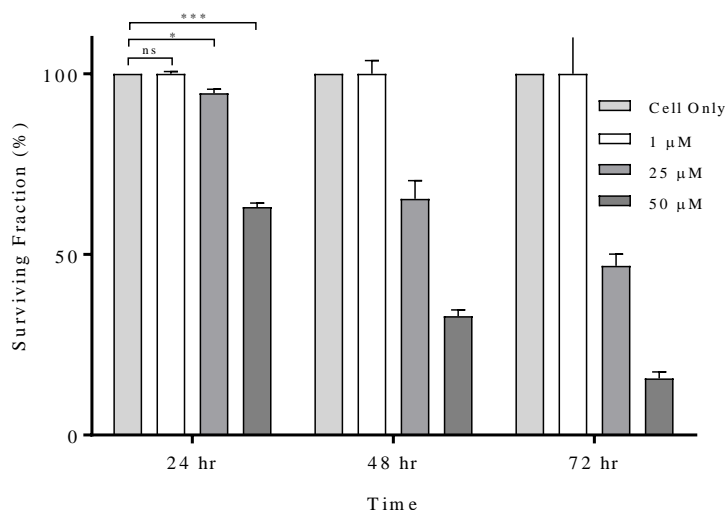


Figure 49. MTT cell number surviving fraction data for **23** in HT-29 (p53 null) measured every 24 hr for 2 hrs. Bars represent $\bar{x} \pm SD$ (n=3). Statistical analysis was performed using multiple double-sided unpaired Student's t-test. ns; p>0.05, *; p<0.05, **; p<0.01, ***; p<0.001, ****; p<0.0001.

2.6.5 5,15-Dinitro-10,20-diphenylporphyrins Cause Sensitization of Colorectal Cancers to Ionizing Radiation

The main radiobiological enhancement factors to be investigated are the dose modifying ratio (DMR, Equation 13), and the radiation enhancement ratio (RER, Equation 14), equations given below.^{204,230} Another useful parameter is the α/β ratio which denotes whether a compound is having an effect on the lethal factor (α) or sub-lethal factor (β) compared to the measured untreated control.²³⁰ For a molecule to be classed as a radiosensitizer the DMRs and RERs must be greater than 1.00. Excellent radiosensitizers will yield values greater than 1.50. Initially, all clonogenic assays were carried out using dosing schedule 1 (Table 20).

$$DMR_{x\%} = \frac{D_{Control}}{D_{Drug}} \text{ (for } x\% \text{ survival)} \quad (13)$$

$$RER_{xGy} = \frac{SF_{xGy Control}}{SF_{xGy Drug}} \text{ (for } x \text{ Gy)} \quad (14)$$

Schedule 1:

Day 1	Day 2	Day 3	Day 4	Day 5	Day 6	Day 7
Incubation with the drug for 1 hr. Media is replenished. Plates are irradiated.	Incubate	Incubate	Incubate	Incubate	Incubate	Cells are fixed. Plates are dried and counted.

Table 20. Schedule 1 ionising radiation therapy routine.

Radiosensitization experiments were performed by carrying out clonogenic assays (**18**) DMR and RER factors were calculated where possible (Table 21). The results fitted to the LQM are given by Figure 50.

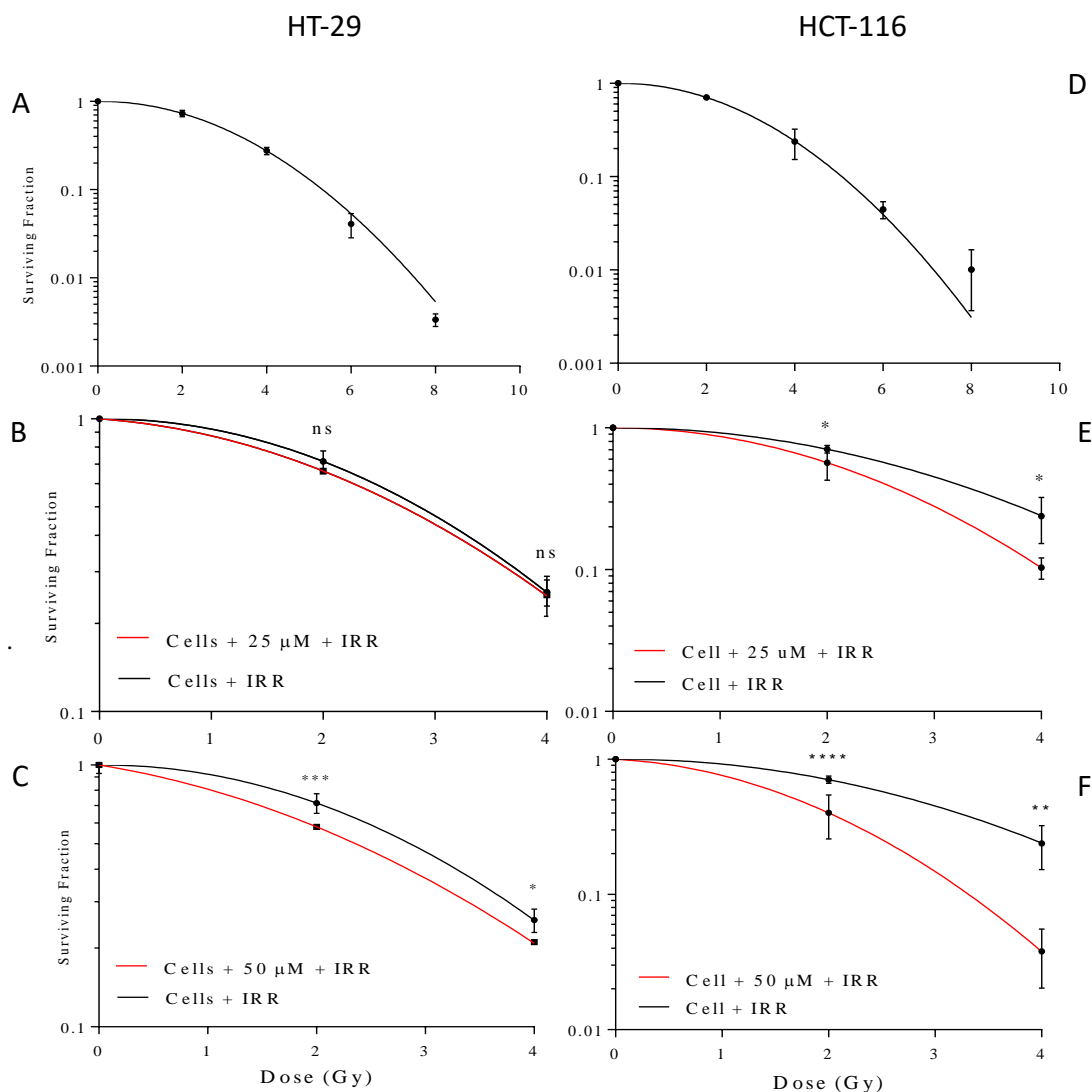


Figure 50. Dose-response curves of HT-29 (p53 null): A; cell only, B; 25 μM , C; 50 μM . Dose-response curve of HCT-116 (p53 WT): D; cell only, E; 25 μM , F; 50 μM . IRR = Irradiated. Data points represent $\bar{x} \pm \text{SD}$ ($n=3$). Statistical analysis was performed using a two-factor ANOVA with Bonferroni's multiple comparisons *post-hoc* significance testing. ns; $p>0.05$, *; $p<0.05$, **; $p<0.01$, ***; $p<0.001$, ****; $p<0.0001$.

A clear dose-dependent relationship was observed within both cell lines with regard to surviving fraction with sensitization occurring in the clinical dose range of 0-4 Gy. Significant sensitization enhancement values were obtained with HCT-116 cells (p53 WT), and less so in HT-29 (p53 null) cells at a dose of 50 μM . Good sensitization enhancement ratios were observed in HCT-116 cells, with a 25 μM incubation of compound **18**, but not in HT-29 (p53 null) at this concentration. These data are summarized in Table 21. At a dose range of 6 Gy to 8 Gy over 90% of the cells become

non-viable, as is expected at high doses, furthermore, at these high doses we cannot determine any clear radiosensitisation, due to the small number of cells counted the error in these measurements increases beyond what is acceptable. We would expect that the presence of p53 in HCT-116, a greater effect on cell viability should be observed, due to the cells entering cell cycle arrest after irradiation, limiting their ability to proliferate thus reducing the observed number of colonies.

Entry	Cell Line	Dose (μM)	RER _{2 Gy}	RER _{4 Gy}	DMR _{10%}	DMR _{25%}	DMR _{50%}
18	HT-29	50	1.24	1.26	1.79	1.48	1.22
	HCT-116	25	-	2.31	-	1.24	1.24
		50	1.74	6.20	2.26	1.74	1.69

Table 21. Tabulated data representing the RER and DMR factors calculated using equations 17 and 18. RER; radiation enhancement ratio, DMR; dose-modifying ratio.

The greatest effects were observed at the highest concentration, with little observable intrinsic toxicity, therefore any observed effects can be said to be due to the effects of the radiotherapy and radiosensitization. These data highlight that a radiation dose-dependent relationship can be seen through the RER. The trend exists whereupon increasing from 2 Gy to 4 Gy the enhancement is greater, additionally, the RER increases with increasing concentration of compound **18**. In HT-29 (p53 null), RER values of 1.24 and 1.26 for 2 Gy and 4 Gy respectively at 50 μM were obtained. At higher doses of radiation, minimal enhancement was observed due to the error in measurement of a small number of colonies. These radiation iso-dose values indicate that at an ionising radiation dose of RER_{2 Gy} a 24% increase in cell death is observed, and similarly for a RER_{4 Gy} a 26% increase in cell death is observed at 50 μM . In HCT-116 (p53 WT), significantly higher values were obtained, likely due to the presence of p53. Again, an increasing trend can be observed for the calculated DMR values. Interestingly, the DMR is higher for the α component of this curve when treated with low LET ionizing radiation. In real terms, a DMR_{10%} of 1.79 means in real terms that in order to achieve a 10% reduction in the number of colonies counted a 79% smaller dose of ionizing radiation is required. In either case, the RER and DMR values obtained are consistent with those of an excellent radiosensitizer (>1.50).

The radiobiological parameters of a drug *in vitro* do not necessarily correlate to its *in vivo* values,²³¹ as low *in vitro* values can have higher *in vivo* values depending on the pharmacokinetics and pharmacodynamics. The SER (RER & DMR) values obtained are in most cases higher than those obtained for nitroimidazole species in some studies.⁹² Furthermore, the concentration of porphyrin administered required to obtain these values at a maximum dose of 8 Gy is around 1000 times less than the nitroimidazole species which require a dose of 15 Gy in another study.⁹² The lower dose of porphyrin radiosensitizers administered also circumvents cytotoxic effects that are experienced by high concentrations of nitroimidazole type drugs.²³²

2.6.6 5,15-Carboxy-10,20-diphenylporphyrins Do Not Cause Sensitization of Colorectal Cancers to Ionizing Radiation

Using the conditions developed for **18**, a preliminary assay was conducted using **23**. Due to the higher hydrophilicity of **23**, it could be dissolved in a diluent of DMSO/PBS (50:50) followed by dilution into media until only trace <0.1% DMSO was present. Schedule II was selected and the results given by Figure 51. Schedule II was used because it emulates clinical conditions most closely. The raw data are given below which have not been fitted to the LQM. Clearly, no statistically significant sensitization could be observed at either of the three concentrations at any of the ionizing radiation doses compared to the cell only controls. Compound **23** was found to have a deleterious effect on the surviving fraction compared to the cell only control, this correlates with what was observed in the MTT assay. Therefore, the data were normalised to eliminate any cytotoxic/cytostatic effects so that only the effects of radiosensitization could be observed which again proved to show no statistically significant sensitization occurring.

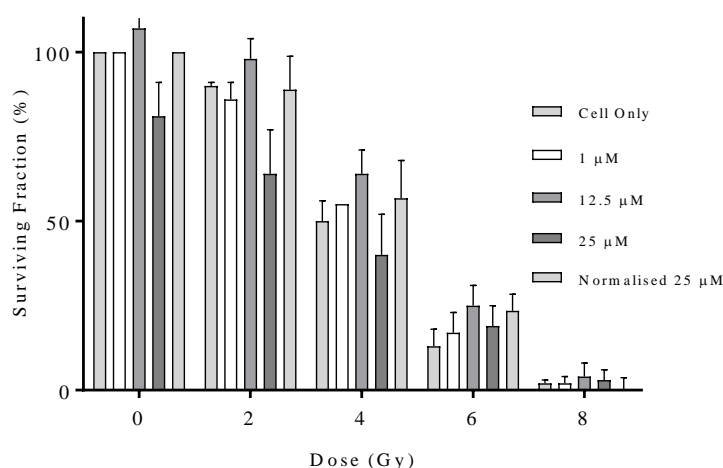


Figure 51. Surviving fraction of HT-29 (p53 null) cells, with various doses of ionising radiation and concentration of **23** after 1 hour incubation.

2.6.7 Evaluation of the Impact on Cell Cycle Progression after Treatment with Ionizing Radiation

Fluorescence-activated cell sorting (FACS) is a powerful technique which sorts cells based on measured fluorescence, typically emanating from dyes and antibodies. In order to elucidate if the decreased long-term clonogenic survival observed in Figure 52 was associated with alterations of cell cycle distribution after irradiation, FACS was utilized. Additionally, FACS can determine the relative number of non-viable (sub-G1) cells present in a sample. Throughout, the negative control was a vehicle control sample, and the positive control was cells that were treated with 10 Gy dose of ionizing X-ray radiation only. Propidium iodide is a well-known cationic DNA intercalating dye which is commonly used in FACS assays to determine cell viability and cell cycle population distribution.²³³ We predict, that the data obtained should accurately reflect that obtained through

clonogenic assays. The HT-29 (p53 null) cells should have a far lower proportion of cells exhibiting the characteristics of cell cycle arrest, while the HCT-116 (p53 WT) cells should have a greater proportion, due to the presence of the p53 protein.

We followed the method according to Nicoletti and co-workers.²³⁴ Upon analysis of the proportion of cells in the radiosensitive G2/M phase, we observed that there was a post-irradiation time-dependent response with HCT-116 (p53 WT) when comparing the 1 hour post-irradiation time point to the 24 hour post-irradiation time point, but not with HT-29 (p53 null) (Figure 52, Figure 53). These data concur with what has previously been reported in the literature.²³⁵

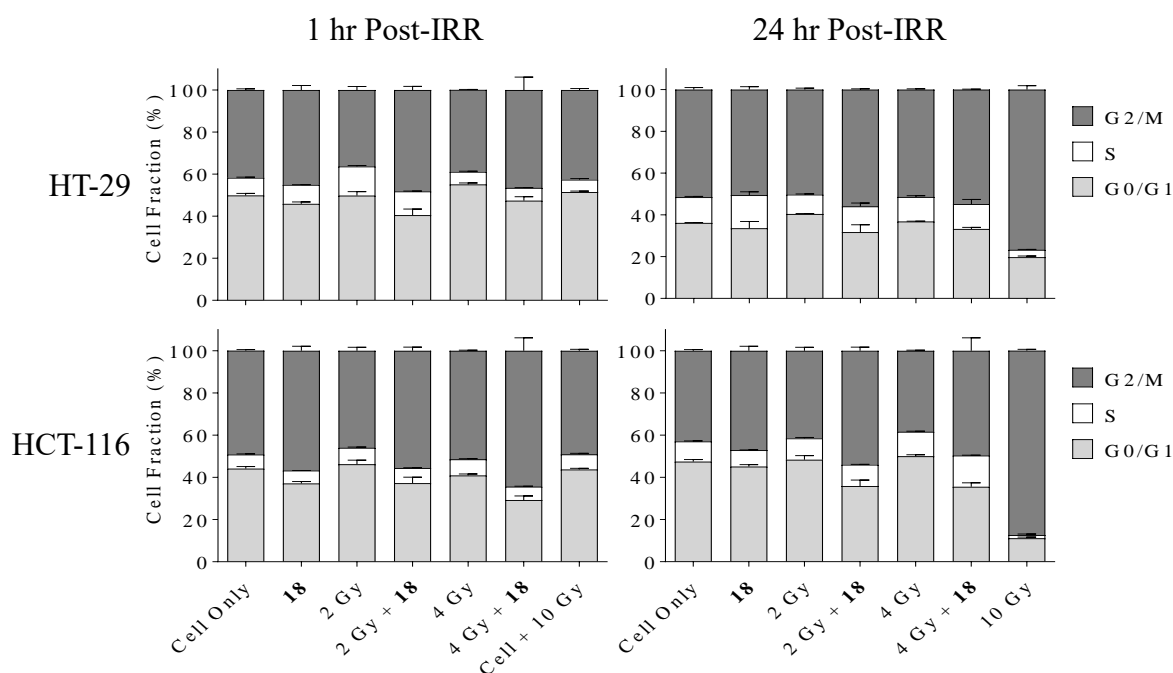


Figure 52. Stacked-columns representing the cell cycle proportions observed by FACS for given treatments at two different time points. IRR = Irradiated. Data points represent $\bar{x} \pm SD$ (n=3). 10 Gy control data points represent $\bar{x} \pm SD$ (n=6).

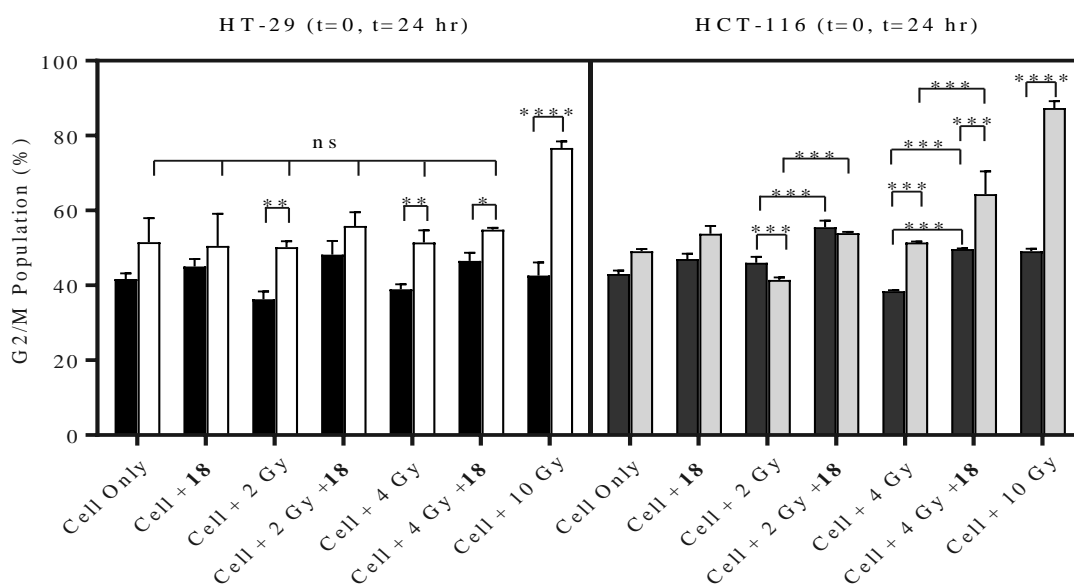


Figure 53. The fraction of the G2/M population (%) observed by FACS for given treatments. IRR = Irradiated. Data points represent $\bar{x} \pm SD$ (n=3). 10 Gy control data points represent $\bar{x} \pm SD$ (n=6). Statistical analysis was performed using three-factor ANOVA with Bonferroni's multiple comparisons *post-hoc* significance testing. ns; p>0.05, *, p<0.05, **, p<0.01, ***, p<0.001, ****, p<0.0001.

With regards to HT-29 (p53 null), there was a statistically significant temporal effect on the measured fraction of cells in the G2/M phase (p<0.01). HCT-116 (p53 WT) was also found to have a time-dependent response (p<0.01). This could be interpreted as 1 hour post-irradiation being insufficient for the molecular machinery within the cells to carry out the processes which cause a G2/M arrest, which is to be expected. In both cell lines, no statically significant differences in the cell cycle distribution of untreated cell only control and cells treated with 50 μ M of **18** were observed (p>0.05), indicating that the mechanism of action was not dominated by cytostatic behaviour. However, significant differences were observed in the proportion of cells in the G2/M phase when comparing treatment with 4 Gy with 50 μ M of **18**, or 2 Gy with 50 μ M of **18** to 4 Gy and 2 Gy alone respectively within HCT-116 (p53 WT) (p<0.001). This effect was observed at both measured time points. At the 24 hour time point, both cell lines treated with 10 Gy showed a substantial increase in G2/M compared to the control samples (0 Gy). On the whole, HT-29 (p53 null) cells were resistant to changes in the measured fraction of cells in the G2/M phase, unless irradiated with a lethal 10 Gy dose.

As expected, when evaluating the non-viable fraction, an increase in non-viable cells (Sub-G1 cell fraction) was observed 24 hours post-IRR. Significant differences in cell viability were observed at both time points when comparing 4 Gy of radiation with **18** to 4 Gy radiation without **18** in both cell lines. Sensitization enhancement was also observed in HT-29 (p53 null) 4 hour

post-treatment at 2 Gy and 4 Gy (Figure 54, Figure 55). When comparing the two cell lines at the same time point, there was a clear and statistically significant relationship between the treatment and the cell line used. This was confirmed by ANOVA. The presence of p53 seems to be associated with increased loss of viability.

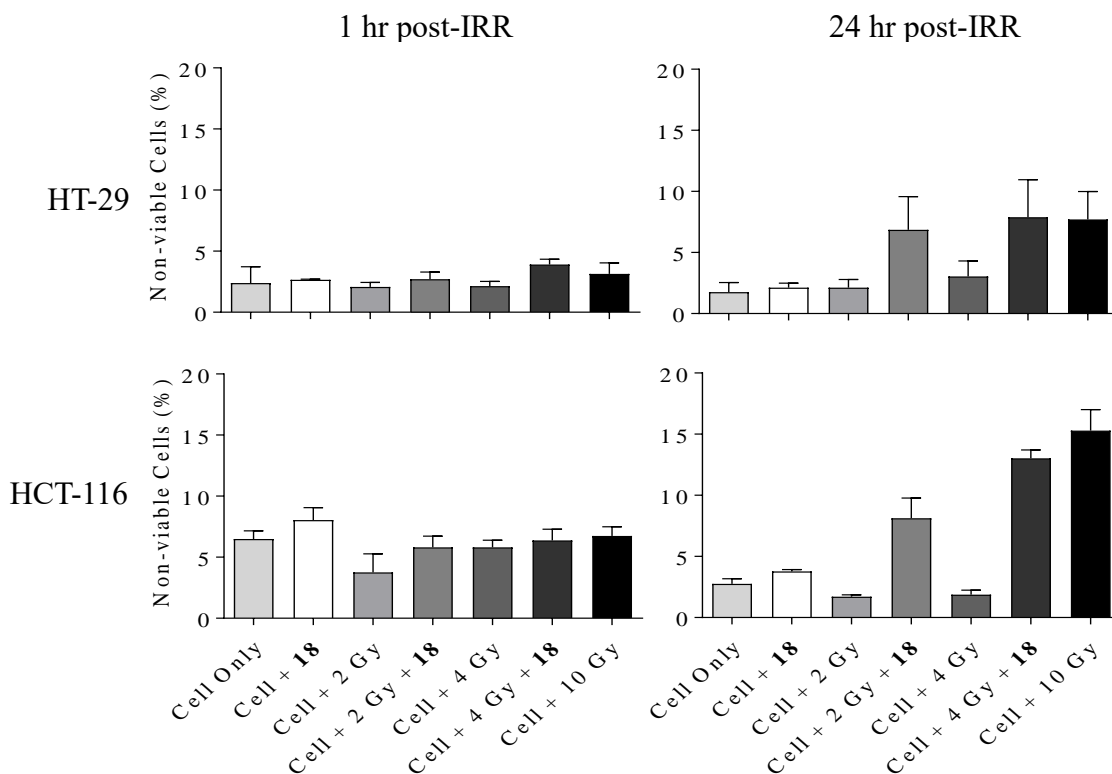


Figure 54. The fraction of Sub-G1 cells (%) observed by FACS for given treatments. IRR = Irradiated. Data points represent $\bar{x} \pm SD$ (n=3). 10 Gy control data points represent $\bar{x} \pm SD$ (n=6).

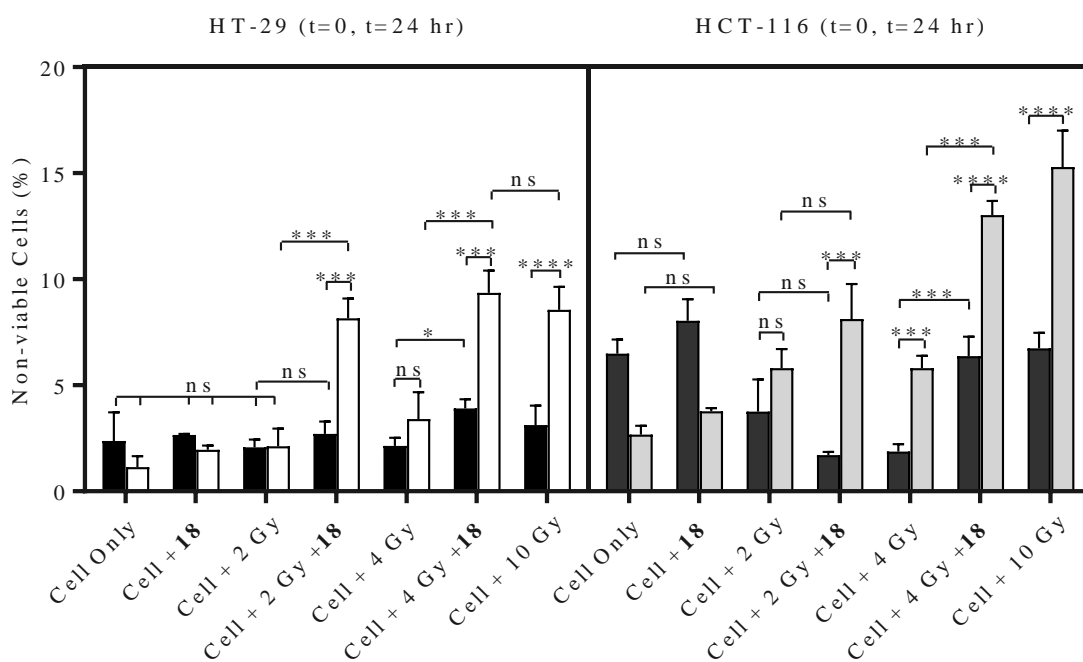


Figure 55. The fraction of Sub-G1 cells (%) observed by FACS for given treatments. IRR = Irradiated. Data points represent $\bar{x} \pm SD$ (n=3). 10 Gy control data points represent $\bar{x} \pm SD$ (n=6). Statistical analysis was performed using three-factor ANOVA with Bonferroni's multiple comparisons *post-hoc* significance testing. ns; p>0.05, *, p<0.05, **, p<0.01, ***, p<0.001, ****, p<0.0001.

Figure 55 reveals that the cell viability for HT-29 (p53 null) and HCT-116 (p53 WT) are time-dependent (p<0.0001). Furthermore, the measured response of both cell lines was found to be highly dependent on the given treatment (p<0.0001). Within both cell lines, at both time points, the compound alone did not significantly increase the observed fraction of non-viable cells. However, both cell lines were found to have a significantly higher proportion of non-viable cells when comparing treatment with 50 μM of **18** and 4 Gy to treatment with 4 Gy alone (p<0.0001). There was no difference in either cell line when comparing treatment with 50 μM of **18** and 4 Gy to treatment with 10 Gy of radiation (p>0.05). Radiobiology data obtained using Mn(II) functionalised pyridylporphyrins concurs with our observations that radiosensitization by porphyrins tends to be followed by an increase in non-viable cells and a G2/M arrest.²³⁶

2.6.8 Evaluation of the Impact on DNA Damage/Repair after Treatment with Ionizing Radiation

It is well understood that treatment of biological material with ionizing radiation causes damage to DNA through either the direct or indirect mechanism yielding either double-strand breaks (DSB) or single strand breaks (SSB), as previously discussed. This DNA damage can be measured and quantified by the single cell gel electrophoresis assay, otherwise known as the 'comet' assay, due to the comet-shaped tails of DNA material that are electrophoretically separated from the nucleic head of the cell.^{237,238} We utilized the alkaline comet assay procedure published by Olive *et al.* to evaluate the impact on DNA damage/repair after treatment with and without ionizing radiation.²³⁹ Below are examples of cell-only controls versus the 10 Gy radiation control for HT-29 (p53 null) and HCT-116 (p53 WT) (Figure 56). Denaturing under alkaline conditions means that replication forks appear as single-strand breaks so S-phase DNA migrates further than G1 DNA and G2 DNA. It is worth noting, that large amounts of DNA in the comet tail is not always due to genotoxicity – it can be induced by mitochondrial or membrane damage *via* apoptosis or necrosis. The half-life for DNA repair is less than 30 mins, therefore, all experiments were carried out in the dark at 4 °C to limit DNA recombination.

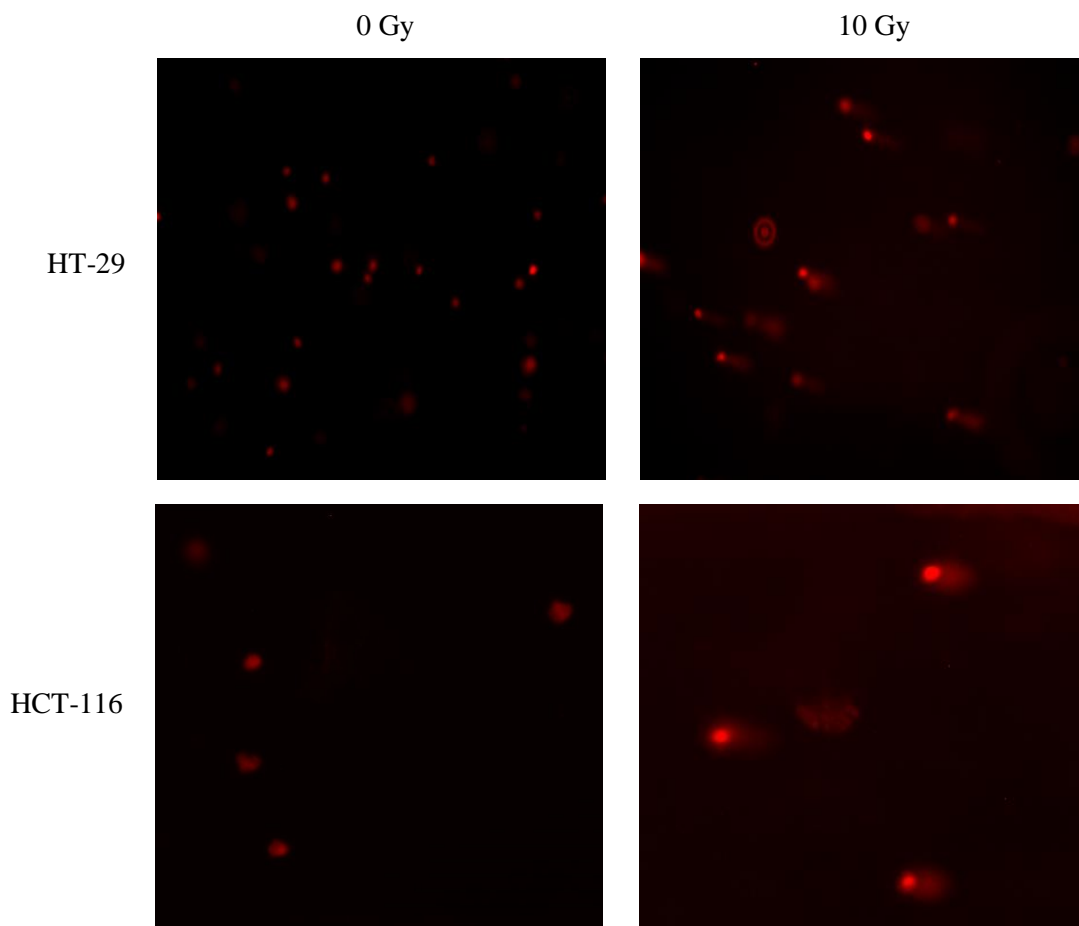


Figure 56. Fluorescence micrographs of treated and untreated HT-29 (p53 null) and HCT-116 (p53 WT) cells seeded into agarose gel stained with propidium iodide after being lysed in alkaline buffer and electrophoretically separated.

In order to produce the characteristic comet tails, the method had to be optimised. Use of high voltages gave higher resistance which caused the gel to melt or dislodge from the silicate glass slide, longer times gave long drawn out comet tails that couldn't reliably be quantified, and shorter times didn't cause sufficient migration of the DNA. The optimisation conditions are summarised by Table 22.

Time (mins)	Voltage (V)	Current (mA)	Power (W)	Qualitative Outcome
10	20	500	250	+
20	20	500	250	++
30	20	500	250	+
40	30	500	250	-
60	30	500	250	-
120	30	500	250	--

Table 22. Tabulated conditions investigated in the optimisation of the alkaline comet assay.

The data obtained the comet assay performed on HT-29 (p53 null) and HCT-116 (p53 WT) cells are given by Figure 57.

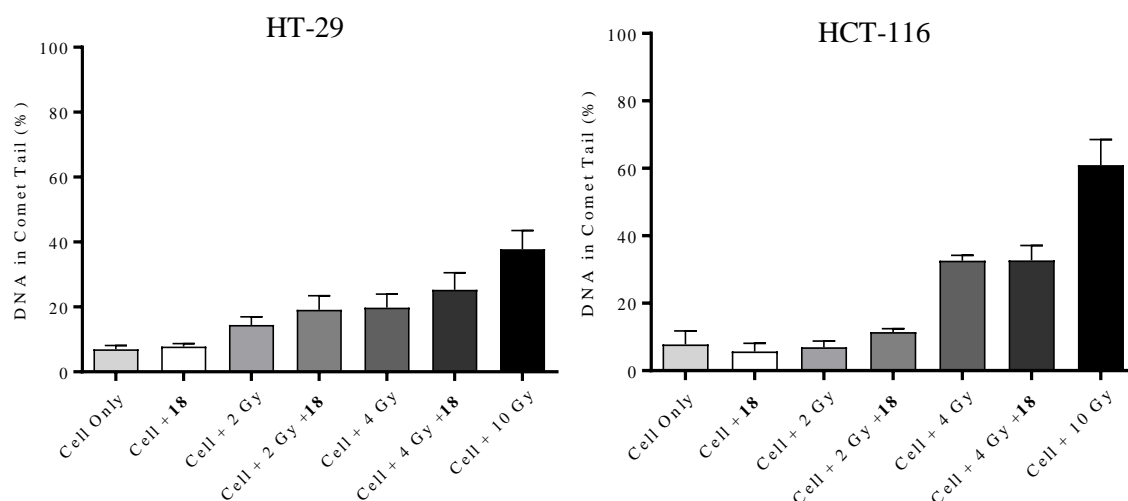


Figure 57. DNA in comet tails observed through the alkaline comet assay for HT-29 (p53 null) (left) an HCT-116 (p53 WT) (right) cells after a given treatment. Data points represent $\bar{x} \pm SD$ (n=3). Statistical analysis was performed using two-factor ANOVA with Bonferroni's multiple comparisons *post-hoc* significance testing. ns; p>0.05, *, p<0.05, **, p<0.01, ***, p<0.001, ****, p<0.0001.

With regards to HT-29 (p53 null) and HCT-116 (p53 WT), ANOVA gave no significant differences between the treated samples with the compound compared to radiation treated samples alone (p>0.05). Therefore, this assay couldn't definitively determine whether or not an increased amount of DNA damage was occurring with the presence of the compound, but it did confirm that DNA damage was occurring and that it was dependent on the treatment administered (p<0.001).

2.6.9 Determination of the Mode of Cell Death

Elucidating the mechanism of cell death is important in determining how a drug molecule functions. This can be achieved qualitatively and quantitatively by immunofluorescence (IF) assays by scoring the morphology of the nuclear material of fluorescence micrographs. The dye of choice for this assay is 4',6-diamidino-2-phenylindole (DAPI). This water-soluble non-ionic fluorescent dye binds to adenine-thymine rich regions in DNA and is able to stain fixed or live cells. The nuclear morphology of untreated HT-29 (p53 null) and HCT-116 (p53 WT) cells grown on silicate glass coverslips are shown below in Figure 58. The fluorescence micrographs also reveal key distinctions in the nuclear morphology of cells treated with 10 Gy of ionizing radiation. HT-29 (p53 null) cells appear to transition through mitotic catastrophe leading to canonical apoptosis, while HCT-116 (p53 WT) undergo cell cycle arrest and apoptosis.

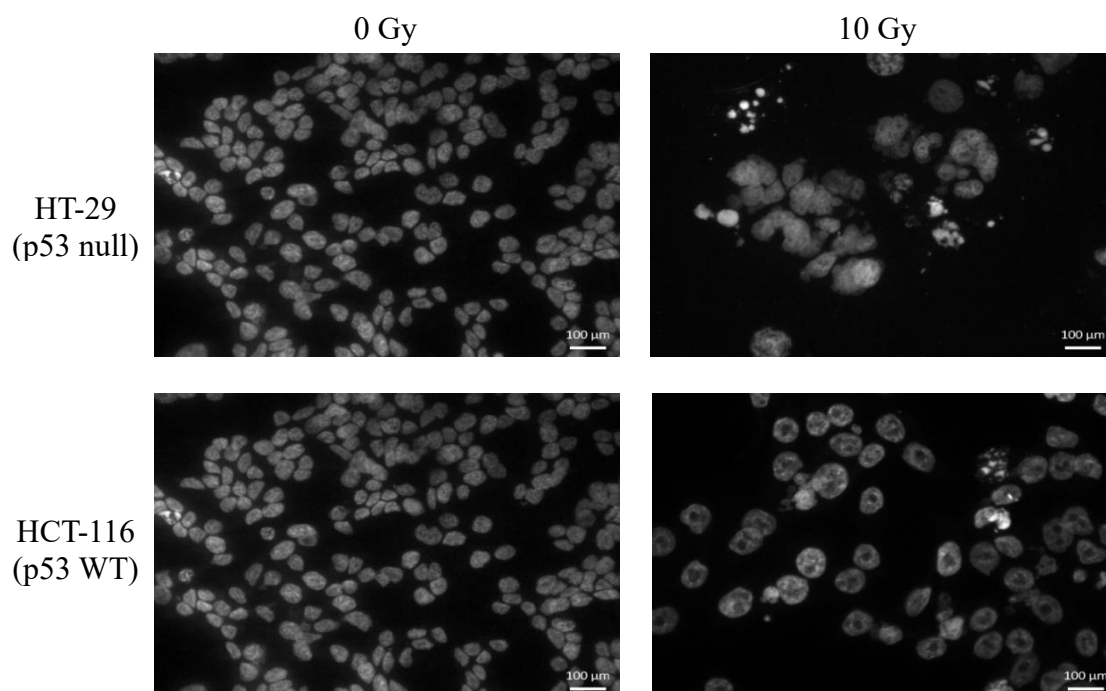


Figure 58. Fluorescence micrographs of the nuclear morphology of HT-29 (p53 null) and HCT-116 (p53 WT) cells with and without ionizing radiation treatment.

In order to determine the mode of action of cell death, firstly the definitions of each possible outcome needed to be determined. Therefore, using the method of Kobayashi *et al.*, the following fluorescent micrographs were used to define the observations (Figure 59).²⁴⁰

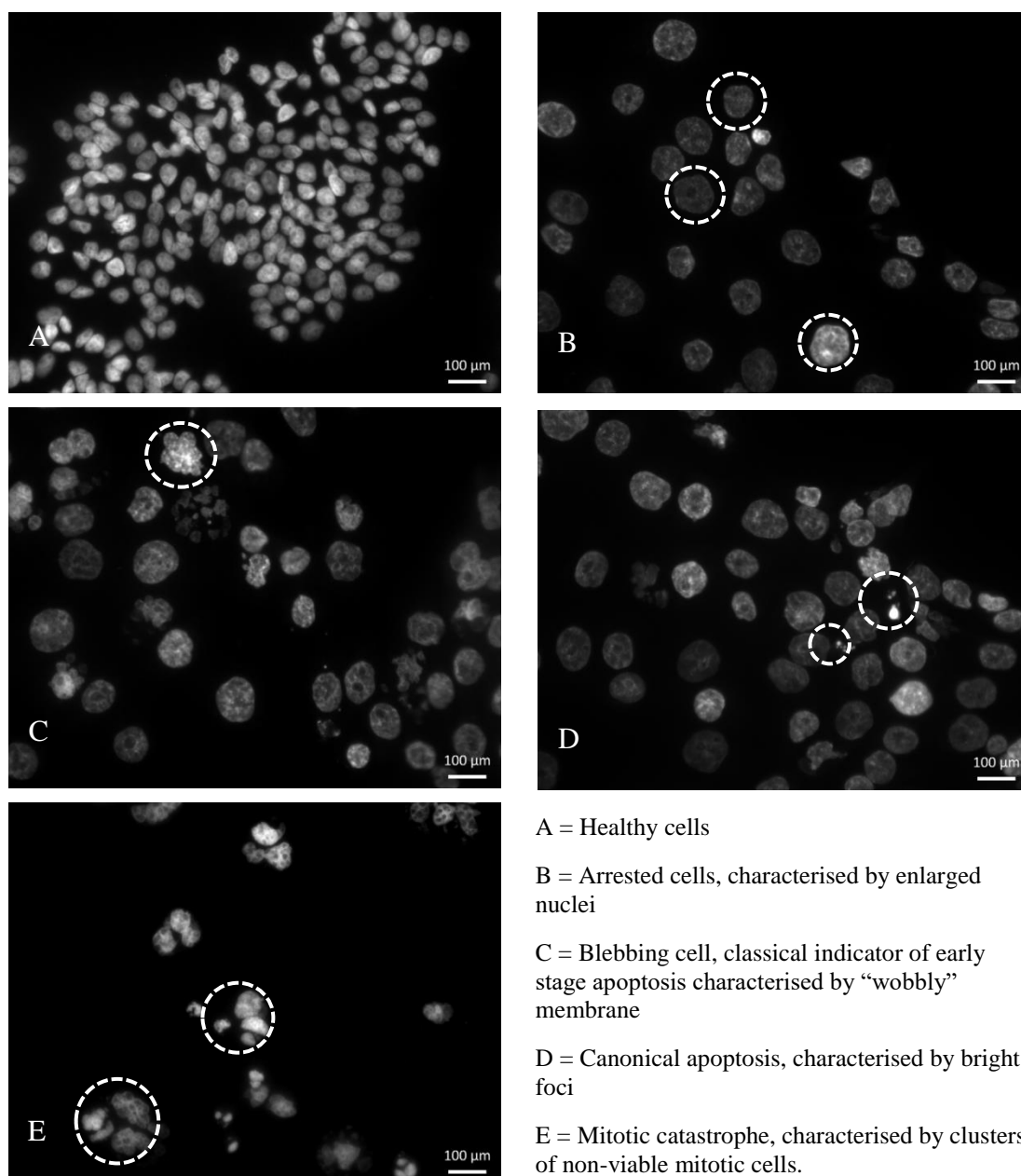


Figure 59. Fluorescence micrographs examples of healthy colorectal cancer cells, and colorectal cells treated with 10 Gy of ionizing radiation displaying typical examples of arrested cells, blebbing cells, canonical apoptotic cells and cells undergoing mitotic catastrophe.

Full assays were carried out and the data can be summarised by the stacked figures below (Figure 60) However, the use of the term ‘mitotic catastrophe’ is disputed in the literature as it is believed to be an early stage of apoptosis which eventually leads to apoptosis. p53 can repress transcription of *cyclin D1* which contributes to a G2 arrest. We perceive that the bulk of HCT-116 (p53 WT) are in an arrested cell cycle which is clear from the vast difference of the size of the nuclei compared to the untreated cells. WT p53 can avoid aberrant mitosis by undergoing cell cycle arrest and senescence followed by expression of cytokines that stimulate cell proliferation and tumour relapse.

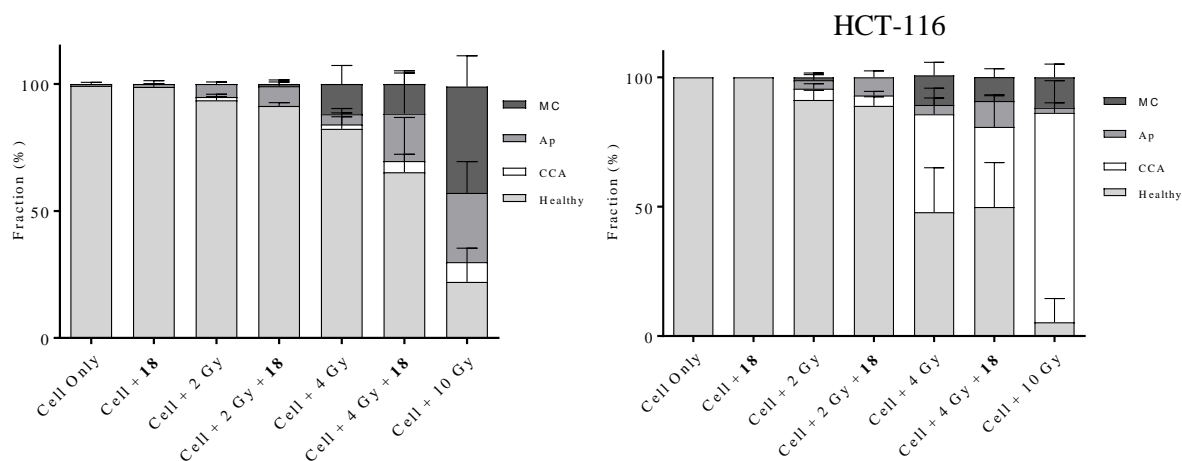


Figure 60. Figures displaying stacked columns of the fraction of cell morphologies observed *via* immunofluorescence microscopy of colorectal cells stained with DAPI. MC; mitotic catastrophe, Ap; canonical apoptosis, CCA; cell cycle arrest, Healthy; cells expressing normal nuclear morphology. Data points represent $\bar{x} \pm SD$ (n=3). Statistical analysis was performed using two-factor ANOVA with Bonferroni's multiple comparisons *post-hoc* significance testing. ns; $p > 0.05$, *; $p < 0.05$, **; $p < 0.01$, ***; $p < 0.001$, ****; $p < 0.0001$.

In all cases, the presence of the drug **18** did not cause any significant morphological abnormalities in either cell lines ($p > 0.05$), nor was it found to increase the fraction of observed cells with a mitotic catastrophe or arrested morphology ($p > 0.05$). The 10 Gy radiation control for HT-29 (p53 null) cells caused a significant increase in apoptotic and mitotic catastrophe morphologies being observed. Within HCT-116 (p53 WT), the same 10 Gy radiation control produced a significant fraction of arrested cells and far fewer canonical apoptotic cells. It's known that when cells lack p53 they will undergo mitosis even though they contain DNA damage. Within HT-29 (p53 null) and HCT-116 (p53 WT) cells, there was no significant difference between the 4 Gy treated sample and the 4 Gy + 50 μM treated samples ($p > 0.05$), furthermore, the presence of the compound did not cause a difference in the observed levels of mitotic catastrophe. However, there was no significant difference ($p > 0.05$) between the 10 Gy treated sample and the 4 Gy + 50 μM treated sample for the fraction of cells expressing canonical apoptotic morphologies, while there was a significant difference ($p < 0.01$) between the 10 Gy treated sample and 4 Gy treated sample. There was a significant increase ($p < 0.05$) in the observed levels of arrested cells in HT-29 (p53 null) cells treated with 4 Gy + 50 μM compared to the 4 Gy treated cells alone. Therefore, it could be said that the presence of the drug causes an increase in canonical apoptosis. The increase in levels of apoptosis, a G2/M arrest, and an increase in radiosensitivity of cells has been found to be key characteristics of many radiosensitizers.²⁴¹ However, these data do not directly support the obtained FACS data due to the difference in the damage/repair time. For FACS a period of 24 hour was used before processing and analysis took place, however for the immunofluorescence a 72 hour time period of incubation was required.

2.7 Chapter Conclusion

Throughout this chapter, a library of aldehydes, dipyrromethanes, and diphenylporphyrin has been synthesised. The structures have been informed from the literature on hydrophilic diphenylporphyrins. A simplistic pair of hydrophilic diphenylporphyrins has been synthesised which are hydrophilic enough to undergo *in vitro* experimentation to determine efficacy as radiosensitizers. Both of the lead molecules are easy to formulate in biological media, they can be taken into a diluent of sterile DMSO and diluted into media or serum to a DMSO concentration of ~1%, which is far below the toxic limit used for *in vitro*, *ex vivo*, and *in vivo* assays. This represents a vast improvement in formulation compared to that of MLT-005. **23** was found to be soluble in PBS without the need for DMSO. *In vitro* comparisons of these two compounds has allowed us to determine that the biological effects might well be modulated by the *meso*-substituents.

We have to the best of our knowledge carried out the first radiobiological study on a diphenylporphyrin to determine the viability, efficacy and mechanism of action. We have successfully quantified the presence of copper in the cancer cells emanating from compounds **18** and **23** through the utilization of ICP-OES studies which proved that the compounds were being internalized. We have evaluated the effect of these two compounds on cell number/viability through MTT assays, **18** was found to be predominantly non-toxic when incubated with cells for less than 24 hours. The use of clonogenic assays has revealed that within HT-29 (p53 null) cells, RER values of 1.24 and 1.26 for doses of 2 Gy and 4 Gy respectively with a 50 μM dose of **20** were obtained. At higher doses of radiation, minimal enhancement was observed. These radiation iso-dose values indicate that at an ionising radiation dose of $\text{RER}_{2\text{ Gy}}$ a 24% increase in cell death is observed, and similarly for a $\text{RER}_{4\text{ Gy}}$ a 26% increase in cell death is observed at 50 μM . In HCT-116, significantly higher values were obtained ($\text{RER}_{2\text{ Gy}} = 1.74$, $\text{RER}_{4\text{ Gy}} = 2.31$). Similarly, DMR values were found to be higher at lower surviving fractions than higher surviving fractions. We have evaluated the effect of the compound **18** on the cell cycle distribution through FACS which revealed that it caused an increase in the arrested cells when irradiated with 4 Gy of ionizing radiation compared to the 4 Gy control. Immunofluorescence showed that there was no significant difference in either cell line between the observed levels of canonical apoptosis for the 10 Gy treated samples and 4 Gy + 50 μM treated samples. Overall, we believe that we have started to reveal the biological mechanism of action of a novel porphyrin radiosensitizer. The next stages are to carry out modification of the existing motif to prepare it for radiochemistry, to perform the radiochemistry and then to biologically re-evaluate the potential theranostic agent.

Chapter 3

Synthesis and Validation of a Theranostic Radiosensitizer

3.1 Introduction

Chapter 3 discusses the modification of **18** into a theranostic agent. The core motif, **18**, has been identified and confirmed as a viable candidate for use as a potential radiosensitizer which is based upon the structure of MLT-005 (Figure 15). As mentioned in Chapter 1 Section 1.2.1.5, ‘click’ chemistry is an important tool not to be overlooked in the field of radiochemistry and molecular imaging; it is associated with high reaction yields, low reaction times, and 100% atom economy.^{242,243} Furthermore, microwave heating has been known to amplify these effects further. While amide bonds are heralded as being highly stable under physiological conditions, the triazole linkage formed by the ‘click’ reaction is even more resistant to physiological enzyme hydrolysis.²⁴⁴ This chemistry has been demonstrated previously by Boyle and co-workers by the conjugation of [¹⁸F]F prosthetics to cationic photosensitizing porphyrins.¹⁵⁴ The Cu(I) catalysed alkyne-azide cycloaddition reaction synthetically requires both an alkyne and an azide moiety, either of which could be the [¹⁸F]F prosthetic. Therefore, a novel ‘clickable’ diphenylporphyrin bearing either azide or alkyne functionality had to be synthesised in order to investigate ‘click’ conjugation in a radiochemistry environment. The trans-A₂-diarylporphyrin would also have to retain some polar properties for further *in vitro* and *in vivo* evaluation, as well as purification by high-performance liquid chromatography (HPLC). We envisaged three possible sites for conjugation to a radionuclide: the first involved conjugation to the carboxylic acid functional groups of compound **18**, the second, to synthesise a new diphenylporphyrin with alkyne/azide groups, and the last strategy, modification of a *meso*-position so that the scaffold contains one less nitro group, but possesses a conjugatable group instead (Figure 61). However, conjugation to one or more of the carboxylic acid residues will reduce the polarity of the molecule, thus this needs to be taken into account.

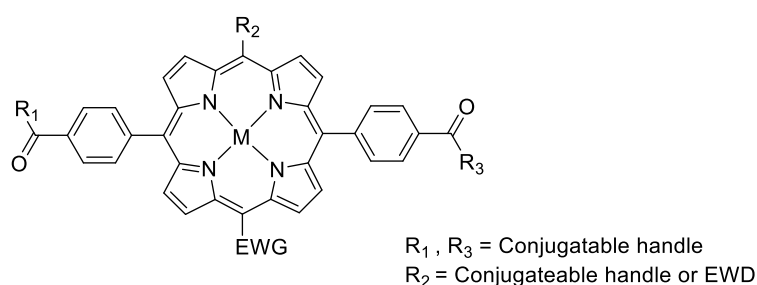
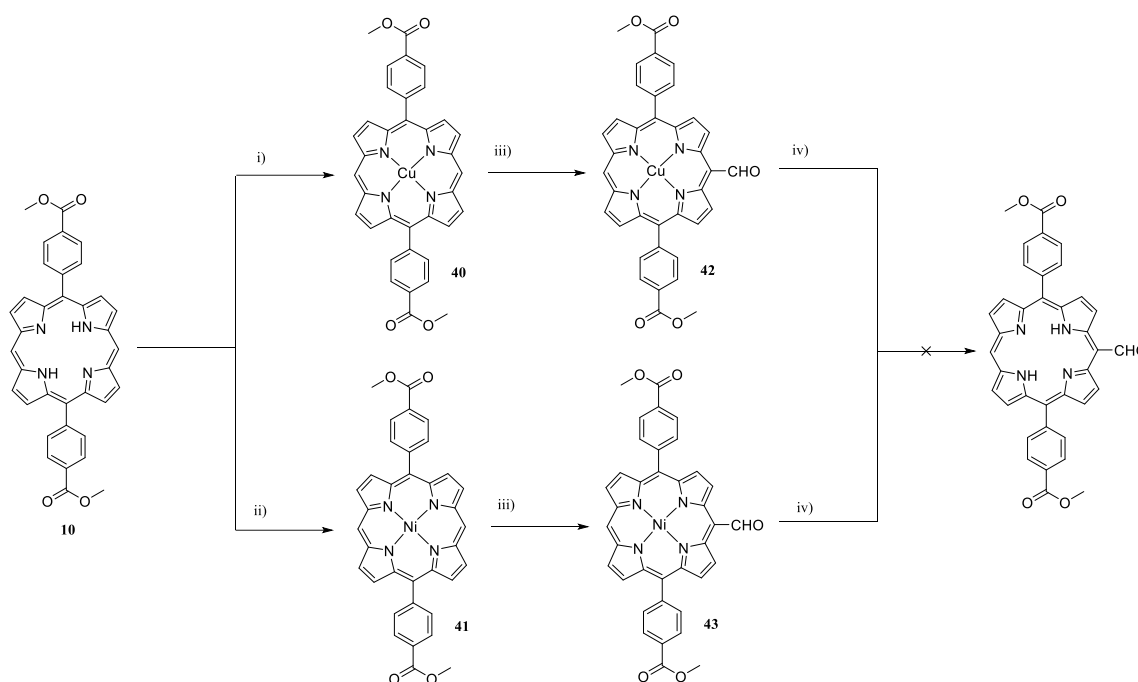


Figure 61. Pictorial representation of the available three sites on the existing scaffold of molecule **18** to append an [¹⁸F]F prosthetic.

3.2 *Meso*-Modification

3.2.1 Formylation

The chemistry available to modify the *meso*-positions of a trans-A₂-diarylporphyrin with a functional handle that can be used for conjugation reactions is limited. The most obvious modification is to introduce an aldehyde functional group; these aromatic aldehydes can undergo a range of reactions including, but not limited to: Grignard reactions, Wittig reactions, reduction/oxidation reactions, and Knoevenagel reactions.^{245,246,247,248} The most direct route to append a porphyrin with a *meso*-formyl group is through the Vilsmeier-Hack formylation. Reportedly, Vilsmeier-Hack formylation of diphenylporphyrins will occur preferentially on the free *meso* carbons,²⁴⁹ and is one of the routine reactions for *meso*-functionalisation and *beta*-functionalisation.²⁵⁰ Formylation reactions would need to be performed before nitration, because the macrocycle needs to be electron-rich and the NO₂ groups withdraw electron density from the macrocycle, deactivating it to the electrophilic aromatic substitution. For successful formylation to occur the pyrrolic hydrogens have to be protected by chelation to a metal cation.²⁵¹ The main properties that a metal should have in this application are that it should be easily inserted into the cavity in high yield, it shouldn't be removed under the acidic conditions of the Vilsmeier-Hack reaction, and it should then be able to be removed with strong mineral acid, giving the free base porphyrin in high yield. Ideally, the cation would form a diamagnetic complex so that NMR spectroscopic analysis can be carried out of the formyl intermediate. Therefore, Ni(II) and Cu(II) were selected. Both of these cations have been found to activate diphenylporphyrins towards *meso*-electrophilic substitution with the Vilsmeier reagent, which is generated *in situ*.^{252,253} While Cu(II) species require treatment with a strong acid before being analysed by NMR, Ni(II) porphyrin chelates do not, due to them being square planar diamagnetic complexes.²⁵⁴ Treatment with POCl₃/DMF with either microwave or conventional heating can give the *meso*-formyl species in reportedly high yields.²⁵²



Scheme 22. Formylation of diphenylporphyrin. Conditions used: i) $\text{Cu}(\text{OAc})_2$ monohydrate, MW heating, 80 °C, 1 hr. ii) $\text{Ni}(\text{OAc})_2$, MW, 160 °C, 1 hr. iii) DMF/ POCl_3 , 60 °C, Ar, 16 hr, . iv) H_2SO_4 , RT, stir 30 mins.

Porphyrin **10** was taken up in THF and complexed to Cu(II) under MW heating to give the Cu(II) chelate, **40**, in a high yield of (97%) and excellent purity by TLC and UV-Vis. **10** was taken up in DMF and complexed to Ni(II) under MW heating at 160 °C. Harsher conditions were required to chelate the tetradentate porphyrin ligand to the Ni(II) cation, which is consistent with the literature.²⁵⁵ Typically, aliphatic nitrogenous chelates have high rate constants (*ca.* 10^5) while porphyrins have low rate constants (*ca.* 10^{-5}) for metal chelation.²⁵⁶ However, porphyrins do form thermodynamically and kinetically stable chelates. Ni-N bonds in porphyrins are shorter than expected, thus causing conformational deformation by a ruffling of the macrocyclic core. **41** was synthesised in good yield (89%) after successive purification by column chromatography. The spectroscopic data show a bathochromic shift of the Soret band from 410 nm to 405 nm, and a reduction in the number of Q bands from four to two could be seen, indicating complete metallation. **40** and **41** were treated with freshly prepared Vilsmeier reagent in refluxing dichloroethane.^{257,258} The reaction yields an intermediate iminium salt which is hydrolysed with base to give the corresponding aldehyde, consumption of the starting material could be seen by TLC. The iminium salt can be seen by TLC as a green fluorescent band which does not elute on the silica plate. The crude products were purified by column chromatography with DCM eluent to give the product as a crystalline solid, **41** was analysed by $^1\text{H-NMR}$, $^{13}\text{C-NMR}$, MS, and UV-Vis analysis (Figure 62). De-metallation of **42** and **43** was carried out in 98% sulfuric acid, however, upon work-up and attempted purification the desired compounds could not be isolated,

nor could any compound resembling a porphyrin. This is likely due to the aldehyde being sensitive to the presence of strong mineral acids, in the case of β -formylporphyrins, treatment with strong acids yields exocyclic hydroporphyrins. Additionally, the *trans*- A_2 -diarylporphyrin macrocycle itself is also susceptible to degradation when treated with strong acids.

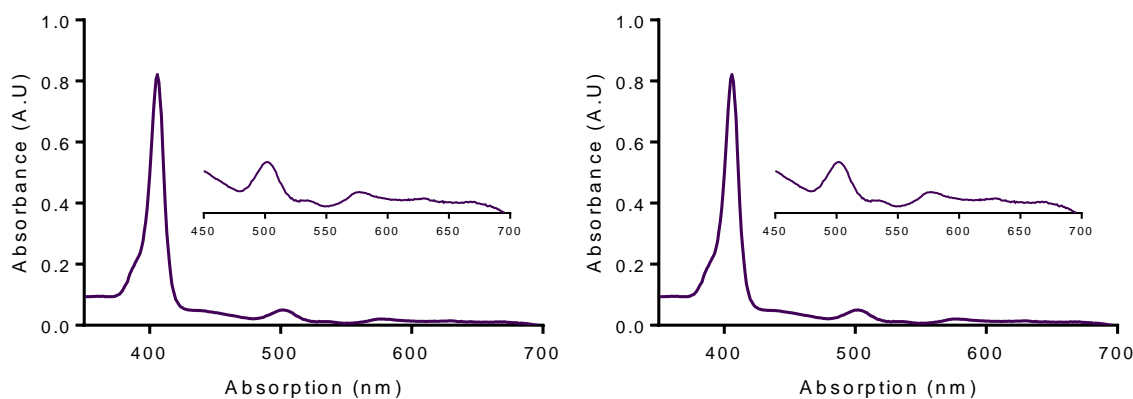
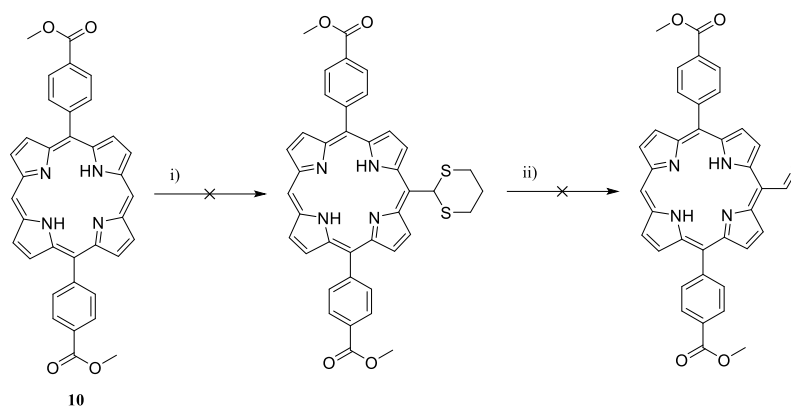


Figure 62. UV-Vis spectrum of compounds **42** (left) and **43** (right), each showing a Soret band and two Q bands.

A modified version of this reaction has been reported in the literature; Bonfantini *et al.* highlighted that isolation of the moisture-sensitive iminium salt is impractical, and found that removal of the metal cation from tetraphenylporphyrins with strong mineral acids (conc. $H_2SO_{4(aq)}$) should take place before treatment of the iminium salt with weak base to give the acid-sensitive formyl substituent was a solution to overcome the problem.²⁵¹ Therefore, this modification was attempted with both a copper(II) chelate and the nickel(II) chelate. Unfortunately, neither **42** nor **43** used in this modified reaction gave the desired metal-free *meso*-formyl porphyrins, again, probably due to the sensitivity of the *meso*-methylene bridgeheads to treatment with concentrated $H_2SO_{4(aq)}$.

Therefore, a second route was attempted which has been established by Senge and co-workers.^{250,257,259,260} Dithiane was treated with *n*-BuLi under anhydrous conditions giving the lithiated salt by removal of the acidic α -proton. The porphyrin, **10**, was subsequently treated with this mixture and brought up to room temperature followed by oxidation with DDQ solution to give the dithiolated product, which could be subsequently removed with BF_3 giving the β -formyl compound.



Scheme 23. Formylation of diphenylporphyrin. Conditions used: i) Dithiane, n-BuLi, 12, -78 °C warming to -40 °C, 2 hr, Ar.

Unfortunately, this reaction only proceeded to give a mixture of compounds which didn't contain the desired product after purification by column chromatography; multiple conditions were attempted, but none were successful. The conditions investigated are summarized in Table 23.

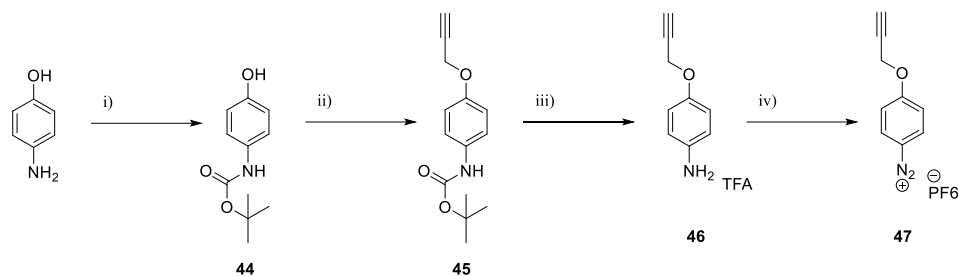
Conditions	BuLi (eq. mol)	Porphyrin (eq. mol)	Time (hr)	Dithiane (eq. mol)	Temperature (°C)	Solvent
A	4	1	0.5	1	-70	THF
B	4	1	1	1	-70	THF
C	4	1	1	1	-70 to -40	Py
D	12	0.5	0.5	1	-40	Py

Table 23. Tabulated conditions attempted to synthesise a dithiolated diarylporphyrin.

3.2.2 Diazotisation

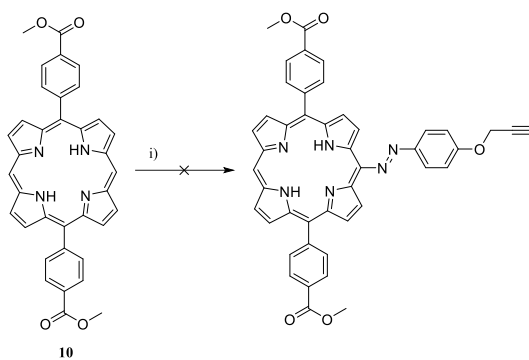
Screen *et al.* reported that diazonium functional groups readily react with electron-rich macrocycles, including porphyrin macrocycles.²⁶¹ While this method would introduce an additional phenyl ring, it has been reported to be a facile way to introduce functional groups which can be used for conjugation reactions, such as 'click' reactions. Azo groups are susceptible to light-activated cis-trans isomerisation, but, they are exceptionally stable to hydrolysis *in vivo*. Through this route, the diazonium linker would need to be appended to the macrocycle and then nitrated as the EWG nitro group reduces electron density on the aromatic tetrapyrrole ring deactivating it to electrophilic substitution. The substituents of the diazonium linker play an important role in the reactivity of the diazonium N_2^+ group, EWGs in the *para* positions increase the rate of reaction, while EDGs reduce the rate of reaction. Using the method according to Cheng

et al., a desired heterobifunctional diazonium linker was synthesised bearing an alkyne functionality.²⁶²



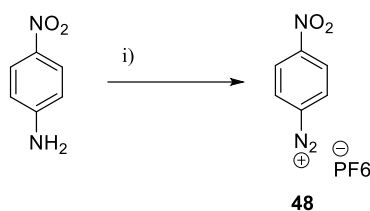
Scheme 24. Synthesis of an aromatic heterobifunctional linker. Conditions used: i) Boc_2O , MeOH, Ar, stir RT 17 hrs. ii) Propargyl bromide, K_2CO_3 , DMF, Ar, stir 17 hrs. iii) TFA, stir RT, 30 mins. iv) TFA, NaNO_2 , HPF_6 , H_2O , Ar, $-10\text{ }^\circ\text{C}$, 1.5 hr.

47 was synthesised exactly according to the method of Cheng *et al.*; all structural determination analysis and data agreed exactly with the published data. While Screen *et al.*, utilized diazonium linkers with a BH_4^- counter-ion, we opted for the PF_6^- , which has a higher solubility in polar organic solvents. An attempted conjugation reaction to yield the target porphyrin was unsuccessful when using the bifunctional linker in 1.2 mol excess. Repeating the reaction with 10.0 mol excess similarly didn't yield the desired compound. Upon heating the reaction mixture to $40\text{ }^\circ\text{C}$ the heterobifunctional diazonium linker degraded, as expected due to their thermal instability by releasing diatomic nitrogen gas rendering it unreactive.



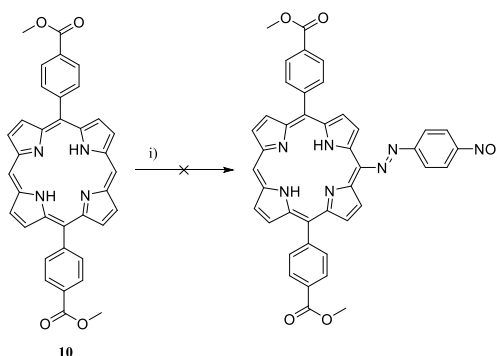
Scheme 25. Formylation of diphenylporphyrin. Conditions used: i) **47**, THF, Ar, RT stir, 17 hr.

Synthesis of a second heterobifunctional diazonium linker bearing a *para* nitro substituent was carried out,²⁶³ this linker theoretically should have had a far higher rate of reaction, and could be reduced to an amine by refluxing in $\text{HCl}_{(\text{aq})}$ with SnCl_2 , which could subsequently be diazotised to an azide. **48** was synthesised according to the method of Maskill *et al.*,²⁶⁴ but was used immediately due to its highly sensitive nature.



Scheme 26. Formylation of diphenylporphyrin. Conditions used: i) TFA, NaNO₂, HPF₆, H₂O, Ar, -10 °C, 1.5 hr.

Again, the conjugation reaction was attempted, and the reaction progress monitored by TLC to reveal no consumption of the porphyrin starting material.



Scheme 27. Formylation of diphenylporphyrin. Conditions used: i) **48**, THF, Ar, RT stir, 17 hr.

3.2.3 Sonogashira Coupling

The main C-C bond forming reactions rely on palladium(II) catalysts. The Suzuki-Miyaura, Heck, Negishi, and Sonogashira reactions have all been performed on the *meso*-substituents of trans-A₂-diarylporphyrins which have been previously pioneered and demonstrated by Boyle and co-workers.^{162,265} The Sonogashira reaction involves the reaction of an aryl/alkyl bromide with an aryl/alkyl alkyne aided by a Pd(II) catalyst and a Cu(I) co-catalyst.

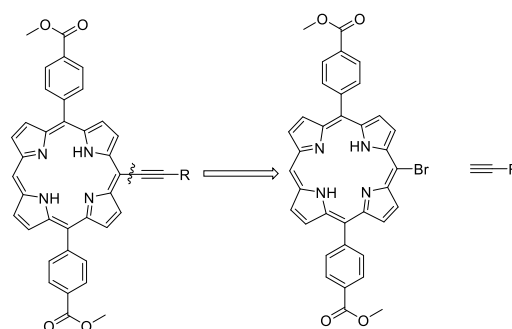
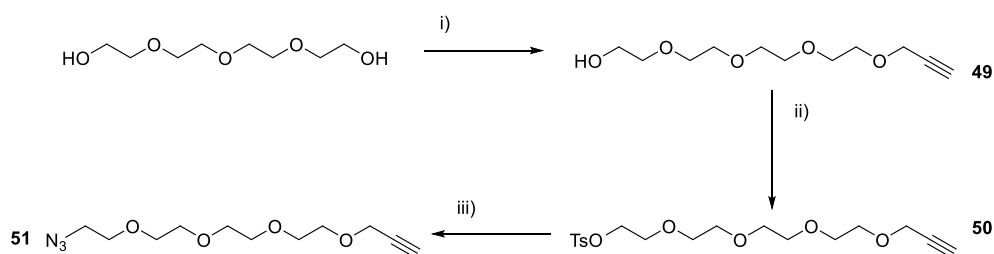


Figure 63. Retrosynthetic breakdown of a porphyrin bearing a *meso*-alkyne functionality.

Initially, the synthesis of porphyrin **17** was carried out, using previously optimised conditions. According to the literature, Balaz *et al.* was unable to isolate the desired mono-brominated compound.²⁶⁶ Using retrosynthetic analysis (Figure 63), the corresponding synthon required would be an alkyne heterobifunctional linker. Therefore, a simple PEG chain was synthesised from commercially available starting material (tetraethylene glycol). This linker chain was reacted with propargyl bromide using mild Williamson ether conditions with potassium hydroxide, sodium iodide and tetrabutylammonium iodide giving the alkyne chain in good yields (64%) once purified by column chromatography. Sodium iodide and tetrabutylammonium iodide were employed to trans-halogenate the propargyl bromide *in situ* into propargyl iodide, which has a greater rate of substitution due to iodide being a superior leaving group. The product was isolated as a colourless oil after purification by column chromatography. The alkyne proton had a chemical shift of 2.41 ppm and the methylene bridge and alkyne carbons were observed at 58.48, 61.80 and 69.15 ppm. The functionalised chain was reacted with *p*-toluenesulfonyl chloride (TosCl) under basic conditions to give the tosylated heterobifunctional PEG chain (95%) after aqueous work-up and column chromatography. The chain was taken up in DMF with excess sodium azide which was used as a good nucleophile with the OTs acting as a good leaving group. Purification of the chain by column chromatography gave the desired linker (**51**) in good yield (86%). MS proved the existence of the product by the $[M+H]^+$ and $[M+Na]^+$ peaks and NMR by the loss of the aromatic and methyl protons on the toluene ring.



Scheme 28. Formylation of a heterobifunctional linker for Sonogashira coupling. Conditions used: i) Propargyl bromide, NaI, TBAI, KOH, THF, Ar, -10 °C warming to RT, 17 hr. ii) TosCl, TEA, DCM, Ar, RT, 17 hr. iii) NaN₃, MeCN, reflux, 48 hr.

Recently, several modifications of the Sonogashira reaction have been published, some with applications in porphyrin modification.²⁶⁷ Most interestingly, a copper-, amine- and solvent-free Sonogashira reaction which tolerates multiple functional groups including PEG chains, and has been devised to limit homo-coupling.²⁶⁸ This reaction, due to it being copper-free, will also extinguish the possibility of any intramolecular and intermolecular CuAAC reactions from occurring. Porphyrin **11** dissolved in tetrabutylammonium fluoride (TBAF) with 10% mol. of Pd(PPh₃)₄ was de-gassed with a stream of argon over 30 mins to prevent Glaser couplings from

occurring followed by the addition of the PEG chain **51**. Investigated conditions are given by Table 24.

Conditions	PEG	Time (mins)	Temperature (°C)	Yield (%) ^a
A	1.1 eq	120	RT	-
B	1.1 eq	180	RT	-
C	1.1 eq	340	RT	-
D	1.1 eq	120	Reflux	-
E	1.1 eq	180	Reflux	-
F	1.1 eq	340	Reflux	-

Table 24. Table of results from optimisation studies of a Sonogashira coupling reaction to a trans-A₂-diarylporphyrin. ^aYields given are isolated yields obtained after column chromatography and precipitation.

Summary:

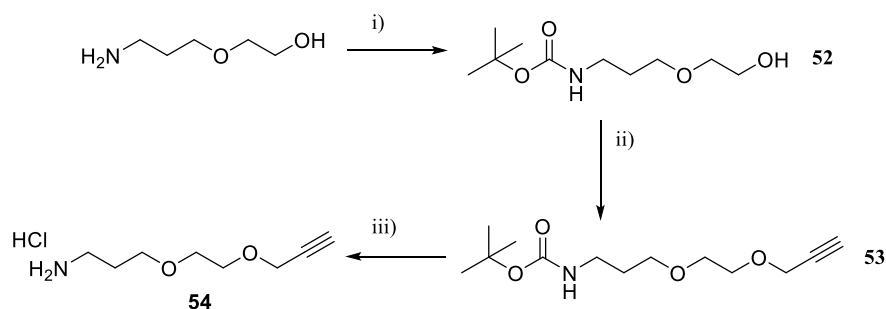
While some success has been achieved, due to the unreliability and difficulty to replicate the success of some of the previously published procedures, the investigation of the modification of the *meso*-positions of the porphyrin macrocycle was halted. Therefore, an investigation into the derivatization of the existing carboxyl groups was carried out.

3.3 *Meso*-phenyl Modification

3.3.1 Synthesis of Bifunctional Linkers

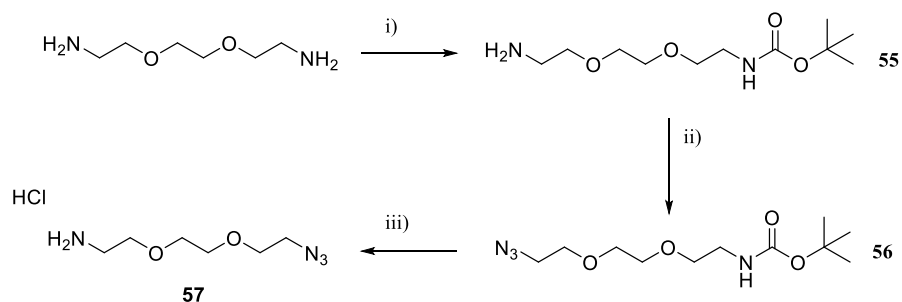
It was reasoned, that due to the high yields of the routes to synthesise **10** and **11**. In order to further increase the solubility of these lipophilic macrocycles, PEG chains were investigated as heterobifunctional linkers not only to increase the hydrophilicity but, to add the all-important conjugation handle.²⁶⁹ An advantage of this route means that the macrocycle can have two nitro groups, and heterobifunctional linkers can contain either alkyne or azide functional groups. 2-(2-aminoethoxy)ethanol was reacted under anhydrous conditions with Boc₂O anhydride to protect the terminal amine group. The reaction proceeded in almost quantitative yield but was purified by column chromatography regardless. The structure of the oil was confirmed by NMR by the presence of the t-butyl group and the N-H amide proton at 1.42 (9 H) and 4.97 (1 H) ppm respectively as well as MS analysis. This linker chain was reacted with propargyl bromide using mild Williamson ether conditions as previously discussed with **51** to give the oil in good yield (64%) once purified by column chromatography. The alkyne proton had a chemical shift of 2.42 ppm and the methylene bridge and alkyne carbons were observed at 69.09, 70.18 and 70.38 ppm. The chain was dissolved in a minimum of ethyl acetate and stirred under argon overnight with HCl in dioxane (4N), the reaction yielded the hydrochloride salt as a beige coloured solid (**54**) in almost quantitative yield when triturated thrice with diethyl ether. The complete loss of the

Bocprotecting group was observed by $^1\text{H-NMR}$ and $^{13}\text{C-NMR}$ by the loss of the large singlet (9 H) at 1.42 ppm.



Scheme 29. Synthesis of an alkyl ether alkyne-amine heterobifunctional linker. Conditions used; i) Boc₂O, TEA, DCM, Ar, 0 °C, 17 hr, RT. ii) TBAI, NaI, KOH, propargyl bromide, Ar, THF, 17 hr, RT. iii) 4 N HCl in dioxane, ethyl acetate, 17 hr, RT.

The corresponding azide-amine heterobifunctional linker was synthesised. Bis(2-aminoethoxy)ethane was reacted under anhydrous conditions with Boc₂O anhydride to protect the terminal amine group, the product was purified by extensive column chromatography to yield the product as a colourless oil in excellent yield (81%). The structure of the oil was confirmed by NMR by the presence of the t-butyl group and the N-H amide proton at 1.38 (9H) and 5.11 (1H) ppm respectively. 1-Imidazole-sulfonyl azide (ISA) was prepared according to the method of Potter *et al.* and used *in situ* due to its explosive nature when exposed to moisture.²⁷⁰ While an alkyl amine is a poor leaving group, ISA is a highly reactive diazo-transfer agent, capable of displacing even alkyl amines which typically aren't displaced in nucleophilic reactions, however, the mechanistic path is not as simplistic as an S_N2 “backside attack” reaction. Under anhydrous conditions, the azide functionality was successfully introduced to the chain. Accurate mass and other spectroscopic techniques were used to confirm the structure. This linker chain was deprotected with HCl in dioxane (4 N), and the product was worked up as a fawn-coloured oil which was triturated thrice with diethyl ether. Accurate mass gave the molecular ion as the HCl salt. The complete loss of the Boc protecting group at 1.42 ppm indicated that complete deprotection had occurred to yield the conjugatable chain.



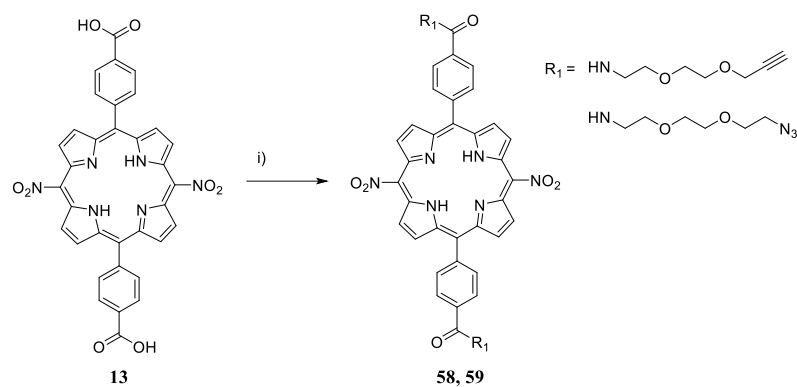
Scheme 30. Synthesis of an alkyl ether azide-amine bifunctional linker. Conditions used; i) Boc_2O , TEA, DCM, Ar, 0 °C, 17 hr, RT. ii) TBAI, NaI, KOH, propargyl bromide, Ar, 17 hr, RT. iii) 4 N HCl in dioxane, ethyl acetate, 17 hr, RT.

3.3.2 Conjugation of Diphenylporphyrins to Heterobifunctional Linkers

13 was synthesised according to the method as discussed previously. **54**, **57** and the porphyrin, **13**, were dissolved in anhydrous amine-free DMF and treated with excess DIPEA with coupling agents. DIPEA was utilized as a non-nucleophilic base which could readily be removed under reduced pressure, facilitating a slightly easier work-up protocol. Three different activating reagents were investigated in order to optimise coupling conditions (Table 25). The three combinations were: HOBt/EDC, HATU and TBTU. HOBt was coupled with EDC, EDC is a dehydrating agent which assists in the elimination of water during the peptide coupling reaction.²⁷¹ HATU and TBTU are hybrid coupling reagents which do not require the addition of dehydrating carbodiimides such as EDC and DCC.²⁷¹ The mixtures were washed with excess water to remove the water-soluble base and coupling reagents. After purification by column chromatography, the structure of the samples were confirmed by the presence of the alkyl ether groups and characteristic triplet and doublet for the alkyne functionality. The products **58** and **59** from the coupling reactions gave compounds which were highly soluble in DCM and methanol, likely due to the amphiphilicity of the ethylene glycol chains. The TLC was stained with basic potassium permanganate and, when revealed with heat, gave a single white spot which co-localised with the characteristic red fluorescence of a porphyrin under long-wave UV light suggesting that conjugation had taken place to the heterobifunctional amine-alkyne chain. Spectroscopic analysis and mass spectrometry confirmed the presence of the chains by the characteristic PEG protons and carbon environments.

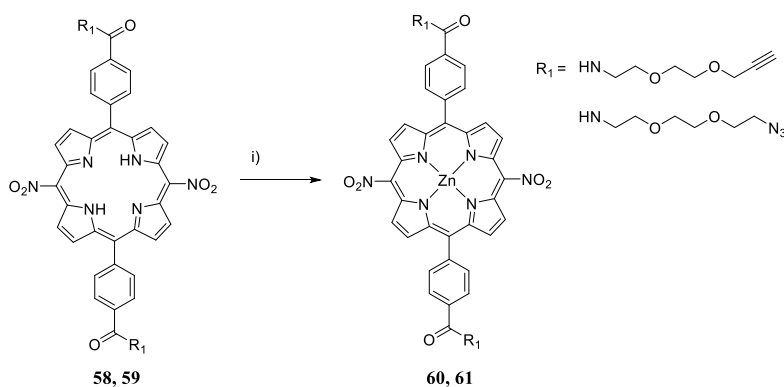
Conditions	Solvent	Base	Activating Agents	Temperature (°C)	Time (hr)	Yield (%) ^a
A	DMF	DIPEA	HOBt/EDC	80	24	67
B	DMF	DIPEA	HATU	80	24	73
C	DMF	DIPEA	TBTU	80	24	84
D	DMF	DIPEA	HOBt/EDC	80	24	57
E	DMF	DIPEA	HATU	80	24	75
F	DMF	DIPEA	TBTU	80	24	85

Table 25. Table of attempted conditions for the formation of peptide linkages. ^aYields given are isolated yields obtained after column chromatography and precipitation.



Scheme 31. Synthesis of a clickable porphyrin. Conditions used; i) PEG chain (**54** or **57**), TBTU, DIPEA, DMF, 80 °C, 17 hr, RT.

In order to prevent the porphyrins from sequestering the Cu(I)/Cu(II) catalyst during the ‘click’ reactions the cavity was protected with Zn(II) which can be later removed by treatment with TFA. The porphyrins were treated with excess zinc(II) acetate dihydrate under microwave irradiation and purified by column chromatography to give the desired compounds. The products yielded were purple crystalline solids.



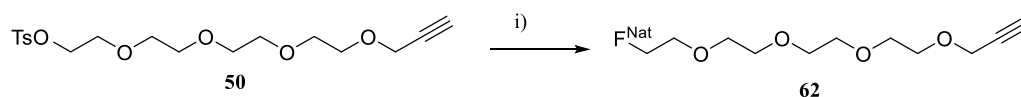
Scheme 32. Zinc(II) protection of **58** and **59**. Conditions used; i) **58** or **59**, Zn(OAc)₂ dihydrate, DMF, MW heating 80 °C, 1 hr.

3.4 Synthesis of a Novel [¹⁸F]F Fluorinated Diphenylporphyrin

3.4.1 Synthesis of the ‘Cold’ Standard PEG Prosthetic

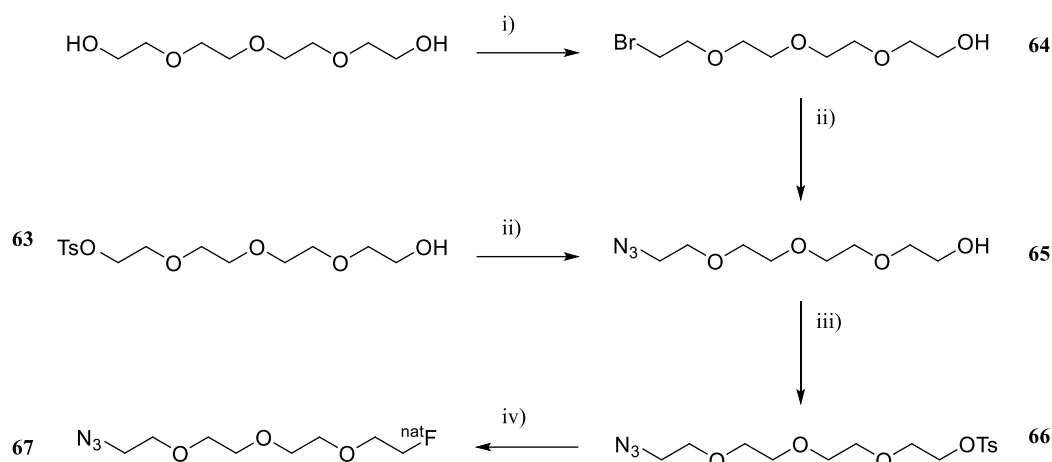
A method published by Entract *et al.* outlines that a two-step radiolabelling procedure was required in order to yield a fully radiolabelled cationic PET/PDT conjugate. Due to the short half-life of ¹⁸F (~110 mins), a facile process has to be used to generate the radiolabelled prosthetic in high specific activity and radiochemical yield. A retrosynthetic approach best describes the reasoning. Firstly, the ‘cold’ standard prosthetic needed to be produced and conjugated to the porphyrin to give the ‘cold’ conjugate, not only to validate whether or not the conjugate could be synthesised, but also to determine an HPLC purification protocol. **50** was re-synthesised and the

'cold' natural fluorine group was introduced by nucleophilic substitution in refluxing THF with tetrabutylammonium fluoride (TBAF). While fluorine has 17 known isotopes, in nature, fluorine is a monoisotopic element and exists in nature almost exclusively as the ^{19}F isotope in 100% abundance,²⁷² otherwise known in the radiochemistry field as ^{nat}F . The product was purified by column chromatography to give the product (**64**) as a pale-yellow oil, the structure was confirmed by NMR, MS and ATR-FT-IR. The ^{19}F -NMR provided the presence of the fluorine atom from the multiplet observed at -222.22 ppm. HRMS gave the product as the $[\text{M}+\text{H}]^+$ species.



Scheme 33. Synthesis of clickable alkyne-fluorine alkyl ether PEG chain. Conditions used; i) TBAF, THF, Ar, reflux, 17 hr.

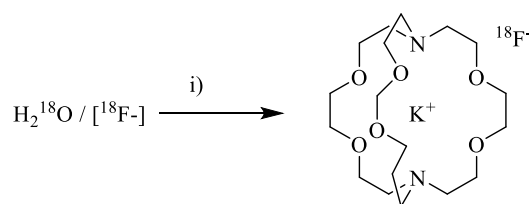
In order to give the corresponding azide-fluorine heterobifunctional prosthetic, the synthesis of **630** was carried out using chemistry as previously described, **64** was synthesised using PBr_3 in DCM under anhydrous conditions, the reaction was quenched with brine, extracted into DCM, and purified by column chromatography to give the desired compound in acceptable yield (43%) as a yellow oil. The leaving groups were exchanged for an N_3 group by refluxing in acetonitrile with excess sodium azide for 48 hours followed by extraction and purification by column chromatography to give the product as a colourless oil. As predicted, the synthesis of **65** progressed with higher yield from **63** than **64** due to the presence of the more superior leaving group (tosylate). Again, the structure was confirmed by NMR, MS and ATR-FT-IR. The remaining hydroxyl was tosylated under previously discussed conditions. Finally, the 'cold' fluorine group was introduced, again, by previously discussed conditions. The product (**67**) was purified by column chromatography to give the product as a pale-yellow oil in nearly quantitative yield (96%), the structure was confirmed by NMR, MS and ATR-FT-IR.



Scheme 34. Synthesis of clickable azide-fluorine alkyl ether PEG chain. Conditions used; i) PBr₃, DCM, Ar, -10 °C warming to RT, 17 hr. ii) NaN₃, MeCN, reflux, 48 hr. iii) TosCl, Et₃N, DCM, Ar, 0 °C warming to RT, 17 hr. iv) TBAF, THF, reflux, 17 hr.

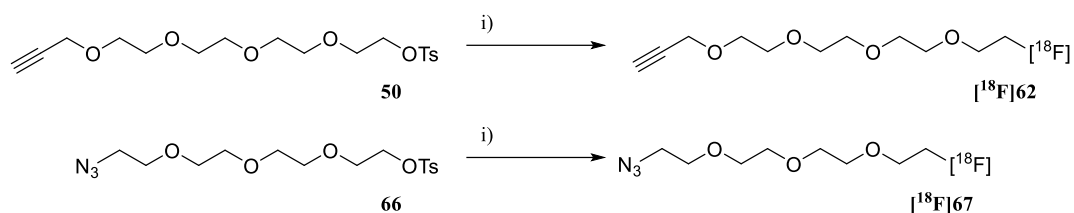
3.4.2 Radiochemical Synthesis of [¹⁸F]F PEG Prosthetics

Naturally, trial ‘hot’ synthesis of the heterobifunctional PEG prosthetics was carried out to determine which one would be most useful in going forward. Approximately 2500 MBq of [¹⁸F]F⁻ was prepared using a BG-75 ABT positive ion 7.5 MeV cyclotron with a current of 4 μA and a beam time of 1 hour delivered from a lead shielded line directly from the cyclotron to the ¹⁸O enriched water and eluted through a bicarbonate QMA ion exchange resin cartridge into a solution basic of Kryptofix® (K₂₂₂) in acetonitrile. The K₂CO₃/K₂₂₂ mixture is commonly used to trap [¹⁸F]F⁻.²⁷³ The water-acetonitrile solution was azeotropically dried for 20 mins under a stream of argon at 110 °C.²⁷⁴ The activity at this stage was measured to be approximately 1000 MBq.



Scheme 35. Trapping of [¹⁸F]F⁻. Conditions used; i) K₂₂₂, MeCN, RT, 20 mins.

The [¹⁸F]K₂₂₂ intermediate was reacted with **50** or **66** for 20 mins at 90 °C in V-shaped vials by an S_N2 reaction as with the ‘cold’ prosthetics in a similar way as reported by Denk *et al.*²⁷⁵ and Entract *et al.*¹⁵⁴ The volume of the solutions were azeotropically reduced, and the solvent exchanged to methanol and passed through a Sep-Pak light alum N cartridge to assist in the removal of unbound [¹⁸F]F⁻. The eluted activity was measured to be 1164 MBq (RCY 85%, non-decay corrected) and 1042 MBq (RCY 76%, non-decay corrected) respectively.



Scheme 36. Radiofluorination of **50** and **66**. Conditions used; i) $[^{18}\text{F}]K_{222}$, acetonitrile, 90 °C, 20 mins.

Radio-TLC of the crude products was carried out with acetonitrile as eluent to follow the progression of the reaction (Figure 64). As expected, the unbound $[^{18}\text{F}]^-$ remained on the bottom of the silica plate, while the radiolabelled PEG chains ($[^{18}\text{F}]\mathbf{62}$ and $[^{18}\text{F}]\mathbf{67}$) eluted to the top of the TLC plate moving with the acetonitrile solvent front, which confirmed that radiolabelling had taken place.

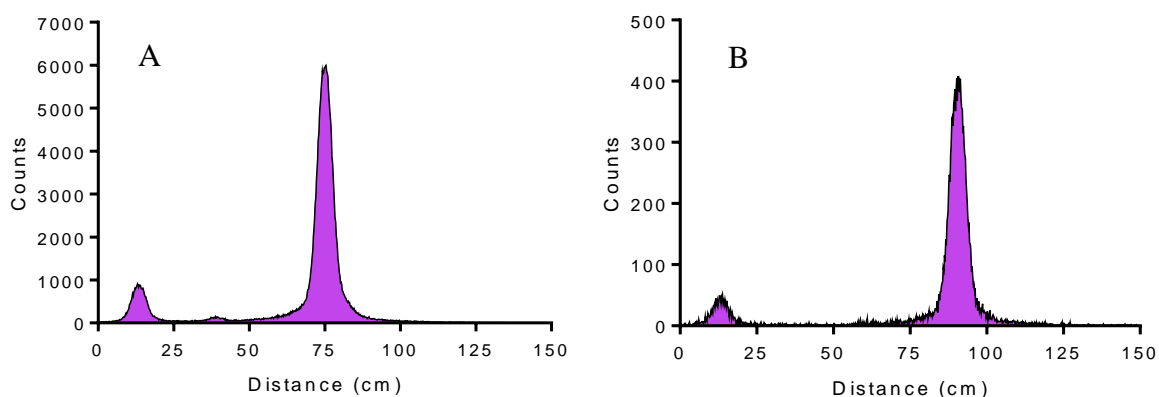


Figure 64. (A) Radio-TLC of the reaction mixture, denoting free unbound $[^{18}\text{F}]^-$ and the $[^{18}\text{F}]$ radiolabelled prosthetic ($[^{18}\text{F}]\mathbf{62}$). (B) Radio-TLC of the reaction mixture, denoting free unbound $[^{18}\text{F}]^-$ and the $[^{18}\text{F}]$ radiolabelled prosthetic ($[^{18}\text{F}]\mathbf{67}$).

Approximately 500 MBq of $[^{18}\text{F}]\mathbf{62}$ and $[^{18}\text{F}]\mathbf{67}$ were taken up by lead shielded HPLC needles and purified by semi-preparative HPLC using solvent method 1 (Chapter 6.1) and the fractions collected in glass vials shielded in a lead pot. It is worth noting, that semi-preparative HPLC of $[^{18}\text{F}]\mathbf{62}$ had notably fewer by-products and less unbound $[^{18}\text{F}]^-$ than that of $[^{18}\text{F}]\mathbf{67}$, this could likely be due to the sensitivity of the azide moiety to thermally decompose when harshly heated during azeotropic distillation, meanwhile, the thermally stable alkyne functionalised $[^{18}\text{F}]\mathbf{62}$ radiolabelled prosthetic had noticeably fewer radiolabelled by-products. The pure fractions were collected, the accumulated activity measured. The pure samples were analysed by QC radio-TLC and radio-HPLC to determine the purity post-semi-preparative HPLC (Figure 65). In both cases, radio-TLC and radio-HPLC gave the products as a single major band. The radiochemical purity

(RCP) of both of the PEG chains ($[^{18}\text{F}]\mathbf{62}$ and $[^{18}\text{F}]\mathbf{67}$) at this stage was found to be >99% by QC radio-HPLC and radio-TLC.

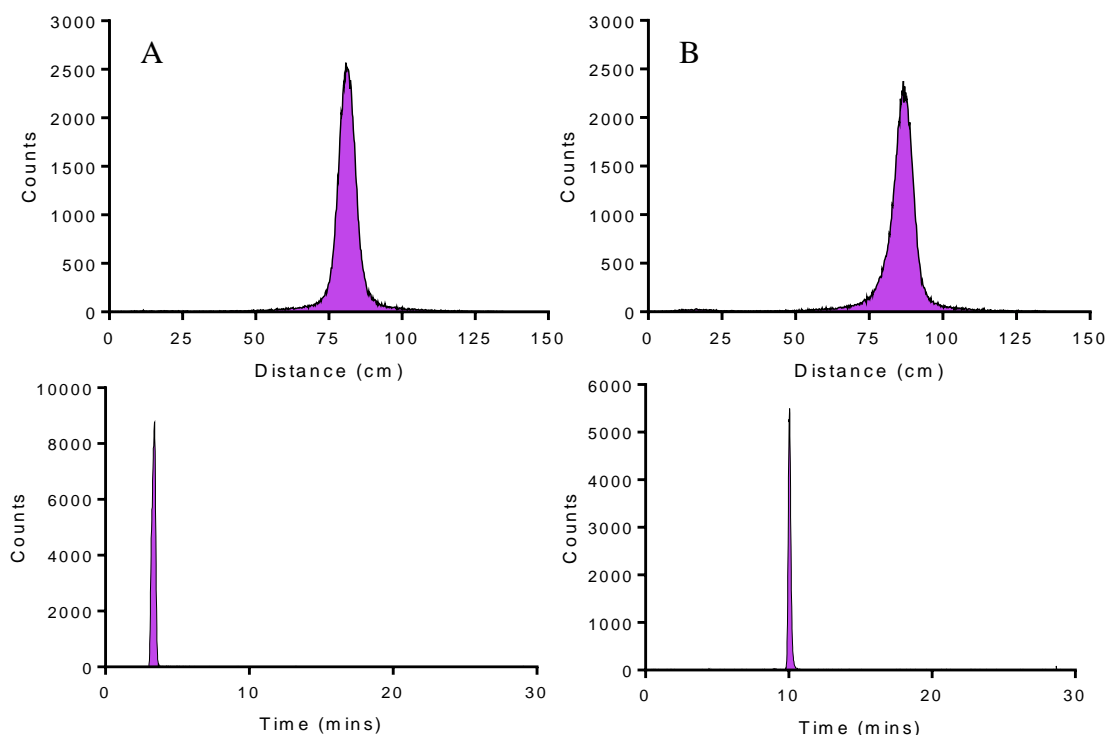


Figure 65. (A) QC radio-TLC of $[^{18}\text{F}]\mathbf{62}$. (B) QC radio-TLC of $[^{18}\text{F}]\mathbf{67}$. (C) QC radio-HPLC (C-18 silica, method 1) of $[^{18}\text{F}]\mathbf{62}$. (D) QC radio-HPLC (C-18 silica, method 1) of $[^{18}\text{F}]\mathbf{67}$.

This protocol has enabled us to identify that the radiolabelling of **50** and **66** could be carried out by nucleophilic substitution with $[^{18}\text{F}]\text{K}_{222}$, and, to determine that the radiochemical synthesis of $[^{18}\text{F}]\mathbf{62}$ (109.1 MBq, non-decay corrected) was more favourable than $[^{18}\text{F}]\mathbf{67}$ (75.6 MBq, non-decay corrected) due to its higher stability during azeotropic drying and higher radiochemical yield. Moving forwards, proof-of-concept conjugation of $[^{18}\text{F}]\mathbf{62}$ to **61** was carried out first due to it being synthetically easier to synthesise and purify $[^{18}\text{F}]\mathbf{62}$ and obtain it in higher RCY.

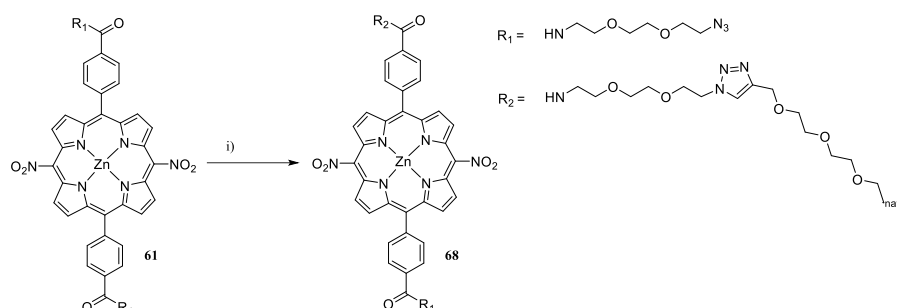
3.4.3 Synthesis of the ‘Cold’ Standard Conjugates

The next step in the protocol was to conjugate the trans- A_2 -diarylporphyrin to its corresponding ‘cold’ heterobifunctional ^{18}F prosthetic. The conjugation was carried out under microwave heating to give a mixture of mono- and bis-adducts (Scheme 35, Table 26). Due to the reaction occurring in a THF/MeOH mixture, $\text{Cu}(\text{OAc})_2$ monohydrate was used as a source of Cu(I) with the aid of a reducing agent (sodium ascorbate). Tris(benzyltriazolylmethyl)amine (TBTA) was used in the reaction mixture to stabilise the Cu(I) active catalyst and promote a higher reaction yield. Strictly speaking, an excess of heterobifunctional linker would give a far higher ratio of the

bis-adduct. However, during radiolabelling and conjugation, only the mono-fluorinated product could be produced due to the minute concentrations of radiolabelled heterobifunctional linker compared to **61**.

Entry	Solvent	Copper Species	Reducing Agent	Temperature (°C)	Time (mins)	Yield ^a (%)
61	THF/Methanol (8:2)	Cu(OAc) ₂	Sodium ascorbate	80	20	75

Table 26. Table of conditions for copper (I) catalysed alkyne-azide cycloaddition reaction. ^a Yield is reported after purification by column chromatography.

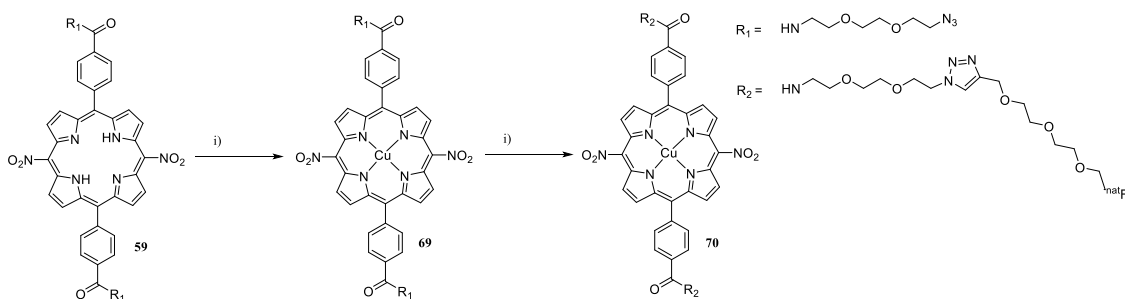


Scheme 37. Click reaction yielding mono- and bis-adducts. Conditions used; i) **61**, Cu(OAc)₂ monohydrate, sodium ascorbate, TBTA, THF/MeOH (8:2), MW heating, 80 °C, 20 mins.

Due to the amphiphilic non-ionic nature of the resulting product, the crude mixtures were highly soluble in DCM and water, but in the presence of both solvents the compound preferred the DCM phase. This allowed for facile removal of the copper species and sodium ascorbate reagents used to catalyse the CuAAC reaction. The crude was purified by solvent extraction and aqueous work-up followed by column chromatography with an eluent of 5% methanol in DCM. The pure product was obtained as a lustrous purple oily substance. This non-ionic porphyrin was rendered amphiphilic due to the high degree of PEGylation, which can reportedly increase circulation lifetime *in vivo*. The pure compound, **68**, was soluble in DMSO and could be diluted into water (final DMSO concentration <1%). All structural determination data matched what was predicted.

Compound **68** was analysed by HPLC using method 2 (Chapter 6.1). It is reasonable to assume that the polarity of the Zn(II) analogue is similar to that of the Cu(II) compounds. So an HPLC method was calibrated to give ideal separation of the precursor and cold compound, which was collected and analysed by NMR, MS, and UV-Vis. The same HPLC gradient would then be used for the copper(II) analogue. **59** was taken up in DMF and reacted with excess copper(II) acetate monohydrate under microwave irradiation. The product was worked up to give a reddish-purple crystalline powder with evidence of full metallation taking place due to the presence of only two Q bands. **69**, was reacted under the same conditions as **61**, this time giving the true ‘cold’ standard. The mixture was purified by column chromatography in DCM/MeOH (95:5) to give a lustrous

reddish-purple crystalline solid in excellent yield (97%). The purified compounds were analysed by analytical HPLC to determine ideal conditions for facile semi-preparative HPLC purification during radiochemistry.



Scheme 38. Metallation of **59** with Cu(OAc)₂ monohydrate under microwave heating, and subsequent CuAAC conjugation to **62**. Conditions used; i) **62**, Cu(OAc)₂ monohydrate, DMF, MW heating, 80 °C, 1 hr. ii) **69**, Cu(OAc)₂ monohydrate, sodium ascorbate, TBTA, THF/MeOH (8:2), MW heating, 80 °C, 20 mins.

3.4.4 Synthesis of a ‘Hot’ [¹⁸F] Radiolabelled Diphenylporphyrin

The radiochemical synthesis of [¹⁸F]**62** was repeated from an initial activity of 3.64 GBq [¹⁸F]F⁻, which was trapped and eluted through an Allox cartridge as before giving the [¹⁸F]K₂₂₂ intermediate (2.82 GBq, RCY 77%, non-decay corrected). [¹⁸F]**62** was synthesised and purified by semi-preparative HPLC, collected, and azeotropically distilled. Aliquots were taken into 1.7 mL champagne vials with sodium ascorbate, Cu(OAc)₂ monohydrate, and TBTA. **70** was added and a series of six reactions were carried out to determine the most efficacious time and concentration of precursor (**70**) required to give the highest yield of radiolabelled conjugate (Figure 66). The reactions were monitored by radio-TLC to reveal that the most efficacious time and concentration to be used for radiochemical conjugation was 0.6 µg/mL and 30 mins at 80 °C. RCP was determined by radio-TLC and radio-HPLC where possible (Table 27). Higher concentrations (>0.6 µg/mL) of **70** used in the reaction were found to deleteriously affect the yield obtained.

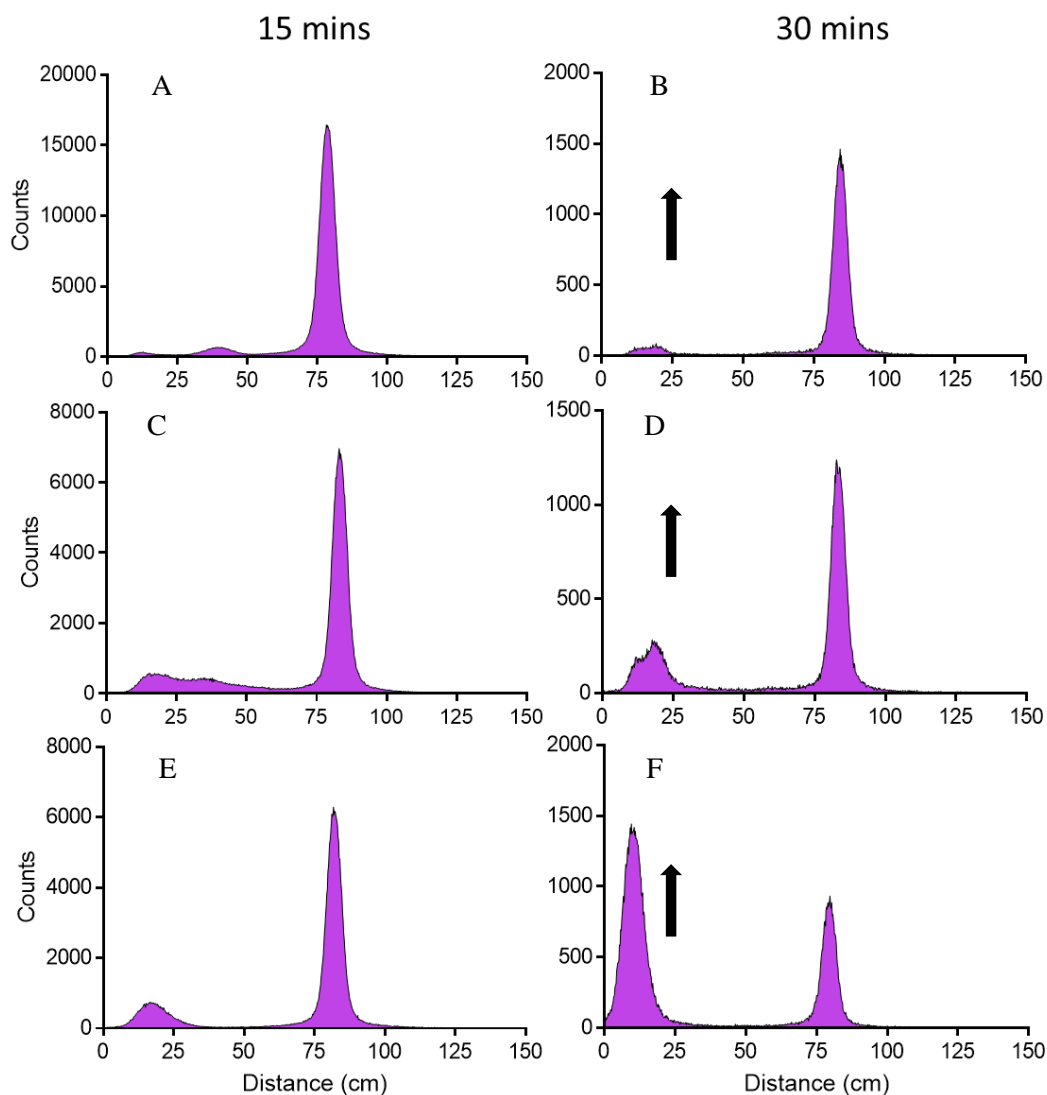


Figure 66. Radio-TLC chromatograms of the reaction optimisation of the radiochemical conjugation of $[^{18}\text{F}]\mathbf{62}$ to $\mathbf{69}$ yielding $[^{18}\text{F}]\mathbf{70}$.

Conditions	Initial Activity (Bq)	Temperature (°C)	Concentration $\mathbf{69}$ ($\mu\text{g/mL}$)	Time (mins)	RCP (%) ^a	RCP (%) ^b
A	100	80	0.2	15	3.41	-
B	100	80	0.2	30	7.72	5.23
C	100	80	0.4	15	24.84	-
D	100	80	0.4	30	27.28	23.64
E	100	80	0.6	15	18.22	-
F	100	80	0.6	30	68.43	54.60

Table 27. Tabulated experimental conditions investigated for the radiochemical conjugation of $[^{18}\text{F}]\mathbf{62}$ to $\mathbf{69}$. ^aRadiochemical purity (RCP) determined by radio-TLC. ^bRadiochemical purity (RCP) determined by radio-HPLC.

QC Radio-HPLC of crude [^{18}F]70 was found to agree with QC HPLC of the ‘cold’ analogue 70, as shown by Figure 67.

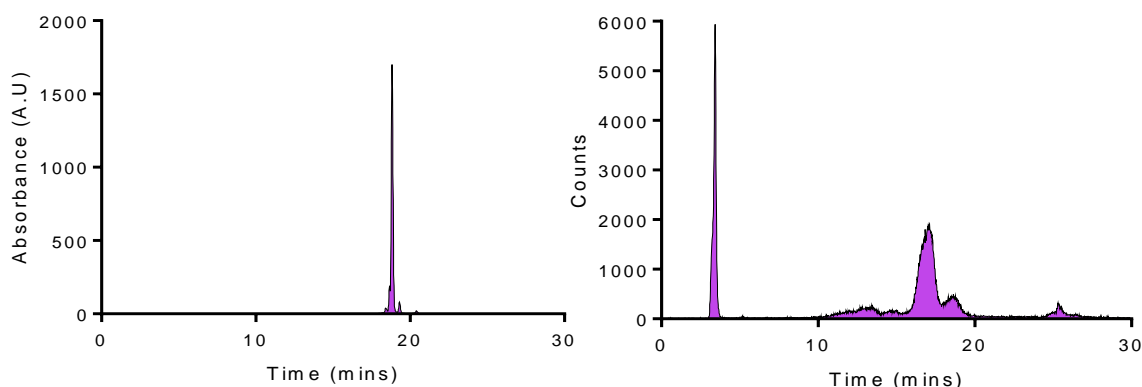


Figure 67. HPLC of 72, $R_t = 18.7$ mins (left). Radio-HPLC of [^{18}F]72, $R_t = 18.1$ mins (right).

These data were used to determine that conditions ‘F’ were the most suitable for radiochemical conjugation of [^{18}F]62 to precursor 69 yielding [^{18}F]70. However, the RCP (~55%) was low for a CuAAC reaction with scope to increase the efficiency of this reaction by varying the concentration of catalyst, reducing agent, and changing solvent azeotropes from THF/MeOH to dioxane/EtOH allowing for higher temperatures to be reached. In either case, semi-preparative HPLC purification and QC analyses are required to obtain reliable RCYs, and azeotropic distillation and solvent exchange to formulate the porphyrin in heparin-water for hot cell-uptake and IV administration to murine orthotopic models for *in vivo* biodistribution acquisition.

3.5 Chapter Conclusion

Throughout this chapter, several strategies have been attempted to append either an alkyne or azide functionality to 10. Initially, efforts to directly introduce an alkyne or azide functionality to one of the free *beta*-positions were attempted. The most efficacious route determined was *via* the use of heterobifunctional PEG chains which could be conjugated to the tetrapyrrole through an amide linkage. Porphyrins with both alkyne and azide PEG chains have been successfully conjugated, purified and characterised. The porphyrin has been subjected to metallation conditions and ‘clicked’ to a cold fluorinated linker group to yield the cold standard. HPLC methodology has been developed to separate the mixture of compounds obtained to give ideal separation conditions for semi-preparative HPLC purification of the ‘hot’ compound. The prosthetic chains [^{18}F]62 and [^{18}F]67 have been successfully radiolabelled using the $\text{K}_2\text{CO}_3/\text{K}_{222}$ nucleophilic radiofluorination method and purified using semi-preparative HPLC. Both of the radiolabelled prosthetics synthesised were found to have an RCP of >99% and could be synthesised in good RCYs >50% (non-decay corrected). Radiochemical method development was

carried out for the CuAAC ‘click’ reaction of [^{18}F]62 and 69 to give the radiolabelled conjugated [^{18}F]70 with a radiochemical purity of >55% as measured by radio-TLC and radio-HPLC, with further method development required. The conjugate could be successfully obtained with an activity within the 100 MBq region required for clinical human diagnostic PET scans, albeit formulation development needs to be carried out.

These proof-of-concept reactions gave us sufficient information to determine that radiochemical conjugation could be carried, however, the RCP and RCP were relatively low for a CuAAC reaction and further method development is required. Furthermore, simplification of the molecule is required in order to increase the overall yield of the final product and to reduce the number of synthetic steps in this lengthy 13-step procedure. This work has also demonstrated that the methodology laid down by Entract *et al.* in the preparation of a novel cationic theranostic PET/PDT conjugate could be applied to a diphenylporphyrin scaffold, which has never been demonstrated before in the literature. Future work would include synthesis of a ‘simpler’ conjugate, hot cell-uptake and *in vivo* biodistribution PET imaging.

Chapter 4
**Synthesis and Biological Evaluation of a Novel Porphyrin-
RAPTA Conjugate**

4.0 Introduction

Increasingly, novel metal-based compounds are being investigated as cytotoxic agents. Chief among these are the ruthenium(II) arene 1,3,5-triaza-7-phosphaadamantane (PTA) species or so-called “RAPTA” complexes which have gained interest in the past two decades as cytotoxic or anti-metastatic agents.^{121,276,277} For an excellent review of biologically active RAPTA complexes see Murray *et al.*¹²² These ruthenium-based agents offer many advantages over traditional platinum-based and organic-based chemotherapy, principally the lack of off-target side effects - with platinum-based therapies associated with more than 40 side effects.¹¹⁶ Secondly, the solubility of RAPTA complexes in polar media is typically far higher than those of platinum based agents such as *cis*-platin, carboplatin and oxaliplatin.²⁷⁸ Thirdly, many cancers become resistant to platinum *via* mechanisms including: decline in adduct levels, reaction with intracellular reducing agents, binding to transporters, reduced endocytosis and cross-linking repair.¹¹⁹ Both ruthenium and platinum based therapy agents have a mechanisms of action dominated by the aquation of the metal center resulting in chloride ligand displacement in the intercellular environment due to low chloride concentrations.²⁷⁹ However, RAPTA complexes are still relatively lipophilic and suffer from a lack of specificity towards cancers and internalization can only be validated by invasive biopsies followed by elemental analysis such as ICP techniques or by labeling with fluorophores or radionuclides.

Porphyryns are well known for possessing exquisite fluorescent properties, and an ability to generate cytotoxic reactive oxygen species (ROS) by acting as photodynamic sensitizers upon interaction with light.²⁸⁰ Porphyryns are the ideal conjugate of choice which have been used to generate theranostic agents for combined cancer therapy and imaging.¹³⁷ Photodynamic therapy (PDT) is a minimally invasive technique requiring a photosensitizer (PS), light and molecular oxygen. Absorption of light of the correct wavelength promotes the porphyrin into an electronically excited singlet state which undergoes Laporte forbidden intersystem crossing to the triplet state.²⁸¹ From here, two main photochemical processes can occur to produce cytotoxic species. The Type I mechanism creates ROS through immediate electron transfer to surrounding substrates, while the Type II mechanism is dominated by interaction with molecular oxygen producing singlet oxygen.²⁸¹ An added and well documented benefit of conjugating to porphyryns is they are able to utilize the enhanced permeation and retention (EPR) effect to passively accumulate and be retained in tumors, this has been proven with many substrates appended to porphyryns in the literature.^{12,154}

It is well understood that cancers are far less resilient when combating two therapies at the same time, and, the combination of PDT with the anti-metastatic/cytotoxic effects of ruthenium(II) represents a novel therapeutic combination.^{4,282} While the conjugation of porphyryns with 2,2'-bipyridine appended moieties has been carried out previously, the work did not use the true

RAPTA motif, and four Ru(II) units were required to obtain IC_{50} values in the low micro molar region.²⁸³ A second group investigated the photophysical properties of first generation ruthenium-porphyrin conjugates using pyridyl groups on the porphyrin macrocycle to act as ligands to the metal center.¹⁶⁰ Both of these reports found that cytotoxicity was only observed in multinuclear ruthenium complexes containing four ruthenium metal centres.^{160,283} These complexes would represent a large economic burden if taken to scale due to the sheer excess of ruthenium required in the synthesis of these complexes. Furthermore, these complexes contained highly lipophilic porphyrins and lipophilic bifunctional linkers which rely on the poorly hydrophilic ruthenium metal complexes to facilitate dissolution of these lipophilic porphyrins in biological media. In order to obtain spectral data studies were carried out in organic solvent, highlighting the aqueous solubility issues of these conjugates.²⁸³

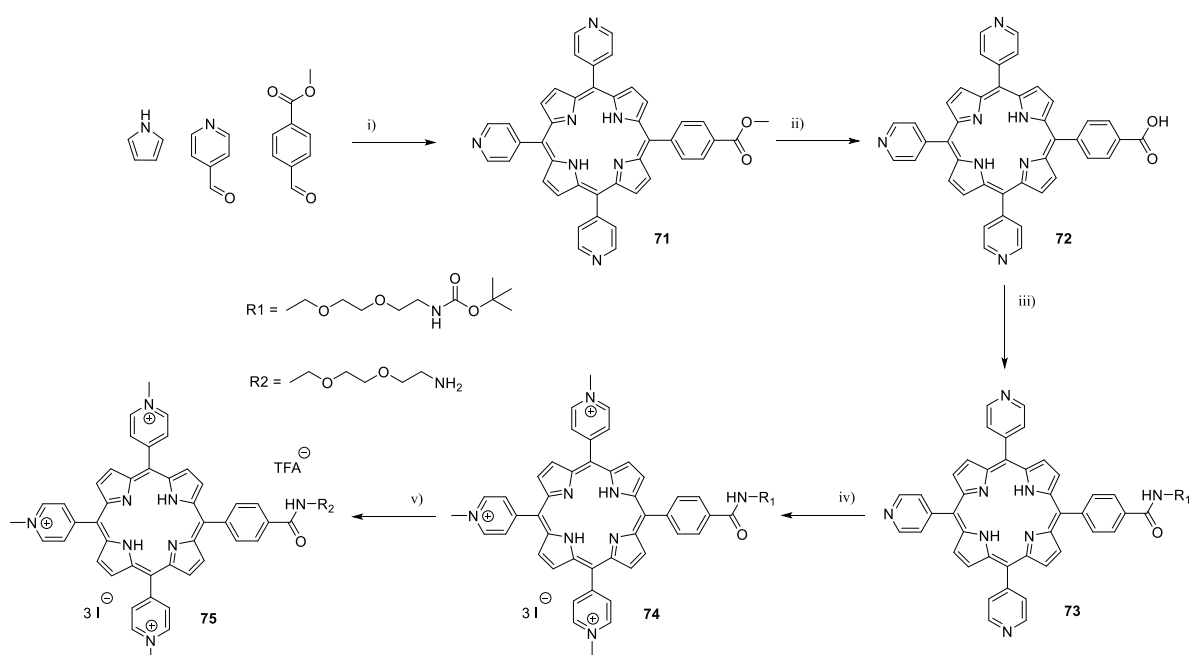
Clearly, further development of RAPTA-porphyrin conjugates is required in order to produce a clinically relevant and economically viable ruthenium conjugate using a single metal centre, while still being a hydrophilic complex. The employment of hydrophilic porphyrins bearing solubilizing methyl pyridinium groups and a hydrophilic bifunctional spacer is obviously advantageous. Furthermore, cationic N-methylpyridylporphyrins possess a natural ability to passively accumulate in cancer cells and neoplastic tissues. Therefore, our studies have focused on a cationic porphyrin covalently tethered to a single RAPTA complex with known anti-cancer activity. As previously discussed in Chapter 1, several attempts to synthesise tetranuclear Ru(II)-porphyrin conjugates has been attempted. However, ruthenium is a scarce precious metal, and a ratio of four Ru(II) ions per porphyrin represents a significant expense. The key difference being that in previous examples the Ru(II) was coordinated to N-pyridyl nitrogen atoms. We wish to investigate the tethering of the RAPTA complex by the arene ring, thus allowing for more labile ligands to be attached to the Ru(II) centre, potentially giving way to a significantly more cytotoxic conjugate. As discussed, the mechanism of action of these Ru(II) RAPTA complexes is said to progress similarly to that of *cis*-platin through the aquation of the metal centre in the intracellular environment giving a highly cytotoxic metal complex.

4.1 Synthesis of a Conjugatable Porphyrin

Our investigations began with the synthesis of a porphyrin which could be derivatized to be water-soluble for simple drug formulation, and, to contain a conjugatable handle for covalent attachment to the RAPTA species. Amide bonds are known to be thermodynamically and hydrolytically stable *in vitro* and *in vivo* and are resilient to esterases, thus we investigated the synthesis of a carboxylic acid reactive porphyrin. Porphyrin **71** was synthesised *via* the Adler-Longo mixed aldehyde condensation [3+1] reaction, condensation of 4-pyridylcarboxaldehyde and methyl 4-formylbenzoate occurred with pyrrole in refluxing propionic acid according to the method of Yap *et al.*²⁸⁴ The desired product was isolated from the obtained statistical mixture of six products

firstly by pre-column chromatography, followed by exhaustive column chromatography to give the product as lustrous purple crystals in 4.5% yield. The NMR gave the exact expected splitting pattern of the aromatic pyridyl, aryl protons, and *beta* protons. This reaction was successfully scaled by a factor of two to obtain a greater mass of product with no significant sacrifice of the obtained yield (4.2%), higher scales than this were not attempted. The methyl ester was saponified by heating at reflux a mixture of the methyl ester porphyrin and KOH in a THF/MeOH (4:1) for 24 hour. Acidic-aqueous workup gave the carboxylic acid porphyrin (**72**) as a purple powder in near quantitative yield (98%) after drying *in vacuo* until reaching constant mass. A hydrophilic bifunctional PEG linker was dissolved in DCM/TEA and protected with the commonly used acid labile Boc group. Purification by column chromatography with a gradient from 5% to 25% MeOH gave the PEG chain as a colourless oil in good yield (87%) with excellent purity.

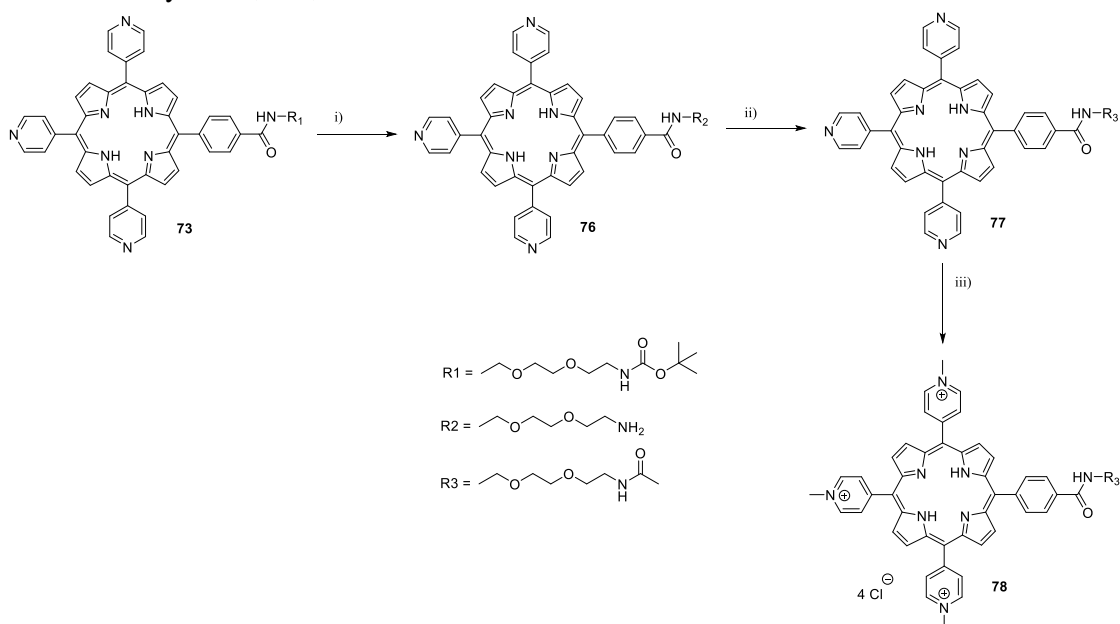
Conjugation of the Boc-protected hydrophilic bifunctional PEG linker (**56**) took place in DMF with TBTU and DIPEA with heating to 50 °C overnight. The complex (**73**) was afforded in excellent yields (87%) after column chromatography. The pre-conjugate was characterised fully by NMR, MS and UV-Vis spectroscopy. Notably, the addition of this PEG spacer produced a porphyrin which was soluble in methanol and ethanol indicating increasing hydrophilicity. Quarternerisation of the pyridyl moieties gave the water-soluble N-methylpyridium groups with iodide as the balancing counter ion after reaction with methyl iodide in DMF with heating overnight. The cationic porphyrin salt was obtained as the iodide salt, this was carried out so that counter-ion exchange could be used as a purification technique for the final desired compound. Finally, facile deprotection of the Boc group took place by reaction in TFA/DCM (1:1) followed by precipitation to yield the hydrochloride-iodide salt (**75**) in excellent yield (81%). All structural determination data agreed with data published previously.



Scheme 39. Synthesis of a carboxylic acid reactive porphyrin. Conditions used; i) propionic acid, reflux 180 °C, 2 hr. ii) KOH, THF/MeOH (4:1), Ar, 60 °C, stir 17 hr. iii) TBTU, DIPEA, DMF, Ar, 40 °C, stir 17 hr. iv) MeI, DMF, DIPEA, Ar, 40 °C, stir 17 hr. v) TFA/DCM (1:1), RT, stir 1 hr.

4.2 Synthesis of an Amide-capped Porphyrin

Synthesis of **73** was repeated, however, this route deviated from the previous route as the compound was to be used as a chemical comparative standard during biological evaluation. The Boc protecting group was removed by treatment with TFA in DCM (1:1) for 1 hour, followed by aqueous work up to give the porphyrin as the TFA salt (**76**). The TFA-amine salt was reacted with acetic anhydride under anhydrous basic conditions followed by purification by column chromatography to give the acylated protected product (**77**). Following this, the porphyrin was rendered water-soluble by methylation of the pyridyl groups in DMF with excess methyl iodide. The product was converted from the iodide salt to the hexafluorophosphate salt by dissolving in methanol with the addition of ammonium hexafluorophosphate. The hexafluorophosphate porphyrin salt was taken up in acetone and the addition of excess tetrabutylammonium chloride gave the cationic porphyrin as the highly water-soluble chloride salt (**80**) in excellent yield (94%), following the method according to the method of Giuntini *et al.*²⁸⁵. All compounds were fully characterised by NMR, MS, and UV-Vis.

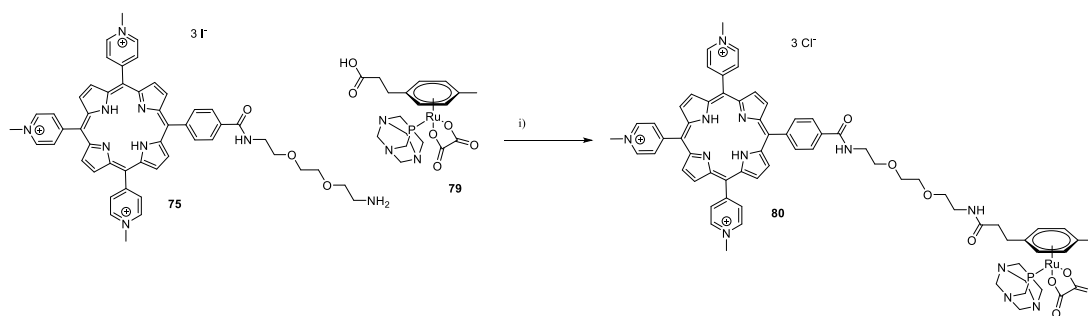


Scheme 40. Synthesis of an amide capped porphyrin. Conditions used; i) TFA/DCM (1:1), RT, stir 1 hr. ii) Ac₂O, DIPEA, DMF, Ar, 40 °C, stir 17 hr. iii) MeI, DMF, DIPEA, Ar, 40 °C, stir 17 hr.

4.3 Synthesis of a Porphyrin-RAPTA Conjugate

The [Ru(η⁶-arene)(C₂O₄)PTA] complex (**79**) was kindly synthesized and provided by Dr Ben Murray (University of Hull).¹²³ The conjugate was covalently linked by carrying out an amide conjugation reaction in DMSO with TBTU and DIPEA which was purified by washing with ethyl

acetate, followed by counter-ion exchange and isolation by lyophilization from acetone. The highly water-soluble cationic RAPTA-porphyrin conjugate (**80**) was found to be highly soluble in DMSO, water and biological media. The cationic porphyrin and hydrophilic PEG spacer had dramatically enhanced the hydrophilicity of the lipophilic RAPTA complex. Interestingly, we observed a down field shift for the conjugated RAPTA arene protons by $^1\text{H-NMR}$ from 7.21 ppm in D_2O to 8.30 ppm in $\text{DMSO-}d_6$. It can be suggested that this effect occurs due to dielectric constant of water being roughly double that of DMSO (at 25 °C) causing a conformational shift in the complex by π - π stacking of the porphyrin aryl rings with the RAPTA arene ring in order to lower the energy of the system by creating a lipophilic core. This effect could be occurring by a thermodynamically controlled process to minimize surface area of the lipophilic RAPTA-arene ring in the polar deuterated solvent, thus lowering the energy of the molecule in polar media. Biological evaluation of this new dual-therapeutic agent could produce desirable results as the 3D conformation of the ligands has been shown to mediate the biological effects of the complex.²⁸⁶



Scheme 41. Synthesis of a porphyrin-RAPTA conjugate. Conditions used; i) TBTU, DIPEA, DMSO, Ar, stir 3 hr.

4.4 Photochemical Studies

Ideally, a photosensitizer should absorb in the red-NIR region for deep tissue penetration, however, optical fibers which can be inserted into the body to negate this requirement somewhat, so strong absorption at longer wavelengths is clinically relevant. Clearly, the absorption data proves that conjugation of the RAPTA to the porphyrin did not deleteriously alter the porphyrins optoelectronic properties. The results of the UV-Vis absorption studies for the two porphyrins **78** and **80** are given by Figure 68 and Table 28 recorded at room temperature (23.5 °C). The conjugate was maintained as the free base rather than undergoing complexation with a metal such as Zn^{2+} , Pt^{2+} or Pd^{2+} in order to profit from the four Q bands allowing for potential deeper tissue penetration due to the red absorption band at 650 nm.

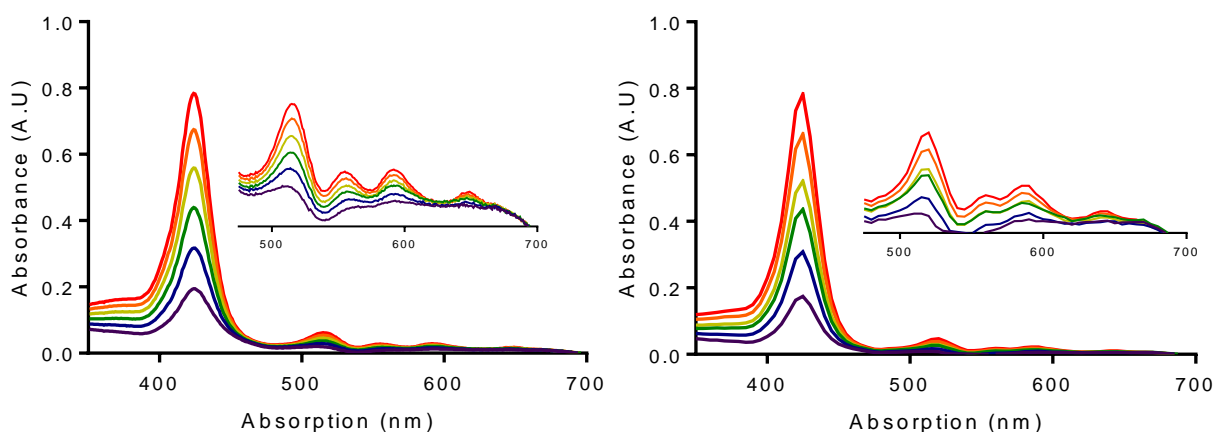


Figure 68. UV-Vis absorption spectra of **78** (left) and **80** (right) determined in d(H₂O).

The Soret bands (*ca.* 420 nm) were found to have the highest molar absorptivity coefficient, while the Q-bands had the lowest. The highest wavelength absorptions were at *ca.* 650 nm. As expected, the tabulated results are extremely similar and don't show any significant variations, this is likely because conjugation of the alkyl amine to the alkyl carboxylic acid of the RAPTA species is unlikely to affect the electronic properties of the tetrapyrrolic core.

Entry	Soret band (nm)	Q band I (nm)	Q band II (nm)	Q band III (nm)	Q band IV (nm)
78	425 (5.10)	518 (3.95)	561 (3.67)	595 (3.64)	649 (3.17)
80	426 (5.12)	525 (3.90)	565 (3.66)	595 (3.53)	650 (3.02)

Table 28. UV-Vis absorption maxima and molar absorptivity coefficients determined in d(H₂O). Molar absorptivity coefficients are given as log₁₀ values in brackets.

The relative singlet oxygen quantum yield is the relative measure of the efficiency of a photosensitizer to convert triplet state molecular oxygen into the highly cytotoxic singlet oxygen. 9,10-anthracenediyl-bis(methylene)dimalonic acid, (ABDA), is commonly used as a diagnostic tool in which photo-oxidation of the central arene ring takes place when in the presence of singlet oxygen yielding an endoperoxide and a reduction in the obtained UV-Vis absorption spectra relative to the control (Figure 69). In this case, the water soluble photosensitizer *meso*-tetra(*N*-methyl-4-pyridyl)porphyrin (**TMePyP**) was used as a standard during singlet oxygen quantum yield experiments with irradiation from red light. **TMePyP** was prepared according to the literature. The results of the irradiation of ABDA (absorption monitored at 380 nm) with time are shown in Table 29. Qualitatively, a decrease in the absorption maxima corresponds to the production of singlet oxygen, it can clearly be seen that the decrease in the absorbance signal of ABDA can be seen over time when irradiated with red light (613–651 nm, 1035.8 W m⁻²). This is an indication that singlet oxygen is being produced. Obviously, irradiation of ABDA without the presence of a photosensitizer didn't produce any statistically significant indication singlet

oxygen. The relative singlet oxygen quantum yields of **78** and **80** were calculated relative to that of **TMePyP**. **80** gave an excellent value of 1.57, this value could be attributed to the subtle combination enhanced steric hindrance and electronic effects of the conjugate when compared to the other two porphyrins. It is well understood that even water-soluble cationic porphyrins aggregate and π - π stack in solution which limits their relative singlet oxygen quantum yields, possibly explaining why **80** and **TMePyP** gave such similar values.

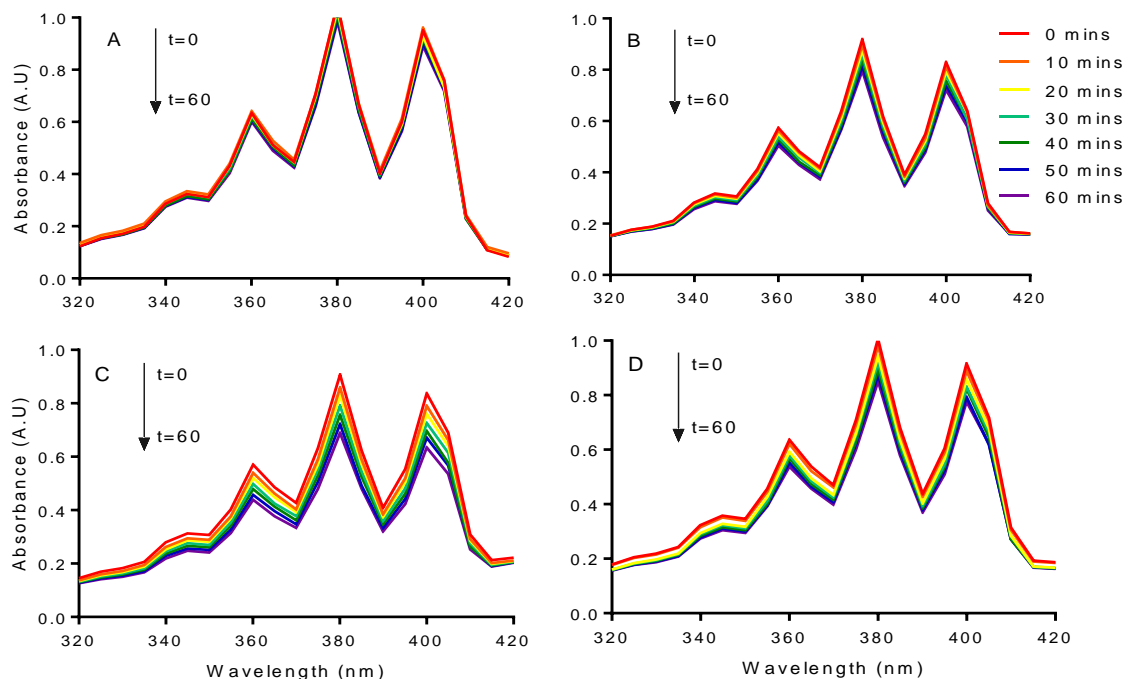


Figure 69. UV-Vis absorbance spectra of ABDA irradiated with red light (617 - 651 nm) with and without photosensitizer (PS). Curves are averages of three independent experiments ($n=3$). A; ABDA (100 μM), B: ABDA (100 μM) irradiated in the presence of 4.75 μM of **TMePyP**, C: ABDA (100 μM) irradiated in the presence of 4.75 μM of **80**, C: ABDA (100 μM) irradiated in the presence of 4.75 μM of **78**.

Entry	Φ_{Δ}
ABDA	-
TMePyP	1.00
78	1.57
80	0.89

Table 29. Data for the relative singlet oxygen quantum yields (Φ_{Δ}) for given compounds obtained by photochemical studies by time-course UV-Vis spectroscopy with the presence of a singlet oxygen radical trap (ABDA). Data presented are averages of three independent experiments ($n=3$).

Photostability is a major concern for any photosensitizer/fluorophore, as small molecule fluorophores often experience irreversible photobleaching upon continuous illumination with light, therefore, limiting their use in biomedical applications. The photostability of **78** and **80** was investigated with Rose Bengal being utilized as a non-porphyrin control for samples irradiated with white light, and **TMePyP** being used as a control for samples irradiated with red light (Figure

70). When irradiated continuously for 60 minutes in d(H₂O), **78**, **80**, and **TMePyP** were all found to behave similarly. This is likely due to the fact that the peripheral substituents rarely have an effect on the photostability of the tetrapyrrolic core. None of the samples were found to have a normalized absorbance of less than 95% after irradiation for 60 minutes. When irradiated continuously with white light for 10 minutes in d(H₂O), **78** and **80** were both found to be appreciably photostable with normalized absorbance values of $88.65 \pm 0.03\%$ and $86.60 \pm 0.01\%$ respectively, which didn't deviate significantly from the normalized absorbance when irradiated continuously for 60 minutes with red light. Meanwhile, the commercially available Rose Bengal control was found to fully photobleach to a normalized absorbance value of $1.58 \pm 0.01\%$ after continuous irradiation with white light for 10 minutes. Therefore, compared to the commercially available photosensitizer/fluorophore, the porphyrin-RAPTA conjugate can be said to be relatively photostable under these specific conditions.

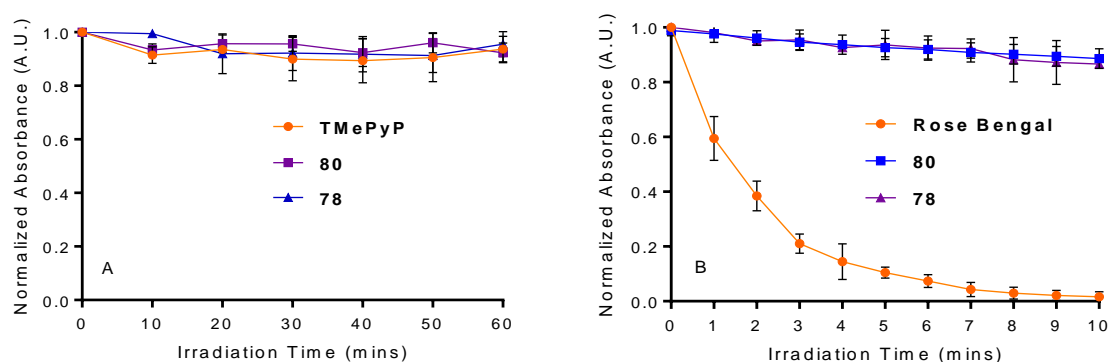


Figure 70. (A) Photostability studies of compounds **78**, **80** and **TMePyP** irradiated continuously with red light (617 - 651 nm, 1035.8 W m^{-2}). (B) Photostability studies of compounds **78**, **80** and **Rose Bengal** irradiated continuously with white light. Data are presented as $\bar{x} \pm SD$ ($n=3$).

In order to probe the photostability of the cytotoxic $[\text{Ru}(\eta^6\text{-arene})(\text{C}_2\text{O}_4)\text{PTA}]$ complex we took a known mass of **14** into D₂O (0.7 mL) in an NMR tube and recorded the ³¹P-NMR and ¹H-NMR spectra at room temperature. The sample was protected from light, then irradiated sequentially with 20 J cm^{-2} fractions of white light and recorded the NMR spectrum after each irradiation. With regards to the ³¹P-NMR spectra, the relative intensity of the peak originating from the bound PTA ligand did not increase or decrease after irradiation with white light, furthermore, no other peaks were observed even at high doses of 60 J cm^{-2} as seen in Figure 71. Again, the ¹H-NMR remained unchanged suggesting that no significant changes to the Ru(II) ligands were occurring from ROS in solution under these conditions. Therefore, we are confident that this unique conjugate consists of not only a photostable tetrapyrrole but also a photostable RAPTA moiety.

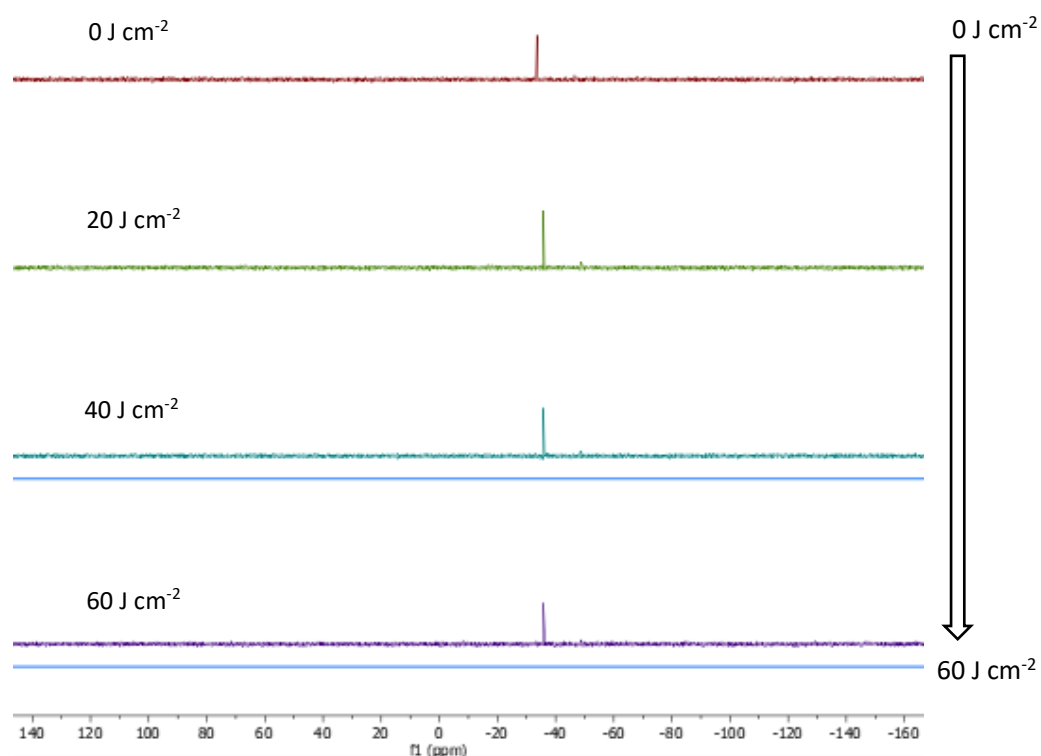


Figure 71. ^{31}P -NMR of **14** after receiving 0, 20, 40, or 60 J cm^{-2} of white light revealing the evolution of PTA phosphine oxide through photoinduced electron transfer. Chemical shifts (δ) measured in ppm.

4.5 *In Vitro* Phototoxicity Studies

In order to determine the biological anti-cancer efficacy of **78**, **79**, and **80**, human colorectal adenocarcinoma (HT-29) cells were treated with varying concentrations and a fixed dose of light (20 J cm^{-1}) over two incubation time periods (24 hours and 48 hours). Cell viability was determined by an MTT assay (Figure 72). The 96-well plates were washed and replenished with fresh media before irradiation with a fixed dose of white light to remove any unbound or non-internalized compound. As previously discussed, mononuclear RAPTA complexes typically have IC_{50} values of $>400 \mu\text{M}$ and exhibit less than favorable solubility.¹²³ The RAPTA-porphyrin conjugate (**80**) had an incubation time-dependent cell viability response. At the 24 hour incubation time period, **79** was found to be clearly non-cytotoxic in the “dark”, but acted as a perfectly viable photosensitizer in its own right when irradiated with white light (20 J cm^{-2}). With regards to **79**, an IC_{50} wasn't observed even at a high concentration of $500 \mu\text{M}$. Obviously, no statistically significant light dependent toxicity was observed with this RAPTA species. Interestingly, we observed a significant decrease in cell viability in the ‘dark’ for conjugate **80** compared to **78**, which we attribute to the presence of the cytotoxic RAPTA. The covalent tethering of the porphyrin to the cytotoxic RAPTA complex *via* a hydrophilic chain was found to yield a 10-fold decrease in the required concentration of Ru(II) compared to the conjugate (**80**) after a 24 hour incubation period to achieve a cell viability of $\sim 70\%$. We attribute this decrease in cell viability

to the natural ability of the cationic porphyrin to increase the internalization of the Ru(II) compared to **79** alone. At the 48 hour incubation period time point, we observed a decrease in the cell viability of cells treated with **79** again, no light dependent cytotoxicity was observed. **80** appears to become appreciably cytotoxic at high concentrations (10 μM) in the 'dark', while still producing a statistically significant difference compared to the irradiated cells. Most interestingly, with regards to **80**, a cell viability of $16.8 \pm 2.0\%$ was observed when the cells were incubated for 48 hours with 10 μM compared to a cell viability of $14.9 \pm 1.7\%$ when incubated for 24 hours with 250 μM , representing a significant 25-fold decrease in effective concentration for a statistically comparable result at the expense of a longer incubation period. With irradiation of light, we observed an excellent $\text{IC}_{90} = <10 \mu\text{M}$ for conjugate **80** (Figure 73). Alternatively, after incubation for 48 hours, **80** gave a cell viability of $16.8 \pm 2.0\%$, while **79** gave a cell viability of $42.8 \pm 3.9\%$ at the 10 μM concentration level. This conjugate yielded cell viabilities comparable to other works while only requiring 48 hour incubations compared to 72 hour incubations, representing a serious advance over other published works.

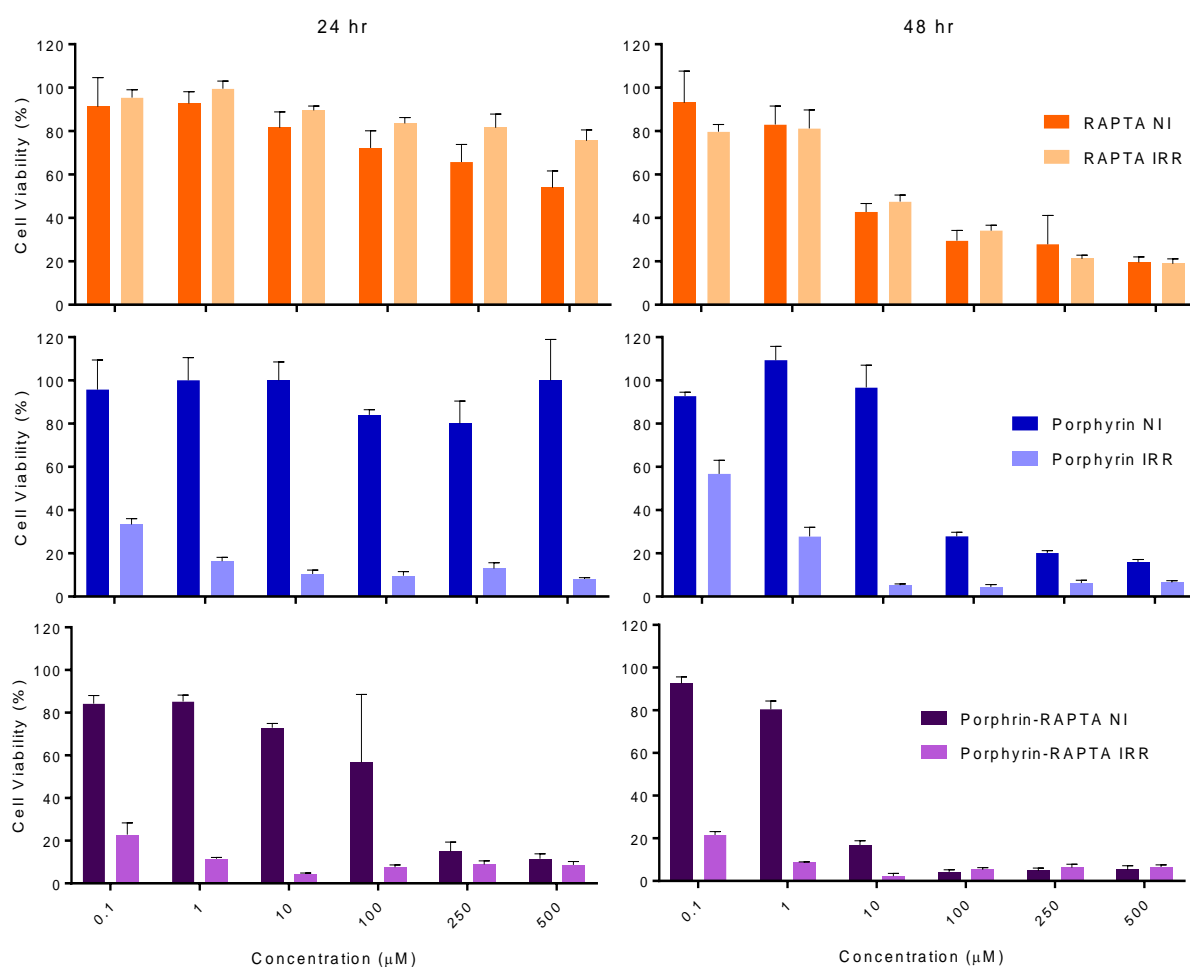


Figure 72. Temporal MTT assay of **78**, **79** and **80** displaying time-dependent and concentration-dependent cell viabilities with 0 J cm^{-2} and 20 J cm^{-2} light doses. NI; non-irradiated, IRR; irradiated. Data are presented

as $\bar{x} \pm SD$ (n=3). ANOVA statistical analysis was carried out with Bonferroni's *post-hoc* significance testing.

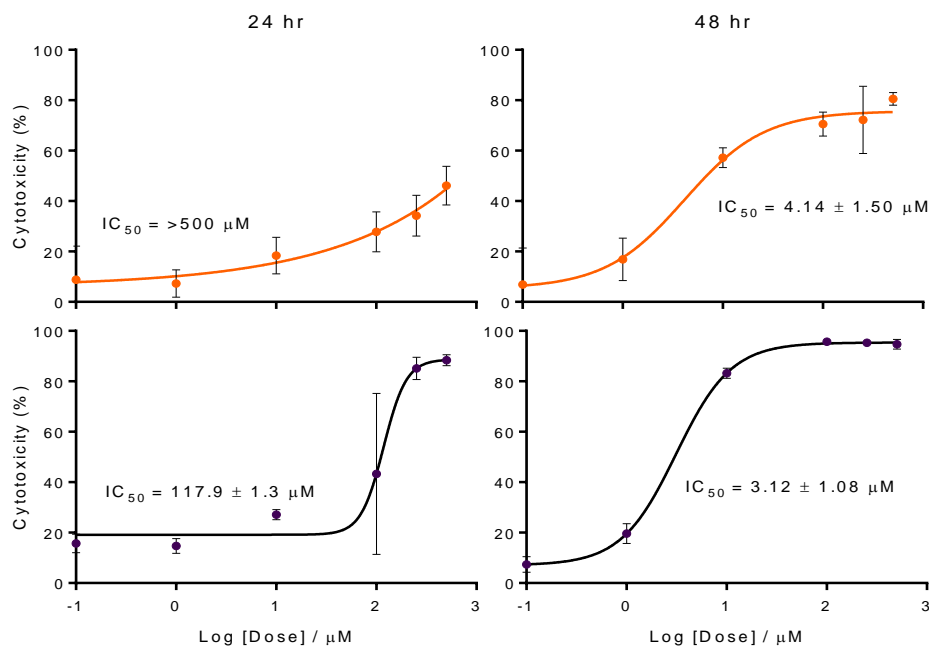


Figure 73. Dose-response cytotoxicity curves of **78** and **80** measured over two incubation periods (24 hour and 48 hour). Data are presented as $\bar{x} \pm SD$ (n=3).

In our hands, we envisage this novel cationic second-generation porphyrin-RAPTA conjugate being used clinically for the combined therapy and imaging of cancers; the non-invasive photodynamic therapy can be initiated using harmless white light, and the remaining retained compound contributes to inhibiting growth of the remaining tumor cells with a concentration and time-dependent effect. 10 μM of **80** gives an ideal balance between phototoxicity when irradiated with 20 J cm^{-1} of white light ($2.3 \pm 1.2\%$ cell viability) and cytotoxicity in the 'dark' ($16.8 \pm 2.0\%$ cell viability).

4.6 Cell Uptake by ICP-MS

Inductively coupled plasma mass spectrometry is a highly sensitive technique used to detect trace elements. In this case, it was employed to determine the relative concentrations of ^{101}Ru in HT-29 cells that had been incubated with compounds **80** or **79** for 48 hours, followed by washing, harvesting, and re-suspending the cells in PBS. The protocol was developed to determine whether **80** or **79** had been internalized by HT-29 cells (Figure 74). Clearly, the concentration of ^{101}Ru was significantly higher ($p < 0.01$) in cells that were treated with $10\ \mu\text{M}$ of **79** compared to $10\ \mu\text{M}$ of **80**, and compared to the cell only sample (vehicle controlled). Therefore, we can predict based on ICP-MS data alone, that the porphyrin-RAPTA conjugate had been internalized by the HT-29 cells, where as a far lower proportion of the RAPTA compound had. It is well documented that cationic N-methylpyridinium porphyrins are known to be internalized by cancer cells and that they mostly localize in the mitochondria,^{289,290} and the lysosomes.^{291,292}

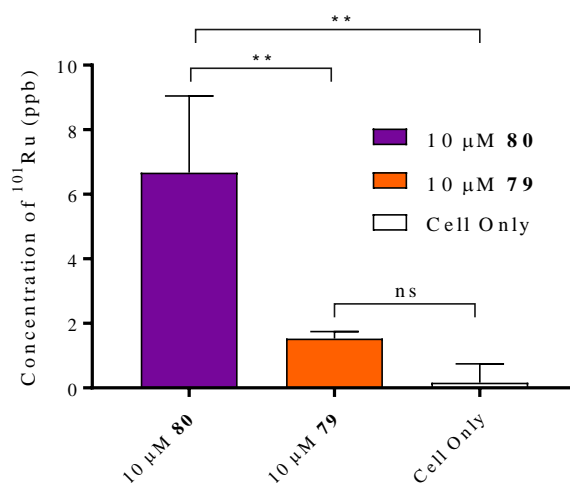


Figure 74. ICP-MS data highlighting the concentration of ^{101}Ru (ppb) in HT-29 cells incubated with $10\ \mu\text{M}$ for 48 hour. Data are presented as $\bar{x} \pm \text{SD}$ ($n=3$). An ordinary ANOVA statistical analysis was carried out with Dunnett's post-hoc multiple comparisons significance testing, ns; ($p > 0.05$), *; ($p < 0.05$), **; ($p < 0.01$).

4.7 Chapter Conclusion

To conclude, we have successfully synthesized a second-generation water-soluble mononuclear porphyrin-RAPTA conjugate (**80**) and evaluated it photochemical and biologically. The photostability of the conjugate was found to be excellent regardless of whether it was irradiated with white light or red light, and the conjugate retained its exquisite optoelectronic absorption properties. Furthermore, it had a relatively higher singlet oxygen quantum yield compared to a known porphyrin standard. Biological evaluation has allowed us to determine that the conjugate is a viable photosensitizer in its own right, but, it also operates as an anti-cancer agent by controlling cell proliferation in the 'dark' at low concentrations ($10\ \mu\text{M}$), while the RAPTA had an $\text{LD}_{50} > 500\ \mu\text{M}$. In fact, a 2.5-fold decrease in cell viability was observed when compared to

the RAPTA conjugate alone at the same concentration in the 'dark'. Furthermore, we obtained this data requiring only 48 hour incubations, while previous work on porphyrin-ruthenium conjugates, and RAPTA compounds, have required 72 hour incubations in order to achieve acceptable LD values. Fluorescence microscopy and ICP-MS has allowed us to obtain bio-distribution and cell uptake data, which has allowed us to attribute this enhanced anti-cancer efficacy of this conjugate to the porphyrin chaperoning the tethered RAPTA into the intracellular environment. In our hands, we envisage this novel cationic second-generation porphyrin-RAPTA conjugate being used clinically for the combined therapy of cancers - the non-invasive photodynamic therapy can be initiated using harmless white light, and the remaining retained compound can contribute to inhibiting growth of the remaining tumor cells with a concentration and time dependent effect. We believe, that these studies have demonstrated that porphyrin-RAPTA conjugates have the potential to be clinically viable, and that we have laid the foundation for further studies to more closely examine the biological efficacy of these conjugates *in vivo*.

Chapter 5

Conclusion, Contributions to the Field, and Future Work

5.0 Conclusion and Contributions to the Field

Throughout this thesis, the field of personalised treatment of cancers through the employment of theranostic and dual-therapeutic porphyrins has been thoroughly reviewed and investigated. We have identified core absences of knowledge in the scientific literature - which we have attempted to bridge. We have recognised that the combination of cancer therapy and diagnostic imaging represents a powerful amalgamation of technologies, which can be applied to personalized medicine. Specifically, with the aim of increasing the effects of radiotherapy by the introduction of a non-toxic tetrapyrrole which is capable of increasing the therapeutic benefits of radiotherapy, which can additionally be monitored by PET imaging, or by the synthesis of a novel dual-therapeutic agent. We have refined the methodology required to functionalise the *meso* positions with electron-withdrawing groups and incorporate paramagnetic and diamagnetic first-row transition metals into the tetrapyrrolic core of a trans-A₂-diarylporphyrin. Furthermore, we have investigated several routes to yield not only a hydrophilic porphyrin, but, also a porphyrin with ‘click’ handles for facile radiolabelling via conjugation. With the support of the literature, we have demonstrated through the synthesis of a library of trans-A₂-diarylporphyrins that a relationship exists between steric and electronic effects in controlling the hydrophilicity of trans-A₂-diarylporphyrins. This synthetic library was reduced to a pair of hydrophilic trans-A₂-diarylporphyrins which have undergone *in vitro* evaluation to determine their efficacies as radiosensitizers. Both of the lead molecules are easy to formulate in biological media, they can be taken into a diluent of sterile DMSO and diluted into media or serum to a DMSO concentration of ~1%, which is far below the toxic limit for *in vitro*, *ex vivo*, and *in vivo* assays. This represents a significant improvement in formulation compared to that of the only porphyrin based radiosensitiser currently in clinical trials, MLT-005. **23** was found to be soluble in PBS without the need for DMSO, while **18** required some DMSO in order to dissolve in polar media.

We have, to the best of our knowledge, carried out the first in-depth radiobiological study on a trans-A₂-diarylporphyrin to elucidate its efficacy and mechanism of action. We have successfully quantified the presence of copper in the cancer cells emanating from compounds **18** and **23** through the utilization of ICP-OES/MS studies which proved that the compounds were being internalized. We have evaluated the effect of these two compounds on cell number/viability through MTT assays, **18** was found to be predominantly non-toxic when incubated with cells for less than 24 hours. The use of clonogenic assays has revealed that within HT-29 (p53 null) cells, RER values of 1.24 and 1.26 for doses of 2 Gy and 4 Gy respectively with a 50 μM dose of **18** were obtained. At higher doses of radiation, minimal enhancement was observed. These radiation iso-dose values indicate that at an ionising radiation dose of RER_{2 Gy} a 24% increase in cell death is observed, and similarly for a RER_{4 Gy} a 26% increase in cell death is observed at 50 μM. In HCT-116, significantly higher values were obtained (RER_{2 Gy} = 1.74, RER_{4 Gy} = 2.31). DMR

values were found to be higher at lower surviving fractions than higher surviving fractions. We have evaluated the effect of the compound **18** on the cell cycle distribution through FACS which revealed that it caused an increase in the arrested cells when irradiated with 4 Gy of ionizing radiation compared to the 4 Gy control. ANOVA analysis of comet assays have revealed that HT-29 (p53 null) and HCT-116 (p53 WT) gave no significant differences between the treated samples with the compound compared to radiation treated samples alone ($p > 0.05$). Therefore, this assay couldn't definitively determine whether or not an increased amount of DNA damage was occurring with the presence of the compound, but it did confirm that DNA damage was occurring and that it was dependent on the treatment administered ($p < 0.001$). Immunofluorescence showed that there was no significant difference in either cell line between the observed levels of canonical apoptosis for the 10 Gy treated samples and 4 Gy + 50 μ M treated samples. Overall, we believe that we have started to reveal the biological mechanism of action of a novel porphyrin radiosensitizer. Our hypothesis is that **18** must be sensitizing the HT-29 (p53 null) and HCT-116 (p53 WT) cells to ionizing radiation, and increasing the observed levels of canonical apoptosis, but not doing so through the enhanced induction of single-strand and double-strand DNA breaks. Regardless, we do believe that **18** is a viable candidate as a radiosensitizer.

The introduction of an [^{18}F]F radionuclide has been attempted in order to produce a theranostic capable of being detected by PET imaging. The modification of **18** to prepare it for 'click' chemistry has been attempted through several routes. Notably, the utilization of heterobifunctional linker groups has proven to be the most useful approach, conferring both enhanced hydrophilicity and a reactive handle for 'click' chemistry. Introduction of both an azide and alkyne to the porphyrin macrocycle have been investigated. Heterobifunctional linkers labelled with ^{nat}F have been synthesised, and test 'click' reactions have been carried out. Owing to this, we investigated the 'hot' synthesis of the Cu(II) chelate, [^{18}F]70. Nucleophilic radiofluorination was successfully carried out on **62** using [^{18}F]F $^-$ mediated by K_{222} which was purified by semi-preparative radio-HPLC. The QC radio-TLC and QC radio-HPLC determined that the RCP was $>99\%$. The 'hot' radiolabelled product ([^{18}F]62) was successfully conjugated to **69** giving [^{18}F]70 which was determined by radio-HPLC in $>55\%$ RCP. This work demonstrated that the porphyrin scaffold could be successfully synthesised 'hot', albeit in low RCY.

Additionally, we have investigated the synthesis of a novel second-generation water-soluble mononuclear porphyrin-RAPTA conjugate and evaluated it photochemically and biologically as a dual-therapeutic compound. The rationale being that cancer cells are less able to combat two different therapies which progress through two different mechanisms of action. We successfully synthesized a conjugatable cationic tetraarylporphyrin and conjugated it to a RAPTA species with known, albeit poor, biological activity. Photochemically, the conjugate was found to be stable

under irradiation with either white light or red light, and the photoelectronic properties were not found to be deleteriously affected, in fact, the relative quantum yield was enhanced compared to a known porphyrin standard. Biologically, we found that the conjugate is a viable photosensitizer in its own right, but, it also operates as an anti-cancer agent by controlling cell proliferation in the 'dark' at low concentrations (10 μM), while the non-conjugated RAPTA had an $\text{LD}_{50} > 500 \mu\text{M}$. In fact, a 2.5-fold decrease in cell viability was observed when compared to the RAPTA conjugate alone at the same concentration in the 'dark'. Furthermore, we obtained this data requiring only 48 hour incubation, while previous work on porphyrin-ruthenium conjugates, and RAPTA compounds, have required 72 hour incubations in order to achieve acceptable LD values.

5.1 Future Work

In terms of synthesis, we believe that the synthesis of a more hydrophilic trans- A_2 -diarylporphyrin would be advantageous and that this could be achieved by emulating the swallow-tail technology developed by Borbas and Lindsay *et al.* Or alternatively, the synthesis of a porphyrin appended to two cyclodextrins would most resemble the structure of MLT-005 in 3D space providing the steric bulk required to prevent π - π stacking/aggregation and enhancing the hydrophilicity at the same time. Additionally, a true structure-activity relationship needs to be determined with a wider range of *meso* EWGs including moieties such as CF_3 , CN and SO_2CF_3 . Cyclic voltammetry and computational studies can be employed as physiochemical/computational methods of determining reduction potentials which can be correlated to *in vitro* activity. Biologically speaking, γH2AX immunofluorescence studies can help to identify radiation-induced stress *in vitro*. While Western blots can be exploited to determine the levels of protein expression for PARP, *cyclin D1*, Chk1, Chk2, p23 and p53, which would allow us to elucidate the downstream effects of the compound on the cells when exposed to ionizing radiation. Furthermore, the determination of whether Cu(II) trans- A_2 -diarylporphyrins have any effect on the regulation of genes that are metallothionein or thioredoxin related would allow us to determine their effect on cellular ability to combat redox stress. This would allow us to elucidate whether the tetrapyrrole was inhibiting cellular antioxidants, which would inevitably lead to higher levels of cell death after exposure to ionizing radiation. Or, whether they are replacing cofactors in the intracellular environment yielding defunct structures preventing repair and reoxygenation. Additionally, carrying out biological evaluation with hypoxic cells or 3D cell cultures would further provide evidence to validate **18** as a clinically viable radiosensitizer. In terms of improving the radiochemistry aspect of this thesis in the synthesis of a theranostic agent, method development and a simplification of the laborious synthetic procedure would be an obvious advantage, as well as increasing the radiochemical yield of radiolabelling, obtaining a molar activity curve, log P, 'hot' cell uptake, and *in vivo* biodistribution data. With regards to dual-therapeutic agents, it is reported that osmium analogues of RAPTA compounds possess serious untapped potential as anti-cancer agents. The synthesis of

an analogous osmium compound would be interesting to determine whether the attachment of the porphyrin still enhances the cell uptake and whether dark toxicity could be amplified meaning that the LD₉₀ has potential to enter more desirable nanomolar concentrations. Additionally, FACS analysis of cells treated with the porphyrin-RAPTA conjugate (**80**) could help determine whether the effect on the cell viability emanating from the conjugate in the 'dark' is either cytotoxic or cytostatic. Overall, trans-A₂-diphenylporphyrins are little studied for their biomedical applications compared to their *meso*-tetraphenyl cousins, mostly due to solubility and aggregation issues, to date, there is no published literature on [⁶⁸Ga] or [¹⁸F] radiolabelled PET/PDT trans-A₂-diarylporphyrin theranostic agents. It is our belief that all of these investigations would further enhance the understanding of trans-A₂-diarylporphyrins as theranostic agents and dual-therapeutic agents for the combined therapy and diagnostic imaging of cancers.

Chapter 6
Experimental

6.0 Experimental

6.1 Methods and Materials

All reagents and solvents were obtained from either Alfa Aesar, Fluorochem, Honeywell, or Sigma Aldrich, and were used as received unless stated otherwise. Dry solvents were obtained by drying the solvent over dried activated 3Å or 4Å molecular sieves or anhydrous metals salts as appropriate using the method according to Williams *et al.*²⁹³

The reaction progress and purity of synthetic compounds were analysed by TLC using Fluka analytical TLC plates of 0.2 mm thickness with a stationary phase of 60 Å pore sized adsorbed silica. Progress of TLC was visualised using long wave or short-wave UV irradiation, potassium permanganate solution, ninhydrin solution, bromine vapour, or iodine chambers as appropriate. Rf values were calculated by measuring the ratio of the distance travelled by the analyte by the distance travelled by the solvent front.

Synthesised compounds were purified by column chromatography using an appropriate mobile phase as stated using a glass chromatography column and a stationary phase of silica gel obtained from Fluorochem; LC60Å 35-70 µm. Progress of column chromatography was visualised using long wave or short-wave UV irradiation, tracked against relevant TLC plates.

NMR were recorded on a JEOL ECZ 400 Spectrometer at 400 MHz for proton NMR and at 100.5 MHz for carbon NMR analyses. All samples submitted contained an internal standard of tetramethylsilane (TMS) in deuterated solvent as stated. NMR spectra splitting patterns were designated as s (singlet), d (doublet), t (triplet), q (quartet), quin (quintet), sex (sextet), m (multiplet) or br s (broad singlet), dt (doublet of triplets) as appropriate. All chemical shifts, δ , for proton (^1H), carbon (^{13}C), fluorine (^{19}F), and phosphorous (^{31}P) NMR spectra were quoted as parts per million, ppm. J values are quoted in Hz unless stated otherwise. Proton, carbon, fluorine, and phosphorous chemical shifts are denoted as follows; ppm (multiplicity, integration, coupling constant, chemical environment or structure) where possible.

Mass spectrometry data were obtained by submitting samples to the EPSRC National Mass Spectrometry Service at Swansea. Matrix assisted laser desorption ionization (MALDI) analysis was performed on a MALDI-TOF Voyager mass spectrometer in positive reflectron mode with DCBT matrix. ESI+ mass spectrometry was performed on a LTD Orbitrap XL mass spectrometer in an appropriate solvent or buffer. Time of flight atmospheric solids analysis probe mass spectrometry (ASAP) was performed on a Xevo GS-2 mass spectrometer in positive reflection mode. ESI- was performed on a LTQ Orbitrap XL mass spectrometer in an appropriate solvent or buffer. All high-resolution mass spectrometry data were within the 5 ppm threshold.

UV-Vis data was obtained from a Varian Cary Bio 50 spectrophotometer by the addition of aliquots of standard solutions into a known volume of solvent in an optical glass cuvette of optical clarity 200-2500 nm. Data obtained by 20 μL additions to 2 mL of solvent from a 10 mL stock solution of concentration $1 \times 10^{-2} \text{ mol dm}^{-3}$. The molar absorptivity (ϵ) at the λ_{max} was calculated from the Soret band by application of the Beer-Lambert law.

Combustion elemental analysis was performed with 15 mg of compound analysed in a Carlo Erba EA1108 CHN Fischer instrument with a thermal conductivity detector for determination of CHN; analysis quoted in %.

ATR-FT-IR was obtained using a Thermo Scientific Nicolet iS5 FT-IR spectrophotometer with an iD6 Diamond ATR attachment using Thermo Scientific OMINC software for analyses for both solid and liquid phase samples.

Microwave reactions were carried out in 35 mL or 15 mL thick-walled glass reaction vials with a PTFE cap in a CEM SP Benchmate microwave reactor with a maximum power output of 200 W, and a maximum pressure of 17 Bar.

Fluorine-18 ($[^{18}\text{F}]\text{F}^-$) was produced by the $^{18}\text{O}(\text{p},\text{n})^{18}\text{F}$ reaction on an enriched ^{18}O water (98% enrichment, Marshal Isotopes Ltd., Israel) using a BG-75 BTA 7.5 MeV Molecular Imaging Cyclotron with a current of 4 μA and a beam time of approximately 1 hour.

Mean values are given ($\bar{X} \pm \text{SD}$) where possible, ($n \geq 3$), all biological experiments were carried out in at least triplicate ($n=3$) unless stated otherwise. Values were statistically evaluated using a GraphPad Prism 5 (San Diego, CA, USA). * denotes ($P < 0.05$); ** denotes ($P < 0.01$); *** denotes ($P < 0.001$), **** denotes ($P < 0.0001$). The normality of the data was assessed to validate the use of parametric statistical analyses. The Skewness and Kurtosis were found to be within acceptable levels suggesting the data are normally distributed calculated using GraphPad Prism 5. The mean was relatively equal to the median in all cases unless stated otherwise.

HPLC analyses were performed on an Agilent series 1200 HPLC system. Separations were carried out on an ACE-5 C-18 column (4.6 x 250 mm). Semi-preparative HPLC was carried out using a Pursuit 10 μm C-18 200 \AA column (250 x 10 mm) (Phenomenex). All solvents were HPLC grade containing 0.1% TFA in both eluents.

Method 1:

Analytical RP-HPLC (ACE-5, C18 column, 4.6 x 250 mm 100) with HPLC grade methanol with 0.1% TFA and HPLC grade water with 0.1% TFA as eluents A and B respectively. The flow rate was 1 mL per minute. Initially, an isocratic gradient of 20% A rising to 30% (20 mins) raising to 95% A (1 min), isocratic 95% (3 mins), falling to 20% (2 mins) and remaining isocratic (3 mins).

Method 2:

Analytical RP-HPLC (ACE-5, C18 column, 4.6 x 250 mm 100) with HPLC grade methanol with 0.1% TFA and HPLC grade water with 0.1% TFA as eluents A and B respectively. The flow rate was 1 mL per minute. Initially, an isocratic gradient of 80% A rising to 83% (18 mins) raising to 95% A (7 mins), then increasing to 80% (3 mins) and remaining isocratic (2 mins).

Method 3:

Analytical RP-HPLC (ACE-5, C18 column, 4.6 x 250 mm 100) with HPLC grade methanol with 0.1% TFA and HPLC grade water with 0.1% TFA as eluents A and B respectively. The flow rate was 1 mL per minute. Initially, an isocratic gradient of 5% A rising to 95% (20 mins), isocratic 95% (3 mins), falling to 5% (2 mins) and remaining isocratic 5% A (5 mins).

6.2 Biological Methodology

Clonogenic Assay

All cell culture was carried out by Huguette Savoie. Cell irradiation and cell counting were performed by Jordon Sandland.

Cells: HT29/HCT-116

Medium: McCoy's 5A modified medium substituted with 1% L-glutamine and 10% foetal calf serum (Life Science Productions).

Environment: humidified 5% CO₂

Cells, with a confluence of 60-70%, were seeded onto 6 well plates (Greiner Bio-one; multiwell 6), 1.5 mL of a 1×10^3 μ L solution McCoy's 5A modified medium substituted with 1% L-glutamine and 10% foetal calf serum (Life Science Productions) and incubated to adhere to the plates for 24 hr at 37°C with a 5% CO₂ humidified environment. Cells were seeded at a concentration of 1.5×10^3 per 1.5 mL of solution. The cells were irradiated with an RS-2000 Biological System animal irradiator at level 3, dose rate of 1.87 Gy/min, 160 kV and 25 mA. The cells were incubated for 7 days and the progress of growth checked by optical microscopy, the media was replenished as previously stated, the cells were fixed with crystal violet (Gerard; microscopical stain), 0.1% w/v in methanol (Honeywell; puris >99.7% GC) 70% v/v and d(H₂O) 30% v/v was used to stain and fix the cells, which was then removed and quenched in concentrated NaOH_(aq) (Fischer; analytical reagent grade) solution. The plates were carefully washed with d(H₂O) until the colonies were distinct, plates were then air-dried for 24 hrs. Colonies were counted using the GelCout instrument (Oxford Optronix, UK) using optimised CHARM for each cell line. Only colonies of 50 cells or greater were counted. The results are expressed with respect to control values (i.e.: cells only, no irradiation).

MTT Assay

All cytotoxicity assays were carried out and analysed by Huguette Savoie.

Cells: HT29/HCT-116

Medium: McCoy's 5A modified medium substituted with 1% L-glutamine and 10% foetal calf serum (Life Science Productions).

Environment: humidified 5% CO₂

Agents: MTT (Sigma M5655; Thiazolyl blue)

The cell viability was determined using MTT (3-[4, 5-dimethylthiazol-2-yl]-2, 5-diphenyltetrazolium bromide) colourimetric assay. Briefly: 10 µL of 12 mM MTT solution is added to each well and incubated between 1 and 4 hours at 37°C to allow MTT metabolism. The crystals formed were dissolved by adding 150 µL of acid-alcohol mixture (0.04 M HCL in absolute 2-propanol). The absorbance at 570 nm is measured on a Biotek ELX800 Universal Microplate Reader. The results are expressed with respect to control values (i.e.: cells only).

Fluorescence Assisted Cell Sorting (Nicoletti Assay)

All cell culture was carried out by Huguette Savoie. Cell irradiation and flow cytometry were performed by Jordon Sandland.

Cells: HT-29/HCT-116

Medium: McCoy's 5A modified medium substituted with 1% L-glutamine and 10% foetal calf serum (Life Science Productions).

Environment: humidified 5% CO₂

Cells with a confluence of 60-70%, were seeded onto 6-well plates (Greiner Bio-one; multiwell 6), 1.5 mL of a 1×10^3 µL solution McCoy's 5A modified medium substituted with 1% L-glutamine and 10% foetal calf serum (Life Science Productions) and incubated to adhere to the plates for 24 hr at 37°C with a 5% CO₂ humidified environment. Cells were seeded at a concentration of 1.5×10^3 per 1.5 mL of solution. The cells were irradiated with an RS-2000 Biological System animal irradiator (Rad Source Technologies; Boca Raton, FL, USA) at level 3, dose rate of 1.87 Gy/min, 160 kV and 25 mA. The wells were rinsed with PBS (2 mL, retained) (Gibco®; PBS tablets) and trypsinised (1 mL) and the medium collected in cold media (1 mL). The cells were centrifuged for 5 min at 1250 RPM (260 g). Decanted and re-suspend into ice-cold PBS (1 mL); transferred into FACS (Falcon) tubes and keep on ice then centrifuged as above. The supernatant was decanted and re-suspended by slowly adding ice-cold 80% EtOH (4 mL) (Honeywell; puris >99.7% GC) to each tube while vortexing, the tubes were frozen for 1 hr. Pre-

prepared PI-RNaseA (Sigma-Aldrich) in PBS mixture (5×10^{-6} g/ml and 10×10^{-6} g/ml) was added. Centrifuged at 1250 RPM (260 g) for 10 minutes. The supernatant was decanted and washed with ice-cold PBS (1 mL). Centrifuged again as above and re-suspend into 1 ml PI-RNaseA PBS mix; incubated at room temperature and in the dark for 1 hour then transferred to ice for FACS analyses (Beckmann).

Cell Uptake by ICP-OES/ICP-MS

All cell culture was carried out by Huguette Savoie. ICP-OES/ICP-MS was performed by Bob Knight.

Cells: HT29/HCT-116

Medium: McCoy's 5A modified medium substituted with 1% L-glutamine and 10% foetal calf serum (Life Science Productions).

Environment: humidified 5% CO₂

Cells (1 mL, 3×10^5 cells/mL), with a confluence of 60-70%, were aliquoted into centrifuge tubes (Falcon). The cells were pelleted by centrifugation and re-suspended in 1 mL of McCoy's 5A modified medium substituted with 1% L-glutamine and 10% foetal calf serum (Life Science Productions) or McCoy's 5A modified medium substituted with 1% L-glutamine and 10% foetal calf serum (Life Science Productions) substituted with 25 or 50 μ M of compounds **18** or **23**. The tubes were incubated for 1 hr at 37°C with a 5% CO₂ humidified environment. The cells were pelleted and the supernatant collected. The cell pellet was re-suspended with PBS (1 mL, Glibco®; PBS tablets) pelleted and the supernatant fractions combined. The pellets and supernatant were frozen at -20 °C for 24 hr before ICP-OES processing. The samples were diluted into concentrated nitric acid and water (Elga Purelab Flex). ICP-OES was carried out using a Perkin Elmer 43000 Optima instrument. The cooling gas was argon (BOC Cryospeed) with a flow rate of 15 L/min, the auxiliary flow rate was 0.2 L/min and the nebuliser was 0.8 L/min. The detector (Perkin Elmer) was Peltier cooled to -43 °C. The nebuliser used was a high solids modified V-groove PEEK unit (Perkin Elmer). The Cu standards used were certified 1000 ppm (Romil, UK), which were appropriately diluted with 2% v/v nitric acid (Spa grade, Romil, UK) and water (Purelab).

Single Cell Gel Electrophoresis Assay (Comet Assay)

All cell culture was carried out by Huguette Savoie. Cell seeding, single-cell gel electrophoresis and fluorescence microscopy were carried out by Jordon Sandland.

Cells: HT-29/HCT-116

Medium: McCoy's 5A modified medium substituted with 1% L-glutamine and 10% foetal calf serum (Life Science Productions).

Environment: humidified 5% CO₂

Cells (1 mL, 3 x 10⁵ cells/mL), with a confluence of 60-70%, were aliquoted into centrifuge tubes (Falcon). The cells were pelleted by centrifugation and re-suspended in 1 mL of McCoy's 5A modified medium substituted with 1% L-glutamine and 10% foetal calf serum (Life Science Productions) or McCoy's 5A modified medium substituted with 1% L-glutamine and 10% foetal calf serum (Life Science Productions) substituted with 25 or 50 µM of compounds **18** or **23**. The tubes were incubated for 1 hr at 37 °C with a 5% CO₂ humidified environment. The cells were pelleted and the supernatant decanted. The pellets were re-suspended in PBS and the cells were irradiated with an RS-2000 Biological System animal irradiator (Rad Source Technologies; Boca Raton, FL, USA) at level 3, dose rate of 1.87 Gy/min, 160 kV and 25 mA at 4 °C. The cell suspension (1 mL) was added to 1% agarose (Flowgen Bioscience, MacroSieve LM Agarose) solution in d(H₂O) (0.4 mL). The mixture was vortexed and pipetted (1 mL) onto pre-prepared agarose coated frosted microscope slide. The slides were left to solidify at 4 °C for 15 mins with protection from light. The cells were lysed at 4 °C for 17 hr with protection from light. The cells were washed twice with alkaline electrophoresis buffer for 5 mins at 4 °C with protection from light. The DNA was separated using electrophoresis in a large horizontal bed tank (Bio-Rad) at 1 V/cm, 25 V, 300 mA and 250 W for 40 mins (Bio-Rad, Power Pac 1000). The cells were incubated in PI staining solution (2.5 µg/mL) in distilled water for 20 mins at 4 °C. The cells were washed twice with water (400 mL) and left to dry at 4 °C with protection from light. 50 images were taken per slide using a Zeiss Axio Vert. A1 fluorescence microscope with an excitation filter at 517 nm. The data were analysed using ImageJ with the OpenComet plug-in.

DAPI Nuclear Staining Immunofluorescence Assay

All cell culture was carried out by Huguette Savoie. Cell irradiation and cell counting were performed by Jordon Sandland.

Cells: HT-29/HCT-116

Medium: McCoy's 5A modified medium substituted with 1% L-glutamine and 10% foetal calf serum (Life Science Productions).

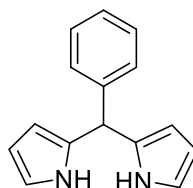
Environment: humidified 5% CO₂

Cells, with a confluence of 60-70%, were seeded onto square glass coverslips (SLS, 24 x 24 mm, No. 1.5) in 6-well plates (Greiner Bio-one; multiwel 6), 1.5 mL of a 1.5x10⁵ µL solution McCoy's 5A modified medium substituted with 1% L-glutamine and 10% foetal calf serum (Life Science Productions) and incubated to adhere to the plates for 24 hr at 37 °C with a 5% CO₂ humidified environment. The cells were irradiated with an RS-2000 Biological System animal irradiator at level 3, dose rate of 1.87 Gy/min, 160 kV and 25 mA. The cells were incubated for 3 days and

the progress of growth checked by optical microscopy. The media was removed, and the coverslips were taken, gently blotted dry, inverted, and mounted with 5 μL of DAPI (Bio Legend) and sealed with clear nail polish. 10 fluorescence images were taken per coverslip using a Zeiss Axio Vert A1 fluorescence microscope with an excitation filter at 358 nm. The data were analysed using ImageJ with a Counters plug-in.

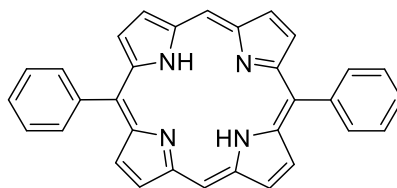
6.3 Synthetic Protocols

5-(Phenyl)dipyrromethane (1)¹⁷³



Under an inert atmosphere, a flask was purged with dry argon for 15 mins. The flask was charged with freshly distilled pyrrole (350 mL, 5.00 mol) and freshly distilled benzaldehyde (5.31 g, 50.00 mmol) and degassed for 15 mins with dry argon while protected from light with a stream of argon. InCl_3 (1.11 g, 5.00 mmol) was added in one portion, and the mixture was stirred under argon at room temperature for 3.5 hr yielding a pale-yellow solution. Freshly powdered NaOH (8.00 g, 0.15 mol) was added to quench the reaction with stirring for 1.5 hr, which afforded a pale-yellow mixture. The mixture was filtered under reduced pressure, the filtrate was collected, and bulk solvent removed under reduced pressure. Traces of pyrrole were removed by trituration with hexane (50 mL) and sonication, bulk solvent was removed under reduced pressure, repeated thrice to yield an amorphous tan solid. The resulting mass was dissolved in ethanol/water (50 mL, 4:1) with gentle heating, and allowed to crystallise overnight at 4 $^\circ\text{C}$ whilst protected from light. The crystals were taken and dissolved in a minimum of ethyl acetate and precipitated over hexane and filtered under reduced pressure to yield a colourless crystalline powder (3.7661 g, 16.9 mmol, 87% yield).

R_F : 0.32 (silica, 50:50, DCM/hexane). $^1\text{H-NMR}$ (CDCl_3): δ 5.57 (s, 1H, C-CH-C), 5.91 (dd, $J=5.9, 1.7$ Hz, 2H, C=CH-C), 6.15 (dd, $J=6.0, 2.7$ Hz, 2H, C-CH=C), 6.69 (m, 2H, C=CH-NH), 7.27 (m, 3H, m-,p-Ar), 7.91 (s, 2H, o-Ar). $^{13}\text{C-NMR}$ (CDCl_3): δ 44.06 (CC-CH-CC), 107.29, 108.52, 117.29, 127.08, 128.48, 128.74, 132.55, 142.13. MS: (ESI+) m/z $[M+H]^+$ 223.1231, HRMS: calcd. For $\text{C}_{15}\text{H}_{16}\text{N}_2$: 223.1231 found 223.1230. CHN Anal. Calcd for $\text{C}_{15}\text{H}_{14}\text{N}_2$: C, 81.05; H, 6.35; N, 12.60. Found C, 80.1; H 6.11; N, 12.89.

5, 15-Di(phenyl)porphyrin (2)¹⁷⁹

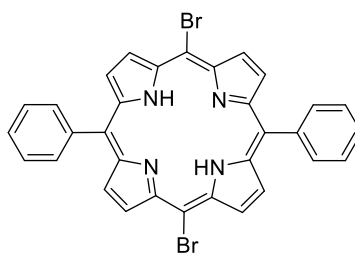
Under an inert atmosphere, 5-di(phenyl)dipyrromethane (500 mg, 2.3 mmol) was added to DCM (800 mL) and degassed following the addition of trimethyl orthoformate (25 mL, 0.165 mol). The mixture was protected from light and a solution of trichloroacetic acid (8.83 g, 54 mmol) in DCM (250 mL) was added over 15 mins under argon. The solution was stirred in the absence of light for 4 hr, excess acid was quenched with pyridine (25 mL, 24.55 g, 310 mmol). The solution was stirred for 17 hr in the absence of light. The solution was purged with compressed air and stirred open to light for 4 hr. Bulk solvent was removed under reduced pressure and triturated with hexane (50 mL), followed by co-evaporation from toluene (20 mL) to remove residual pyridine. The crude was dissolved in a minimum of DCM and eluted onto a silica chromatography column, the porphyrin eluted as the first major red fraction. Bulk solvent was removed under reduced pressure and the powder dissolved in a minimum of DCM and precipitated over MeOH and filtered under reduced pressure to yield lustrous purple crystals (75 mg, 0.0756 mmol, 14% yield).

R_F : 0.90 (silica, 70:30, DCM/hexane). $^1\text{H-NMR}$ (400 MHz, CDCl_3): δ 7.81 (m, 6H, *m*-,*p*-Ar), 8.28 (m, 4H, *o*-Ar), 9.09 (d, 4H, $J=4.6$ Hz, β -H), 9.40 (d, 4H, $J=4.6$ Hz, β -H), 10.32 (s, 2H, *meso*-H). $^{13}\text{C-NMR}$ (100 MHz, CDCl_3): δ 105.36, 119.226, 127.07, 127.82, 131.15, 131.71, 131.15, 131.70, 134.95, 141.54, 145.30, 147.33. MS: (ESI+) m/z $[M+H]^+$ 463.1910, HRMS: calcd. $\text{C}_{32}\text{H}_{22}\text{N}_4$ For: 463.1910 found 463.1917. UV-Vis (DCM): λ_{max} 407, 503, 536, 577, 626. $\log \epsilon$ (417) = 5.50.

Zinc(II) 5, 15-di(phenyl)porphyrin (3)

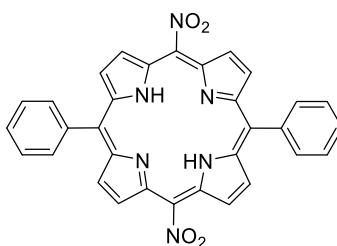
Under an inert atmosphere, 5-di(phenyl)dipyrromethane (500 mg, 2.3 mmol) was added to DCM (800 mL) and degassed following the addition of trimethyl orthoformate (25 mL, 0.165 mol). The mixture was protected from light and a solution of trichloroacetic acid (8.83 g, 54 mmol) in DCM (250 mL) was added over 15 mins under argon. The solution was stirred in the absence of light for 3 hr, a methanolic (30 mL) solution of zinc(II) acetate dihydrate (500 mg, 2.28 mmol) was added, the reaction mixture was stirred for 1 hr, excess acid was quenched with pyridine (25 mL, 24.55 g, 310 mmol). The solution was stirred for 17 hr in the absence of light. The solution was purged with compressed air and stirred open to light for 4 hr. Bulk solvent was removed under reduced pressure and triturated with hexane (50 mL), followed by co-evaporation from toluene (20 mL) to remove residual pyridine. The crude was dissolved in a minimum of DCM and eluted onto a silica chromatography column, the porphyrin eluted as the first major red fraction. Bulk solvent was removed under reduced pressure and the powder dissolved in a minimum of DCM and precipitated over MeOH and filtered under reduced pressure to yield lustrous purple crystals (175 mg, 0.333 mmol, 29% yield).

R_F : 0.86 (silica, DCM). 1H -NMR (400 MHz, DMSO- d_6): δ 7.81 (s, 6H, *p*-,*m*-Ar), 8.19 (s, 4H, *o*-Ar), 8.90 (s, 4H, β -H), 9.46 (s, 4H, β -H), 10.33 (s, 2H, *meso*-H). ^{13}C -NMR (100 MHz, DMSO- d_6): δ 55.44, 106.63, 119.47, 127.25, 127.98, 132.19, 132.65, 134.98, 143.10, 143.16, 149.43, 149.72. UV-Vis (DMSO): λ_{max} 415, 550, 585. $\log \epsilon$ (415) = 5.55.

5,15-Dibromo-10,20-di(phenyl)porphyrin (4)

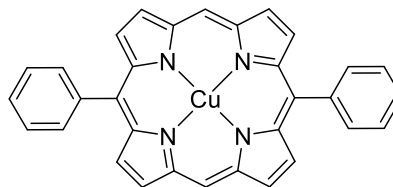
Under an inert atmosphere, 5,15-di(phenyl)porphyrin (25mg, 0.0560 mmol) was dissolved in chloroform (12.5 mL) and cooled to 0 °C and maintained for the duration of the experiment. Pyridine (0.05 mL, 0.05 g, 0.63 mmol) was added as an acid scavenger. N-Bromosuccinimide (20 mg, 0.11 mmol) was added directly to the flask and stirred for 10 min. The reaction progress was checked by TLC, DCM/hexane (50:50). The reaction was quenched with 20 mL of acetone. Bulk solvent was removed under reduced pressure, the crude was dissolved in 5 mL of toluene and entrained by sonication then bulk solvent removed under reduced pressure to remove residual pyridine. The crude product was triturated with methanol (2x10 mL) and dried under reduced pressure to yield an amorphous solid. The crude was precipitated from DCM over MeOH and filtered under reduced pressure to yield purple microcrystals (24.5 mg 0.040 mmol, 71% yield).

R_F : 0.70 (silica, 50:50, DCM/hexane). $^1\text{H-NMR}$ (400 MHz, CDCl_3): δ -2.74 (s, 2H, N-H), 7.77 (m, 6H, m-, p-Ar), 8.15 (d, 4H, o-Ar), 8.83 (d, 4H, β -H), 9.61 (d, 4H, β -H). $^{13}\text{C-NMR}$ (100 MHz, CDCl_3): δ 103.85, 121.50, 126.93, 128.15, 134.60, 141.45. MS: (ESI+) m/z $[M+H]^+$ 621.0101, HRMS: calcd. For $\text{C}_{32}\text{H}_{20}\text{N}_4\text{Br}_2$: 619.0123 found 619.0127. UV-Vis (DCM): λ_{max} 420, 520, 560, 601, 658. $\log \epsilon$ (420) = 5.22.

5,15-Dinitro-10,20-di(phenyl)porphyrin (5)

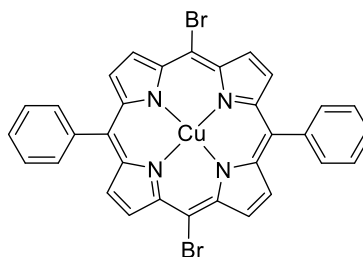
To a solution of 5,15-di(phenyl)porphyrin (300 mg, 0.079 mmol) in trifluoroacetic acid (3 mL) was added sodium nitrite (40 mg, 0.16 mmol) in one portion. The solution was stirred at RT for 10 mins. The mixture was poured into 50 ml of water, neutralized with sodium bicarbonate until the colour change from green to red-brown was observed. The nitroporphyrin was extracted into DCM (3x50 mL) and dried over anhydrous MgSO_4 . Bulk solvent was removed under reduced pressure. The crude was dissolved in a minimum of DCM and chromatographed onto a column. The fractions were collected and bulk solvent removed under reduced pressure. The powder was taken in DCM and precipitated over MeOH and filtered under reduced pressure to yield a lustrous purple powder (237 mg, 0.043 mmol, 54% yield).

R_F : 0.50 (silica, DCM). $^1\text{H-NMR}$ (400 MHz, CDCl_3): δ 7.81 (m, $J=7.8$ Hz, 6H, Ar-H), 8.18 (dd, $J=7.6, 1.7$ Hz, 4H, Ar-H), 8.94 (d, $J=4.6$ Hz, 2H, β -H), 9.03 (d, $J=4.9$ Hz, 2H, β -H), 9.26 (d, $J=4.6$ Hz, 2H, β -H), 9.33 (d, $J=4.9$ Hz, 2H, β -H). $^{13}\text{C-NMR}$ (100 MHz, CDCl_3): δ 117.22, 121.67, 122.03, 126.94, 127.98, 128.15, 134.63, 135.19, 142.72, 147.88, 148.97. MS: (ESI+) m/z $[M+H]^+$ 553.1613, HRMS: calcd. For $\text{C}_{32}\text{H}_{20}\text{N}_6\text{O}_4$: 553.1613 found 553.1619. UV-Vis (DCM): λ_{max} 416, 513, 550, 591, 640. $\log \epsilon$ (416) = 5.09.

Copper(II) 5,15-di(phenyl)porphyrin (6)

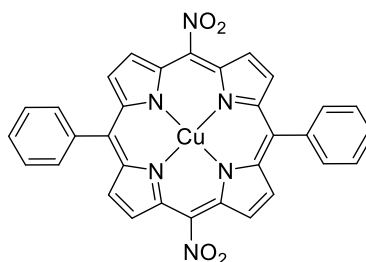
To a sample of 5,15-di(phenyl)porphyrin (100 mg, 0.216 mmol) in DMF (20 mL) in a thick-walled glass microwave vial was added copper(II) acetate monohydrate (100 mg, 0.50 mmol). The solution was heated by microwave for 1 hr at 90 °C. Bulk solvent was removed under reduced pressure and the DMF residues triturated and co-evaporated with toluene. The crude was dissolved in DCM and washed with water. The DCM was removed under reduced pressure and concentrated. The crude product was loaded onto a chromatography column and purified by flash chromatography in DCM/ hexane (70:30). The fractions were collected and bulk solvent removed under reduced pressure to yield a pink crystalline solid, the powder was taken in a minimum of DCM and precipitated over hexane and filtered under reduced pressure to yield lustrous purple-red crystals (85 mg, 0.138 mmol, 64% yield).

R_F: 0.50 (silica, 70:30, DCM/hexane). *MS*: (ASAP) $[M+H]^+$ *m/z* 614.0770, *HMRS*: calcd. For $C_{32}H_{18}N_6O_4Cu$: 614.0764 found 614.0770. *UV-Vis* (DCM): λ_{max} 408, 580, 610. $\log \epsilon$ (408) = 5.34.

Copper(II) 5,15-dibromo-10,20-di(phenyl)porphyrin (7)

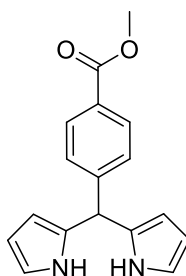
To a sample of 5,15-dibromo-10,20-di(phenyl)porphyrin (25mg, 0.0560 mmol) and excess copper(II) acetate monohydrate (20 mg, 0.10 mmol) were dissolved in chloroform (20 mL) and the mixture heated to 50 °C for 1 hr by microwave-assisted heating. Bulk solvent was removed under reduced pressure. The crude was loaded onto a silica chromatography column in DCM, the product eluted in the first major red fraction from DCM/hexane (50:50). The fractions were collected and bulk solvent removed under reduced pressure. The powder was taken in DCM and precipitated over hexane to yield reddish-purple microcrystals when filtered under reduced pressure (36 mg 0.053 mmol, 96% yield).

R_F : 0.67(silica, 70:30, DCM/hexane). MS: (ASAP) m/z $[M+H]$ 681.9255, HRMS: calcd. For $C_{32}H_{18}N_4Br_2Zn$: 679.9272 found 679.9277. UV-Vis (DCM): λ_{max} 425, 548, 586. $\log \epsilon$ (425) = 5.51.

Copper(II) 5,15-dinitro-10,20-di(phenyl)porphyrin (8)

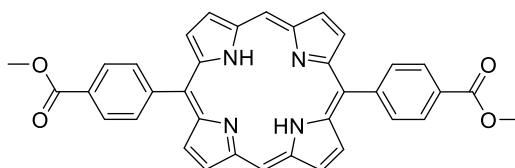
To a sample of 5,15-dinitro-10,20-di(phenyl)porphyrin (100 mg, 0.018 mmol) in DMF (20 mL) in a thick-walled microwave vial was added copper(II) acetate monohydrate (100 mg, 0.50 mmol). The solution was heated for 1 hr at 90 °C by microwave-assisted heating. Bulk solvent was removed under reduced pressure. The crude was loaded onto a silica chromatography column in DCM, the product eluted in the first major red fraction from DCM. The fractions were collected and bulk solvent removed under reduced pressure. The powder was taken in DCM and precipitated over hexane and filtered under reduced pressure to yield reddish-purple (85 mg, 0.014 mmol, 75% yield).

R_F : 0.50 (silica, 70:30, DCM/hexane). MS: (ASAP) $[M+H]^+$ m/z 614.0770, HMRS: calcd. For $C_{32}H_{18}N_6O_4Cu$: 614.0764 found 614.0770. UV-Vis (DCM): λ_{max} 408, 580, 610. $\log \epsilon$ (408) = 5.34.

5-(4-Methoxycarbonylphenyl)dipyrromethane (9)¹⁷³

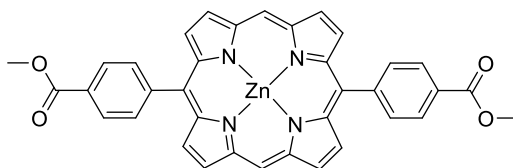
Under an inert atmosphere, a flask was purged with dry argon for 15 mins. The flask was charged with freshly distilled pyrrole (173 mL, 2.50 mol) and methyl 4-formylbenzoate (4.10 g, 25.0 mmol), then degassed for 15 min with dry argon while protected from light to afford a pale-yellow solution. InCl_3 (555 mg, 2.50 mmol) was added, and the mixture was stirred under argon at room temperature for 3 hr yielding a pale-yellow solution. Freshly powdered NaOH (6.00 g, 0.15 mol) was added to quench the reaction with stirring for 1.5 hr, which afforded a pale-green mixture. The mixture was filtered under reduced pressure, the filtrate collected and bulk solvent removed under reduced pressure. Traces of pyrrole were removed by trituration with hexane (50 mL) and sonication, bulk solvent was removed under reduced pressure, this procedure was repeated thrice to yield a beige powder. The crude was taken in ethanol/water (4:1) and allowed to crystallise overnight at 4 °C whilst protected from light, the supernatant was discarded and the solids dissolved in a minimum of ethyl acetate and precipitated over hexane, the product was filtered under reduced pressure to yield a white crystalline powder. (4.01 g, 14.29 mmol, 57% yield).

R_F : 0.30 (silica, 9:1, DCM/ethyl acetate). $^1\text{H-NMR}$ (400 MHz, CDCl_3): δ 3.90 (s, 3H, COOCH_3), 5.52 (s, 1H, C- $\underline{\text{CH}}-\text{C}$), 5.88 (dd, $J=4.0, 2.8$ Hz, 2H, C= $\underline{\text{CH}}-\text{C}$), 6.15 (dd, $J = 5.6, 2.7$ Hz, 2H, C- $\underline{\text{CH}}=\text{C}$), 6.71 (dd, $J = 4.2, 2.5$ Hz, 2H, C= $\underline{\text{CH}}-\text{NH}$), 7.28 (d, $J=8.2$ Hz, 2H, *m-Ar*), 7.97 (d, $J=8.4$ Hz, 2H, *o-Ar*), 10.59 (s, 2H, C- $\underline{\text{NH}}-\text{C}$). $^{13}\text{C-NMR}$ (100 MHz, CDCl_3): δ 45.06, 52.21 (COOCH_3), 107.60, 108.68, 117.65, 128.52, 130.03, 131.66, 147.38, 166.97 ($\underline{\text{C}}=\text{O}$). MS: (ASAP) m/z $[\text{M}-\text{H}]^+$ 279.1136, HMRS: *calcd.* For $\text{C}_{17}\text{H}_{16}\text{N}_2\text{O}_2$: 279.1133 *found* 279.1136. CHN Anal. *Calcd* for $\text{C}_{17}\text{H}_{16}\text{N}_2\text{O}_2$: C, 72.84; H, 5.75; N, 9.99. *Found* C, 72.94; H 5.92; N, 10.13.

5,15-Di(4-methoxycarbonylphenyl)porphyrin (10)

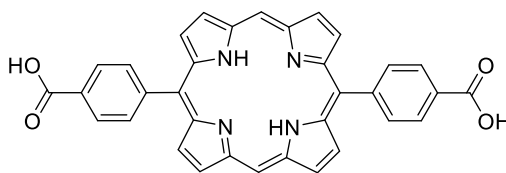
Under an inert atmosphere, 5-(4-methoxycarbonylphenyl)dipyrromethane (645 mg, 2.3 mmol) in DCM (700 mL) was added trimethyl orthoformate (25 mL, 0.165 mol). The solution was protected from light and a solution of trichloroacetic acid (8.83 g, 54 mmol) in DCM (250 mL) was added over 15 mins to afford a red solution. The solution was stirred in the absence of light for 4 hr, excess acid was quenched with pyridine (25 mL, 24.55 g, 310 mmol). The solution was stirred for 17 hr in the absence of light. The flask was purged with compressed air and stirred open to air and ambient light for 4 hr. Bulk solvent was removed under reduced pressure and triturated with hexane (50 mL), followed by toluene (20 mL) to remove residual pyridine. Bulk solvent was removed under reduced pressure and dissolved in a minimum of solvent, DCM/MeOH (95:5) and loaded onto a flash chromatography column. The porphyrin eluted in the first major red fraction, bulk solvent removed under reduced pressure, the product was precipitated from DCM over MeOH and filtered under reduced pressure to yield a purple crystalline solid (115 mg, 0.200 mmol, 17% yield).

R_F : 0.30 (silica, DCM). 1H -NMR (400 MHz, CF_3COOD): δ 4.32 (s, $COOCH_3$), 8.76 (m, $J=11.6$ Hz, 8H, *o*-,*m*-Ar), 8.84 (d, $J=4.9$ Hz, 4H, β -H), 9.29 (d, $J=4.6$ Hz, 4H, β -H), 11.25 (s, 2H, meso-H). ^{13}C -NMR (100 MHz, CF_3COOD): δ 53.16 ($COOCH_3$), 129.62, 130.47, 130.84, 137.30, 137.69, 142.83, 143.50, 145.56, 170.34 ($C=O$). MS: (ASAP) m/z $[M+H]^+$ 579.2027, HMRS: calcd. $C_{36}H_{26}N_4O_4$ For: 579.2032 found 579.2027. UV-Vis (DCM): λ_{max} 410, 505, 540, 580, 635. $\log \epsilon$ (417) = 5.43.

Zinc(II) 5,15-di(4-methoxycarbonylphenyl)porphyrin (11)

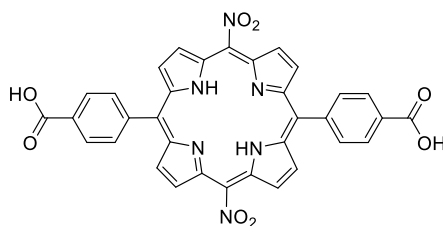
Under an inert atmosphere, to 5-(4-methoxycarbonylphenyl)dipyrromethane (645 mg, 2.3 mmol) in DCM (700 mL) was added trimethyl orthoformate (25 mL, 0.165 mol) dropwise with stirring. The solution was protected from light and a solution of trichloroacetic acid (8.83 g, 54 mmol) in DCM (250 mL) was added over 15 mins to afford a red solution. The solution was stirred in the absence of light for 3 hr, a methanolic (30 mL) solution of zinc(II) acetate dihydrate (500 mg, 2.28 mmol) was added, the reaction mixture was stirred for 1 hr. Excess acid was quenched with pyridine (25 mL, 24.55 g, 310 mmol). The solution was stirred for 17 hr in the absence of light. The flask was purged with compressed air and stirred open to air and ambient light for 4 hr. Bulk solvent was removed under reduced pressure and triturated with hexane (50 mL), followed by toluene (20 mL) to remove residual pyridine. Bulk solvent was removed under reduced pressure and dissolved in a minimum of solvent, DCM/MeOH (95:5) and loaded onto a flash chromatography column. The porphyrin eluted in the first major red fraction, bulk solvent removed under reduced pressure, the product was precipitated from DCM over MeOH and filtered under reduced pressure to yield a purple crystalline solid (360 mg, 0.280 mmol, 24% yield).

R_F : 0.40 (silica, DCM). $^1\text{H-NMR}$ (400 MHz, CF_3COOD): δ 4.32 (s, 6H, COOCH_3), 8.76 (m, $J=11.6$ Hz, 8H, *o*-,*m*-Ar), 8.84 (d, $J=4.9$ Hz, 4H, $\beta\text{-H}$), 9.29 (d, $J=4.6$ Hz, 4H, $\beta\text{-H}$), 11.25 (s, 2H, *meso*-H). $^{13}\text{C-NMR}$ (100 MHz, CF_3COOD): δ 53.16 (COOCH_3), 129.62, 130.47, 130.84, 137.30, 137.69, 142.83, 143.50, 145.56, 170.34 ($\text{C}=\text{O}$). MS: (ASAP) m/z $[M+H]^+$ 641.1169, HMRS: calcd. $\text{C}_{36}\text{H}_{24}\text{N}_4\text{O}_4\text{ZnFor}$: 641.1167 found 641.1169. UV-Vis (MeOH): λ_{max} 412, 504, 547. $\log \epsilon$ (412) = 5.45.

5,15-Di(4-carboxyphenyl)porphyrin (12)

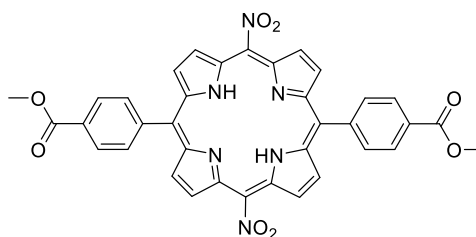
To a stirred solution of 5,15-di(4-methoxycarbonylphenyl)porphyrin (200 mg, 0.345 mmol) in THF (40 mL) was added a solution of potassium hydroxide (1.60 g, 28.6 mmol) in methanol (10 ml) and the mixture stirred at 80 °C for 24 hr. The solution was poured into water and diluted, bulk solvent was removed to give a slurry. To the slurry was added 6M HCl_(aq) dropwise until a red-brown precipitate was formed. The product was collected by filtration under reduced pressure to yield a pure crystalline purple solid (178 mg, 0.0323 mmol, 96% yield).

R_F: 0.90 (silica, THF). ¹H-NMR (400 MHz, CF₃COOD): δ 8.81-8.70 (d, J=6.5 Hz, 4H, *o*-Ar), 8.89 (d, J=6.5 Hz, 4H, *m*-Ar), 9.28 (m, 4H, β-H), 9.80 (m, 4H, β-H), 11.27 (s, 2H, meso-H). ¹³C-NMR (100 MHz, CF₃COOD): δ 107.16, 121.44, 130.12, 130.43, 130.84, 137.50, 143.29, 143.55, 145.51, 172.42 (C=O). MS: (ESI-) *m/z* [M-H]⁻ 549.1568 HRMS: *calcd.* For C₃₄H₂₂N₄O₄: 549.1568 *found* 549.1568. UV-Vis (DCM/MeOH (1:1)): λ_{max} 410, 505, 540, 580, 630. log ε (410) = 5.55.

5,15-Dinitro-10,20-di(4-carboxyphenyl)porphyrin (13)

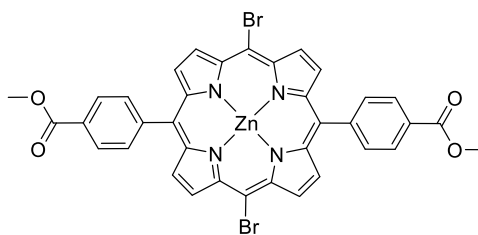
To a solution of 5,15-di(4-carboxyphenyl)porphyrin (300 mg, 0.079 mmol) in trifluoroacetic acid (3 mL) was added sodium nitrite (20 mg, 0.079 mmol) in one portion. The solution was stirred at RT for 10 mins. The mixture was poured into water (50 mL), neutralized with sodium bicarbonate until the colour change from green to red-brown was observed. The nitroporphyrin was extracted into DCM (3x50 mL) and dried over anhydrous MgSO₄. Bulk solvent was removed under reduced pressure. The crude was dissolved in a minimum of DCM and chromatographed onto a column. The fractions were collected and bulk solvent removed under reduced pressure. The powder was taken in DCM and precipitated over MeOH and filtered under reduced pressure to yield a lustrous purple (188 mg, 0.282 mmol, 89% yield).

R_F : 0.57 (silica, THF). $^1\text{H-NMR}$ (400 MHz, CF₃COOD): δ 8.81-8.70 (d, $J=6.5$ Hz, 4H, *o*-Ar), 8.89 (d, $J=6.5$ Hz, 4H, *m*-Ar), 9.28 (m, 4H, β -H), 9.80 (m, 4H, β -H). $^{13}\text{C-NMR}$ (100 MHz, CF₃COOD): δ 107.16, 121.44, 130.12, 130.43, 130.84, 137.50, 143.29, 143.55, 145.51, 172.42 (C=O). UV-Vis (DCM): λ_{max} 405, 501, 541, 580, 631. $\log \epsilon$ (405) = 5.26.

5,15-Dinitro-10,20-di(4-methylcarbonylphenyl)porphyrin (14)

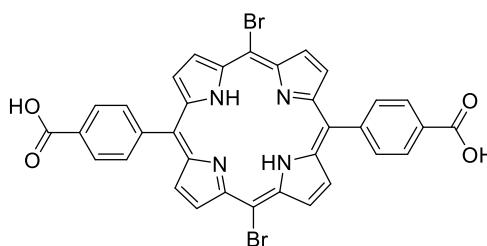
To a stirred solution of 5,15-di(4-methylcarbonylphenyl)porphyrin in THF (40 mL) was added a solution of potassium hydroxide (1.60 g, 28.6 mmol) in methanol (10 ml) and the mixture stirred at 80 °C for 17 hr. The solution was poured into water and diluted, bulk solvent was removed to give a slurry. To the slurry was added 6M HCl_(aq) dropwise until a red-brown precipitate was formed. The product was dissolved in THF and purified by column chromatography, the product eluted as the third major purple band. The fractions were collected and bulk solvent removed under reduced pressure. The crystals were collected in hexane and filtered under reduced pressure to yield a pure crystalline purple solid (0.122 mg, 0.182 mmol, 67% yield).

R_F: 0.45 (silica, DCM). ¹H-NMR (400 MHz, DMSO-*d*₆): δ 4.32 (s, 6H, COOCH₃), 8.74 (d, *J*=6.5 Hz, 4H, *o*-Ar), 8.85 (d, *J*=6.5 Hz, 4H, *m*-Ar), 9.32 (m, 4H, β-H), 9.78 (m, 4H, β-H). ¹³C-NMR (100 MHz, DMSO-*d*₆): δ 53.16 (COOCH₃), 107.16, 121.44, 130.12, 130.43, 130.84, 137.50, 143.29, 143.55, 145.51, 172.42.

Zinc(II) 5,15-di(4-methoxycarbonylphenyl)porphyrin (15)

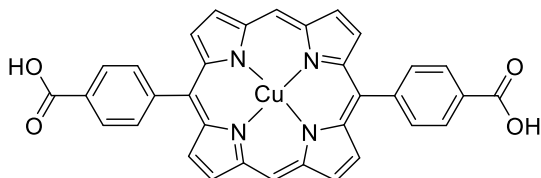
Under an inert atmosphere, to a sample of zinc(II) 5,15-di(4-methoxycarbonylphenyl)porphyrin (50 mg, 78.1 μmol) in chloroform (5 mL) was added pyridine (0.2 mL) followed by N-bromosuccinimide (14 mg, 78 μmol) in one portion. The mixture was stirred at room temperature while protected from light. The reaction progress was monitored by TLC over 10 mins. Bulk solvent was removed under reduced pressure and the residues dissolved in acetone and co-evaporated to remove traces of pyridine. The crude was eluted onto a silica chromatography column in DCM. The product eluted as the first major purple band. The fractions were collected and bulk solvent removed under reduced pressure to yield a purple powder. The powder was taken in DCM and precipitated over methanol to give burgundy-purple crystals (27 mg, 19.46 μmol , 25% yield).

R_F : 0.40 (silica, DCM). $^1\text{H-NMR}$ (400 MHz, CDCl_3): δ 4.03 (s, 6H, COOCH_3), 8.26 (d, $J=8.0$ Hz, *o*-Ar), 8.37 (d, $J=8.0$ Hz, 4H, *m*-Ar), 8.75 (d, $J=4.7$ Hz, 4H, β -H), 9.60 (d, $J=4.7$ Hz, 4H, β -H). $^{13}\text{C-NMR}$ (100 MHz, CDCl_3): δ 53.03 (COOCH_3), 121.14, 128.07, 129.54, 133.80, 133.89, 135.15, 147.21, 150.08, 150.16, 167.00 ($\text{C}=\text{O}$). MS: (ASAP) m/z $[M+H]^+$ 800.9352, HRMS: calcd. For $\text{C}_{36}\text{H}_{22}\text{N}_4\text{O}_4\text{Br}_2\text{Zn}$: 796.9378 found 796.9395. UV-Vis (DCM): λ_{max} 412, 515, 551. $\log \epsilon$ (405) = 5.23.

5,15-Dibromo-10,20-di(4-carboxyphenyl)porphyrin (16)

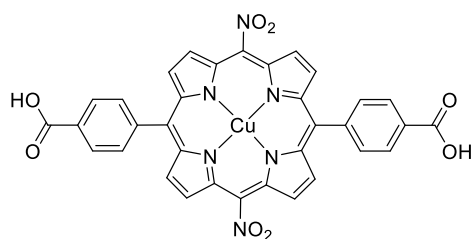
To a stirred solution of zinc(II) 5,15-dibromo-10,20-di(4-methylbenzoatephenyl)porphyrin (200 mg, 0.345 mmol) in THF (40 mL) was added a solution of potassium hydroxide (1.60 g, 28.6 mmol) in methanol (10 ml) and the mixture stirred at 80 °C for 24 hr. The solution was poured into water and diluted, bulk solvent was removed to give a slurry. To the slurry was added 6M HCl_(aq) dropwise until a red-brown precipitate was formed. The product was collected by filtration under vacuum to yield a pure crystalline purple solid (173 mg 0.245 mmol, 71% yield).

R_F : 0.70 (silica, 50:50, DCM/hexane). $^1\text{H-NMR}$ (400 MHz, CF_3COOD): δ 8.81-8.70 (d, $J=6.5$ Hz, 4H, *o*-Ar), 8.89 (d, $J=6.5$ Hz, 4H, *m*-Ar), 9.28 (m, 4H, $\beta\text{-H}$), 9.80 (m, 4H, $\beta\text{-H}$). $^{13}\text{C-NMR}$ (100 MHz, CF_3COOD): δ 107.16, 121.44, 130.12, 130.43, 130.84, 137.50, 143.29, 143.55, 145.51, 172.42. MS:(ESI+) m/z $[\text{M}+\text{H}]^+$ 708.9894, HRMS: calcd. For $\text{C}_{32}\text{H}_{21}\text{N}_4\text{Br}_2$: 708.9907 found 708.9894. UV-Vis (DMSO): λ_{max} 410, 505, 540, 580, 630. $\log \epsilon$ (420) = 5.45.

Copper(II) 5,15-di(4-carboxyphenyl)porphyrin (17)

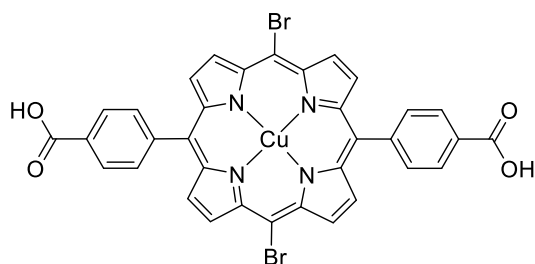
To a sample of 5,15-di(4-carboxyphenyl)porphyrin (100.0 mg, 0.200 mmol) in DMF (20 mL) was added copper(II) acetate monohydrate (100.0 mg, 0.50 mmol) to a thick-walled microwave vessel. The solution was heated for 1 hr at 90 °C by microwave-assisted heating. Bulk solvent was removed under reduced pressure. The crystals were sonicated in water, filtered and washed with copious amounts of water then dried under reduced pressure to give deep purple crystals (111 mg, 0.181 mmol, 90% yield).

R_F: 0.23 (silica, THF). *MS*: (ESI-) *m/z* [M-H]⁻ 610.0708 *HRMS*: *calcd.* For C₃₄H₂₀N₄O₄Cu: 610.0705 *found* 610.0708. *UV-Vis* (DCM): λ_{max} 410, 520, 578. log ε (410) = 5.52.

Copper(II) 5,15-dinitro-10,20-di(4-carboxyphenyl)porphyrin (18)

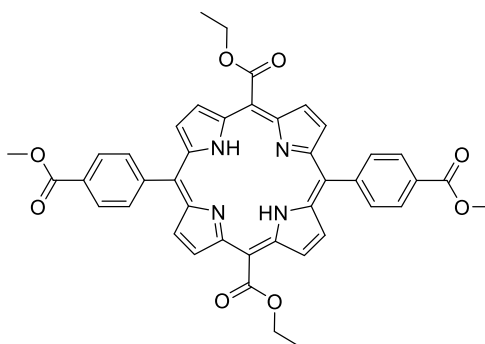
A sample of 5,15-dinitro-10,20-di(4-carboxyphenyl)porphyrin (75.0 mg, 0.112 mmol) in DMF (20 mL) and copper(II) acetate monoacetate (75.0 mg, 0.38 mmol) were added to a microwave vessel. The solution was heated by microwave for 1 hr at 90 °C. Bulk solvent was removed under reduced pressure and the DMF residues triturated with toluene, then removed under reduced pressure. The residue was sonicated with purified water (50 mL) and filtered under vacuum to give a pinky-red solid which was dried overnight at 40 °C under vacuum until reaching constant mass (78.6 mg, 0.111 mmol, 99% yield).

R_t (solvent method 1): 21.2 mins. *R_F*: 0.90 (silica, THF). UV-Vis (DMSO): λ_{max} 410, 535, 570. $\log \epsilon$ (410) = 5.23. Florescence (DMSO): λ_{max} (exc/em) 410/640 nm.

Copper(II) 5,15-dibromo-10,20-di(4-carboxyphenyl)porphyrin (19)

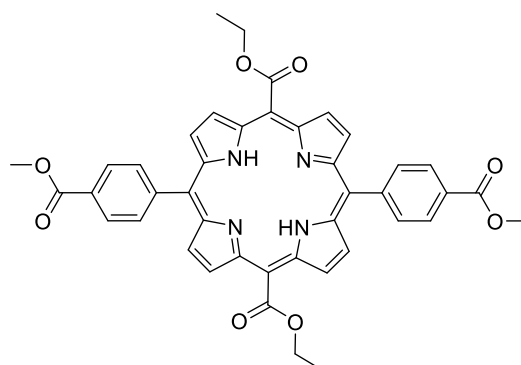
To a sample of 5,15-dibromo-10,20-di(4-carboxyphenyl)porphyrin (75.0 mg, 0.112 mmol) in DMF (20 mL) in a microwave vessel was added copper(II) acetate monohydrate(75.0 mg, 0.38 mmol). The solution was heated in a microwave for 1 hr at 90 °C. Bulk solvent was removed under reduced pressure and the DMF residues entrained with toluene, then removed under reduced pressure. The residue was entrained with purified water (50 mL) and filtered under reduced pressure to give a pinky-red solid which was dried overnight at 40 °C under reduced pressure until reaching constant mass (78.6 mg, 0.111 mmol, 99% yield).

MS: (ASAP) m/z [M^+] 769.0344, HRMS: calcd. For $C_{32}H_{18}N_6O_4Cu$: 768.8968 found 769.0344.

5,15-Di(ethoxycarbonyl)-10,20-di(4-methoxycarbonylphenyl)porphyrin (20)

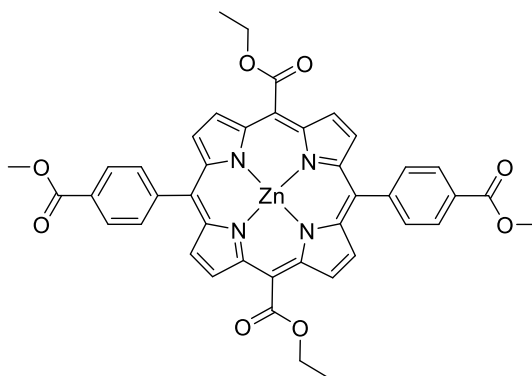
Under an inert atmosphere, to a sample of 5-(4-methylbenzoate)dipyrromethane (645 mg, 2.3 mmol) in DCM (700 mL) was added to a flask, ethyl glyoxylate (2.5 mL, 0.165 mol) was added dropwise with stirring. The mixture was protected from light and a solution of trichloroacetic acid (8.83 g, 54 mmol) in DCM (250 mL) was added over 15 mins to afford a red solution. The solution was stirred in the absence of light for 4 hr, excess acid was quenched with pyridine (25 mL). The solution was stirred for 17 hr in the absence of light. The flask was purged with compressed air and stirred open to air and ambient light for 4 hr. Bulk solvent was removed under reduced pressure and triturated with hexane (50 mL), followed by toluene (20 mL) to remove residual pyridine. Bulk solvent was removed under reduced pressure and dissolved in a minimum of solvent, DCM/MeOH (95:5) and loaded onto a flash chromatography column. The porphyrin eluted in the first major red fraction.

This method failed to yield any significant amount of product, a large amount of scrambling was seen.

5,15-Di(ethoxycarbonyl)-10,20-di(4-methoxycarbonylphenyl)porphyrin (20)

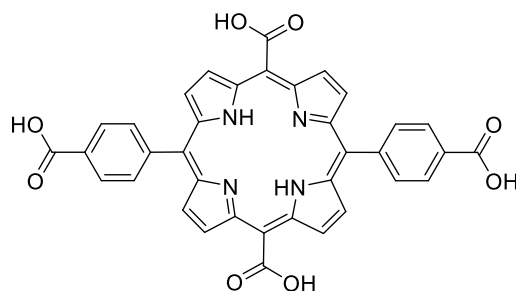
Under an inert atmosphere, to a sample of 5-(4-methylbenzoate)dipyrromethane (645 mg, 2.3 mmol) in DCM (280 mL) was added to a flask, ethyl glyoxylate (470 mL 2.3 mmol, 50% in toluene) was added dropwise with stirring. The solution was protected from light and boron trifluoride diethyletherate (0.1 mL) to afford a red solution. The solution was stirred in the absence of light for 2 hr. DDQ (500 mg) was added in one portion and the mixture stirred open to air and light for 30 mins. Bulk solvent was removed under reduced pressure and dissolved in a minimum of solvent, DCM/MeOH (95:5) and loaded onto a flash chromatography column. The porphyrin eluted in the first major red fraction, bulk solvent was removed under reduced pressure. The product was sonicated in hexane and filtered to give lustrous purple microcrystals (237 mg, 0.328 mmol, 28% yield).

R_F : 0.80 (silica, 97:3, DCM/MeOH). $^1\text{H-NMR}$ (400 MHz, CDCl_3): δ -3.07 (s, 2H, N-H), 1.74-1.80 (m, 6H, $\text{COO-CH}_2\text{-CH}_3$), 4.08-4.18 (m, 6H, Ar-COO-CH_3), 5.09 (m, 4H, $\text{COO-CH}_2\text{-CH}_3$), 8.27 (d, $J=7.9$ Hz, 4H, $m\text{-Ar}$), 8.46 (d, $J=7.1$ Hz, $o\text{-Ar}$), 8.90 (m, 4H, $\beta\text{-H}$), 9.37-9.57 (m, 4H, $\beta\text{-H}$). $^{13}\text{C-NMR}$ (100 MHz, CDCl_3): δ 14.24, 14.88, 22.76, 31.69, 52.53, 63.34, 63.54, 110.36, 111.52, 120.01, 120.28, 128.18, 130.05, 134.50, 134.60, 146.20, 146.26, 146.26, 170.79 (C=O), 170.97 (C=O). MS : (ASAP) m/z $[M+H]^+$ 723.2447, HMRS : *calcd.* $\text{C}_{42}\text{H}_{34}\text{N}_4\text{O}_8$ *For*: 723.2455 *found* 723.2447. UV-Vis (DCM): λ_{max} 415, 509, 550, 590, 644. $\log \epsilon$ (415) = 5.46.

Zinc(II) 5,15-di(ethoxycarbonyl)-10,20-di(4-methoxycarbonylphenyl)porphyrin (21)

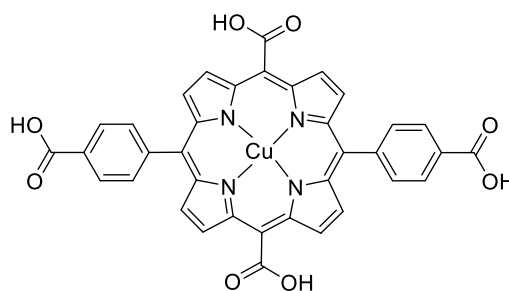
Under an inert atmosphere, to a sample of 5-(4-methylbenzoate)dipyrromethane (645 mg, 2.3 mmol) in DCM (280 mL) was added to a flask, ethyl glyoxylate (1 mL, 0.165 mol) was added dropwise with stirring. Zinc(II) acetate dihydrate (500 mg, 2.28 mmol) was added in one portion. The solution was protected from light and boron trifluoride diethyletherate (0.1 mL) to afford a red solution. The solution was stirred in the absence of light for 2 hr. DDQ (1.0 g) was added in one portion and the mixture stirred for 2 hr. Bulk solvent was removed under reduced pressure and dissolved in a minimum of solvent, DCM/MeOH (95:5) and loaded onto a flash chromatography column. The porphyrin eluted in the first major red fraction, bulk solvent was removed under reduced pressure, the product was sonicated in hexane and filtered to give lustrous purple microcrystals (97 mg, 0.123 mmol, 10% yield).

R_F : 0.73 (silica, 95:5, DCM/MeOH). $^1\text{H-NMR}$ (400 MHz, CDCl_3): δ 1.74-1.80 (m, 6H, $\text{COO-CH}_2\text{-CH}_3$), 4.08-4.18 (m, 6H, Ar- COO-CH_3), 5.09 (m, 4H, $\text{COO-CH}_2\text{-CH}_3$), 8.27 (d, $J=7.9$ Hz, 4H, *m*-Ar), 8.46 (d, $J=7.1$ Hz, 4H, *o*-Ar), 8.90 (m, 4H, $\beta\text{-H}$), 9.37-9.57 (m, 4H, $\beta\text{-H}$). $^{13}\text{C-NMR}$ (100 MHz, CDCl_3): δ 14.24, 14.88, 22.76, 31.69, 52.53, 63.34, 63.54, 110.36, 111.52, 120.01, 120.28, 128.18, 130.05, 134.50, 134.60, 146.20, 146.26, 146.26, 170.79 ($\underline{\text{C}}=\text{O}$), 170.97 ($\underline{\text{C}}=\text{O}$). UV-Vis (DCM): λ_{max} 415, 550, 585. $\log \epsilon$ (415) = 5.37.

5,15-di(Carboxy)-10,20-di(4-carboxyphenyl)porphyrin (22)

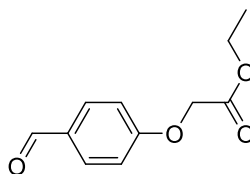
To a solution of potassium hydroxide (1.60 g) in THF/MeOH (4:1, 50 mL) was added 5,15-di(carboethoxyphenyl)-10,20-di(4-methoxycarbonylphenyl)porphyrin (48 mg, 0.066 mmol) in one portion. The mixture was heated at 80 °C for 48 hr. Bulk solvent was removed under reduced pressure. The crude was dissolved in a minimum of water (50 mL) and a mixture of DCM/THF (1:1, 200 mL) added. The mixture was acidified with HCl (1 M) until reaching pH 2 and the porphyrin changes phase. The organic layer was extracted twice into DCM/THF (1:1, 200 mL) and bulk solvent removed under reduced pressure, the solid was sonicated with hexane and filtered to give purple microcrystals (37 mg, 0.058 mmol, 88% yield).

R_F : 0.24 (silica, THF). 1H -NMR (400 MHz, DMSO- d_6): 8.27 (d, $J=7.9$ Hz, 4H, *m*-Ar), 8.46 (d, $J=7.1$ Hz, 4H, *o*-Ar), 8.90 (m, 4H, β -H), 9.37-9.57 (m, 4H, β -H). ^{13}C -NMR (100 MHz, DMSO- d_6): δ 109.36, 120.72, 127.96, 130.12, 132.42, 134.46, 147.12, 147.63, 149.96, 167.44 ($\underline{C=O}$), 172.02 ($\underline{C=O}$). UV-Vis (DMSO): λ_{max} 419, 515, 560, 595, 650. $\log \epsilon$ (419) = 5.19.

Copper(II) 5,15-di(carboxy)-10,20-di(4-carboxyphenyl)porphyrin (23)

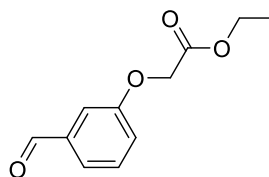
A sample of 5,15-di(carboxy)-10,20-di(4-carboxyphenyl)porphyrin (25 mg, 0.039 mmol) and copper(II) acetate monohydrate (25 mg, 0.13 mmol) were added to a microwave vessel in DMF (20 mL). The solution was heated for 1 hr at 90 °C by microwave-assisted heating. Bulk solvent was removed under reduced pressure. The crystals were sonicated in water, filtered and washed with copious amounts of water then dried under reduced pressure at 40 °C to give deep purple crystals (12 mg, 0.017 mmol, 45% yield).

R_F: 0.32 (silica, THF). *MS*: (ESI-) *m/z* [M-H]⁻ 698.0498, *HMRS*: *calcd.* C₃₆H₁₉N₄O₈Cu *For*: 698.0498 *found* 698.0504. *UV-Vis* (DMSO/PBS (0.1M) (50:50)): λ_{max} 415, 500, 545. log ε (415) = 5.19.

4-(Ethoxycarbonylmethoxy)benzaldehyde (24)

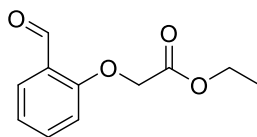
Under an inert atmosphere, 4-hydroxybenzaldehyde (5.0 g, 40.9 mmol) in anhydrous DMF (50 mL) was treated with K_2CO_3 (11.32 g, 81.88 mmol) and heated to 60 °C for 30 mins. Ethyl bromoacetate (6.7 mL, 61.4 mmol) was added dropwise to the reaction and the mixture heated to 80 °C for 1 hr. The mixture was allowed to cool and treated with water (20 mL). The product was extracted into DCM. The organic layer was washed with brine and dried with anhydrous Na_2SO_4 , filtered and concentrated under reduced pressure to give an orange oil. The crude was loaded onto a silica flash chromatography column and eluted in DCM as the first major band. Bulk solvent was removed under reduced pressure to give a pale-yellow oil which solidified upon standing to give a waxy substance (6.94 g, 33.3 mmol, 81% yield).

Mp: 35-36 °C. *R_F*: 0.40 (silica, 7:3, DCM/hexane). ¹H-NMR (400 MHz, $CDCl_3$): δ 1.27 (t, $J=7.1$ Hz, 3H, O-CH₂-CH₃), 4.25 (q, $J=7.2$ Hz, 2H, O-CH₂-CH₃), 4.68 (s, 2H, O-CH₂-COO-C₂H₅), 6.98 (d, $J=8.7$ Hz, 2H, *o*-Ar), 7.82 (d, $J=8.8$ Hz, 2H, *m*-Ar), 9.87 (s, 1H, Ar-CHO). ¹³C-NMR (100 MHz, $CDCl_3$): δ 14.22 (CH₂-CH₃), 62.77 (CH₂-CH₃), 65.26, 114.96, 130.77, 132.06, 162.68, 168.15, 190.84. *MS*: (ESI+) m/z $[M+H]^+$ 209.0810, *HMRS*: calcd. $C_{12}H_{12}O_4$ For: 209.0808 found 209.0810. *CHN Anal*. Calcd for $C_{11}H_{12}O_4$: C, 63.45; H, 5.81. Found C, 63.25; H 5.89. *ATR-FT-IR*: 2987.36 (C-H str), 2754.89 (COC-H str), 1749.36 (C=O str), 1670.07 (C=O), 1577.47 (C-H bnd), 1479.21 (C-H methyl str), 1158.96 (C-O str).

3-(Ethoxycarbonylmethoxy)benzaldehyde (25)

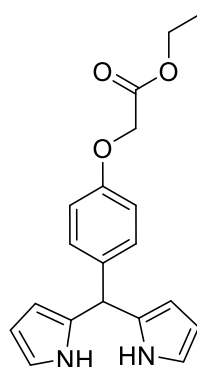
Under an inert atmosphere, 3-hydroxybenzaldehyde (15.0 g, 122.7 mmol) in anhydrous DMF (100 mL) was treated with K_2CO_3 (30.00 g, 245.6 mmol) and heated to 60 °C for 30 mins to give a yellow mixture. Ethyl bromoacetate (20 mL, 184.2 mmol) was added dropwise to the reaction mixture and heated to 80 °C for 2 hr to give a white mixture. The mixture was allowed to cool and treated with water (100 mL). The product was extracted into DCM. The organic layer was washed with brine and dried with anhydrous Na_2SO_4 , filtered and concentrated under reduced pressure to give an orange oil. The crude was loaded onto a silica flash chromatography column and eluted in DCM as the first major band. Bulk solvent was removed under reduced pressure to afford a pale-yellow oil which solidified upon standing to give a waxy substance (24.05 g, 115.5 mmol, 94% yield).

Mp: 34-34 °C. *R_F*: 0.64 (silica, DCM). ¹H-NMR (400 MHz, $CDCl_3$): δ 1.27 (t, $J=7.1$ Hz, 3H, O-CH₂-CH₃), 4.25 (q, $J=7.2$ Hz, 2H, O-CH₂-CH₃), 4.66 (s, 2H, O-CH₂-COO-C₂H₅), 7.20 (m, $J=7.9$ Hz, 1H, *m*-Ar), 7.33 (dd, 1H, *p*-Ar), 7.47 (m, 2H, *o*-Ar), 9.94 (s, 1H, Ar-CHO). ¹³C-NMR (100 MHz, $CDCl_3$): δ 14.22 (CH₂-CH₃), 61.64 (CH₂-CH₃), 65.37, 112.87, 122.14, 124.55, 130.65, 137.56, 158.46, 168.49 (Ar-O), 191.90 (C=O). *MS*: (ESI+) m/z [M+H]⁺ 209.0809, *HMRS*: *calcd.* C₁₁H₁₂O₄ *For*: 209.0808 *found* 209.0809. *CHN Anal.* *Calcd for* C₁₁H₁₂O₄: C, 63.45; H, 5.81. *Found* C, 63.70; H 6.11. *ATR-FT-IR*: 2983.09 (C-H str), 2737.32 (COC-H str), 1752.34 (C=O str), 1698.55 (C=O), 1586.67 (C-H bnd), 1483.59 (C-H methyl str), 1167.78 (C-O str).

2-(Ethoxycarbonylmethoxy)benzaldehyde (26)

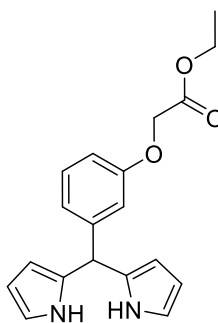
Under an inert atmosphere, 2-hydroxybenzaldehyde (15.00 g, 122.7 mmol) in anhydrous DMF (100 mL) was treated with K_2CO_3 (30.00 g, 245.6 mmol) and heated to 60 °C for 30 mins to give a yellow mixture. Ethyl bromoacetate (20 mL, 184.2 mmol) was added dropwise to the reaction mixture and heated to 80 °C for 2 hr to give a white mixture. The mixture was allowed to cool. Bulk solvent was removed under reduced pressure. The slurry was treated with water (100 mL) and the product was extracted into DCM. The organic layer was washed with brine and dried with anhydrous Na_2SO_4 , filtered and concentrated under reduced pressure to give an orange oil. The crude was loaded onto a silica flash chromatography column and eluted in DCM as the second major band. Bulk solvent was removed under reduced pressure to give a pale-yellow oil (14.94 g, 71.75 mmol, 59% yield).

R_F : 0.35 (silica, DCM). 1H -NMR (400 MHz, $CDCl_3$): δ 1.28 (t, $J=7.1$ Hz, 3H, O-CH₂-CH₃), 4.26 (q, $J=7.2$ Hz, 2H, O-CH₂-CH₃), 4.74 (s, 2H, O-CH₂-COO-C₂H₅), 6.84 (d, $J=8.4$ Hz, 1H, *p*-Ar), 7.07 (t, $J=7.5$ Hz, 1H, *o*-Ar), 7.52 (dt, $2J=8.9$ Hz, 1H, *o*-Ar), 7.85 (dd, $J=7.7$ Hz, 1H, *o*-Ar), 10.55 (s, 1H, Ar-CHO). ^{13}C -NMR (100 MHz, $CDCl_3$): δ 14.21 (CH₂-CH₃), 61.73 (CH₂-CH₃), 65.69, 112.62, 121.92, 125.43, 128.69, 135.84, 160.18, 168.28 (Ar-O), 189.72 (C=O). MS: (ESI+) m/z [$M+H$]⁺ 209.0808, HMRS: calcd. $C_{11}H_{12}O_4$ For: 209.0808 found 209.0812. CHN Anal. Calcd for $C_{11}H_{12}O_4$: C, 63.45; H, 5.81. Found C, 63.52; H 5.67. ATR-FT-IR: 2986.06 (C-H str), 2764.53 (COC-H str), 1736.63 (C=O str), 1681.38 (C=O), 1598.20 (C-H bnd), 1479.80 (C-H methyl str), 1189.98 (C-O str).

5-[4-(Ethoxycarbonylmethoxy)phenyl]dipyrromethane (27)

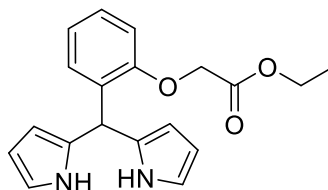
Under an inert atmosphere, a flask was purged with dry argon for 15 mins. The flask was charged with freshly distilled pyrrole (87 mL, 1.25 mol) and 4-(ethoxycarbonylmethoxy)benzaldehyde (5.40 g, 25.0 mmol) and degassed for 15 mins with dry argon while protected from light giving a pale-yellow solution. InCl_3 (555 mg, 2.50 mmol) was added, and the mixture was stirred under argon at room temperature for 3 hr yielding a darkening of the solution. NaOH (6.00 g, 0.15 mol) was added to quench the reaction with stirring for 45 mins, which afforded a pale-yellow mixture. The mixture was filtered under reduced pressure, the filtrate was collected and bulk solvent removed under reduced pressure. Traces of pyrrole was removed by trituration with hexane (50 mL) and sonication, bulk solvent was removed under reduced pressure, repeated thrice to yield an oil. The crude was dissolved in a minimum of eluent, hexane/DCM/ethyl acetate (7:2:1) and the product eluted as the first yellow major fraction. The fractions were collected and bulk solvent removed under reduced pressure to yield a pale-yellow oil (7.06 g, 21.75 mmol, 87% yield).

R_F : 0.50 (silica, DCM). $^1\text{H-NMR}$ (400 MHz, CDCl_3): δ 1.33 (t, 3H, $\text{COO-CH}_2\text{-CH}_3$), 4.29 (q, 2H, $\text{COO-CH}_2\text{-CH}_3$), 4.62 (s, 2H, $\text{O-CH}_2\text{-COO-C}_2\text{H}_5$), 5.42 (s, 1H, C-CH=C), 6.18 (dd, $J = 5.8, 2.8$ Hz, 2H, C=CH-C), 6.69 (dd, $J = 4.6, 2.2$ Hz, 2H, C-CH=C), 6.56 (dd, $J = 4.2, 2.5$ Hz, 2H, C=CH-NH), 6.87 (d, $J = 8.7$ Hz, 2H, *o*-Ar), 7.14 (d, $J = 8.7$ Hz, 2H, *m*-Ar), 10.48 (s, 2H, C-NH-C). CHN Anal. Calcd for $\text{C}_{19}\text{H}_{20}\text{N}_2\text{O}_3$: C, 70.35; H, 6.21; N, 8.64. Found C, 70.55; H, 6.54; N, 8.72.

5-[3-(Ethoxycarbonylmethoxy)phenyl]dipyrromethane (28)

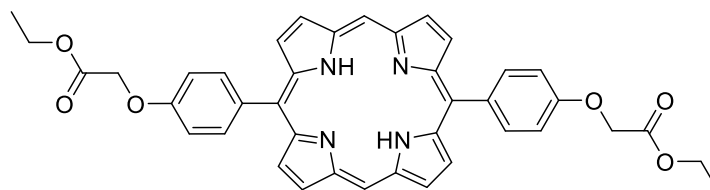
Under an inert atmosphere, a flask was purged with dry argon for 15 mins. The flask was charged with freshly distilled pyrrole (87 mL, 1.25 mol) and 4-(ethoxycarbonylmethoxy)benzaldehyde (2.60 g, 12.50 mmol) and degassed for 15 mins with dry argon while protected from light giving a pale-yellow solution. InCl_3 (555 mg, 2.50 mmol) was added, and the mixture was stirred under argon at room temperature for 3 hr yielding a darkening of the solution. NaOH (3.00 g, 0.15 mol) was added to quench the reaction with stirring for 45 mins, which afforded a pale-yellow mixture. The mixture was filtered under reduced pressure, the filtrate was collected and bulk solvent removed under reduced pressure. Traces of pyrrole was removed by trituration with hexane (50 mL) and sonication, bulk solvent was removed under reduced pressure, repeated thrice to yield an oil. The crude was dissolved in a minimum of eluent, hexane/DCM/ethyl acetate (7:2:1) and the product eluted as the first yellow major fraction. The fractions were collected and bulk solvent removed under reduced pressure to yield a pale-brown oil (2.71 g, 8.37 mmol, 67% yield).

R_F : 0.43 (silica, DCM). $^1\text{H-NMR}$ (400 MHz, CDCl_3): δ 1.28 (t, 3H, $\text{COO-CH}_2\text{-CH}_3$), 4.24 (q, 2H, $\text{COO-CH}_2\text{-CH}_3$), 4.56 (s, 2H, Ar-O- $\text{CH}_2\text{-COO}$), 5.42 (s, 1H, C- CH=C), 6.14 (dd, $J=4.1, 2.8$ Hz, 2H, C= CH-C), 6.26 (dd, $J = 4.3$ Hz, 2H, C- CH=C), 7.20 (m, $J=7.9$ Hz, 1H, *m-Ar*), 7.33 (dd, 1H, *p-Ar*), 7.47 (m, 2H, *o-Ar*), 7.93 (s, 2H, N- H). $^{13}\text{C-NMR}$ (100 MHz, CDCl_3): δ 14.25 ($\text{CH}_2\text{-CH}_3$), 43.98 ($\text{CH}_2\text{-CH}_3$), 61.54, 65.38, 107.73, 108.24, 108.49, 112.99, 115.06, 117.39, 117.80, 121.98, 129.83, 132.19, 144.04, 158.11, 169.05 (C=O). MS: (ASAP) m/z $[\text{M}+\text{H}]^+$ 325.1548, HMRS: calcd. For $\text{C}_{19}\text{H}_{21}\text{N}_2\text{O}_3$: 325.1547 found 325.1548. CHN Anal. Calcd for $\text{C}_{19}\text{H}_{20}\text{N}_2\text{O}_3$: C, 70.35; H, 6.21; N, 8.64. Found C, 70.03; H 6.37; N, 8.56.

5-[2-(Ethoxycarbonylmethoxy)phenyl]dipyrromethane (29)

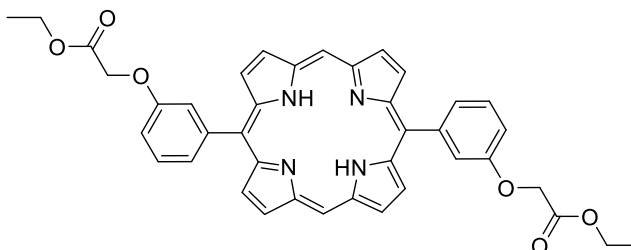
Under an inert atmosphere, a flask was purged with dry argon for 15 mins. The flask was charged with freshly distilled pyrrole (178.5 mL, 1.25 mol) and 2-(ethoxycarbonylmethoxy)benzaldehyde (5.20 g, 25.00 mmol) and degassed for 15 mins with dry argon while protected from light giving a pale-yellow solution. InCl_3 (555 mg, 2.50 mmol) was added, and the mixture was stirred under argon at room temperature for 3 hr yielding a darkening of the solution. NaOH (3.00 g, 0.15 mol) was added to quench the reaction with stirring for 45 mins, which afforded a pale-yellow mixture. The mixture was filtered under reduced pressure, the filtrate was collected and bulk solvent removed under reduced pressure. Traces of pyrrole was removed by trituration with hexane (50 mL) and sonication, bulk solvent was removed under reduced pressure, repeated thrice to yield a reddish oil. The crude was dissolved in a minimum of ethyl acetate, precipitated with hexane and filtered under reduced pressure to yield a salmon coloured crystalline powder (4.80 g, 17.80 mmol, 59% yield).

R_F : 0.26 (silica, DCM). $^1\text{H-NMR}$ (400 MHz, CDCl_3): δ 1.31 (t, $J=7.1$ Hz, 3H, O-CH₂-CH₃), 4.27 (q, $J=7.2$ Hz, 2H, O-CH₂-CH₃), 4.54 (s, 2H, O-CH₂-COO-C₂H₅), 5.78 (s, 1H, C-CH=C), 6.11 (dd, $J=5.9, 2.8$ Hz, 2H, C=CH-C), 6.68 (dt, $2J=8.9$ Hz, 1H, o-Ar), 6.80 (d, $J=8.2$ Hz, 2H, C-CH=C), 6.69 (td, $J=7.4$ Hz, 1H, m-Ar), 7.33 (dd, 1H, p-Ar), 7.47 (m, 2H, o-Ar), 8.84 (bs, 2H, N-H). $^{13}\text{C-NMR}$ (100 MHz, CDCl_3): δ 14.26 (CH₂-CH₃), 39.39 (CH₂-CH₃), 61.76, 65.80, 106.59, 107.99, 112.92, 116.88, 122.61, 128.22, 130.54, 132.29, 154.83, 169.55 (C=O). MS: (ESI+) m/z [M+H]⁺ 325.1550, HMRS: calcd. For $\text{C}_{19}\text{H}_{20}\text{N}_2\text{O}_3$: 325.1547 found 325.1150. CHN Anal. Calcd for $\text{C}_{19}\text{H}_{20}\text{N}_2\text{O}_3$: C, 70.35; H, 6.21; N, 8.64. Found C, 70.14; H 6.49; N, 8.77.

5,15-Di((3-ethoxycarbonylmethoxy)phenyl)porphyrin (30)

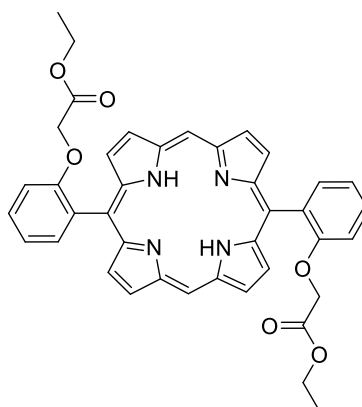
Under an inert atmosphere, 5-[4-(ethoxycarbonylmethoxy)phenyl]dipyrromethane (745 mg, 2.3 mmol) in DCM (800 mL) was added to a flask, trimethyl orthoformate (25 mL, 0.165 mol) was added dropwise with stirring. The solution was protected from light and a solution of trichloroacetic acid (8.83 g, 54 mmol) in DCM (250 mL) was added over 15 mins to afford a red solution. The solution was stirred in the absence of light for 4 hr, excess acid was quenched with pyridine (25 mL, 24.55 g, 310 mmol). The solution was stirred for 17 hr in the absence of light. The flask was purged with compressed air and stirred open to air and ambient light for 4 hr. Bulk solvent was removed under reduced pressure and triturated with hexane (50 mL), followed by toluene (20 mL) to remove residual pyridine. Bulk solvent was removed under reduced pressure and dissolved in a minimum of solvent, DCM/MeOH (95:5) and loaded onto a flash chromatography column. The porphyrin eluted in the first major red fraction, bulk solvent removed under reduced pressure, to yield purple crystals which was precipitated from MeOH over DCM.

This method failed to yield any significant amount of the desired porphyrin.

5,15-Di((3-ethoxycarbonylmethoxy)phenyl)porphyrin (31)

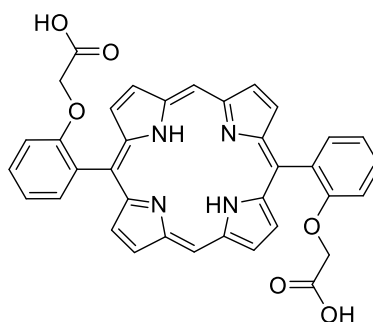
Under an inert atmosphere, 5-[3-(ethoxycarbonylmethoxy)phenyl]dipyrromethane (745 mg, 2.3 mmol) in DCM (800 mL) was added to a flask, trimethyl orthoformate (25 mL, 0.165 mol) was added dropwise with stirring. The solution was protected from light and a solution of trichloroacetic acid (8.83 g, 54 mmol) in DCM (250 mL) was added over 15 mins to afford a red solution. The solution was stirred in the absence of light for 4 hr, excess acid was quenched with pyridine (25 mL, 24.55 g, 310 mmol). The solution was stirred for 17 hr in the absence of light. The flask was purged with compressed air and stirred open to air and ambient light for 4 hr. Bulk solvent was removed under reduced pressure and triturated with hexane (50 mL), followed by toluene (20 mL) to remove residual pyridine. Bulk solvent was removed under reduced pressure and dissolved in a minimum of solvent, DCM/MeOH (95:5) and loaded onto a flash chromatography column. The porphyrin eluted in the first major red fraction, bulk solvent removed under reduced pressure, to yield purple crystals which was precipitated from MeOH over DCM (20 mg, 0.029 mmol, 3% yield).

R_F : 0.89 (silica, 95:5, DCM/MeOH). $^1\text{H-NMR}$ (400 MHz, CDCl_3): δ -3.17 (s, 2H, N-H), 1.27 (t, 3H, $\text{COO-CH}_2\text{-CH}_3$), 4.30 (q, 2H, $\text{COO-CH}_2\text{-CH}_3$), 4.84 (s, 2H, $\text{Ar-O-CH}_2\text{-COO}$), 7.39 (d, $J=7.0$ Hz, 2H, Ar-H), 7.80 (m, $J=7.9$ Hz, 6H, Ar-H), 9.10 (d, $J=4.4$ Hz, 4H, $\beta\text{-H}$), 9.39 (d, $J=4.4$ Hz, 4H, $\beta\text{-H}$), 10.31 (s, 2H, meso-H). $^{13}\text{C-NMR}$ (100 MHz, CDCl_3): δ 14.27 ($\text{CH}_2\text{-CH}_3$), 29.81 ($\text{CH}_2\text{-CH}_3$), 61.59, 65.68, 105.46, 114.44, 118.56, 121.09, 128.09, 128.90, 131.13, 132.79, 142.86, 145.35, 147.06, 156.58 (Ar-O-CH_2), 169.06 (C=O). MS : (ESI+) m/z [$M+H$] $^+$ 667.2543, HMRS : calcd. $\text{C}_{40}\text{H}_{34}\text{N}_4\text{O}_6$ For: 667.2551 found 667.2543. UV-Vis (DCM): λ_{max} 410, 505, 540, 580, 635. $\log \epsilon$ (410) = 5.54.

5,15-Di((2-ethoxycarbonylmethoxy)phenyl)porphyrin (32)

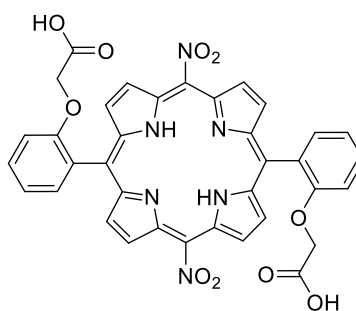
Under an inert atmosphere, 5-[2-(ethoxycarbonylmethoxy)phenyl]dipyrromethane (745 mg, 2.3 mmol) in DCM (800 mL) was added to a flask, trimethyl orthoformate (25 mL, 0.165 mol) was added dropwise with stirring. The solution was protected from light and a solution of trichloroacetic acid (8.83 g, 54 mmol) in DCM (250 mL) was added over 15 mins to afford a red solution. The solution was stirred in the absence of light for 4 hr, excess acid was quenched with pyridine (25 mL, 24.55 g, 310 mmol). The solution was stirred for 17 hr in the absence of light. The flask was purged with compressed air and stirred open to air and ambient light for 4 hr. Bulk solvent was removed under reduced pressure and triturated with hexane (50 mL), followed by toluene (20 mL) to remove residual pyridine. Bulk solvent was removed under reduced pressure and dissolved in a minimum of solvent, DCM/MeOH (95:5) and loaded onto a flash chromatography column. The porphyrin eluted in the first major red fraction, bulk solvent removed under reduced pressure, to yield a purple crystalline solid (88 mg, 0.029 mmol, 9% yield).

R_F : 0.89 (silica, 98:2, DCM/MeOH). 1H -NMR (400 MHz, $CDCl_3$): δ 1.05 (t, $J=7.1$ Hz, 3H, $O-CH_2-CH_3$), 4.04 (q, $J=7.2$ Hz, 2H, $O-CH_2-CH_3$), 4.36 (s, 2H, $O-CH_2-COO-C_2H_5$), 7.44 (d, $J=8.4$ Hz, 1H, p -Ar), 7.77 (t, $J=7.5$ Hz, 1H, o -Ar), 8.07 (dt, $2J=8.9$ Hz, 1H, o -Ar), 7.85 (dd, $J=7.7$ Hz, 1H, o -Ar), 9.08 (d, $J=4.6$ Hz, 4H, β -H), 9.35 (d, $J=4.6$ Hz, 4H, β -H), 10.25 (s, 2H, meso-H). ^{13}C -NMR (100 MHz, $CDCl_3$): δ 14.05 (CH_2-CH_3), 29.83 (CH_2-CH_3), 40.99, 55.71, 61.15, 65.77, 104.39, 105.04, 106.26, 112.17, 114.62, 120.73, 121.63, 123.45, 127.07, 129.92, 130.72, 131.09, 131.52, 136.48, 145.35, 147.32, 157.66, 158.62, 169.03, (Ar-O- CH_2), 189.70 ($C=O$). MS: (ESI+) m/z $[M+H]^+$ 667.2541, HMRS: calcd. $C_{40}H_{34}N_4O_6$ For: 667.2551 found 667.2541. UV-Vis (DCM): λ_{max} 405, 500, 535, 580, 630. $\log \epsilon$ (405) = 5.38.

5,15-Di((2-ethoxycarboxy)phenyl)porphyrin (33)

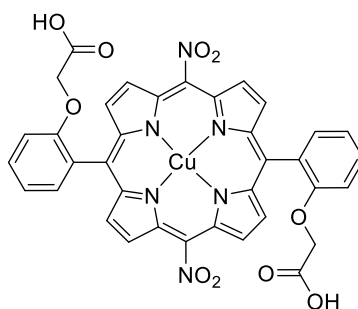
To a solution of potassium hydroxide (1.60 g) in THF/MeOH (4:1, 50 mL) was added 5,15-di((2-ethoxycarbonylmethoxy)phenyl)porphyrin (200 mg, 0.300 mmol) in one portion. The mixture was heated at 80 °C for 17 hrs. Bulk solvent was removed under reduced pressure. The crude was dissolved in a minimum of water (50 mL) and a mixture of DCM/THF (1:1, 200 mL) added. The mixture was acidified with HCl (1 M) until reaching pH 7, the porphyrin was extracted into the organic layer. The aqueous layer was washed with DCM/THF (1:1, 200 mL) and the organic layers combined. The organic layer was washed with saturated brine solution (300 mL), the organic layer was separated, dried with anhydrous MgSO₄, filtered, and bulk solvent removed under reduced pressure, the solid was sonicated with hexane and filtered to give purple microcrystals (157 mg, 0.257 mmol, 85% yield).

R_F: 0.35 (silica, 9:1, DCM/MeOH). ¹H-NMR (400 MHz, DMSO-*d*₆): δ 4.36 (s, 2H, O-CH₂-COOH), 7.44 (d, *J*=8.4 Hz, 1H, *p*-Ar), 7.77 (t, *J*=7.5 Hz, 1H, *o*-Ar), 8.07 (dt, 2*J*=8.9 Hz, 1H, *o*-Ar), 7.85 (dd, *J*=7.7 Hz, 1H, *o*-Ar), 9.08 (d, *J*=4.6 Hz, 4H, β-H), 9.35 (d, *J*=4.6 Hz, 4H, β-H), 10.25 (s, 2H, meso-H). ¹³C-NMR (100 MHz, DMSO-*d*₆): δ 67.54, 105.80, 112.47, 115.45, 120.51, 125.45, 128.52, 129.48, 130.63, 131.45, 132.66, 136.39, 136.44, 139.73, 145.21, 147.19, 152.00, 157.56, (Ar-O-CH₂), 170.51 (C=O). MS: (ASAP) *m/z* [M+H]⁺ 611.1929, HMRS: *calcd.* C₃₆H₂₆N₄O₆ For: 611.1931 found 611.1929.

5,15-Dinitro-10,20-di((2-ethoxycarboxy)phenyl)porphyrin (34)

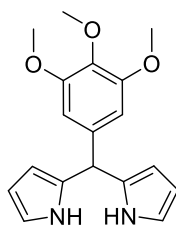
Sodium nitrite (60 mg, 0.908 mmol) was added to a solution of 5,15-di((2-ethoxycarboxy)phenyl)porphyrin (120 mg, 0.197 mmol) in trifluoroacetic acid (2.5 mL). The solution was stirred at 0 °C for 30 mins. The mixture was poured into 50 ml of water, neutralized with sodium bicarbonate until the colour change from green to red-brown was observed. The nitroporphyrin was extracted into DCM (3x50 mL) and dried over MgSO₄. Bulk solvent was removed under reduced pressure. The product was entrained with hexane, sonicated, and filtered under reduced pressure to yield a purple crystalline solid (90.0 mg, 0.128 mmol, 65% yield).

R_F: 0.45 (silica, THF). *MS*: (ASAP) *m/z* [M+H]⁺ 701.1639, *HMRS*: *calcd.* C₃₄H₂₆N₄O₂ *For*: 701.1632 *found* 701.1639.

Copper(II) 5,15-dinitro-10,20-di((2-ethoxycarboxy)phenyl)porphyrin (35)

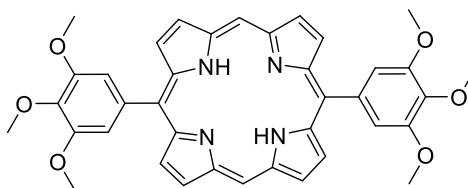
To a sample of 5,15-dinitro-10,20-di((2-ethoxycarboxy)phenyl)porphyrin (50.0 mg, 0.0714 mmol) in DMF (20 mL) in a microwave vessel was added copper(II) acetate monohydrate (50 mg, 0.25 mmol). The solution was heated in a microwave for 60 mins at 100 °C, 200 W and 200 PSI. Bulk solvent was removed under reduced pressure and the DMF residues entrained with toluene, then removed under reduced pressure. The product was dissolved in a minimum of DCM and washed repeatedly with water, the organic layers collected, dried with anhydrous MgSO₄ and bulk solvent removed under reduced pressure. The metalloporphyrin was sonicated in hexane and filtered under reduced pressure to yield purple crystals (38 mg, 0.049 mmol, 80% yield).

R_F: 0.90 (silica, THF). *MS*: (ESI-) *m/z* [M-H]⁻ 760.0622, *HRMS*: *calcd.* For C₃₆H₂₂N₆O₁₀Cu: 760.0621 *found* 760.0622.

5-(3,4,5-Trimethoxyphenyl)dipyrromethane (36)

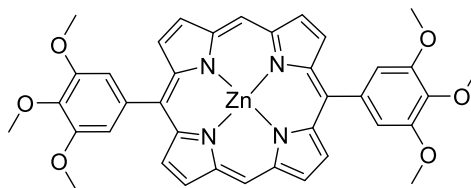
Under an inert atmosphere, a flask was purged with dry argon for 15 mins. The flask was charged with freshly distilled pyrrole (173.5 mL, 2.50 mol) and 3,4,5-trimethoxybenzaldehyde (4.9050 g, 25.0 mmol) were degassed for 15 mins with dry argon while protected from light. InCl_3 (555 mg, 2.50 mmol) was added, and the mixture was stirred under argon at room temperature for 3 hr yielding a pale-yellow solution. NaOH (6.0 g, 0.15 mol) was added to quench the reaction with stirring for 45 min, which afforded a pale-yellow mixture. The mixture was filtered under reduced pressure, the filtrate was collected and bulk solvent removed under reduced pressure. Traces of pyrrole were removed by trituration with hexane (50 mL) and sonication, bulk solvent was removed under reduced pressure, repeated thrice to yield an off white solid. The crude was dissolved in a minimum of ethyl acetate and precipitated from hexane to yield a white solid when filtered under reduced pressure (3.7661 g, 16.9 mmol, 87% yield).

R_F : 0.10 (silica, DCM). $^1\text{H-NMR}$ (400 MHz, $\text{DMSO-}d_6$): δ 3.63 (d, 3H, *para*- O-CH_3), 3.69 (2, 6H, *meta*- O-CH_3), 5.29 (s, 1H, C-(CH)-C), 5.73 (m, C=CH-C), 5.91 (dd, 2H, $J=5.4, 2.8$ Hz, C=CH-C), 6.53 (s, 2H, *Ph-H*), 6.64 (m, 2H, N-CH=C) 10.53 (s, 1H, *N-H*). $^{13}\text{C-NMR}$ (100 MHz, $\text{DMSO-}d_6$): δ 44.50, 56.34 (*Ar-OCH}_3*), 60.51 (*Ar-OCH}_3*), 106.21, 106.67, 107.45, 117.39, 117.50, 133.53, 136.44, 139.98. *MS*: (*ESI*⁺) m/z [$M+H$]⁺ 313.1551, *HMRS*: *calcd.* For $\text{C}_{18}\text{H}_{21}\text{N}_2\text{O}_3$: 313.1551 *found* 313.1547. *CHN Anal.* *Calcd* for $\text{C}_{18}\text{H}_{20}\text{N}_2\text{O}_3$: C, 69.21; H, 6.45. *Found* C, 69.29; H 6.39.

5,15-Di(3,4,5-trimethoxyphenyl)porphyrin (37)

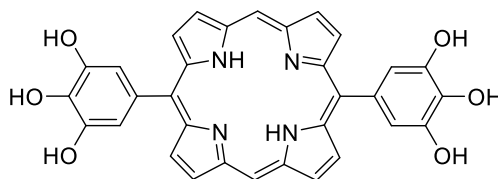
Under an inert atmosphere, 5-(3,4,5-trimethoxyphenyl)dipyrromethane (720 mg, 2.3 mmol) in DCM (700 mL) was added to a flask, trimethyl orthoformate (25 mL, 0.165 mol) was added dropwise with stirring. The solution was protected from light and a solution of trichloroacetic acid (8.83 g, 54 mmol) in DCM (250 mL) was added over 15 mins to afford a red solution. The solution was stirred in the absence of light for 4 hr, excess acid was quenched with pyridine (25 mL, 24.55 g, 310 mmol). The solution was stirred for 17 hr in the absence of light. The flask was purged with compressed air and stirred open to air and ambient light for 4 hr. Bulk solvent was removed under reduced pressure and triturated with hexane (50 mL), followed by toluene (20 mL) to remove residual pyridine. Bulk solvent was removed under reduced pressure and dissolved in a minimum of solvent, DCM/MeOH (99:1) and loaded onto a flash chromatography column. The porphyrin eluted in the first major red fraction, bulk solvent removed under reduced pressure, to yield purple crystals which was precipitated from MeOH over DCM (173 mg, 0.269 mmol, 13% yield).

R_F : 0.80 (silica, 99:1, DCM/MeOH). 1H -NMR (400 MHz, CF_3COOD): δ 4.26 (s, 12H, m -O-CH₃), 4.38 (s, 6H, p -O-CH₃), 7.99 (s, 4H, o -Ar), 9.34 (d, J =4.8 Hz, 4H, β -H), 9.73 (d, J =4.8 Hz, 4H, β -H), 11.5 (s, 2H, meso-H). ^{13}C -NMR (100 MHz, CF_3COOD): δ 55.85 (Ar-OCH₃), 61.18 (Ar-OCH₃), 130.35, 135.72, 138.56, 143.20, 146.38, 152.31. MS: (ESI+) m/z $[M+H]^+$ 643.2545, HMRS: calcd. $C_{38}H_{34}N_4O_6$ For: 643.2545 found 643.2551. UV-Vis (DMSO): λ_{max} 405, 505, 545, 585, 635 nm. $\log \epsilon$ (405) = 5.37.

Zinc(II) 5,15-Di(3,4,5-trimethoxyphenyl)porphyrin (38)

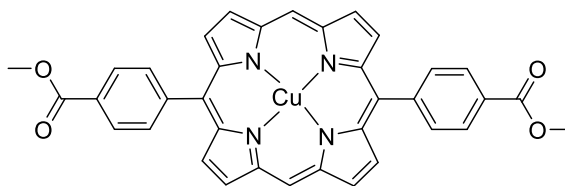
Under an inert atmosphere, 5-(3,4,5-trimethoxyphenyl)dipyrromethane (720 mg, 2.3 mmol) in DCM (700 mL) was added to a flask, trimethyl orthoformate (25 mL, 0.165 mol) was added dropwise with stirring. The solution was protected from light and a solution of trichloroacetic acid (8.83 g, 54 mmol) in DCM (250 mL) was added over 15 mins to afford a red solution. The solution was stirred in the absence of light for 3 hr, a methanolic (30 mL) solution of zinc(II) acetate dihydrate (500 mg, 2.28 mmol) and the mixture stirred for a further 1 hr. Excess acid was quenched with pyridine (25 mL, 24.55 g, 310 mmol). The solution was stirred for 17 hr in the absence of light. The flask was purged with compressed air and stirred open to air and ambient light for 4 hr. Bulk solvent was removed under reduced pressure and triturated with hexane (50 mL), followed by toluene (20 mL) to remove residual pyridine. Bulk solvent was removed under reduced pressure and dissolved in a minimum of solvent, DCM/MeOH (99:1) and loaded onto a flash chromatography column. The porphyrin eluted in the first major red fraction, and bulk solvent was removed under reduced pressure. The porphyrin was dissolved in a minimum of DCM and precipitated upon addition of hexane and filtered under reduced pressure to yield a burgundy powder (215 mg, 0.305 mmol, 26% yield).

R_F : 0.83 (silica, 99:1, DCM/MeOH). $^1\text{H-NMR}$ (400 MHz, CF_3COOD): δ 4.26 (s, 12H, $m\text{-O-CH}_3$), 4.38 (s, 6H, $p\text{-O-CH}_3$), 7.99 (s, 4H, $o\text{-Ar}$), 9.34 (d, $J=4.8$ Hz, 4H, $\beta\text{-H}$), 9.73 (d, $J=4.8$ Hz, 4H, $\beta\text{-H}$), 11.5 (s, 2H, $meso\text{-H}$). $^{13}\text{C-NMR}$ (100 MHz, CF_3COOD): δ 55.89 ($Ar\text{-OCH}_3$), 61.33 ($Ar\text{-OCH}_3$), 116.17, 130.37, 135.61, 135.69, 138.50, 143.19, 146.36, 152.21. MS: (ASAP) m/z [$M\text{-CH}_3+H$] 690.1458, HMRS: calcd. $\text{C}_{38}\text{H}_{34}\text{N}_4\text{O}_6\text{Zn}$ For: 690.1457 found 690.1458. UV-Vis (DMSO): λ_{max} 415, 550, 590. $\log \epsilon$ (415) = 5.61.

5,15-Di(3,4,5-trihydroxyphenyl)porphyrin (39)

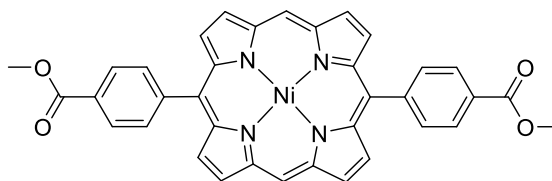
Under an inert atmosphere, to a stirred solution of 5,15-di(3,4,5-trimethoxyphenyl)porphyrin (500 mg, 0.683 mmol) in DCM (10 mL), boron tribromide in DCM (2.5 mL, 1M) was added dropwise at 0 °C under argon and stirred and to warm to room temperature overnight and stirred for 72 hr followed by three more additions of boron tribromide in DCM (2.5 mL, 1M). Methanol (20 mL) was added dropwise and the mixture maintained at room temperature under argon for 30 mins. Bulk solvent was removed under reduced pressure and stirred for 10 mins at room temperature. The crude was washed with water successively to remove salts and filtered under reduced pressure to give a purple crystalline solid.

Analysis of the compound proved that the isolated product wasn't the desired product.

Copper(II) 5,15-di(4-methoxycarbonylphenyl)porphyrin (40)

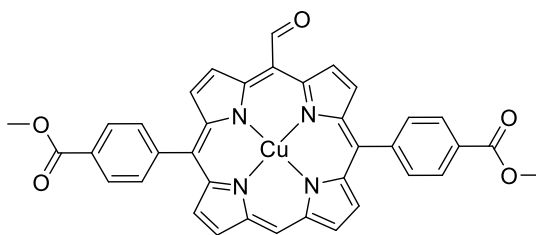
To a sample of 5,15-di(4-methoxycarbonylphenyl)porphyrin (25 mg, 0.039 mmol) and copper(II) acetate monohydrate (25 mg, 0.13 mmol) in a microwave vessel was added THF (20 mL). The solution was heated in a microwave for 1 hr at 80 °C. Bulk solvent was removed under reduced pressure. The crystals were sonicated in water, filtered and washed with copious amounts of water then dried under reduced pressure at 40 °C to give deep purple crystals (23 mg, 0.037 mmol, 97% yield).

R_F: 0.80 (silica, DCM). *MS*: (ASAP) *m/z* [M+H] 640.1172, *HRMS*: *calcd.* For C₃₃H₂₄N₄O₄Cu: 640.1171 *found* 640.1172. *UV-Vis* (DCM): λ_{max} 405, 530, 567. $\log \epsilon$ (405) = 5.68.

Nickle(II) 5,15-di(4-methoxycarbonylphenyl)porphyrin (41)

A sample of 5,15-di(4-methoxycarbonylphenyl)porphyrin (250 mg, 0.39 mmol) and nickel(II) acetate tetrahydrate (250 mg, 1.00 mmol) was added to a microwave vessel in DMF (25 mL). The solution was heated in a microwave for 1 hr at 130 °C. Aliquots were taken for TLC to monitor reaction progress. The flask was charged again with a mixture of nickel(II) acetate tetrahydrate (100 mg, 0.40 mmol) and the mixture heated for a further 30 mins at 130 °C. Bulk solvent was removed under reduced pressure. The crystals were sonicated in water, filtered and washed with copious amounts of water then dried under reduced pressure at 40 °C to give deep burgundy crystalline solid (222 mg, 0.35 mmol, 89% yield).

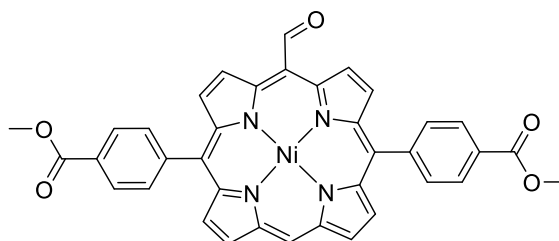
R_F : 0.80 (silica, 99:1, DCM/MeOH). MS: (ASAP) m/z $[M+H]$ 663.1179, HRMS: calcd. For $C_{37}H_{24}N_4O_5Ni$: 663.1178 found 663.1185. UV-Vis (DCM): λ_{max} 405, 515, 550. $\log \epsilon$ (405) = 5.14.

Copper(II) 15-formyl, 10,20-di(4-methoxycarbonylphenyl)porphyrin (42)

Under an inert atmosphere, DMF (1 mL, 0.94 g, 12.9 mmol) was added to POCl₃ (1 mL, 1.64 g, 10.70 mmol) with mixing and cooling to 0 °C with a salt-ice bath for 10 mins to form the Vilsmeier complex. To this mixture was added copper(II) 5,15-di(4-methoxycarbonylphenyl)porphyrin (100 mg, 0.156 mmol) in dry dichloroethane (20 mL) with stirring. The mixture was heated to 40 °C overnight. Saturated sodium carbonate was added and the mixture heated for 1 hr. The organic layer was separated and extracted with DCM, dried with anhydrous sodium sulfate and bulk solvent removed under reduced pressure. The crude was eluted onto a silica chromatography column in DCM/hexane (9:1) with gradient to DCM/hexane (95:5). The product eluted as the third major band. The fractions were collected and bulk solvent removed under reduced pressure to give a reddy-purple solid (75.0 mg, 0.112 mmol, 72%).

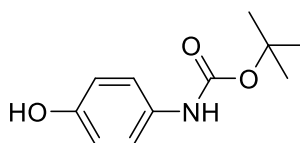
R_F: 0.48 (silica, DCM).

Product was paramagnetic so couldn't obtain NMR, insoluble in all common solvents for MS. Couldn't remove the metal to obtain NMR without destroying the acid sensitive aldehyde group.

Nickel(II) 5-formyl-10,20-di(4-methoxycarbonylphenyl)porphyrin (43)

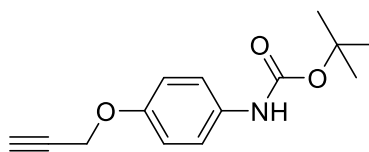
Under an inert atmosphere, DMF (1 mL, 0.94 g, 12.9 mmol) was added to POCl₃ (1 mL, 1.64 g, 10.70 mmol) with mixing and cooling to 0 °C with a salt-ice bath for 10 mins to form the golden-coloured Vilsmeier complex. To this mixture was added nickel(II) 5,15-di(4-methoxycarbonylphenyl)porphyrin (150 mg, 0.234 mmol) in dry dichloroethane (20 mL) with stirring. The mixture was heated to 40 °C overnight. Saturated sodium carbonate was added and the mixture heated at 90 °C for 1 hr. The organic layer was separated and extracted with DCM, dried with anhydrous sodium sulfate and bulk solvent removed under reduced pressure. The crude was eluted onto a silica chromatography column in DCM with gradient to DCM/MeOH (99:1) after elution of the first major band. The product eluted as the second major band. The fractions were collected and bulk solvent removed under reduced pressure. The crystals were entrained in methanol and precipitated over diethyl ether to give the product as a deep purple crystalline solid (118 mg, 0.178 mmol, 76%).

R_F: 0.45 (silica, DCM). ¹H-NMR (400 MHz, CDCl₃): δ 4.10 (s, 6H, COO-CH₃), 7.94 (d, *J*=8.1 Hz, 4H, *p*-Ar), 8.34 (d, *J*=8.1 Hz, 4H, *o*-Ar), 8.56 (d, *J*=4.7 Hz, β-H), 8.67 (d, *J*=5.0 Hz, β-H), 8.93 (d, *J*=4.7 Hz, β-H), 9.59 (s, 1H, meso-H) 8.56 (d, *J*=4.7 Hz, β-H), 11.92 (s, 1H, CHO). ¹³C-NMR (100 MHz, CDCl₃): δ 52.57 (COOCH₃), 106.57, 108.75, 119.18, 128.32, 130.03, 130.83, 132.04, 133.59, 134.79, 141.89, 143.54, 144.17, 144.65, 167.13 (COOCH₃), 192.91 (CHO). MS: (ASAP) *m/z* [*M*+*H*] 663.1179, HRMS: calcd. For C₃₇H₂₄N₄O₅Ni: 663.1178 found 663.1185. UV-Vis (DCM): λ_{max} 415, 545, 591. log ε (415) = 5.15.

Tert-butyl(4-hydroxyphenyl)carbamate (44)²⁶²

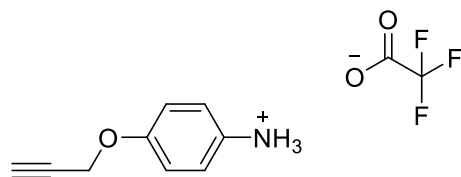
Under an inert atmosphere, to 4-aminophenol (4.40 g, 40.2 mmol) in MeOH (80 mL) was added TEA (2 mL) and di-tert butyl carbonate (12.00 g, 44.12 mmol) and the mixture stirred overnight. Bulk solvent was removed under reduced pressure to give a fawn coloured oil. The oil was taken up in DCM and washed with water. The organic later was separated and dried with anhydrous MgSO₄, filtered under reduced pressure and bulk solvent removed under reduced pressure to yield a white power (8.97 g, 41.88 mmol, 99%).

Mp: 147-151 °C. *R_F*: 0.25 (silica, DCM). ¹H-NMR (400 MHz, CDCl₃): δ 1.47 (s, 12H, NH-CO-C(CH₃)₃), 6.69 (d, *J*=8.1 Hz, 2H, *o*-Ar), 7.13 (d, *J*=8.2 Hz, 2H, *p*-Ar). ¹³C-NMR (100 MHz, CDCl₃): δ 28.45 (NH-CO-C(CH₃)₃), 31.67, 115.81, 121.47, 130.95, 152.14 (Ar-OH), 153.64 (C=O). CHN Anal. Calcd for C₁₁H₁₅O₃N: C, 63.14; H, 7.23; N, 6.69. Found C, 63.16; H 7.45; N, 6.66. ATR-FT-IR: 3359.80 (Ar-OH str), 2969.97 (C-H str), 1526.25 (N-H bnd), 1165,37 (C-O str), 1058.45 (C-N str).

Tert-butyl (4-(prop-2-yn-1-lyoxy)phenyl)carbamate (45)²⁶²

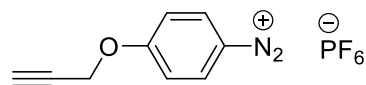
Under an inert atmosphere, to tert-butyl(4-hydroxyphenyl)carbamate (4.00 g, 20.0 mmol) in anhydrous DMF (60 mL) was added K_2CO_3 (4.0 g, 30.0 mmol) and propargyl bromide (3.0 g, 2 mL, 27.6 mmol, 80% in toluene) and the mixture stirred at 40 °C. Bulk solvent was removed under reduced pressure to give a fawn coloured oil. The oil was taken up in DCM and washed with water. The organic later was separated and dried with anhydrous $MgSO_4$, filtered under reduced pressure and bulk solvent removed under reduced pressure to yield a white power. The crude was eluted onto a silica chromatography column and eluted in DCM as the first major fraction to give a pale-yellow oil which solidified upon standing to a pale-yellow crystalline solid (4.00 g, 19.1 mmol, 99%).

Mp: 81-83 °C. *R_F*: 0.84 (silica, DCM). ¹H-NMR (400 MHz, $CDCl_3$): δ 1.49 (s, 12H, NH-CO-C(CH₃)₃), 2.49 (t, *J*=2.5 Hz, 1H, C≡C-H), 4.64 (d, *J*=2.4 Hz, 2H, O-CH₂-C≡C-H), 6.89 (d, *J*=8.1 Hz, 2H, *o*-Ar), 6.91 (d, *J*=8.2 Hz, 2H, *p*-Ar). ¹³C-NMR (100 MHz, $CDCl_3$): δ 28.44 (NH-CO-C(CH₃)₃), 56.28, 75.55 (C≡C), 78.81 (C≡C), 115.53, 120.42, 132.39, 153.57 (C=O). CHN Anal. Calcd for $C_{14}H_{17}O_3N$: C, 68.00; H, 6.96; N, 5.66. Found C, 68.26; H 7.00; N, 5.63. ATR-FT-IR: 3362.16 (C≡C-H str), 2865.40 (C-H str), 2134.08 (C≡C str), 1511.52 (N-H bnd), 1155.09 (C-O str), 1021.73 (C-N str).

(4-(Prop-2-yn-1-lyoxy)aniline trifluoroacetate (46))²⁶²

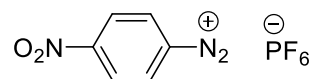
Tert-butyl (4-(prop-2-yn-1-lyoxy)phenyl)carbamate (4.00 g, 19.12mmol) was dissolved in TFA (5 ml, 7.45 g, 65.34 mmol) and stirred at room temperature for 30 mins. Bulk solvent was removed under reduced pressure and the product precipitated from diethyl ether to give a white crystalline solid (2.89 g, 19.00 mmol, 99%).

Mp: 140-141 °C. ¹H-NMR (400 MHz, CD₃OD): δ 3.38 (t, *J*=2.5 Hz, 1H, C≡C-H), 4.15 (d, *J*=2.4 Hz, 2H, O-CH₂-C≡C-H), 5.68 (t, 2H, Ar-NH₂), 7.97 (d, *J*=8.2 Hz, 2H, *o*-Ar), 8.16 (d, *J*=8.3 Hz, 2H, *p*-Ar). ¹³C-NMR (100 MHz, CD₃OD): δ 56.53, 76.81 (C≡C), 78.71 (C≡C), 116.94, 124.53, 158.69 (C=O). CHN Anal. Calcd for C₁₁H₉O₂N: C, 54.11; H, 3.72 N, 5.74. Found C, 53.87; H 3.52; N, 5.69. ATR-FT-IR: 3309.12 (C≡C-H str), 2909.60 (N-H salt str), 2634.18 (C-H str), 2137.47 (C≡C str), 1578.20 (N-H bnd), 1199.79 (C-O str), 1013.74 (C-N str), 1025.07 (C-O str).

(4-(Prop-2-yn-1-lyoxy)benzene diazonium hexafluorophosphate (47))²⁶²

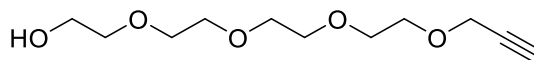
(4-(Prop-2-yn-1-lyoxy)aniline (1.00 g, 6.80 mmol) was dissolved in TFA (10 ml) and cooled in a salt-ice bath. Sodium nitrite (1.76 g, 20.40 mmol) in water (5 mL) was added dropwise and the temperature maintained for 1.5 hr. HPF₆ (60% w/w aq. 27.2 mmol) was added dropwise. The reaction was maintained at -10 °C for a further 1.5 hr. The mixture was filtered under reduced pressure to yield the product as a white crystalline solid (1.06 g, 3.49 mmol, 51%).

Mp: 149-152 °C. ¹H-NMR (400 MHz, DMSO-*d*₆): δ 3.78 (*t*, *J*=2.3 Hz, 1H, C≡C-H), 5.12 (*d*, *J*=2.4 Hz, 2H, O-CH₂-C≡C-H), 7.48 (*d*, *J*=9.4 Hz, 2H, *o*-Ar), 8.60 (*d*, *J*=9.3 Hz, 2H, *p*-Ar). ¹³C-NMR (100 MHz, DMSO-*d*₆): δ 58.06, 77.78 (C≡C), 80.71 (C≡C), 105.20 (Ar-O-CH₂), 118.89, 136.57, 166.97 (C=O).

4-Nitrobenzenediazonium hexafluorophosphate(V) (48)

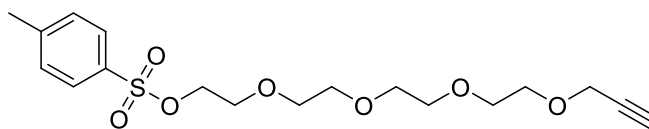
p-Nitroaniline (1.00 g, 7.24 mmol) was dissolved in TFA (10 ml) and cooled in a salt-ice bath. Sodium nitrite (1.76 g, 20.40 mmol) in water (5 mL) was added dropwise and the temperature maintained for 1.5 hr. HPF₆ (60% w/w aq. 27.2 mmol) was added dropwise. The reaction was maintained at -10 °C for 1.5 hr. The mixture was filtered under reduced pressure to yield the product as an off-white crystalline solid (1.08 g, 3.69 mmol, 51%).

The product was used immediate without further purification or characterisation.

3,6,9,12-Tetraoxapentadec-14-yn-1-ol (49)¹⁵⁴

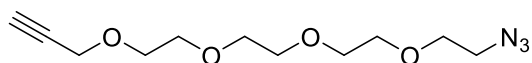
Under an inert atmosphere, tetraethyleneglycol (5.40 g, 35.95 mmol) was slowly added to a solution of NaH (0.466 g, 19.42 mmol) in anhydrous THF (40 mL) at -20 °C. Propargyl bromide (3.0 g, 2 mL, 27.6 mmol, 80% in toluene) was added dropwise after all bubbling had stopped, the mixture was allowed to warm to room temperature and stirred overnight under argon. The mixture was filtered to remove solid residues and the filter cake washed with DCM, bulk solvent was removed under reduced pressure. The crude was purified by flash column chromatography, DCM/MeOH (95.5:4.5), the product eluted in the second major band, the fractions were collected and bulk solvent removed under reduced pressure to yield the product as a pale tan oil (2.17 g, 9.34 mmol, 35% yield).

R_F: 0.20 (silica, 94.5:4.5, DCM/MeOH). ¹H-NMR (400 MHz, CDCl₃): δ 2.41 (s, 1H, CC-H), 2.43 (s, 3H, 3.66 (m, 16H, O-CH₂-CH₂-O, overlapping CH₂-OH), 4.18 (d, J=2.4 Hz, 2H, O-CH₂-CCH). ¹³C-NMR (100 MHz, CDCl₃): δ 58.48 (C≡CH), 61.80 (C≡CH), 69.15, 70.33, 70.43, 70.58, 70.61, 70.68, 72.69, 77.72, 79.61 (CH₂-CCH). MS: (ESI+) *m/z* [M+H]⁺ 233.1380, HMRS: calcd. C₁₁H₂₀O₅ For: 233.1384 found 233.1380. ATR-FT-IR: 3448.79 (O-H str), 3250.53(C≡C-H str), 2868.42(C-H str), 2112.90 (C≡C str), 1349.16 (C-H bnd), 1248.40 (C-OH str), 1095.29 (C-O str).

3,6,9,12-Tetraoxapentadec-14-(4-methylbenzenesulfonate) (50)¹⁵⁴

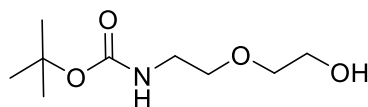
Under an inert atmosphere, to 3,6,9,12-tetraoxapentadec-14-yn-1-ol (2.00 g, 8.61 mmol) in anhydrous DCM (20 mL) was added trimethylamine (3 mL, 21.5 mmol). The solution was cooled to 0 °C and p-toluenesulfonyl chloride (6.16 g, 32.2 mmol) in anhydrous DCM (20 mL) was added slowly and the mixture was stirred for 42 hr affording a tan solution. The bulk solvent was removed under reduced pressure, the crude was dissolved in DCM and washed sequentially with water. The organic layer was dried with anhydrous MgSO₄, filtered under gravity and bulk solvent removed under reduced pressure to yield a light-yellow oil (3.17 g, 8.20 mmol, 95% yield).

R_F: 0.40 (silica, 95:5, DCM/MeOH). ¹H-NMR (400 MHz, CDCl₃): δ 2.41 (s, 1H, CC-H), 2.43 (s, 3H, Ar-CH₃), 3.64 (m, 16H, O-CH₂-CH₂-O), 4.14 (d, J=2.4 Hz, 2H, O-CH₂-CCH), 7.32 (d, J=8.0 Hz, 2H, m-Ar), 7.78 (d, J=8.0 Hz, 2H, o-Ar). ¹³C-NMR (100 MHz, CDCl₃): δ 21.75, 58.48 (C≡CH), 68.75 (C≡CH), 69.17, 69.35, 70.47, 70.60, 70.65, 70.81, 74.65, 79.71 (CH₂-CCH), 128.08, 129.92, 132.99, 144.91. MS: (ASAP) *m/z* [M+H]⁺ 387.1473, HMRS: *calcd.* C₁₈H₂₇SO₇ For: 387.1477 found 387.1473. ATR-FT-IR: 3519.34 (O-H str), 3277.15 (C≡C-H str), 2869.00 (C-H str), 2114.91 (C≡C str), 1597.63 (C=C arom str), 1451.19 (C-H bnd), 1351.11 (C-OH str), 1189.27, 1174.78 (O=S=O str), 1094.39 (C-O str), 916.91 (O-S str), 661.96 (S-C str)

1-Azido-3,6,9,12-tetraoxapentadec-14-yne (51)

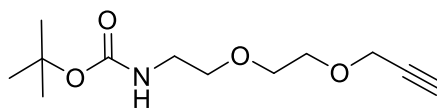
To a solution of 3,6,9,12-tetraoxapentadec-14-(4-methylbenzenesulfonate) (2.50 g, 6.47 mmol) in acetonitrile (20 mL) was added excess sodium azide (1.50 g, 23.08 mmol). The mixture was heated at reflux overnight. The reaction was cooled and the organic phase washed with water (3x50 mL). The organic layer was dried with anhydrous MgSO₄, filtered under reduced pressure and bulk solvent removed under reduced pressure. The crude was taken up in a minimum of ethyl acetate/hexane (1:1) and eluted onto a silica chromatography column. The product eluted in the first major fraction from ethyl acetate/hexane (1:1). Bulk solvent was removed under reduced pressure to give a pale-fawn coloured oil (1.33 g, 5.18 mmol, 80%).

R_F: 0.72 (silica, 98:2, DCM/MeOH). ¹H-NMR (400 MHz, CDCl₃): δ 2.41 (s, 1H, CC-H), 2.43 (s, 3H, 3H), 3.66 (m, 16H, O-CH₂-CH₂-O, overlapping CH₂-OH), 4.18 (d, J=2.4 Hz, 2H, O-CH₂-CCH). ¹³C-NMR (100 MHz, CDCl₃): δ 58.48 (C≡CH), 61.80 (C≡CH), 69.15, 70.33, 70.43, 70.58, 70.61, 70.68, 72.69, 77.72, 79.61 (CH₂-CCH). MS: (ESI+) *m/z* [M]⁺ 257.1, [M+Na-H]⁺ 277.2.

Tert-butyl (2-(2-hydroxyethoxy)ethyl)carbamate (52)

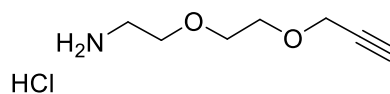
Under an inert atmosphere, 2-(2-aminoethoxy)ethan-1-ol (18.60 g, 176.90 mmol) was dissolved in anhydrous DCM (50 mL) and cooled to 0 °C in an salt-ice bath. Di-tert-butyl dicarbonate (43.65 g, 200.00 mmol) was dissolved in dry dichloromethane (20 mL) and added dropwise, the reaction was stirred overnight and allowed to warm to room temperature. Bulk solvent was removed under reduced pressure. The crude was loaded onto a flash silica column and eluted in DCM/MeOH (95.5:4.5) as the second major fraction. The fractions were collected, bulk solvent was removed under reduced pressure to yield the product as a pale-yellow oil (33.04 g, 160.98 mmol, 91% yield).

R_F: 0.13 (silica, 95.5:4.50, DCM/MeOH). ¹H-NMR (400 MHz, CDCl₃): δ 1.42 (s, 9H, NH-CO-O-C(CH₃)₃), 2.42 (t, 1H, J=2.3 Hz, CH₂-OH), 3.31 (dd, 2H, HO-CH₂-CH₂-NH), 3.54 (t, 2H, J=5.1 Hz, O-CH₂-CH₂-NH), 3.72 (m, 2H, O-CH₂-CH₂-O), 3.66 (m, 2H, O-CH₂-CH₂-O), 4.97 (s, 1H, CH₂-NH-CO). ¹³C-NMR (100 MHz, CDCl₃): δ 27.48, 28.47, ((CH₃)₃-O), 40.41, 53.51, 61.81, 70.39, 72.62, 79.48, 85.28, 156.18 (C=O). MS: (ESI+) [M+H]⁺ m/z 206.1386, HRMS: calcd. For C₉H₂₀NO₄: 206.1387 found 206.1386. ATR-FT-IR: 3373.67 (O-H str), 2992.15 (C-H str), 1692.14 (C=O str), 1513.38 (N-H bnd), 1355.87 (C-H bnd), 1172.05 (C-O str), 1103.57 (C-N str), 1034.53 (C-O str).

Tert-butyl (2-(2-(prop-2-yn-1-yloxy)ethoxy)ethyl)carbamate (53)

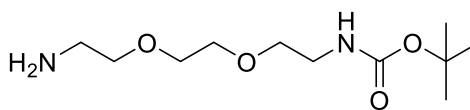
Under an inert atmosphere, tert-butyl (2-(2-hydroxyethoxy)ethyl)carbamate (12.50 g, 60.9 mmol) was dissolved in anhydrous THF (50 mL). Tetrabutylammonium iodide (29.54 g, 80.00 mmol) and sodium iodide (29.54 g, 197.07 mmol) were added in one portion. Propargyl bromide (8.8 mL, 80% in toluene, 11.76 g, 80.00 mmol) was added dropwise. To this mixture was added freshly powdered potassium hydroxide (3.00 g, 60.00 mmol) in portions over 30 mins. The reaction was stirred overnight. Bulk solvent was removed under reduced pressure and the crude was dissolved in a minimum of DCM/MeOH (97:3) and loaded onto a flash silica chromatography column. The product eluted as the first major fraction. The fractions were collected and bulk solvent removed under reduced pressure to yield a yellow-orange oil (9.42 g, 38.72 mmol, 64% yield).

R_F : 0.45 (silica, 97:3, DCM/MeOH). $^1\text{H-NMR}$ (400 MHz, CDCl_3): δ 1.43 (s, 9H, $\text{NH-CO-O-C}(\text{CH}_3)_3$), 2.42 (t, 1H, $J=2.3$ Hz, $\text{H-CC-CH}_2\text{-O}$), 3.31 (dd, 2H, $\text{HO-CH}_2\text{-CH}_2\text{-NH}$), 3.53 (t, 2H, $J=5.1$ Hz, $\text{O-CH}_2\text{-CH}_2\text{-NH}$), 3.63 (m, 2H, $\text{O-CH}_2\text{-CH}_2\text{-O}$), 3.68 (m, 2H, $\text{O-CH}_2\text{-CH}_2\text{-O}$), 4.20 (d, $J=2.4$ Hz, 2H, $\text{O-CH}_2\text{-CC-H}$), 4.98 (s, 1H, $\text{CH}_2\text{-NH-CO}$). $^{13}\text{C-NMR}$ (100 MHz, CDCl_3): δ 28.48, 40.39, 53.52, 58.50, 69.09, 70.18, 70.38, 74.76, 79.27, 79.59, 156.05. MS: (ESI+) $[M+H]^+$ m/z 244.1547, HRMS: calcd. For $\text{C}_{12}\text{H}_{22}\text{NO}_4$: 244.1543 found 244.1547. ATR-FT-IR: 3300.03 (C \equiv C-H str), 2868.80 (C-H str), 2112.80 (C \equiv C str), 1698.10 (C=O str), 1509.20 (N-H bnd), 1365.60 (C-H bnd), 1168.76 (C-O str), 1034.89 (C-N str), 1033.19 (C-O str).

2-(2-(prop-2-yn-1-yloxy)ethoxy)ethan-1-amine hydrochloride (54)

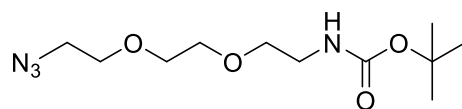
To a stirred solution of tert-butyl (2-(2-(prop-2-yn-1-yloxy)ethoxy)ethyl)carbamate (6.00 g, 24.66 mmol) in ethyl acetate (15 mL) was added HCl in dioxane (4M, 12 mL). The reaction was stirred at room temperature overnight and the solvent removed under reduced pressure. The residue was triturated thrice with diethyl ether (50 mL) to yield the hydrochloride product as a beige solid (3.72 g, 20.59 mmol, 84% yield).

$^1\text{H-NMR}$ (400 MHz, CD_3OD): δ 2.89 (t, 1H, $J=2.5$ Hz, $\underline{\text{H}}\text{-CC-CH}_2\text{-O}$), 3.10 (m, 2H, $\text{HO-CH}_2\text{-CH}_2\text{-NH}$), 3.28 (dt, 2H, $J=5.1$ Hz, $\text{O-CH}_2\text{-CH}_2\text{-NH}$), 3.63 (m, 4H, $\text{O-CH}_2\text{-CH}_2\text{-O}$), 4.19 (d, $J=2.4$ Hz, 2H, $\text{O-CH}_2\text{-CC-H}$), 4.60 (brs, 1H, $\text{CH}_2\text{-NH-CO}$). $^{13}\text{C-NMR}$ (100 MHz, CD_3OD): δ 39.39, 57.82, 66.56, 68.91, 69.80, 74.97, 78.98. MS: (ESI+) m/z $[M]^+$ 144.1015, HRMS: calcd. For $[\text{C}_7\text{H}_{13}\text{NO}_2]\text{HCl}$: 144.1019 found 144.1015.

Tert-butyl (2-(2-(2-aminoethoxy)ethoxy)ethyl)carbamate (55)²⁸⁴

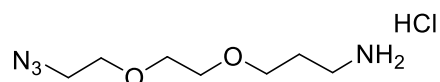
Under an inert atmosphere, 2,2'-(ethane-1,2-diylbi(oxy)diethanamine (10 mL, 10.15 g, 68.49 mmol) was dissolved in anhydrous DCM (20 mL) and cooled to 0 °C under argon with stirring. Di-tert-butyl dicarbonate (5.00 g, 22.91 mmol) was dissolved in dry dichloromethane (20 mL) and added dropwise, the reaction was stirred overnight and allowed to warm to room temperature. Bulk solvent was removed under reduced pressure. The crude was eluted onto a flash silica column and eluted in DCM/MeOH with gradient (95:5 to 75:25) as the second major fraction. The fractions were collected, bulk solvent was removed under reduced pressure to yield the product as a pale-yellow oil (4.61 g, 18.56 mmol, 81% yield).

R_F: 0.10 (silica, 75:25, DCM/MeOH). ¹H-NMR (400 MHz, CDCl₃): δ 1.38 (s, 9H, NH-CO-(CH₃)₃), 2.09 (s, 2H, NH₂), 2.84 (t, J=5.2 Hz, 2H, CH₂-NH₂), 3.26 (m, 2H, CH₂-NHBoc), 3.48 (m, 4H, O-CH₂-CH₂-O), 3.56 (s, 4H, O-CH₂-CH₂-O). ¹³C-NMR (100 MHz, CDCl₃): δ 28.46, 40.35, 41.60, 50.23, 70.25, 73.60, 79.20, 156.10 (C=O). MS: (ESI+) *m/z* [M+H]⁺ 249.1811, HMRS: *calcd.* C₁₁H₂₄N₂O₄ *For*: 249.1809 *found* 249.1811. ATR-FT-IR: 3359.22 (N-H str), 2915.36 (C-H str), 1690.04 (C=O str), 1526.54 (N-H bnd), 1365.12 (C-H bnd), 1173.69 (C-O str), 1103.23 (C-N str), 1027.15 (C-O str).

Tert-butyl (2-(2-(2-aminoethoxy)ethoxy)ethyl)carbamate (56)

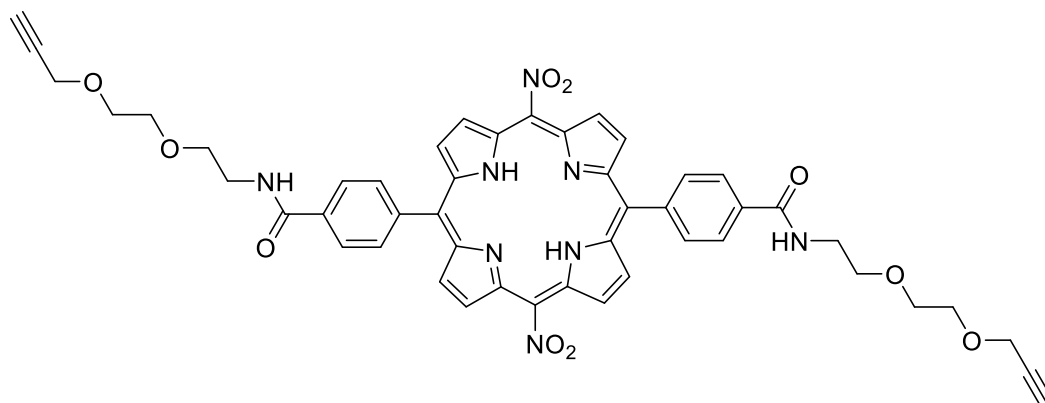
Under an inert atmosphere, to a stirred solution of tert-butyl (2-(2-(2-aminoethoxy)ethoxy)ethyl)carbamate (2.50 g, 10.00 mmol) in anhydrous methanol (50 mL) was added copper(II) sulfate pentahydrate (1 mg, 0.25 μ mol), and anhydrous potassium carbonate (2.75 g, 20.00 mmol). Imidazole-1-sulfonyl azide hydrochloride (2.50 g, 12.00 mmol) was added. The mixture was stirred at room temperature overnight. Bulk solvent was removed under reduced pressure and the crude was loaded onto a flash silica column and eluted with DCM/MeOH (95:5) to yield the product as a pale-yellow oil (1.60 g, 5.83 mmol, 58% yield).

R_F : 0.60 (silica, 95:5, DCM/MeOH). 1H -NMR (400 MHz, $CDCl_3$): δ 1.43 (s, 9H, NH-CO-(CH_3)₃), 3.31 (dd, $J=10.4, 5.2$ Hz, 2H, CH_2-N_3), 3.39 (t, 2H, $CH_2-NHBoc$), 3.54 (t, 2H, O- CH_2-CH_2-O), 3.64 (s, 6H, O- CH_2-CH_2-O), 5.00 (s, 1H, NH-CO-(CH_3)₃). ^{13}C -NMR (100 MHz, $CDCl_3$): δ 20.48, 40.40, 50.72, 70.16, 70.31, 70.39, 70.65, 79.28, 156.08 ($C=O$). MS: (ESI+) m/z [$M+H$]⁺ 275.1718, HMRS: calcd. $C_{11}H_{22}N_4O_4$ For: 275.1714 found 274.1718. ATR-FT-IR: 2869.02 (C-H str), 2100.84 (N-N⁺=N str) 1707.98 (N-H str), 1510.44 (C-H bnd), 1116.64 (C-O str).

3-(2-(2-Azidoethoxy)ethoxy)propan-1-amine hydrochloride (57)

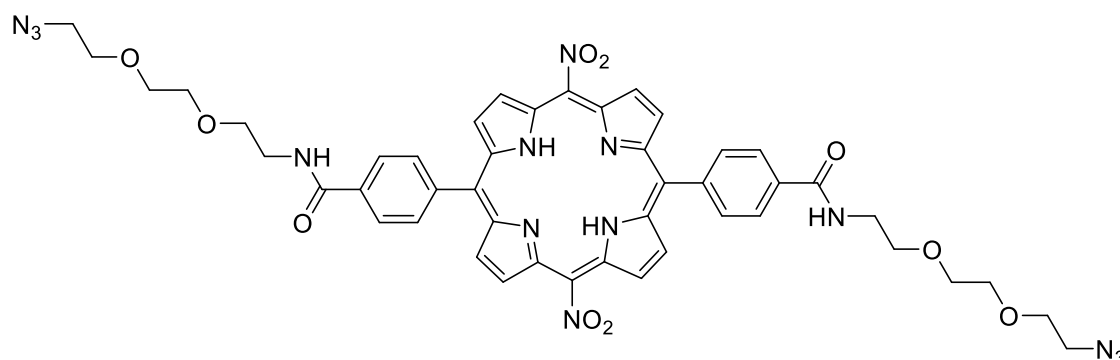
To a stirred solution of tert-butyl (2-(2-(2-aminoethoxy)ethoxy)ethyl)carbamate (1.20 g, 4.37 mmol) in ethyl acetate (3 mL) was added HCl in dioxane (4M, 5 mL) The reaction was stirred at room temperature overnight and the solvent removed under reduced pressure. The residue was triturated thrice with diethyl ether (50 mL) to yield the hydrochloride product as a fawn coloured oily residue (0.860 g, 3.84 mmol, 88% yield).

¹H-NMR (400 MHz, CD₃OD): δ 3.11 (t, 2H, CH₂-NH₂), 3.39 (t, 2H, CH₂-N₃), 3.66 (m, 6H CH₂-CH₂ overlapping O-CH₂), 4.89 (brs, 2H, NH₂). ¹³C-NMR (100 MHz, CD₃OD): δ 39.40, 50.40, 66.57, 69.71, 70.05, 70.12. MS: (ESI+) m/z [M]⁺ 189.1346, HRMS: calcd. For [C₆H₉NO]HCl: 114.0913 found 189.1346. ATR-FT-IR: 3356.25 (N-H salt, str), 2854.53 (C-H str), 2099.67 (N-N⁺=N str) 1604.42 (N-H str), 1453.91 (C-H bnd), 1108.89 (C-O str).

Conjugate (58)

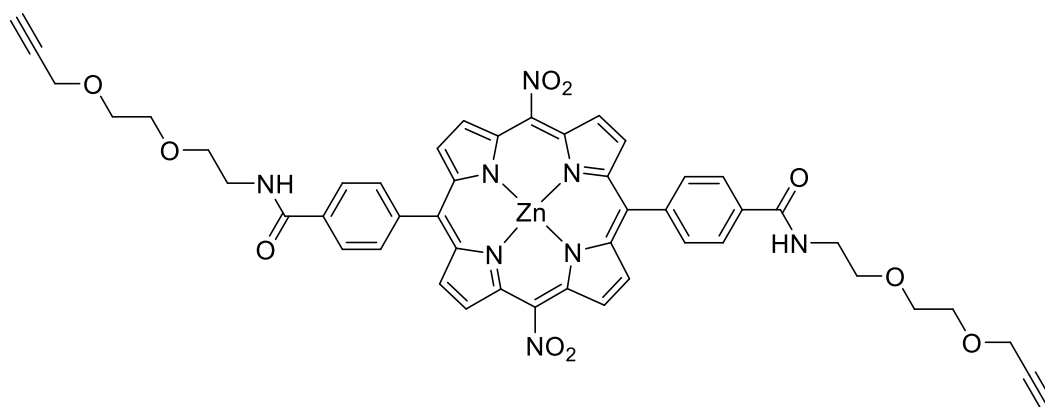
Under an inert atmosphere, 5,15-di(carboxyphenyl)porphyrin (50.0 mg, 0.078 mmol) and 2-(2-(prop-2-yn-1-yloxy)ethoxy)ethan-1-amine hydrochloride (33.00 mg, 0.17 mmol) were dissolved in anhydrous amine free DMF (5 mL). DIPEA (0.11 mL, 80.65 mg, 0.62 mmol) and TBTU (54.57 mg, 0.17 mmol) in anhydrous amine free DMF (2 mL). The reaction was stirred at 40 °C for 72 hr protected from light. Bulk solvent was removed under reduced pressure and the crude was sonicated in water and filtered under reduced pressure. The crude was loaded onto a flash chromatography column and eluted in DCM/MeOH with gradient (98:2 – 93:7) to give the product as the first major red band. Bulk solvent was removed under reduced pressure to give a purple crystalline solid. (44.5 mg, 0.050 mmol, 64% yield).

R_F : 0.63 (silica, 98:2, DCM/MeOH). $^1\text{H-NMR}$ (400 MHz, CDCl_3): δ -3.03 (s, 2H, N-H), 2.45 (t, 2H, $J=2.3$ Hz, $\text{H-CC-CH}_2\text{-O}$), 3.82 (m, 16H, $\text{HO-CH}_2\text{-CH}_2\text{-NH}$), 4.28 (d, $J=2.5$ Hz, 4H, $\text{O-CH}_2\text{-CC-H}$), 5.60 (brs, 2H, $\text{CH}_2\text{-NH-CO}$), 8.27 (dd, $J=8.1$ Hz, 8H, *o,m*-Ar), 8.96 8.97 (dd, $J=10.8$ Hz, 4H, $\beta\text{-H}$), 9.35 (dd, $J=11.0$ Hz, 4H, $\beta\text{-H}$), $^{13}\text{C-NMR}$ (100 MHz, CDCl_3): δ 29.80, 40.02, 58.65, 69.28, 70.00, 70.27, 74.99, 79.52, 109.12, 120.96, 125.96, 128.56, 129.54, 131.57, 132.89, 134.78, 143.90, 167.46 (C=O). MS: (ESI+) m/z [$\text{M-NO}_2\text{+H}$] $^+$ 846.3257, HRMS: calcd. For $\text{C}_{48}\text{H}_{43}\text{N}_7\text{O}_8$: 846.3246 found 846.3257. UV-Vis (DCM): λ_{max} 415, 515, 555, 585, 645. $\log \epsilon$ (415) = 5.44.

Conjugate (59)

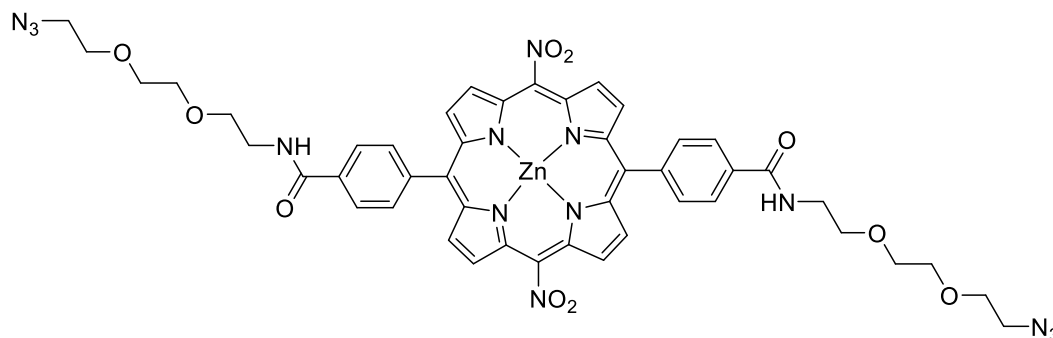
Under an inert atmosphere, 5,15-di(carboxyphenyl)porphyrin (50.0 mg, 0.078 mmol) and 3-(2-(2-azidoethoxy)ethoxy)propan-1-amine hydrochloride (38.20 mg, 0.17 mmol) were dissolved in anhydrous amine free DMF (5 mL). To this mixture was added DIPEA (0.11 mL, 80.65 mg, 0.62 mmol) and TBTU (54.57 mg, 0.17 mmol) in anhydrous amine free DMF (2 mL). The reaction was stirred at 40 °C for 72 hr protected from light. Bulk solvent was removed under reduced pressure and the crude was sonicated in water and filtered under reduced pressure. The crude was loaded onto a flash chromatography column and eluted in DCM/MeOH with gradient (98:2 – 95:5) to give the product as the first major red band. Bulk solvent was removed under reduced pressure to give a purple crystalline solid. (50.5 mg, 0.053 mmol, 68% yield).

R_F : 0.70 (silica, 97:3, DCM/MeOH). $^1\text{H-NMR}$ (400 MHz, CDCl_3): δ -3.17 (s, 2H, N-H), 3.38 (t, 4H, $\text{CH}_2\text{-N}_3$), 3.39 (t, 2H, $\text{CH}_2\text{-N}_3$), 3.71 (m, 14H $\text{O-CH}_2\text{-CH}_2\text{-O-CH}_2\text{-CH}_2\text{-N}_3$), 3.80 (m, 8H, $\text{CO-NH-CH}_2\text{-CH}_2\text{-O}$) 8.18 (d, $J=8.2$ Hz, 4H, *o*-Ar), 8.23 (d, $J=8.2$ Hz, 4H, *m*-Ar), 8.92 (dd, $J=12.2$ Hz, 4H, $\beta\text{-H}$), 9.30 (dd, $J=12.1$ Hz, 4H, $\beta\text{-H}$). $^{13}\text{C-NMR}$ (100 MHz, CDCl_3): δ 14.23, 22.79, 29.41, 29.80, 30.31, 32.02, 40.10, 50.74, 70.14, 70.27, 70.47, 70.73, 120.96, 125.94, 128.55, 132.89, 134.59, 134.78, 143.91, 167.53 (C=O).

Zinc(II) Conjugate (60)

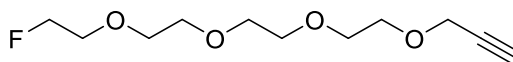
A sample of **58** (50 mg, 0.078 mmol) and zinc(II) acetate dihydrate (45 mg, 8.25 mmol) were added to a microwave vessel in DMF (10 mL). The solution was heated in a microwave for 1 hr at 90 °C. Bulk solvent was removed under reduced pressure. The crystals were sonicated in water, filtered and washed with copious amounts of water then dried under reduced pressure to give deep purple crystals. The crude was loaded onto a flash chromatography column and eluted using DCM/MeOH with gradient (98:2 – 93:7) to give the product as the first major red band. Bulk solvent was removed under reduced pressure to give a purple crystalline solid (44.5 mg, 0.050 mmol, 64% yield).

R_F : 0.63 (silica, 98:2, DCM/MeOH). MS: (ESI+) m/z $[M+H]^+$ 908.2387, HRMS: calcd. For $C_{48}H_{40}N_8O_{10}Zn$: 908.2381 found 908.2387.

Zinc(II) Conjugate (61)

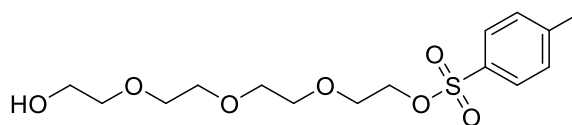
A sample of **59** (45 mg, 0.017 mmol) and zinc(II) acetate dihydrate (45 mg, 8.25 mmol) were added to a microwave vessel in DMF (10 mL). The solution was heated in a microwave for 1 hr at 90°C. Bulk solvent was removed under reduced pressure. The crystals were sonicated in water, filtered and washed with copious amounts of water then dried under reduced pressure to give deep purple crystals. The crude was loaded onto a flash chromatography column and eluted in DCM/MeOH with gradient (98:2 – 93:7) to give the product as the first major red band. Bulk solvent was removed under reduced pressure to give a purple crystalline solid (49 mg, 0.016 mmol, 98% yield).

R_F : 0.82 (silica, 98:2, DCM/MeOH). 1H -NMR (400 MHz, $CDCl_3$): δ 3.38 (t, 4H, \underline{CH}_2 - N_3), 3.39 (t, 2H, \underline{CH}_2 - N_3), 3.71 (m, 14H O - \underline{CH}_2 - \underline{CH}_2 - O - \underline{CH}_2 - \underline{CH}_2 - N_3), 3.80 (m, 8H, CO - NH - \underline{CH}_2 - \underline{CH}_2 - O) 8.18 (d, $J=8.2$ Hz, 4H, o -Ar), 8.23 (d, $J=8.2$ Hz, 4H, m -Ar), 8.92 (dd, $J=12.2$ Hz, 4H, β -H), 9.30 (dd, $J=12.1$ Hz, 4H, β -H). ^{13}C -NMR (100 MHz, $CDCl_3$): δ 14.23, 22.79, 29.41, 29.80, 30.31, 32.02, 40.10, 50.74, 70.14, 70.27, 70.47, 70.73, 120.96, 125.94, 128.55, 132.89, 134.59, 134.78, 143.91, 167.53 ($\underline{C}=\underline{O}$). UV-Vis (DCM): λ_{max} 415, 447, 490. $\log \epsilon$ (415) = 5.18.

1-Fluoro-3,6,9,12-tetraoxapentadec-14-yne (62)¹⁵⁴

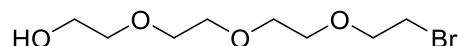
3,6,9,12-Tetraoxapentadec-14-(4-methylbenzenesulfonate) (2.50 g, 6.40 mmol) was dissolved in anhydrous THF (10 mL) under argon with heating at 80°C. TBAF in THF (4.84 mL, 4.84 mmol, 1M) was added dropwise. The mixture was stirred at 80°C for 1 hr. The mixture was cooled to room temperature. Bulk solvent was removed under reduced pressure and the crude purified by column chromatography and eluted in DCM/ethyl acetate (25:75). The fractions were collected and bulk solvent was removed under reduced pressure to yield a pale-yellow oil (1.13 g, 4.82 mmol, 75% yield).

R_F : 0.40 (silica, 25:75, DCM/ethyl acetate). $^1\text{H-NMR}$ (400 MHz, CDCl_3): δ 2.41 (s, 1H, CC-H), 3.07 (m, 14H, $\text{O-CH}_2\text{-CH}_2\text{-O}$), 4.18 (d, 2H, $\text{O-CH}_2\text{-CCH}$), 4.49 (t, 1H, $\text{CH}_2\text{-F}$), 4.60 (t, 1H, $\text{CH}_2\text{-F}$). $^{13}\text{C-NMR}$ (100 MHz, CDCl_3): δ 58.48, 69.18, 70.38, 70.84, 70.68, 70.87, 74.61, 79.72, 82.41, 84.09 ($\text{CH}_2\text{-F}$). $^{18}\text{F-NMR}$ (377 MHz, CDCl_3): δ -222.81 (tt, 1F, $J = 47.7, 29.7$ Hz, $\text{CH}_2\text{-F}$). MS: (ASAP) m/z $[M+H]^+$ 235.1350, HMRS: calcd. $\text{C}_{11}\text{H}_{20}\text{O}_4\text{F}$ For: 235.1346 found 235.1350. ATR-FT-IR: 3274.94 ($\text{C}\equiv\text{C-H}$ str), 2876.36 (C-H str), 2149.79 ($\text{C}\equiv\text{C}$ str), 1455.62 (C-H bnd), 1355.27 (C-F str), 1027.37 (C-O str).

3,6,9,12-Tetraoxapentadec-14-(4-methylbenzenesulfonate) (63)

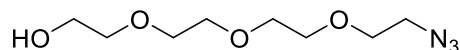
Under an inert atmosphere, tetraethylene glycol (5.40 g, 35.95 mmol) in anhydrous DCM (20 mL) was added trimethylamine (5.95 mL, 43.00 mmol). The solution was cooled to 0 °C and p-toluenesulfonyl chloride (6.16 g, 32.2 mmol) in DCM (20 mL) was added slowly and stirred for 20 mins at this temperature, and then for 40 mins while warming to room temperature. The mixture was poured into water and extracted into DCM. The organic layer was washed exhaustively to remove any unreacted TEG. The organic layer was collected and dried with anhydrous MgSO₄, bulk solvent was removed under reduced pressure. The crude was purified by column chromatography, the oil was eluted onto the column in DCM/MeOH (95.5:4.5) and the product collected as the third major fraction to give a pale-yellow oil (2.11 g, 6.06 mmol, 19% yield).

R_F: 0.40 (silica, 95:5, DCM/MeOH). ¹H-NMR (400 MHz, CDCl₃): δ 2.43 (s, 3H, Ar-CH₃), 3.64 (m, 16H, O-CH₂-CH₂-O), 4.15 (s, 2H, CH₂-OH), 7.33 (d, 2H, J=7.9 Hz, o-Ar), 7.78 (d, 2H, J=7.9 Hz, m-Ar). ¹³C-NMR (100 MHz, CDCl₃): δ 21.76, 61.82, 68.78, 69.33, 70.38, 70.53, 70.72, 70.81, 72.56, 128.08, 129.93, 132.96, 144.94. MS: (ESI+) *m/z* [M+H]⁺ 349.1314, HMRS: calcd. C₁₅H₂₄O₇S For: 349.1315 found 349.1314. ATR-FT-IR: 3441.29 (O-H str), 2871.02 (C-H str), 1597.53 (C=C arom str), 1351.86 (C-H bnd), 1188.91, 1174.33 (O=S=O str), 1095.29 (C-O str), 918.06 (O-S str), 662.19 (S-C str).

2-(2-(2-(2-Bromoethoxy)ethoxy)ethoxy)ethan-1-ol (64)

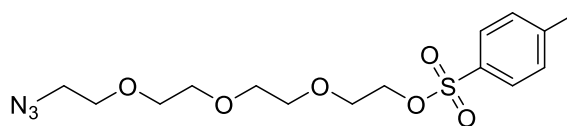
Under an inert atmosphere, tetraethyleneglycol (5.40 g, 35.95 mmol) was dissolved in anhydrous DCM (20 mL) with stirring at -10 °C under argon. To this was added PBr₃ (5.40 g, 2 mL, 20 mmol) dropwise over 10 mins. The reaction was left to stir under argon and allowed to warm to room temperature overnight. The reaction was quenched with the addition of brine dropwise with stirred for 30 mins. Bulk solvent was removed under reduced pressure. The crude was eluted onto a silica flash chromatography column and eluted in DCM/MeOH (97:3). The product eluted as the first major orange band. The fractions were collected and bulk solvent removed under reduced pressure to yield an orange oil (3.22 g, 12.58 mmol, 35% yield).

R_F: 0.70 (silica, 95:5, DCM/MeOH). ¹H-NMR (400 MHz, CDCl₃): δ 3.64 (t, *J*=6.3 Hz, 4H, CH₂-CH₂-OH), 3.66 (d, *J*=5.1 Hz, 9H, -CH₂-CH₂-), 3.79 (td, *J*=6.3 Hz, 2.8 Hz, 4H, -CH₂-CH₂-Br). ¹³C-NMR (100 MHz, CDCl₃): δ 30.46, 64.82, 70.29, 70.62, 70.73, 71.28. MS: (ESI+) *m/z* [*M*+*H*]⁺ 257.0385, HMRS: calcd. C₈H₁₇O₆Br For: 257.0383 found 257.0385.

2-(2-(2-(2-Azidoethoxy)ethoxy)ethoxy)ethan-1-ol (65)

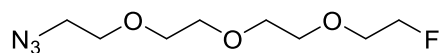
3,6,9,12-Tetraoxapentadec-14-(4-methylbenzenesulfonate) (2.00 g, 5.74 mmol) was dissolved in acetonitrile (5 mL), and sodium azide (0.75 g, 11.48 mmol) was added. The reaction was stirred at 95 °C for 48 hr. The mixture was filtered and the filtrate collected. Bulk solvent was removed under reduced pressure to yield a fawn colour oil. The crude was loaded onto a silica chromatography column in DCM and eluted from a solvent gradient of DCM to DCM/MeOH (98:2), the fractions were collected and bulk solvent removed under reduced pressure to yield a colourless oil (981 mg, 4.48 mmol, 78% yield).

R_F : 0.57 (silica, 98:2, DCM/MeOH). 1H -NMR (400 MHz, $CDCl_3$): δ 3.38 (t, 2H, CH_2 - $\underline{CH_2}$ - N_3), 3.59 (t, 2H, $\underline{CH_2}$ - CH_2 - N_3), 3.65 (m, 11H, O- $\underline{CH_2}$ - $\underline{CH_2}$ -O), 3.71 (t, 2H, HO- $\underline{CH_2}$). ^{13}C -NMR (100 MHz, $CDCl_3$): δ 50.75, 61.81, 70.13, 70.40, 70.66, 70.73, 70.77, 72.56. MS: (ESI+): m/z [$M+H$]⁺ 220.5, m/z [$M+Na$]⁺ 242.5. MS: (ASAP) m/z [$M+H$]⁺ 220.1301, HMRS: calcd. $C_8H_{17}O_4N_3$ For: 220.1297 found 220.1301. ATR-FT-IR: 3419.08 (O-H str), 2861.12 (C-H str), 2104.93 (N-N⁺=N str), 1118.45 (C-N str), 1065.53 (C-O str).

2-(2-(2-(2-Azidoethoxy)ethoxy)ethoxy)ethyl 4-methylbenzenesulfonate (66)

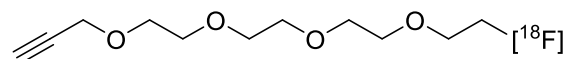
Under an inert atmosphere, 2-(2-(2-(2-azidoethoxy)ethoxy)ethoxy)ethan-1-ol (1.00 g, 4.56 mmol) was dissolved in anhydrous DCM and trimethylamine (5.95 mL, 43.00 mmol). The solution was cooled to 0 °C and p-toluenesulfonyl chloride (6.16 g, 32.2 mmol) in DCM (20 mL) was added slowly and stirred for 20 mins at this temperature, and then for 40 mins while warming to room temperature. The mixture was poured into water and extracted into DCM. The organic layer was washed exhaustively. The organic layer was collected and dried with anhydrous MgSO₄, bulk solvent was removed under reduced pressure. The crude was purified by column chromatography, the oil was eluted onto the column in DCM with gradient to DCM/MeOH (97:3) and the product collected as the second major fraction to give a pale-yellow oil (1.49 g, 3.99 mmol, 88% yield).

R_F: 0.28 (silica, 98:2, DCM/MeOH). ¹H-NMR (400 MHz, CDCl₃): δ 2.43 (s, 3H, Ar-CH₃), 3.37 (t, 2H, CH₂-CH₂-OTs), 3.58 (m, 4H, O-CH₂-CH₂-O), 3.66 (m, 8H, CH₂-CH₂), 4.14 (t, 2H, CH₂-CH₂-N₃), 7.33 (d, 2H, J=8.3 Hz, o-Ar), 7.78 (d, 2H, J=8.3 Hz, m-Ar). ¹³C-NMR (100 MHz, CDCl₃): δ 21.74 (CH₃-Ar), 50.75, 68.76, 69.33, 70.13, 70.68, 70.75, 70.84, 128.07, 129.91, 133.04, 144.90. MS: (ESI⁺): m/z [M]⁺ 373.5, m/z [M+H]⁺ 374.5, m/z [M+Na]⁺ 396.9. ATR-FT-IR: 2869.50 (C-H str), 2099.69 (N=N=N str), 1597.99 (C=C arom str), 1174.55 (O=S=O str), 1095.61 (C-O str), 815.45 (S-O str), 690.04 (S-C str).

1-Azido-2-(2-(2-(2-fluoroethoxy)ethoxy)ethoxy)ethane (67)

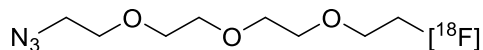
2-(2-(2-(2-Azidoethoxy)ethoxy)ethoxy)ethyl 4-methylbenzenesulfonate (2.50 g, 6.40 mmol) was dissolved in anhydrous THF (10 mL) under argon with heating to 80 °C. TBAF in THF (4.84 mL, 4.84 mmol, 1M) was added dropwise. The mixture was stirred at 80 °C for 5 hr. The mixture was cooled to room temperature. Bulk solvent was removed under reduced pressure and the crude purified by column chromatography and eluted in DCM/MeOH (95:5) as the first major fraction. The fractions were collected and bulk solvent was removed under reduced pressure to yield a pale-yellow oil (1.36 g, 6.14 mmol, 96% yield).

R_F : 0.90 (silica, 95:5, DCM/MeOH). $^1\text{H-NMR}$ (400 MHz, CDCl_3): δ 3.38 (t, 2H, $\text{CH}_2\text{-CH}_2\text{-N}_3$), 3.68 (m, 11H, $\text{O-CH}_2\text{-CH}_2\text{-O}$), 3.77 (t, 2H, $\text{CH}_2\text{-CH}_2\text{-F}$), 4.50 (t, 1H, $\text{CH}_2\text{-CH}_2\text{-F}$), 4.62 (t, 1H, $\text{CH}_2\text{-CH}_2\text{-F}$). $^{13}\text{C-NMR}$ (100 MHz, CDCl_3): δ 50.75 ($\text{CH}_2\text{-N}_3$), 70.14, 70.39, 70.58, 70.78, 70.89, 82.42, 84.10 ($\text{CH}_2\text{-F}$). $^{18}\text{F-NMR}$ (377 MHz, CDCl_3): δ -222.79 (ddd, 1F, $J = 47.7, 30.3, 17.4$ Hz, $\text{CH}_2\text{-F}$). ATR-FT-IR: 2921.07 (C-H str), 2098.09 ($\text{N}^-\text{-N}^+=\text{N}$ str), 1284.64 (C-F str), 1125.02 (C-O str).

1-(fluoro- ^{18}F)-3,6,9,12-tetraoxapentadec-14-yne (^{18}F 62)¹⁵⁴

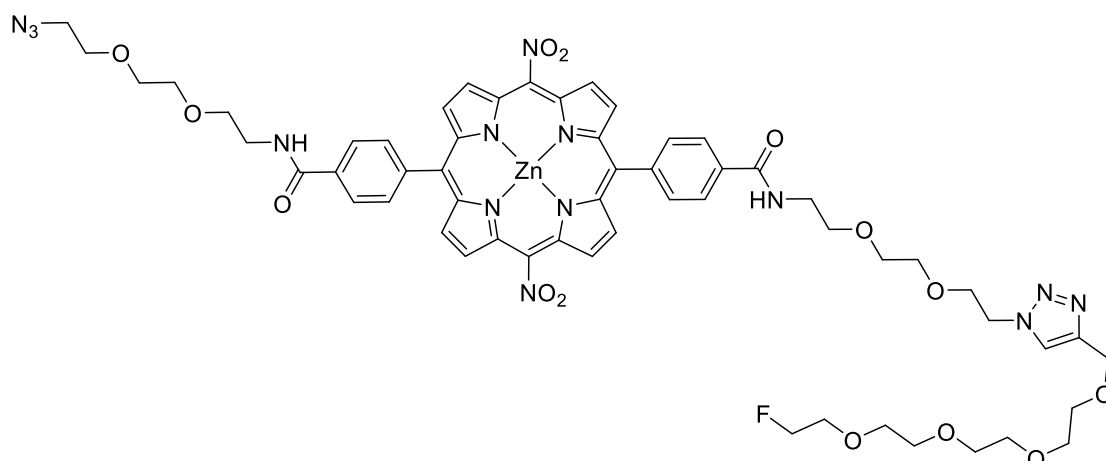
^{18}O water (~140 μL) containing 3.64 GBq of ^{18}F was transferred to a 5 mL V-vial containing potassium hydrogen carbonate solution (0.5 mL, 5 mg/mL) and Kryptofix® K₂₂₂ (10.0 mg in 1 mL of dry acetonitrile). The water was removed *via* azeotropic distillation with acetonitrile under a compressed argon stream at 90 °C for 20 mins. To a 5 mL V-vial containing dried ^{18}F (1347 MBq) was added **50** (5.0 mg) in dry acetonitrile (1 mL), and the mixture was heated to 90 °C for 20 min. The crude reaction mixture was passed through a Sep-Pak Light Alum N cartridge. Eluted activity: 1164 MBq (RCY 88%, non-decay corrected). The solvent was reduced to ~0.2 mL at 90 °C under a compressed argon stream and the residue diluted with water (0.5 mL). The crude was purified on semi-preparative HPLC (MeOH/water, 20% to 30% in 15 min), with ^{18}F 62 eluting at 10–12 min (109.1 MBq). The collected HPLC fraction was diluted to 10 mL with water and azeotropically dried at 90 °C for 15 mins.

Rt = 10-12 min (C-18 silica, solvent method 1).

1-Azido-2-(2-(2-(2-(fluoro-[¹⁸F])ethoxy)ethoxy)ethoxy)ethane ([¹⁸F]67)

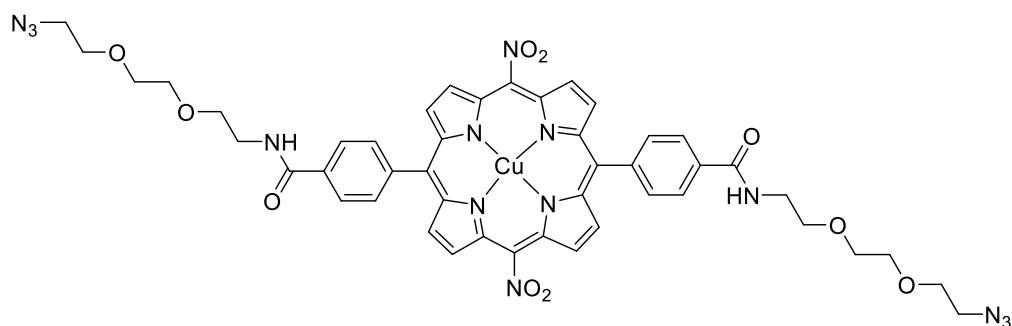
¹⁸O water (~140 μL) containing 3.64 GBq of ¹⁸F was transferred to a 5 mL V-vial containing potassium hydrogen carbonate solution (0.5 mL, 5 mg/mL) and Kryptofix® K₂₂₂ (10.0 mg in 1 mL of dry acetonitrile). The water was removed *via* azeotropic distillation with acetonitrile under a compressed argon stream at 90 °C for 20 mins. To a 5 mL V-vial containing dried ¹⁸F (1368 GMq) was added **66** (5.0 mg) in dry acetonitrile (1 mL), and the mixture was heated to 90 °C for 20 min. The crude reaction mixture was passed through a Sep-Pak Light Alum N cartridge. Eluted activity: 1042 MBq (RCY 76%, non-decay corrected). The solvent was reduced to ~0.2 mL at 90 °C under a compressed argon stream and the residue diluted with water (0.5 mL). The crude was purified on semi-preparative HPLC (MeOH/water, 20% to 30% in 15 min), with [¹⁸F]**67** eluting at 10–12 min (75.6 MBq). The collected HPLC fraction was diluted with water (10 mL) and azeotropically dried at 90 °C for 15 mins.

Rt = 10-12 min (C-18 silica, solvent method 1).

Conjugate (68)

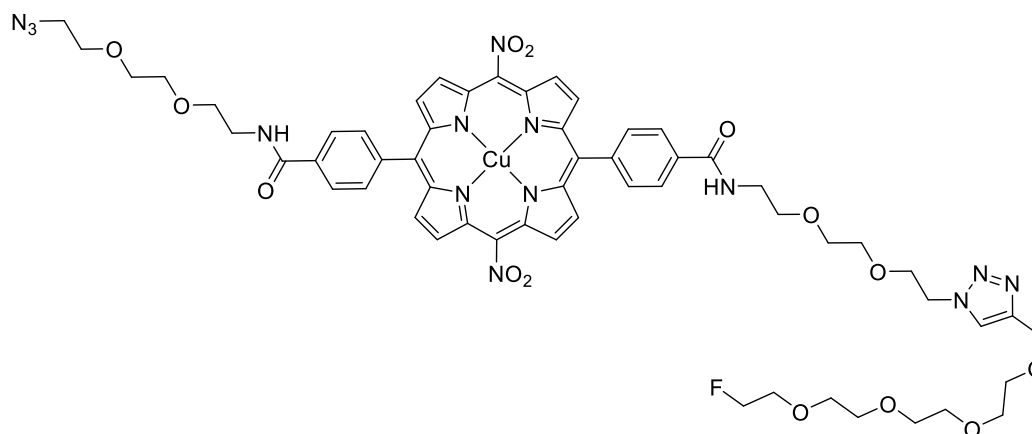
61 (282.1 mg, 0.198 mmol), 1-fluoro-3,6,9,12-tetraoxapentadec-14-yne (50 mg, 0.198 mmol), sodium ascorbate (5.00 mg, 1.00 μ mol) and copper(II) acetate monohydrate (5.00 mg, 0.02 mmol) were added to a microwave reactor tube with THF/methanol (9:1) (30 mL). The mixture was stirred at 80 °C under microwave irradiation for 20 mins. Bulk solvent was removed under reduced pressure. The compound was dissolved in DCM and washed with water. The organic layer was dried with MgSO_4 and bulk solvent removed under reduced pressure. The crude was loaded onto a silica chromatography column and the product eluted in DCM/MeOH with gradient (95:5–90:10) as the first major coloured fraction. The fractions were collected and bulk solvent removed under reduced pressure to yield a purple oily solid (186.0 mg, 0.149 mmol, 75%).

R_F : 0.65 (silica, 95:5, DCM/MeOH). $R_t = 9.21$ min (C-18 silica, solvent method 2). $^1\text{H-NMR}$ (400 MHz, CDCl_3): δ 3.18 (t, 2H, $\text{CH}_2\text{-N}'\text{-triazole}$), 3.39 (m, 30H, $\text{O-CH}_2\text{-CH}_2\text{-O}$), 4.30 (t, 2H, $\text{CH}_2\text{-CH}_2\text{-F}$), 4.42 (t, 2H, $\text{CH}_2\text{-CH}_2\text{-F}$), 4.49 (t, 1H, $\text{CH}_2\text{-CH}_2\text{-F}$), 4.61 (t, 1H, $\text{CH}_2\text{-CH}_2\text{-F}$), 7.02 (s, 2H, triazole-H), 7.77 (d, $J=7.6$ Hz, 4H, *o*-Ar), 8.14 (d, $J=7.5$ Hz, 4H, *m*-Ar), 8.87 (d, 4H, β -H), 9.31 (d, 4H, β -H). $^{13}\text{C-NMR}$ (100 MHz, CDCl_3): δ 14.24, 22.79, 29.60, 29.79, 32.02, 39.71, 40.31, 48.70, 49.97, 50.75, 69.44, 70.11, 70.20, 70.40, 70.61, 82.26, 83.94, 98.55, 110.12, 121.45, 123.15, 125.26, 128.59, 129.59, 132.36, 133.00, 133.14, 133.75, 134.53, 143.90, 144.58, 145.75, 149.75, 150.00, 151.03, 167.33. $^{18}\text{F-NMR}$ (377 MHz, CDCl_3): δ -222.73 (m, 1F). UV-Vis (DCM): λ_{max} 419, 552, 595 nm. $\log \epsilon$ (419) = 5.26

Conjugate (69)

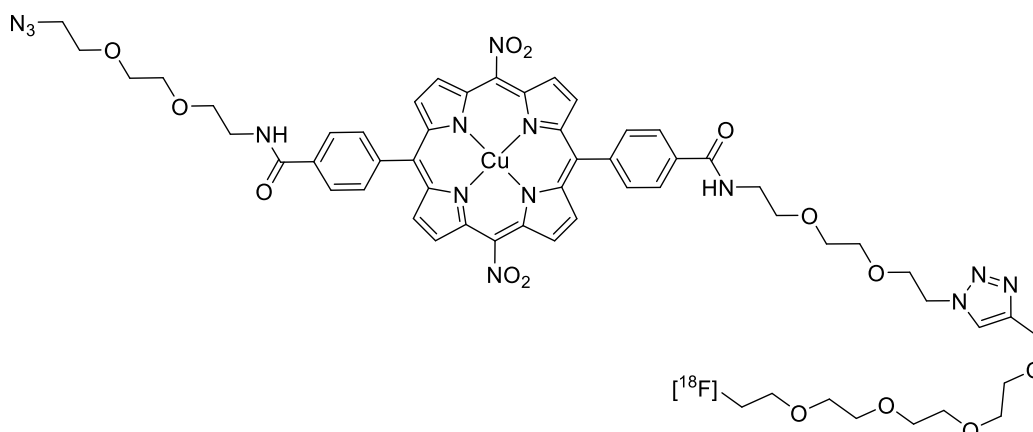
A sample of **59** (200 mg, 0.210 mmol) and copper(II) acetate monohydrate (200 mg, 1.00 mmol) was added to a microwave vessel in DMF (20 mL). The solution was heated in a microwave for 1 hr at 80 °C, 200 W and 200 PSI. Bulk solvent was removed under reduced pressure. The crystals were sonicated in water, filtered and washed with copious amounts of water then dried under reduced pressure to give a deep red-purple powder. The crude was dissolved into DCM/MeOH (98:2 – 98:5) and eluted onto a silica chromatography column to yield deep red-purple crystals (200 mg, 0.197 mmol, 94% yield).

R_F: 0.78 (silica, 98:2, DCM/MeOH). *R_t*: 27.35 (C-18 silica, solvent method 2). *MS*: (ESI+) *m/z* [*M*+2*H*]⁺ 507.6224, *HMRS*: calcd. C₄₆H₄₂N₁₄O₁₀Cu For: 507.6325 found 507.6224. *UV-Vis* (DMSO): λ_{max} 420, 550, 600. log ε (420) = 4.89.

Conjugate (70)

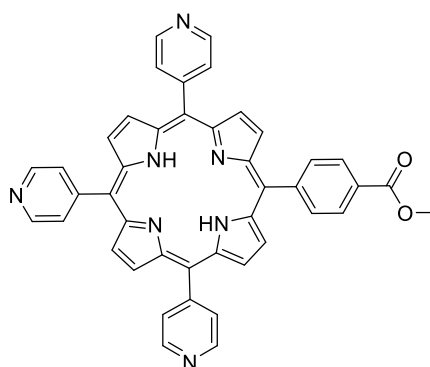
Conjugate **69** (100.0 mg, 98.6 μmol), 1-fluoro-3,6,9,12-tetraoxapentadec-14-yne (23 mg, 98.6 μmol , 1 eq.), sodium ascorbate (5.00 mg, 1.00 μmol) and copper(II) acetate monohydrate (5.00 mg, 0.02 mmol) were added to a microwave reactor tube with THF/methanol (9:1) (20 mL). The mixture was stirred at 80 °C under microwave irradiation for 20 mins. Bulk solvent was removed under reduced pressure. The compound was dissolved in DCM and washed with water. The organic layer was dried with MgSO₄ and bulk solvent removed under reduced pressure. The crude was loaded onto a silica chromatography column and the product eluted in DCM/MeOH with gradient (95:5 – 90:10) as the first major coloured fraction. The fractions were collected and bulk solvent removed under reduced pressure to yield a purple oily solid (13.3 mg, 0.01 mmol, 87%).

R_F: 0.90 (silica, 95:5, DCM/MeOH). *R_t*: 13.45 (C-18 silica, solvent method 2). UV-Vis (DMSO): λ_{max} 421, 549, 600. $\log \epsilon$ (421) = 4.56.

Conjugate ([¹⁸F]70)

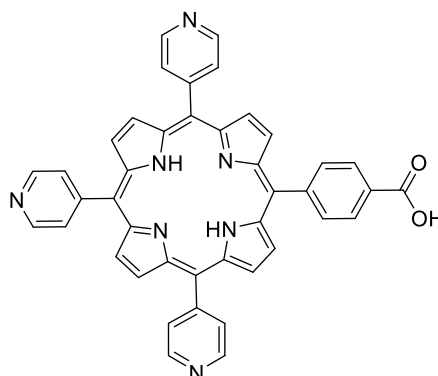
To a sample of pre-azeotropically dried [¹⁸F]**62** (100 MBq) in a 1.7 mL champagne HPLC vial was added to copper(II) acetate monohydrate (0.5 mg in 12.5 μ L of water), sodium ascorbate (3.75 mg in 50 μ L of water), TBTA (0.5 mg in 160 μ L of MeOH), and **Conjugate 69** (0.6 μ g/mL, 200 μ L) in THF/MeOH (4:1). The mixture was heated to 80 $^{\circ}$ C for 30 mins. The crude was passed through a Sep-Pak Light Alum N cartridge in MeOH (1 mL). An aliquot was taken and diluted into water (1:1) and analysed by radio-TLC and radio-HPLC.

Rt: 13.45 (C-18 silica, solvent method 2).

5-[4-Carboxmethoxyphenyl]-10,15,20-tri-(4-pyridyl) porphyrin (71)²⁸⁴

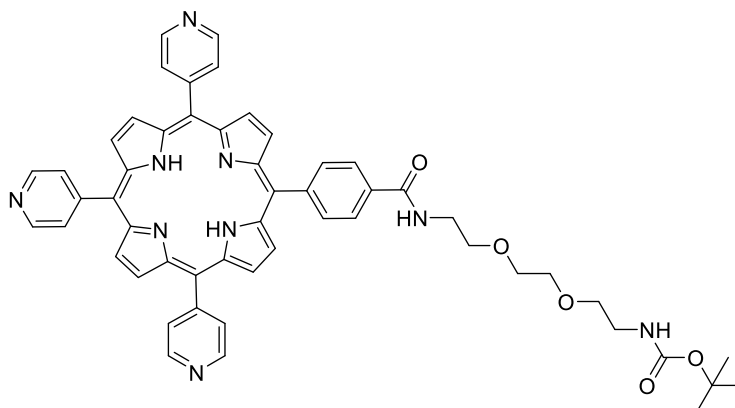
To a refluxing solution of methyl 4-formylbenzoate (3.67 g, 22.5 mmol) and pyridine 4-carboxaldehyde (6.40 mL, 67.5 mmol) in propionic acid (400 mL) was added pyrrole dropwise (5.54 mL, 90.0 mmol). The reaction was heated to reflux for 1 hr. The solution was allowed to cool, and bulk solvent removed under reduced pressure to yield a black sticky solid. The crude was eluted onto a silica pre-column in DCM/MeOH (95:5). The crude eluted as the first major red band. The fractions were collected and bulk solvent removed under reduced pressure to yield a semi-crude purple solid. The semi-crude solid was eluted onto a silica chromatography column in DCM/MeOH (94.5:4.5). The product eluted as the fifth major red band. The fractions were collected and bulk solvent was removed under reduced pressure. The solid was dissolved in a minimum of DCM and precipitated over MeOH and filtered under reduced pressure to give a purple powder (677 mg, 1.00 mmol, 4.5% yield).

R_F : 0.40 (silica, 95.5:4.5, DCM/MeOH). 1H -NMR (400 MHz, $CDCl_3$): δ -3.01 (s, 2H, N-H), 4.12 (s, 3H, Ar-COOCH₃), 8.15 (d, J =5.80 Hz, 6H, *o*-Ar), 8.29 (d, J =8.1 Hz, 2H, *o*-Ar), 8.46 (d, J =8.1 Hz, 2H, *p*-Ar), 8.84 (d, J =6.8 Hz, 8H, β -H), 9.05 (d, J =5.6 Hz, 6H, *p*-Ar). ^{13}C -NMR (100 MHz, $CDCl_3$): δ 52.63 (COOCH₃), 117.74, 120.19, 128.17, 129.43, 130.06, 134.61, 146.33, 148.52, 149.94, 167.26. MS: (MALDI) m/z M^+ 676.2, $[M+H]^+$ 676.2, HRMS: calcd. For $C_{43}H_{29}N_7O_2$: 675.2380 found 675.2377. UV-Vis (DCM): λ_{max} 418, 517, 552, 594, 649. $\log \epsilon$ (418) = 5.17.

5-[4-Carboxyphenyl]-10,15,20-tri-(4-pyridyl) porphyrin (72)²⁸⁴

To a solution of 5-[4-carboxymethoxyphenyl]-10,15,20-tri-(4-pyridyl) porphyrin (600 mg, 0.887 mmol) in THF/MeOH (9:1) was added potassium hydroxide (5.00 g, 89.12 mmol) and the reaction heated to 80 °C overnight. The solution was allowed to cool to room temperature and bulk solvent removed under reduced pressure to give a slurry. The slurry was neutralised with dilute HCl (aq) to cause precipitation and the precipitate filtered under reduced pressure and dried overnight at 60 °C to yield a lustrous purple powder (550 mg, 0.860 mmol, 98% yield).

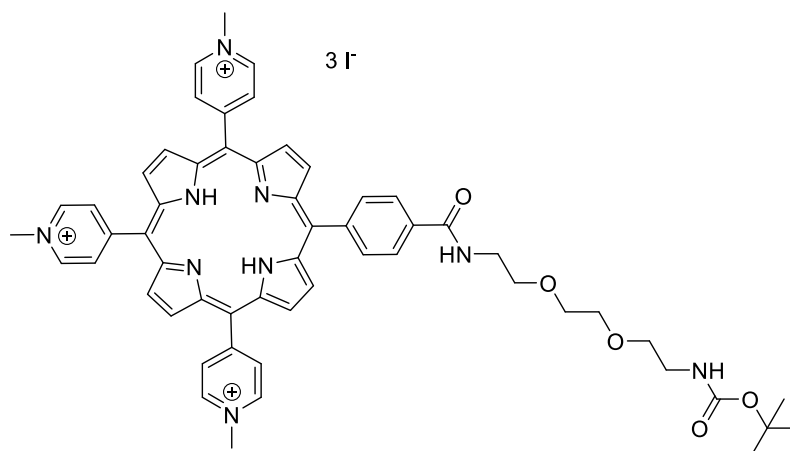
R_F : 0.05 (silica, 95.5:4.5, DCM/MeOH). $^1\text{H-NMR}$ (400 MHz, CDCl_3): δ -2.98 (s, 2H, N-H), 8.15 (d, $J=5.80$ Hz, 6H, o-Ar), 8.29 (d, $J=8.1$ Hz, 2H, o-Ar), 8.46 (d, $J=8.1$ Hz, 2H, p-Ar), 8.84 (d, $J=6.8$ Hz, 8H, β -H), 9.05 (d, $J=5.6$ Hz, 6H, p-Ar). $^{13}\text{C-NMR}$ (100 MHz, CDCl_3): δ 52.63 (COOCH_3), 117.74, 120.19, 128.17, 129.43, 130.06, 134.61, 146.33, 148.52, 149.94, 167.26. MS: (MALDI) m/z $[M+H]^+$ 662.2, HRMS: calcd. For $\text{C}_{42}\text{H}_{27}\text{N}_7\text{O}_2$: 661.2233 found 661.2221. UV-Vis (MeOH): λ_{max} 415, 510, 544]5, 590, 645. $\log \epsilon$ (415) = 5.38.

5-[4-(2-(2-(2-(2-Boc-aminoethoxy)ethoxy)ethoxy)ethaneaminocarbonyl)phenyl]-10,15,20-tris-(4-pyridyl)porphyrin (73)²⁸⁴

Under an inert atmosphere, to a solution of 5-[4-carboxyphenyl]-10,15,20-tri-(4-pyridyl) porphyrin (500.0 mg, 0.775 mmol) in DMF (20 mL) was added tert-butyl (2-(2-(2-aminoethoxy)ethoxy)ethyl)carbamate (280 mg, 1.133 mmol) and TBTU (600.0 mg, 1.133 mmol) and DIPEA (1 mL, 0.742 g, 5.74 mmol). The reaction was stirred at 80 °C overnight. Bulk solvent was removed under reduced pressure. The crude was taken in DCM and washed with copious amounts of water. The organic layer was separated and dried with anhydrous MgSO₄. The semi-crude was dissolved in a minimum of DCM and eluted onto a silica chromatography column. The product eluted in DCM/MeOH (93:7) as the first major red band. The fractions were collected and bulk solvent removed under reduced pressure. The solids were dissolved in a minimum of MeOH and precipitated over Et₂O to yield a deep purple crystalline powder (555.7 mg, 623.0 mmol, 82% yield).

R_F: 0.50 (silica, 9:1, DCM/MeOH). ¹H-NMR (400 MHz, CDCl₃): δ -2.92 (s, 2H, N-H), 1.24 (s, 9H, NH-CO-O-C(CH₃)₃), 3.73 (m, 12H, CH₂-CH₂), 8.16 (dd, J=4.4 Hz, 10H, o-Py, overlapping 4H, β-H), 8.85 (d, 4H, o-Ar, m-Ar), 9.05 (dd, J=4.4 Hz, 10H, o-Py, overlapping 4H, β-H). ¹³C-NMR (100 MHz, CDCl₃): δ 12.44, 14.23, 17.45, 18.75, 22.79, 28.46, 29.80, 40.41, 43.21, 45.31, 55.12, 70.37, 70.62, 110.30, 117.45, 118.54, 118.93, 124.45, 124.49, 125.72, 126.70, 126.88, 128.45, 129.66, 134.42, 134.70, 142.90, 147.90, 150.95 (NH-O-C(CH₃)₃), 156.08 (C=O). MS: (MALDI) *m/z* M⁺ 891.4 HRMS: *calcd.* For C₅₃H₄₉N₉O₅: 891.3868 *found* 891.3851. UV-Vis (DCM): λ_{max} 418, 516, 550, 590, 651. log ε (410) = 5.26.

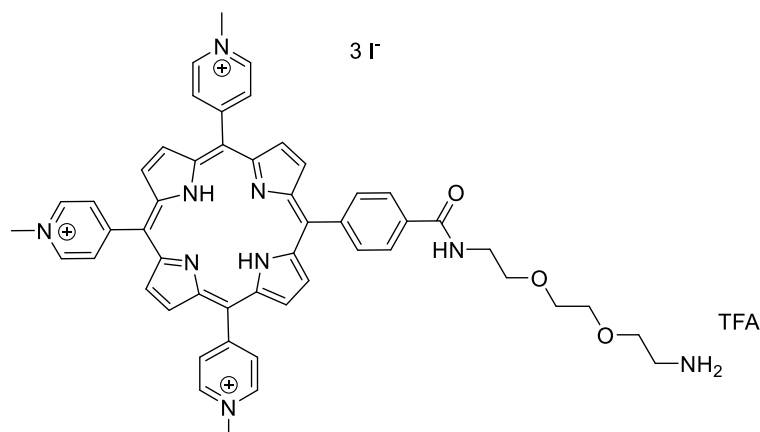
5-[4-(2-(2-(2-Boc-aminoethoxy)ethoxy)ethaneaminocarbonyl)phenyl)-10,15,20-tris-(N-methyl-4-pyridinium)porphyrin triiodide (74)²⁸⁴



Under an inert atmosphere, **73** (200 mg, 0.224 mmol) was dissolved in DMF (80 mL) and the flask fitted with a triethylamine trap bubbler. Methyl iodide (1 mL, 2.16 g, 16.0 mmol) was added dropwise and the reaction stirred at 40 °C overnight. Excess diethyl ether (200 mL) as added to the flask and the precipitate filtered off under gravity through a plug of cotton wool. The crude precipitate was dissolved in methanol and precipitated from diethyl ether (100 mL). The product was filtered under reduced pressure to give a burgundy solid which was washed copiously with diethyl ether. The powder was dissolved in a minimum of methanol and precipitated over diethyl ether to give lustrous purple crystals (250 mg, 0.190 mmol, 84% yield).

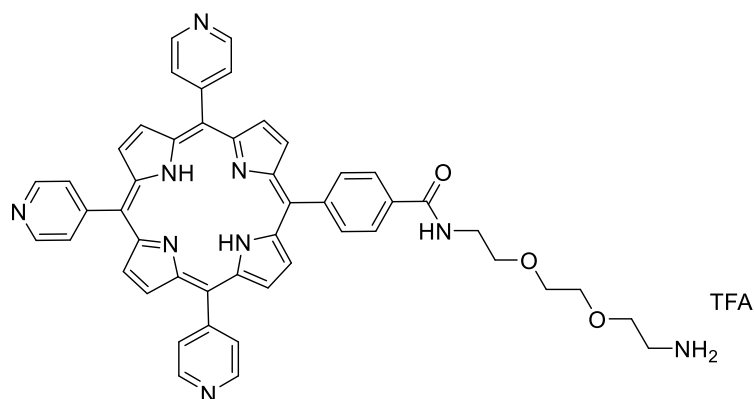
R_F: 0.37 (silica, 8:1:1, acetonitrile/water/*KNO*_{3(aq)}). *R_t*: 9.75 mins (C-18 silica, solvent method 3). ¹H-NMR (400 MHz, DMSO-*d*₆): δ -3.08 (s, 2H, N-H), 1.32 (s, 9H, NH-CO-O-C(CH₃)₃), 3.14 (m, 4H, O-CH₂-CH₂-O), 4.60 (m, 9H, Py-CH₃), 6.90 (s, 1H, NH-CO), 7.91 (d, 2H, *o*-Ar), 8.31 (d, 2H, *m*-Ar), 8.97 (d, 6H, *o*-Py), 9.14 (m, 8H, β-H), 9.44 (d, 6H, *m*-Py). ¹³C-NMR (100 MHz, DMSO-*d*₆): δ 15.00, 23.84, 30.29, 79.72, 80.14, 91.49, 92.21, 125.54, 126.95, 128.65, 130.84, 135.39, 136.18, 137.15, 144.64, 163.56, 164.01, 166.68, 168.68 (C=O), 173.99 (C=O). MS: (ESI+) *m/z* [M-3I]³⁺ 312.1507 HRMS: *calcd.* For C₅₆H₅₈N₉O₅: 312.1507 *found* 312.1515. UV-Vis (MeOH): λ_{max} 426, 519, 560, 595, 650. log ε (426) = 5.16.

5-[4-(2-(2-(2-Aminoethoxy)ethoxy)ethaneaminocarbonyl)phenyl]-10,15,20-tris-(N-methyl-4-pyridinium)porphyrin triiodide (75)²⁸⁴



74 (200 mg, 0.152 mmol) was dissolved in DCM/TFA (10 mL, 1:1) and stirred for 3 hr. Bulk solvent was removed under reduced pressure and the product precipitated from a minimum of methanol over diethyl ether to yield a deep purple crystalline powder (182 mg, 0.127 mmol, 81%).

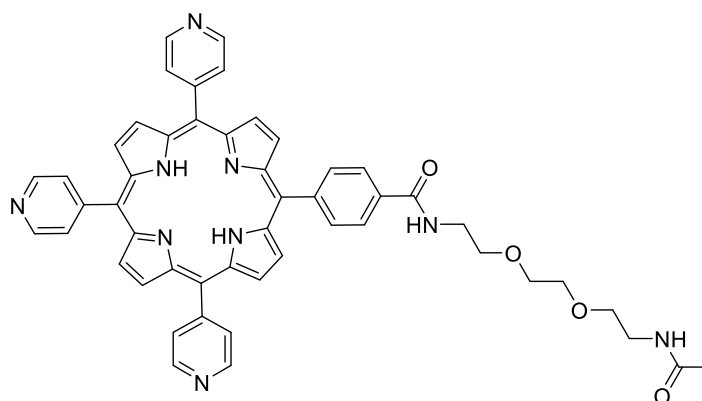
R_F: 0.16 (silica, 8:1:1, acetonitrile/water/ $\text{KNO}_3(\text{aq})$). *R_t*: 11.0 mins (C-18 silica, solvent method 3). ¹H-NMR (400 MHz, $\text{DMSO-}d_6$): δ -3.06 (s, 2H, N-H), 3.00 (t, 2H, $\text{CH}_2\text{-CH}_2$), 3.63 (m, 10H, $\text{CH}_2\text{-CH}_2$), 4.69 (s, 9H, Py- CH_3), 7.87 (d, 3H, NH_3), 8.31 (d, 4H, o-Ar, m-Ar), 8.99 (d, 6H, o-Py, overlapping 8H, $\beta\text{-H}$), 9.44 (d, 6H, m-Py). ¹³C-NMR (100 MHz, $\text{DMSO-}d_6$): δ 39.18, 48.40, 67.29, 69.55, 70.04, 70.30, 115.28, 115.92, 116.42, 119.40, 122.38, 126.43, 126.61, 132.66, 134.74, 143.61, 144.74, 157.05, 158.14, 158.44, 166.68 (C=O). MS: (ESI+) *m/z* [*M-3I*] 278.8001 HRMS: calcd. For $\text{C}_{51}\text{H}_{50}\text{N}_9\text{O}_3$: 278.8007 found 278.8001. UV-Vis (MeOH): λ_{max} 426, 518, 555, 595, 650. $\log \epsilon$ (426) = 5.29

5-[4-(2-(2-(2-Aminoethoxy)ethoxy)ethaneaminocarbonyl)phenyl]-10,15,20-tris-(4-pyridyl)porphyrin (76)

To a solution of **73** (200.0 mg, 0.220 mmol) in DCM (10 mL) was added TFA (5 mL). The mixture was stirred for 3 hrs at room temperature. Bulk solvent was removed under reduced pressure and the crude dissolved in a minimum of methanol and precipitated over diethyl ether (187 mg, 0.207 mmol, 94% yield).

R_F : 0.37 (silica, 8:2, DCM/MeOH). 1H -NMR (400 MHz, DMSO- d_6): δ -3.08 (s, 2H, N-H), 3.13 (m 2H, CH₂-CH₂), 3.60 (m, 10H, CH₂-CH₂), 7.81 (d, J =8.1 Hz, *o*-Py), 8.28 (m, 4H, *m*-Ar, *o*-Ar), 8.87 (s, 8H, β -H), 9.01 (d, 6H, *m*-Py). ^{13}C -NMR (100 MHz, DMSO- d_6): δ 57.08, 69.52, 70.13, 70.24, 117.93, 118.18, 126.44, 129.69, 134.59, 134.68, 143.11, 148.88, 149.34, 169.01(C=O). MS: (ASAP) m/z [M+H]⁺ 792.3, HRMS: calcd. For C₄₈H₄₂N₉O₃: 792.3411 found 792.3403. UV-Vis (MeOH): λ_{max} 415, 511, 548, 591, 647. $\log \epsilon$ (415) = 5.35

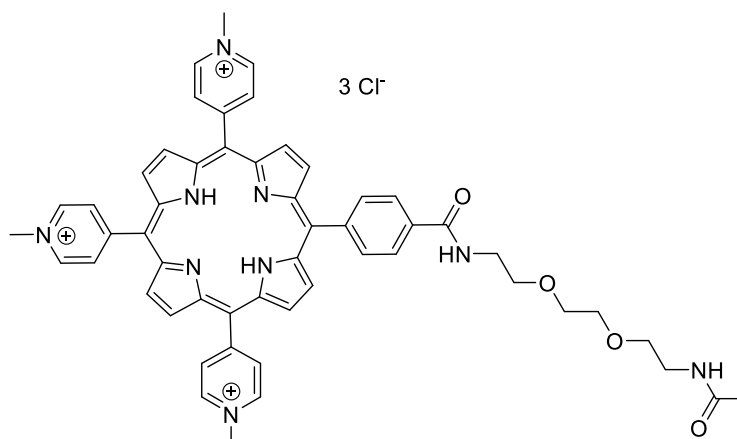
5-[4-(2-(2-(2-Acetimideethoxy)ethoxy)ethaneaminocarbonyl)phenyl]-10,15,20-tris-(4-pyridyl)porphyrin (77)



To a solution of **76** (100.0 mg, 0.111 mmol) in DMF (10 mL) was added DIPEA (5 mL, 3.71 g, 28.7 mmol). Acetic anhydride (2 mL, 2.16 g, 21.16 mmol) was added dropwise and the reaction stirred overnight at room temperature. A second aliquot of acetic anhydride (2 mL, 2.16 g, 21.16 mmol) was added and the mixture heated to 70 °C for 4 hr with stirring. Bulk solvent was removed under reduced pressure. The crude was taken in DCM and washed with copious amounts of water. The organic layer was separated and dried with anhydrous MgSO₄. The semi-crude was dissolved in a minimum of DCM and eluted onto a silica chromatography column. The product eluted in DCM/MeOH (93:7) as the first major red band. The fractions were collected and bulk solvent removed under reduced pressure. The solids were dissolved in a minimum of DCM and precipitated over hexane to yield a deep purple crystalline powder (66.6 mg, 0.080 mmol, 72% yield).

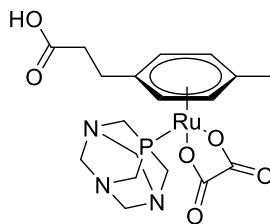
R_F: 0.87 (silica, 95:5, DCM/MeOH). ¹H-NMR (400 MHz, CDCl₃): δ -2.91 (s, 2H, N-H), 1.96 (m, 12H, CH₂-CH₂), 3.32 (s, 3H, NHCO-CH₃) 7.86 (d, J=7.8 Hz, 2H, o-Ar), 8.16 (d, J=5.5 Hz, 6H, o-Ar), 8.25 (d, J=7.9 Hz, 2H, p-Ar), 8.86 (d, J=5.80 Hz, 6H, p-Ar), 9.05 (d, J=4.6 Hz, 8H, β-H). ¹³C-NMR (100 MHz, CDCl₃): δ 14.23, 22.79, 29.46 (NHCO-CH₃), 32.02, 35.72, 40.08, 117.39, 117.65, 120.56, 125.87, 129.46, 134.51, 136.14, 142.94, 148.46, 150.03, 171.51 (C=O), 171.57 (C=O). UV-Vis (DCM): λ_{max} 425, 518, 561, 595, 650. log ε (425) = 5.10.

5-[4-(2-(2-(2-Acetimideethoxy)ethoxy)ethaneaminocarbonyl)phenyl]-10,15,20-tris-(N-methyl-4-pyridinium)porphyrin trichloride (78)

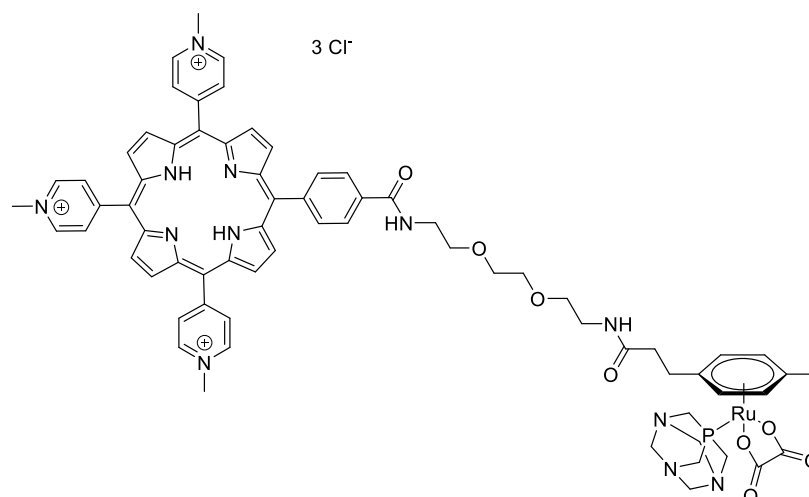


77 (50 mg, 0.060 mmol) was dissolved in DMF (80 mL) and the flask fitted with a triethylamine trap bubbler. Methyl iodide (1 mL, 2.16 g, 16.0 mmol) was added dropwise and the reaction stirred at 40 °C overnight. Excess diethyl ether (100 mL) as added to the flask and the precipitate filtered off under gravity through a plug of cotton wool. The crude precipitate was dissolved in methanol and precipitated from diethyl ether (100 mL). The product was filtered under reduced pressure to give a burgundy solid which was washed copiously with diethyl ether to yield the product as a deep purple crystalline solid (55.5 mg, 0.0564 mmol, 94% yield).

R_F : 0.34 (silica, 8:1:1, acetonitrile/water/ $KNO_3(aq)$). R_t : 10.10 mins (C-18 silica, solvent method 3). 1H -NMR (400 MHz, $DMSO-d_6$): δ -3.08 (s, 2H, N-H), 2.91 (m, 12H, CH_2-CH_2), 3.32 (s, 3H, $NHCO-CH_3$ overlapping with HOD), 4.69 (s, 9H, Py- CH_3), 7.87 (d, $J=7.7$ Hz, 2H, o -Ar), 8.25 (d, $J=7.8$ Hz, 2H, p -Ar), 9.02 (d, 6H, o -Py 6H, overlapping 8H, β -H), 9.48 (d, 6H, m -Py). ^{13}C -NMR (100 MHz, $DMSO-d_6$): δ 36.32 ($NHCO-CH_3$), 48.35 (Py- CH_3), 115.24, 115.93, 122.56, 126.42, 132.66, 134.61, 137.03, 141.71, 144.74, 157.02 ($C=O$), 170.48 ($C=O$). MS: (ESI+) m/z $M+244.4462$ HRMS: calcd. For $C_{47}H_{41}N_8O_1$: 244.4462 found 244.4456. UV-Vis (H_2O): λ_{max} 423, 521, 562, 588, 645. $\log \epsilon$ (410) = 5.21.

[Ru(η^6 -arene)(C₂O₄)PTA] (79)

The RAPTA complex (**79**) was generously provided by Dr Ben Murray (University of Hull) synthesised according to the method of Murray *et al.*

Conjugate (80)

75 (49 mg, 0.096 mmol) and TBTU (31 mg, 0.097 mmol) were suspended in DMSO (1 ml) followed by the addition of DIPEA (49 μ l, 0.286 mmol). The mixture was stirred for 5 min followed by the addition of **75** (40 mg, 0.032 mmol). The dark coloured mixture was stirred for 3 hr whilst protected from light then diluted with acetone (12 ml) and left to stand for 13 hr at 4 °C, the precipitate was collected by centrifugation. The collected solid residue was suspended in acetone (10 ml) and the solids collected by centrifugation. The combined solids were dried under reduced pressure then dissolved in H₂O (0.5 ml) followed by the addition of a solution of NH₄PF₆ (31 mg, 0.190 mmol) in H₂O (0.5 ml) to yield a precipitate that was collected by centrifugation. The solids were taken in H₂O (3 ml) then collected by centrifugation. The collected solid was dried under reduced pressure then dissolved in acetone (2.5 ml) followed by the addition of a solution of tetrabutylammonium chloride (93 mg, 0.335 mmol) in acetone (0.5 ml). The precipitate was collected by centrifugation then the collected solid dispersed in acetone (1 ml) and collected by centrifugation. The solid was suspended in acetone:H₂O (9:1, 10 ml) and the insoluble material collected by centrifugation. The collected solid was then dissolved in H₂O (1 ml) followed by the addition of acetone (9 ml), the mixture was vigorously shaken then allowed to stand for 30 min, followed by centrifugation to collect the solid. This process was repeated followed by washing of the collected solid in acetone (3 x 10 ml) and collection by centrifugation. The solid was dissolved in H₂O (1 ml) then lyophilized to yield a purple solid (8 mg, 5.51 μ mol, 17% yield).

R_F : 0.32 (silica, 8:1:1, acetonitrile/water/KNO_{3(aq)}). ¹H-NMR (400 MHz, DMSO-*d*₆): δ 1.84 (s, 3H, Ar-CH₃), 3.56 (m, 12H, O-CH₂-CH₂-O), 4.68 (m, 10H, phosphaadamantane), 5.76 (s, 1H, CONH), 5.87 (s, 1H, CONH), 8.30 (m, 4H, *o*-,*m*-Ar), 8.96 (m, 12H, β -H, overlapping *o*-,*m*-Ar), 9.07 (m, 6H, *o*-Py), 9.44 (m, 6H, *m*-Py). ¹³C-NMR (100 MHz, DMSO-*d*₆): δ 26.75, 34.36, 38.90, 39.66, 47.79, 47.93, 48.38, 68.55, 69.42, 70.06, 85.11, 86.72, 114.60, 114.85, 121.63, 125.38, 132.86, 143.86, 157.15, 164.44, 169.80 (C=O), 173.02 (C=O). ³¹P-NMR (162 MHz, D₂O): δ -33.67 (s, phoshaadamantane). MS: (ESI+) *m/z* [*M* (Ru-ligand)]³⁺ 327.4910, HRMS: calcd. For C₆₁H₆₀N₄O₉: 327.4910 found 327.4917. UV-Vis (H₂O): λ_{max} 426, 525, 565, 595, 650. log ϵ (426) = 5.12. Fluorescence: (H₂O): λ_{max} (exc/exm) 425/661 nm.

Chapter 7
References

7.0 References

- 1 T. Burki, *Lancet. Oncol.*, 2015, **16**, 108.
- 2 J. Mayles, P. Nahum, A. Rosenwald, *Handbook of Radiotherapy Physics*, CRP Press, New York, 2nd edn., 2007.
- 3 G. Hewitt, D. Jurk, F. D. M. Marques, C. Correia-melo, T. Hardy, A. Gackowska, R. Anderson, M. Taschuk, J. Mann and J. F. Passos, *Nat. Commun.*, 2012, **3**, 1–9.
- 4 B. Bukowska, A. Gajek and A. Marczak, *Wspolczesna Onkol.*, 2015, **19**, 350–353.
- 5 I. Koturbash, M. Merrifield and O. Kovalchuk, *Int. J. Radiat. Biol.*, 2017, **93**, 148–155.
- 6 X. Zhu, W. Han, W. Xue, Y. Zou, C. Xie, J. Du and G. Jin, *Sci. Rep.*, 2016, **6**, 1–10.
- 7 A. Bernal and L. Tusell, *Int. J. Mol. Sci.*, 2018, **19**, 1–21.
- 8 M. Krause, A. Dubrovskaya, A. Linge and M. Baumann, *Adv. Drug Deliv. Rev.*, 2017, **109**, 63–73.
- 9 N. Nishida, H. Yano, T. Nishida, T. Kamura and M. Kojiro, *Vasc. Health Risk Manag.*, 2006, **2**, 213–219.
- 10 M. Rajabi and S. A. Mousa, *Biomedicines*, 2017, **5**, 1–12.
- 11 T. Tonini, F. Rossi and P. P. Claudio, *Oncogene*, 2003, **22**, 6549–6556.
- 12 H. Maeda, *J. Control. Release*, 2012, **164**, 138–144.
- 13 H. Maeda, H. Nakamura and J. Fang, *Adv. Drug Deliv. Rev.*, 2013, **65**, 71–79.
- 14 J. W. Kim and C. V. Dang, *Cancer Res.*, 2006, **66**, 8927–8930.
- 15 O. Warburg, *Science.*, 1956, **123**, 309–314.
- 16 J. I. E. Zheng, *Oncol. Lett.*, 2012, **4**, 1151–1157.
- 17 J. H. Lee, H. Ji and Z. Lu, *Cell Cycle*, 2016, **15**, 1391–1392.
- 18 D. Lafont, Y. Zorlu, H. Savoie, F. Albrieux, V. Ahsen, R. W. Boyle and F. Dumoulin, *Photodiagnosis Photodyn. Ther.*, 2013, **10**, 252–259.
- 19 F. Giuntini, F. Bryden, R. Daly, E. M. Scanlan and R. W. Boyle, *Org. Biomol. Chem.*, 2014, **12**, 1203–1206.
- 20 C. Wigerup, S. Pählman and D. Bexell, *Pharmacol. Ther.*, 2016, **164**, 152–169.
- 21 S. Kakkad, B. Krishnamachary, D. Jacob, J. Pacheco-Torres, E. Goggins, S. K. Bharti, M. F. Penet and Z. M. Bhujwala, *Cancer Metastasis Rev.*, 2019, **38**, 51–64.
- 22 K. Graham and E. Unger, *Int. J. Nanomedicine*, 2018, **13**, 6049–6058.
- 23 M. R. Horsman and J. Overgaard, *J. Radiat. Res.*, 2016, **57**, i90–i98.
- 24 J. Zhou, T. Schmid, S. Schnitzer and B. Brüne, *Cancer Lett.*, 2006, **237**, 10–21.
- 25 W. R. Wilson and M. P. Hay, *Nat Rev Cancer*, 2011, **11**, 393–410.
- 26 C. A. Robertson, D. H. Evans and H. Abrahamse, *J. Photochem. Photobiol. B Biol.*, 2009, **96**, 1–8.
- 27 J. P. . Knisely and S. Rockwell, *Neuroimaging Clin. N. Am.*, 2002, **12**, 525–536.
- 28 S. Antoun, D. Atallah, R. Tahtouh, N. Alaeddine, M. Moubarak, A. Khaddage, E. N. Ayoub, G. Chahine and G. Hilal, *Cancer Cell Int.*, 2018, **18**, 1–10.
- 29 A. Aviv, J. J. Anderson and J. W. Shay, *Trends in Cancer*, 2017, **3**, 253–258.
- 30 N. R. Rodrigues, A. Rowan, M. E. F. Smith, I. A. N. B. Kerr, W. F. Bodmer, J. V Gannon and D. P. Lane, *Proc Natl Acad Sci USA*, 1990, **87**, 7555–7559.
- 31 S. Niazi, M. Purohit and J. H. Niazi, *Eur. J. Med. Chem.*, 2018, **158**, 7–24.
- 32 A. Mandinova and S. W. Lee, *Sci. Transl. Med.*, 2011, **3**, 1–13.
- 33 T. Ozaki and A. Nakagawara, *Cancers.*, 2011, **3**, 994–1013.
- 34 A. C. Joerger and A. R. Fersht, *Annu. Rev. Biochem.*, 2016, **85**, 375–404.
- 35 J. U. Yinghua, X. U. Taojun, H. Zhang and Y. U. Aiming, *Int. J. Oncol.*, 2014, **44**, 1284–1292.
- 36 M. J. Pfaff, S. Mukhopadhyay and M. Hoofnagle, *J. Vasc. Surg.*, 2018, **68**, 1–13.
- 37 M. Cordani, G. Butera, R. Pacchiana and M. Don, *Biochim Biophys Acta Rev Cancer*, 2017, **1867**, 19–28.
- 38 K. Suzuki and H. Matsubara, *J. Biomed. Biotechnol.*, 2011, **2011**, 1–7.
- 39 R. S. DiPaola, *Clin. Cancer Res.*, 2002, **8**, 3311–3314.
- 40 Y. Altundal, G. Cifter, A. Detappe, E. Sajo, P. Tsiamas, P. Zygmanski, R. Berbeco, R. A. Cormack, M. Makrigiorgos and W. Ngwa, *Phys. Medica*, 2015, **31**, 25–30.

- 41 H. A. Gay, M. G. Sanda, J. Liu, N. Wu, D. A. Hamstra, J. T. Wei, R. L. Dunn, E. A. Klein, H. M. Sandler, C. S. Saigal, M. S. Litwin, D. A. Kuban, L. Hembroff, M. M. Regan and P. Chang, *Radiat. Oncol. Biol.*, 2017, **98**, 304–317.
- 42 H. Tatsuzaki, M. M. Urie and G. Willett, *Int. J. Radiat. Oncol. Biol. Phys.*, 1991, **22**, 369–374.
- 43 I. Baccarelli, I. Bald, F. A. Gianturco, E. Illenberger and J. Kopyra, *Phys. Rep.*, 2011, **508**, 1–44.
- 44 M. Scholz, *Nucl. Instruments Methods Phys. Res. Sect. B Beam Interact. with Mater. Atoms*, 2000, **161**, 76–82.
- 45 D. Tan and B. Heaton, *Appl. Radiat. Isot.*, 1994, **45**, 1101–1111.
- 46 M. Niemantsverdriet, M. Van Goethem, R. Bron, W. Hogewerf, S. Brandenburg, J. A. Langendijk, P. Van Luijk, and R. P. Coppes, *Radiat. Oncol. Biol.*, 2012, **83**, 1291–1297.
- 47 T. G. Sazykina and A. I. Kryshev, *J. Environ. Radioact.*, 2016, **165**, 227–242.
- 48 N. Zhao, R. Yang, J. Wang, X. Zhang and J. Li, *Biomed Res Int.*, 2015, **2015**, 1–7.
- 49 M. R. Horsman, L. S. Mortensen, J. B. Petersen, M. Busk and J. Overgaard, *Nat. Rev. Clin. Oncol.*, 2012, **9**, 674–687.
- 50 M. Teoh, C. H. Clark, K. Wood, S. Whitaker and A. Nisbet, *Br J Radiol.*, 2011, **84**, 967–996.
- 51 G. Boily, É. Filion, G. Rakovich, N. Kopek, L. Tremblay, B. Samson, S. Goulet and I. Roy, *J. Thorac. Oncol.*, 2015, **10**, 872–882.
- 52 B. Bucci, S. Misiti, A. Cannizzaro, R. Marchese, G. H. Raza, R. Miceli, A. Stigliano, D. Amendola, O. Monti, M. Biancolella, F. Amati, G. Novelli, A. Vecchione, E. Brunetti and U. De Paula, *Anticancer Res.*, 2006, **26**, 4549–4557.
- 53 I. Koturbash, N. M. Jadavji, K. Kutanzi, R. Rodriguez-Juarez, D. Kogosov, G. A. S. Metz and O. Kovalchuk, *Environ. Epigenetics*, 2016, **2**, 1–13.
- 54 T. S. Lawrence, D. Ph, M. A. Davis, D. Ph, J. Maybaum, D. Ph, P. L. Stetson and D. Ph, *Int. J. Oncol.*, 1990, **18**, 1393–1398.
- 55 P. P. Connell and S. Hellman, *Cancer Res.*, 2009, **69**, 383–392.
- 56 J. Yarnold, *Radiother. Oncol.*, 1997, **44**, 1–7.
- 57 A. T. Gordon and T. J. McMillan, *Clin. Oncol.*, 1997, **9**, 70–78.
- 58 R. G. Bristow and R. P. Hill, *Nat. Rev. Cancer*, 2008, **8**, 180–192.
- 59 H. Ali and J. E. van Lier, *Chem. Rev.*, 1999, **99**, 2379–2450.
- 60 T. Helleday, E. Petermann, C. Lundin, B. Hodgson and R. A. Sharma, *Nat Rev Cancer*, 2008, **8**, 193–204.
- 61 W. Han and K. N. Yu, *Adv. Genet. Res.*, 2010, **4**, 1–13.
- 62 E. Ito, PhD Thesis, University of Toronto, 2010.
- 63 L. B. Harrison, M. Chadha, R. J. Hill, K. Hu and D. Shasha, *Oncologist*, 2002, **7**, 492–508.
- 64 S. Rockwell, I. T. Dobrucki, E. Y. Kim, S. T. Marrison and V. T. Vu, *Curr Mol Med*, 2010, **9**, 442–458.
- 65 M. Koritzinsky and B. G. Wouters, *Semin. Radiat. Oncol.*, 2013, **23**, 252–261.
- 66 A. M. Shannon, D. J. Bouchier-Hayes, C. M. Condron and D. Toomey, *Cancer Treat. Rev.*, 2003, **29**, 297–307.
- 67 J. D. J. F Fowler, G. E Adams, *Cancer Treat. Rev.*, 1976, **3**, 227–256.
- 68 M. De Ridder, D. Verellen, V. Verovski and G. Storme, *Nitric Oxide*, 2008, **19**, 164–169.
- 69 H. Maeda, *Adv. Enzyme Regul.*, 2001, **41**, 189–207.
- 70 H. Maeda, T. Sawa and T. Konno, *J. Control. Release*, 2001, **74**, 47–61.
- 71 J. Fang, H. Nakamura and H. Maeda, *Adv. Drug Deliv. Rev.*, 2011, **63**, 136–151.
- 72 J. M. Brown, *Mol. Med. Today*, 2000, **6**, 157–62.
- 73 R. P. Hill, R. G. Bristow, A. Fyles, M. Koritzinsky, M. Milosevic and B. G. Wouters, *Semin. Radiat. Oncol.*, 2015, **25**, 260–272.
- 74 M. Schaffer, B. Ertl-Wagner, P. M. Schaffer, U. Kulka, G. Jori, E. Dühmke and a Hofstetter, *Curr. Med. Chem.*, 2005, **12**, 1209–1215.
- 75 J. A. O'Hara, E. B. Douple, M. J. Abrams, D. J. Picker, C. M. Giandomenico and J. F. Vollano, *Int. J. Radiat. Oncol.*, 1989, **16**, 1049–1052.

- 76 U. Kulka, M. Schaffer, A. Siefert, P. M. Schaffer, A. Ölsner, K. Kasseb, A. Hofstetter, E. Dühmke and G. Jori, *Biochem. Biophys. Res. Commun.*, 2003, **311**, 98–103.
- 77 G. Wilson, S. Bentzen and P. Harari, *Semin. Radiat. Oncol.*, 2006, **16**, 2–9.
- 78 T. Y. Seiwert, J. K. Salama and E. E. Vokes, *Nat. Clin. Pract. Oncol.*, 2007, **4**, 86–100.
- 79 P. Wardman, *Clin. Oncol.*, 2007, **19**, 397–417.
- 80 B. Bigdeli, B. Goliaei, N. Masoudi-khoram, N. Jooyan and A. Nikoofar, *Toxicol. Appl. Pharmacol.*, 2016, **313**, 180–194.
- 81 I. Cristina, F. Primitivo, R. Bordin, F. Carla, F. Barbisan, V. Farina, C. Ferreira, T. Baumhardt, I. Beatrice, M. Maria, M. Frescura and L. De Freitas, *Chem. Biol. Interact.*, 2018, **282**, 85–92.
- 82 S. Huerta, X. Gao, E. H. Livingston and P. Kapur, *Surgery*, **148**, 346–353.
- 83 M. J. Rybak-smith and H. E. Townley, *Encycl. Nanotechnol.*, 2015, 1–12.
- 84 L. S. Kappen, T. R. Lee and I. H. Goldberg, *Biochemistry*, 1989, **28**, 4540–4542.
- 85 P. Xue, S. Liu, L. Zhang, Q. Guan and J. Zhu, *Colloid Interface Sci. Commun.*, 2018, **23**, 45–51.
- 86 A. C. Begg, F. a. Stewart and C. Vens, *Nat. Rev. Cancer*, 2011, **11**, 239–253.
- 87 T. C. Ramalho, R. B. De Alencastro, M. A. La-Scalea and J. D. Figueroa-Villar, *Biophys. Chem.*, 2004, **110**, 267–279.
- 88 P. W. and M. E. W. G. E. Adams, I. R. Flockhart, C. E. Smithen, I. J. Stratford, 1976, **67**, 9–20.
- 89 W. W. L. J. M. Brown, N. Y. Yu, D. M. Brown, *Int. J. Radiat. Oncol. Biol.*, 1981, **7**, 695–703.
- 90 B. T. Oronsky, S. J. Knox and J. Scicinski, *Transl. Oncol.*, 2011, **4**, 189–198.
- 91 M. Gál, M. Hromadová, L. Pospí, J. Híve, R. Sokolová, V. Kolivo and J. Bulí, *Bioelectrochemistry*, 2010, **78**, 118–123.
- 92 M. Bonnet, C. R. Hong, W. W. Wong, L. P. Liew, A. Shome, J. Wang, Y. Gu, R. J. Stevenson, W. Qi, R. F. Anderson, F. B. Pruijn, W. R. Wilson, S. M. F. Jamieson, K. O. Hicks and M. P. Hay, *J. Med. Chem.*, 2018, **61**, 1241–1254.
- 93 I. Ahmed, T. C. Jenkins, J. M. Walling, I. J. Stratford, P. W. Shedon, G. E. Adams and E. M. Fielden, *Int. J. Radiat. Oncol. Biol. Phys.*, 1986, **12**, 1079–1081.
- 94 M. A. Hassam Metwally, K. Diemer Frederkisen and J. Overgaard, *Acta Oncol.*, 2014, **53**, 654–661.
- 95 B. Pauwels, A. E. C. Korst, G. G. O. Pattyn, H. A. J. Lambrechts, D. R. Van Bockstaele, K. Vermeulen, M. Lenjou, C. M. J. De Pooter, J. B. Vermorken and F. Lardon, *Int. J. Radiat. Oncol. Biol. Phys.*, 2003, **57**, 1075–1083.
- 96 B. R. James, G. G. Meng, J. J. Posakony, J. a Ravensbergen, C. J. Ware and K. a Skov, *Met. Based. Drugs*, 1996, **3**, 85–89.
- 97 J. M. Khreis, S. Pandeti, L. Feketeová and S. Denifl, *Int. J. Mass Spectrom.*, 2018, **431**, 1–7.
- 98 L. B. Josefsen and R. W. Boyle, *Br. J. Pharmacol.*, 2008, **154**, 1–3.
- 99 E. S. Nyman and P. H. Hynninen, *J. Photochem. Photobiol. B Biol.*, 2004, **73**, 1–28.
- 100 X. Huang, K. Nakanishi and N. Berova, *Chirality*, 2000, **12**, 237–255.
- 101 G. Meng, University of British Columbia, 1993.
- 102 K. M. Kadish, F. D'Souza, A. Villard, M. Autret, E. Van Caemelbecke, P. Bianco, A. Antonini and P. Tagliatesta, *Inorg. Chem.*, 1994, **33**, 5169–5170.
- 103 L. C. Gong and D. Dolphin, *Can. J. Chem.*, 1985, **63**, 401–405.
- 104 J. A. Hodge, M. G. Hill and H. B. Gray, *Inorg. Chem*, 1995, **125**, 809–812.
- 105 J. A. S. L. D. Sparks, C. J. Medforth, M. S. Park, J. R. Chamberlain, M. R. Ondrias, M. O. Senge, K. M. Smith, *J. Am. Chem. Soc.*, 1993, **115**, 581–592.
- 106 K. M. Kadish and Æ. E. Van Caemelbecke, 2003, 254–258.
- 107 A. E. K. Jenna Barbee, *Comput Theor Chem*, 2013, **4**, 73–85.
- 108 E. R. Ranyuk, N. Cauchon, H. Ali, R. Lecomte, B. Guérin and J. E. van Lier, *Bioorg. Med. Chem. Lett.*, 2011, **21**, 7470–7473.
- 109 M. Kumar and P. Neta, 1992, 9571–9575.
- 110 D. Meisel and P. Neta, *J. Am. Chem. Soc.*, 1975, **97**, 5198–5203.
- 111 M. B. Gariboldi, R. Ravizza, P. Baranyai, E. Caruso, S. Banfi, S. Meschini and E. Monti,

- Bioorg. Med. Chem.*, 2016, **17**, 2009–2016.
- 112 B. A. Weaver, *Mol. Biol. Cell*, 2014, **25**, 2677–2681.
- 113 M. A. Cahan, K. A. Walter, O. M. Colvin and H. Bremi, *Cancer Chemother Pharmacol*, 1994, **33**, 441–444.
- 114 C. F. Thorn, C. Oshiro, S. Marsh, T. Hernandez-Boussard, H. McLeod, T. E. Klein and R. B. Altman, *Pharmacogenet Genomics*, 2011, **21**, 440–446.
- 115 U. Ndagi, N. Mhlongo and M. E. Soliman, *Drug Des. Devel. Ther.*, 2017, **11**, 599–616.
- 116 R. Oun, Y. E. Moussa and N. J. Wheate, *Dalt. Trans.*, 2018, **47**, 6635–6870.
- 117 D. Corinti, C. Coletti, N. Re, S. Piccirillo, M. Giampà, M. E. Crestoni and S. Fornarini, *RSC Adv.*, 2017, **7**, 15877–15884.
- 118 R. P. Wernyj and P. J. Morin, *Drug Resist. Updat.*, 2004, **7**, 227–232.
- 119 D. W. Shen, L. M. Pouliot, M. D. Hall and M. M. Gottesman, *Pharmacol. Rev.*, 2012, **64**, 706–721.
- 120 V. Venkatesh and P. J. Sadler, *Met. Ions Life Sci.*, 2018, **18**, 69–108.
- 121 C. Scolaro, A. Bergamo, L. Brescacin, R. Delfino and M. Cocchietto, *J. Med. Chem.*, 2005, **48**, 4161–4171.
- 122 B. S. Murray, M. V Babak, C. G. Hartinger and P. J. Dyson, *Coord. Chem. Rev.*, 2016, **306**, 86–114.
- 123 B. S. Murray, L. Menin, R. Scopelliti and P. J. Dyson, *Chem. Sci.*, 2014, **2**, 2536–2545.
- 124 T. J. Prior, H. Savoie, R. W. Boyle and B. S. Murray, *Organometallics*, 2018, **37**, 294–297.
- 125 J. S. Hill, M. D. Daniell, *Aust. N. Z. J. Surg.*, 1991, **61**, 340–348.
- 126 C. C. Byeon, M. M. Mckerns, W. Sun, T. M. Nordlund, C. M. Lawson, G. M. Gray, C. C. Byeon, M. M. Mckerns, W. Sun and G. M. Gray, *Appl. Phys. Lett.*, 2004, **84**, 5174–5176.
- 127 B. I. Kruft and A. Greer, *Photochem. Photobiol. Sci.*, 2012, **87**, 1204–1213.
- 128 H. Ding, H. Yu, Y. Dong, R. Tian, G. Huang, D. A. Boothman, B. D. Sumer and J. Gao, *J Control Release*, 2011, **156**, 276–280.
- 129 P. Hayley, I. Stamati, G. Yahioğlu, M. A. Butt and M. Deonarain, *Antibodies*, 2013, **2**, 270–305.
- 130 C. Spagnul, L. C. Turner and R. W. Boyle, *J. Photochem. Photobiol. B*, 2015, **150**, 11–30.
- 131 L. Zhai and K. Yang, *Dye. Pigment.*, 2015, **120**, 228–238.
- 132 A. Gorman, J. Killoran, C. O’Shea, T. Kenna, W. M. Gallagher and D. F. O’Shea, *J. Am. Chem. Soc.*, 2004, **126**, 10619–10631.
- 133 F. Giuntini, V. M. Chauhan, J. W. Aylott, G. A. Rosser, A. Athanasiadis, A. Beeby, A. J. MacRobert, R. A. Brown and R. W. Boyle, *Photochem. Photobiol. Sci.*, 2013, **13**, 1039–1051.
- 134 A. Tovmasyan, N. Babayan, D. Poghosyan, K. Margaryan, B. Harutyunyan, R. Grigoryan, N. Sarkisyan, I. Spasojevic, S. Mamyán, L. Sahakyan, R. Aroutiounian, R. Ghazaryan and G. Gasparyan, *J. Inorg. Biochem.*, 2014, **140**, 94–103.
- 135 F. Dandash, D. Yannick, C. Fidanzi-dugas, S. Nasri, F. Brégier, R. Granet, W. Karam, M. Diab-assaf, V. Sol and B. Liagre, *J. Inorg. Biochem.*, 2017, **177**, 27–38.
- 136 H. Kuhn, *J. Chem. Phys.*, 1949, **17**, 1198–1212.
- 137 J. Sandland, N. Malatesti and R. Boyle, *Photodiagnosis Photodyn. Ther.*, 2018, **23**, 281–294.
- 138 C. G. Hadjipanayis, G. Widhalm and W. Stummer, *Neurosurgery*, 2016, **77**, 663–673.
- 139 J. E. Blume and A. R. Oseroff, *Dermatol. Clin.*, 2007, **25**, 5–14.
- 140 G. Huber and J. Levy, *Semin. Ophthalmol.*, 2015, **16**, 213–217.
- 141 R. Y. Kim, *Clin. Ophthalmology*, 2010, **4**, 1073–1079.
- 142 P. Cramers, M. Ruevekamp, H. Oppelaar, O. Dalesio, P. Baas and F. A. Stewart, *Br. J. Cancer*, 2003, **88**, 283–290.
- 143 H. Gattuso, A. Monari and M. Marazzi, *RSC Adv.*, 2017, **7**, 10992–10999.
- 144 J. Nanobiotechnol, J. Son, G. Yi, M. H. Kwak, S. M. Yang, J. M. Park, B. I. Lee, M. G. Choi and H. Koo, *J. Nanobiotechnology*, 2019, **17**, 1–12.
- 145 J. Asta, *Photodiagnosis Photodynamic Ther.*, 2009, **6**, 94–96.

- 146 W. W. L. Chin, P. W. S. Heng, P. S. P. Thong, R. Bhuvanewari, W. Hirt, S. Kuenzel, K. C. Soo and M. Olivo, *Eur. J. Pharm. Biopharm.*, 2008, **69**, 1083–1093.
- 147 L. Allott, University of Hull, 2014.
- 148 M. L. Bailey, Dale. W. Townsend, David. E. Valk, Peter. N. Maisey, Ed., *Positron Emission Tomography*, Springer, London, 3rd edn., 2005, vol. 27.
- 149 Z. Li and P. S. Conti, *Adv. Drug Deliv. Rev.*, 2010, **62**, 1031–1051.
- 150 H. J. Wester, U. Keller, M. Schottelius, A. Beer, K. Philipp-abbrederis, F. Hoffmann, J. Šimeček, C. Gerngross, M. Lassmann, K. Herrmann, M. Rudelius, H. Kessler and M. Schwaiger, *Theranostics*, 2015, **5**, 618–630.
- 151 P. A. Waghorn, *J. Label. Compd. Radiopharm.*, 2014, **57**, 304–309.
- 152 B. Wahab, G. Ellames, S. Passey and P. Watts, *Tetrahedron*, 2010, **66**, 3861–3865.
- 153 E. Ranyuk, H. Ali, B. Guérin and J. E. Van Lier, *J. Porphyr. Phthalocyanines*, 2013, **17**, 850–856.
- 154 G. M. Entract, F. Bryden, J. Domarkas, H. Savoie, L. Allott, S. J. Archibald, C. Cawthorne and R. W. Boyle, *Mol. Pharm.*, 2015, **12**, 4414–4423.
- 155 P. Kumar, V. Bacchu and L. I. Wiebe, *Semin. Nucl. Med.*, 2015, **45**, 122–135.
- 156 H. Wang, Y. Zhang, W. Yu, Y. Xue, L. Xiao and H. Xu, *Biomed Reseach Int.*, 2018, **2018**, 1–9.
- 157 L. Hoigebazar, J. M. Jeong, J.-Y. Lee, D. Shetty, B. Y. Yang, Y. Lee, D. S. Lee, J. Chung and M. C. Lee, *J. Med. Chem.*, 2012, **55**, 3155–3162.
- 158 C. Lottner, K. Bart, G. Bernhardt and H. Brunner, *J. Med. Chem.*, 2002, **45**, 2079–2089.
- 159 F. Schmitt, P. Govindaswamy, G. Süß-Fink, H. A. Wee, P. J. Dyson, L. Juillerat-Jeanneret and B. Therrien, *J. Med. Chem.*, 2008, **51**, 1811–1816.
- 160 T. Gianferrara, A. Bergamo, I. Bratsos, B. Milani, C. Spagnul and G. Sava, *J. Med. Chem.*, 2010, **53**, 4678–4690.
- 161 R. W. Boyle, C. K. Johnson and D. Dolphin, *J. Chem. Soc., Chem. Commun.*, 1995, 527–528.
- 162 S. Shanmugathasan, C. K. Johnson, C. Edwards, E. K. Matthews, D. Dolphin and R. W. Boyle, *J. Porphyr. Phthalocyanines*, 2000, **232**, 228–232.
- 163 S. Hiroto, Y. Miyake and H. Shinokubo, *Chem. Rev.*, 2017, **117**, 2910–3043.
- 164 A. G. Hyslop, M. A. Kellett, P. M. Iovine and M. J. Therien, *J. Am. Chem. Soc.*, 1998, **120**, 12676–12677.
- 165 M. O. Senge, M. Pinteá and A. A. Ryan, *Zeitschrift für Naturforsch. - Sect. B J. Chem. Sci.*, 2011, **66**, 553–558.
- 166 A. Wickramasinghe, L. Jaquinod, D. J. Nurco and K. M. Smith, *Tetrahedron*, 2001, **57**, 4261–4269.
- 167 R. Guillard, K. Perie, J. Barbe, D. J. Nurco, K. M. Smith, E. Van Caemelbecke, K. M. Kadish and D. Bourgogne, *Water*, 1998, **1669**, 973–981.
- 168 W. Jentzen, J. Ma and J. A. Shelnutt, *Biophys. J.*, 1998, **74**, 753–763.
- 169 N. A. M. Pereria and T. M. V. D. Pinho e Melo, *Org. Prep. Proced. Int.*, 2014, **46**, 183–213.
- 170 T. D. Lash, *J. Porphyr. Phthalocyanines*, 2016, **20**, 855–888.
- 171 C. Brückner, J. J. Posakony, C. K. Johnson, R. W. Boyle, B. R. James and D. Dolphin, *J. Porphyrins Phthalocyanines*, 1998, **02**, 455–465.
- 172 Z. Abada, L. Ferrié, B. Akagah, A. Tuan and B. Figadère, *Tetrahedron Lett.*, 2011, **52**, 3175–3178.
- 173 J. K. Laha, S. Dhanalekshmi, M. Taniguchi, A. Ambroise and J. S. Lindsey, *Org. Process Res. Dev.*, 2003, **7**, 799–812.
- 174 G. R. Geier III, B. J. Littler and J. S. Lindsey, *J. Chem. Soc. Perkin Trans. 2*, 2001, 701–711.
- 175 M. R. Silva, A. M. Beja and J. A. Paixa, *Tetrahedron Lett.*, 2003, **44**, 3971–3973.
- 176 B. J. Littler, Y. Ciringh and J. S. Lindsey, *J. Org. Chem.*, 1999, **64**, 2864–2872.
- 177 A. N. Cammidge and O. Öztürk, *Tetrahedron Lett.*, 2001, **42**, 355–358.
- 178 S. J. Shaw, K. J. Elgie, C. Edwards and R. W. Boyle, *Tetrahedron Lett.*, 1999, **40**, 1595–1596.
- 179 S. Fox, R. Hudson and R. W. Boyle, *Tetrahedron Lett.*, 2003, **44**, 1183–1185.

- 180 D. K. Lavalley, *Coord. Chem. Rev.*, 1985, **61**, 55–96.
- 181 W. Shi, Q. Shen, Y. Wang, L. Lan and J. Tao, *J. Heterocycl. Chem.*, 2010, **47**, 1221–1224.
- 182 J. Zhang, W. Chan, C. Xie, Y. Zhou, H. Chau, P. Maity, G. T. Harrison, A. Amassian, O. F. Mohammed, P. A. Tanner, W. Wong and K. Wong, *Light Sci. Appl.*, 2019, **8**, 1–10.
- 183 R. F. Pasternack, R. A. Brigandi, M. J. Abrams, A. P. Williams and E. J. Gibbs, *Inorg. Chem.*, 1990, **29**, 4483–4486.
- 184 M. J. C. Eisener, U. Harding, *J. Chem. Soc.*, 1964, **33**, 4089–4101.
- 185 A. Z. Muresan and J. S. Lindsey, 2009, **64**, 11440–11448.
- 186 T. Sahin, P. Vairaprakash, K. E. Borbas, T. Balasubramanian and J. S. Lindsey, *J. Porphyr. Phthalocyanines*, 2015, **19**, 663–678.
- 187 O. J. Clarke and R. W. Boyle, *Tetrahedron Lett.*, 1998, **39**, 7167–7168.
- 188 M. A. Smith, R. M. Barkley and G. B. Ellison, *J. Am. Chem. Soc.*, 1980, **102**, 6852–6854.
- 189 A. C. Serra, M. António and A. R. Gonsalves, *Tetrahedron Lett.*, 2010, **51**, 4192–4194.
- 190 D. E. Chumakov, A. V. Khoroshutin, A. V. Anisimov and K. I. Kobrakov, *Chem. Heterocycl. Compd.*, 2009, **45**, 259–283.
- 191 N. W. Smith and S. V Dzyuba, *Online J. Org. Chem.*, 2010, **2010**, 10–18.
- 192 J. D. J. Baldwin, M. Crossley, *Tetrahedron*, 1982, **38**, 685–692.
- 193 M. Tanaka, E. Muro, H. Ando, Q. Xu and M. Fujiwara, *J. Org. Chem.*, 2000, **65**, 2972–2978.
- 194 S. Banfi, E. Caruso, E. Fieni, L. Buccafurni, M. B. Gariboldi, R. Ravizza and E. Monti, *J. Porphyr. Phthalocyanines*, 2006, **10**, 1319–1326.
- 195 K. Smith, N. Malatesti, N. Cauchon, D. Hunting, R. Lecomte, J. E. Van Lier and J. Greenman, *Immunology*, 2010, **132**, 256–265.
- 196 K. E. Borbas, V. Chandrashaker, C. Muthiah, H. L. Kee, D. Holten and J. S. Lindsey, *J. Org. Chem.*, 2008, **73**, 3145–3158.
- 197 K. E. Borbas, P. Mroz, M. R. Hamblin and J. S. Lindsey, *Bioconjug. Chem.*, 2006, **17**, 638–653.
- 198 K. E. Borbas, H. L. Kee, D. Holten and J. S. Lindsey, *Org. Biomol. Chem.*, 2008, **6**, 187–194.
- 199 R. Luguaya, L. Jaquinod, F. R. Fronczek, M. G. H. Vicente and K. M. Smith, *Tetrahedron*, 2004, **60**, 2757–2763.
- 200 D. P. Arnold, B. R. C. Bott, C. H. Eldridge, F. M. Elms, G. Smith and M. Zojaji, *Aust. J. Chem.*, 1997, **50**, 495–504
- 201 B. J. D. M. P. Trova, P. Jolicia, F. Gauuan, A. D. Pechulis, S. M. Bubb, S. B. Bocckino and J. D. Crapo, *Bioorg. Med. Chem.*, 2003, **11**, 2695–2707.
- 202 C. S. Moore, T. J. Wood, C. Cawthorne, K. L. Hilton, S. Maher, J. R. Saunderson, S. Archibald and A. W. Beavis, *Biomed. Phys. Eng. Express*, 2000, **2**, 1–11.
- 203 T. Tanaka, S. Ikeda, N. Aratani and A. Osuka, *J. Porphyr. Phthalocyanines*, 2017, **21**, 803–810.
- 204 S. Alcorn, A. J. Walker, N. Gandhi, A. Narang and A. T. Wild, *Int. J. Mol. Sci.*, 2013, **14**, 14800–14832.
- 205 K. Buch, T. Peters, T. Nawroth, M. Sanger, H. Schmidberger and P. Langguth, *Radiat. Oncol.*, 2012, **7**, 1.
- 206 Z. Liu, L. Xiong, G. Ouyang, L. Ma, S. Sahi and K. Wang, *Sci. Rep.*, 2017, **7**, 1–11.
- 207 F. M. Frame, H. Savoie, F. Bryden, F. Giuntini, V. M. Mann, M. S. Simms, R. W. Boyle and N. J. Maitland, *Cancer Med.*, 2015, **1**, 61–73.
- 208 A. M. Surin, R. R. Sharipov, I. A. Krasil, D. P. Boyarkin, O. Y. Lisina, L. R. Gorbacheva, A. V. Avetisyan and V. G. Pinelis, *Biochemistry*.
- 209 T. Bernas and J. Dobrucki, *Cytometry*, 2002, **242**, 236–242.
- 210 N. A. P. Franken, H. M. Rodermond, J. Stap, J. Haveman and C. Van Bree, *Nat. Protoc.*, 2006, **1**, 2315–2319.
- 211 H. Fujimori, A. Sato, S. Kikuhara, J. Wang, T. Hirai, Y. Sasaki, Y. Murakami, R. Okayasu and M. Masutani, *Sci. Rep.*, 2015, **5**, 18231.
- 212 R. A. Miller, K. Woodburn, Q. Fan, M. F. Renschler, J. L. Sessler and J. A. Koutcher,

- Int. J. Radiat. Oncol. Biol. Phys.*, 1999, **45**, 981–989.
- 213 L. P. G. Wakelin, A. Adams, C. Hunter and M. J. Waring, *Biochemistry*, 1981, **20**, 5779–5787.
- 214 J. R. Williams, Y. Zhang, H. Zhou, D. S. Gridley, C. J. Koch, J. M. Slater and J. B. Little, *Int. J. Radiat. Oncol. Biol. Phys.*, 2008, **72**, 909–917.
- 215 N. A. P. Franken, S. Hovingh, H. Rodermond, L. Stalpers, G. W. Barendsen and J. Crezee, *Cancer Sci. Ther.*, 2011, **5**, 1–35.
- 216 D. J. Brenner, *Semin. Radiat. Oncol.*, 2009, **18**, 234–239.
- 217 H. Y. Nam, M. W. Han, H. W. Chang, Y. S. Lee, M. Lee, H. J. Lee, B. W. Lee, H. J. Lee, K. E. Lee, M. K. Jung, H. Jeon, S. Choi, N. H. Park, S. Y. Kim and S. W. Kim, *Cancer Res.*, 2013, **73**, 6–17.
- 218 A. L. Dunne, M. E. Price, C. Mothersill, S. R. Mckeown, T. Robson and D. G. Hirst, *Br. J. Cancer*, 2003, **2**, 2277–2283.
- 219 S. B. Schwarz, P. M. Schaffer, U. Kulka, B. Ertl-wagner, R. Hell and M. Schaffer, *Radiat. Oncol.*, 2008, **6**, 1–6.
- 220 D. Ahmed, P. W. Eide, I. A. Eilertsen, S. A. Danielsen, M. Eknæs, M. Hektoen, G. E. Lind and R. A. Lothe, *Oncogenesis*, 2013, **2**, 1–8.
- 221 X. Chen, H. Guan, X. D. Liu, D. Xie, Y. Wang, T. Ma, B. Huang and P.-K. Zhou, *Oncol. Lett.*, 2018, **16**, 431–438.
- 222 A. Rajput, I. Dominguez San Martin, R. Rose, A. Beko, C. LeVea, E. Sharratt, R. Mazurchuk, R. M. Hoffman, M. G. Brattain and J. Wang, *J. Surg. Res.*, 2008, **147**, 276–281.
- 223 G. Schettino, M. Folkard, K. M. Prise, B. Vojnovic, K. D. Held and B. D. Michael, *Radiat. Res.*, 2003, **160**, 505–511.
- 224 R. Ravizza, M. B. Gariboldi, L. Passarelli and E. Monti, *BMC Cancer*, 2004, **10**, 1–10.
- 225 S. Haupt, M. Berger, Z. Goldberg and Y. Haupt, *J. Cell Sci.*, 2003, **116**, 4077–4085.
- 226 F. Bunz, A. Dutriaux, C. Lengauer, T. Waldman, S. Zhou, J. P. Brown, J. M. Sedivy, K. W. Kinzler and B. Vogelstein, *Sci. Reports*, 1998, **282**, 1497–1502.
- 227 N. Issaeva, A. Friedler, P. Bozko, K. G. Wiman, A. R. Fersht and G. Selivanova, *PNAS*, 2003, **100**, 13303–13307.
- 228 Y. Liu and W. F. Bodmer, *PNAS*, 2006, **103**, 976–981.
- 229 C. Spagnol, L. C. Turner, F. Giuntini and R. W. Boyle, *J. Mater. Chem. B*, 2017, **5**, 1834–1845.
- 230 A. Subiel, R. Ashmore and G. Schettino, *Theranostics*, 2016, **6**, 1651–1671.
- 231 Y. Shibamoto, Y. Kitakabu, R. Murata, R. Oya, T. Shibata, T. Sasai, M. Takahashi and M. Abe, *Int. J. Radiat. Biol.* 1994, **29**, 583–586.
- 232 M. Bonnet, C. R. Hong, Y. Gu, R. F. Anderson, W. R. Wilson, F. B. Pruijn, J. Wang, K. O. Hicks and M. P. Hay, *Bioorg. Med. Chem.*, 2014, **22**, 2123–2132.
- 233 A. M. Rieger, K. L. Nelson, J. D. Konowalchuk and D. R. Barreda, *J. Vis. Exp.*, 2011, **3**, 3–6.
- 234 C. Riccardi and I. Nicoletti, *Nat. Protoc.*, 2006, **1**, 1458–1461.
- 235 M. Bache, S. Pigorsch, J. Dunst, P. Würfl, A. Meye, F. Bartel, H. Schmidt, F. W. Rath and H. Taubert, *Int. J. Cancer*, 2001, **96**, 110–117.
- 236 S.-W. Shin, C. Choi, G. Lee, A. Son, S. Kim, H. C. Park, I. Batinic-haberle and W. Park, *Antioxidants Redox Signal.*, 2017, **27**, 1067–1082.
- 237 W. Liao, M. A. Mcnutt and W. Zhu, *Methods*, 2009, **48**, 46–53.
- 238 A. R. Collins, *Mol. Biotechnol.*, 2004, **26**, 246–261.
- 239 P. L. Olive and J. P. Banáth, *Nat. Protoc.*, 2006, **1**, 23–29.
- 240 D. Kobayashi, A. Shibata, T. Oike and T. Nakano, *J. Vis. Exp.*, 2017, **2017**, 1–6.
- 241 Q. qing Zang, L. Zhang, N. Gao and C. Huang, *J. Integr. Med.*, 2016, **14**, 51–59.
- 242 J. Y. Choi and B. C. Lee, *Nucl. Med. Mol. Imaging*, 2015, **49**, 258–267.
- 243 J.-P. Meyer, P. Adumeau, J. S. Lewis and B. M. Zeglis, *Bioconjug. Chem.*, 2017, **27**, 2791–2807.
- 244 M. Gajewski, B. Seaver and C. S. Esslinger, *Bioorg. Med. Chem.*, 2007, **17**, 4163–4166.
- 245 A. F. R. Cerqueira, N. M. M. Moura, V. V. Serra and M. A. F. Faustino, *Molecules*, 2017, **22**, 1269–1314.

- 246 B. Temelli, O. Ozasik and D. Yuksel, *European J. Org. Chem.*, 2017, **56**, 4905–4915.
- 247 A. M. G. Silva and J. A. S. Cavaleiro, *Prog. Heterocycl. Chem.*, 2008, **19**, 44–69.
- 248 E. M. P. Silva, F. Giuntini, M. A. F. Faustino, P. C. Tome, A. M. S. Silva, M. G. P. M. S. Neves, A. C. Tome, J. Ferrer-correia, M. G. Santana-marques, M. F. Caeiro, R. R. Duarte, S. A. P. Tavares and B. Ô. Almeida, *Bioorg. Med. Chem. Lett.*, 2005, **15**, 3333–3337.
- 249 P. P. Liu, Y. Q. Feng, C. Z. Gu, S. X. Meng and B. Zhang, *Chinese Chem. Lett.*, 2012, **23**, 505–508.
- 250 M. O. Senge, *Chem. Commun.*, 2011, **47**, 1943–1960.
- 251 E. E. Bonfantini, A. K. Burrell, W. M. Campbell, M. J. Crossley, J. J. Gosper, M. M. Harding, D. L. Officer and D. C. W. Reid, *J. Porphyr. Phthalocyanines*, 2006, **6**, 708–719.
- 252 N. M. M. Moura, M. A. F. Faustino, M. G. P. M. S. Neves, A. C. Duarte and J. A. S. Cavaleiro, *J. Porphyr. Phthalocyanines*, 2011, **15**, 652–658.
- 253 O. B. Locos and D. P. Arnold, *Org. Biomol. Chem.*, 2006, **4**, 902–916.
- 254 M. Yeung, A. C. H. Ng, M. G. B. Drew, E. Vorpapel, E. M. Breitung, R. J. McMahon and D. K. P. Ng, *J. Org. Chem.*, 1998, **63**, 7143–7150.
- 255 M. L. Dean, J. R. Schmink, N. E. Leadbeater and C. Brückner, *J. Chem. Soc. Dalton Trans.*, 2008, 1341–1345.
- 256 D. K. Lavalley, *Comments Inorg. Chem.*, 2015, **5**, 37–41.
- 257 K. Dahms, M. O. Senge and M. B. Bakar, *European J. Org. Chem.*, 2007, 3833–3848.
- 258 S. Plunkett, K. Dahms and M. O. Senge, *Eur. J. Cancer*, 2013, **2013**, 1566–1579.
- 259 M. O. Senge, *Acc. Chem. Res.*, 2005, **38**, 733–743.
- 260 M. O. Senge, S. S. Matscher, A. Wiehe, K. Dahms and A. Kelling, *J. Am. Chem. Soc.*, 2004, **126**, 13634–13635.
- 261 T. E. O. Screen, I. M. Blake, L. H. Rees, W. Clegg, J. Borwick and H. L. Anderson, *J. Chem. Soc.*, 2002, **2**, 320–329.
- 262 M. Cheng, H. Savoie, F. Bryden and R. W. Boyle, *Photochem. Photobiol. Sci.*, 2017, **16**, 1260–1267.
- 263 E. Merino, *Chem. Soc. Rev.*, 2011, **40**, 3835–3853.
- 264 P. S. J. Canning, K. McCrudden, H. Maskill and B. Sexton, *J. Chem. Soc. Perkin Trans. 2*, 1999, 2735–2740.
- 265 B. Shi and R. W. Boyle, *J. Chem. Soc. Perkin Trans. 1*, 2002, 1397–1400.
- 266 M. Balaz, H. A. Collins, E. Dahlstedt and H. L. Anderson, *Org. Biomol. Chem.*, 2009, **7**, 874–888.
- 267 A. Jiblaoui, C. Baudequin, V. Chaleix, G. Ducourthial, F. Louradour, Y. Ramondenc, V. Sol and S. Leroy-Lhez, *Tetrahedron*, 2013, **69**, 5098–5103.
- 268 Y. Liang, Y.-X. Xie and J.-H. Li, *J. Org. Chem.*, 2006, **71**, 379–381.
- 269 R. E. Mewis, H. Savoie, S. J. Archibald and R. W. Boyle, *Photodiagnosis Photodyn. Ther.*, 2009, **6**, 200–206.
- 270 G. T. Potter, G. C. Jayson, G. J. Miller and J. M. Gardiner, *J. Org. Chem.*, 2016, **81**, 3443–3446.
- 271 A. El-faham and F. Albericio, *Chem. Rev.*, 2011, **111**, 6557–6602.
- 272 A. O. Okaru, T. S. Brunner, S. M. Ackermann, T. Kuballa, S. G. Walch, M. Kohlhimmelseher and D. W. Lachenmeier, *J. Analytical Methods Chem.*, 2017, **2017**, 1–7.
- 273 R. Iwata, C. Pascali, K. Terasaki, Y. Ishikawa, S. Furumoto and K. Yanai, *Appl. Radiat. Isot.*, 2017, **125**, 113–118.
- 274 T. Kniess, M. Laube and J. Steinbach, *Appl. Radiat. Isot.*, 2017, **127**, 260–268.
- 275 C. Denk, M. Wilkovitsch, P. Skrinjar, D. Svatunek, S. Mairinger, C. Kuntner, T. Filip, J. Fröhlich, T. Wanek and H. Mikula, *Org. Biomol. Chem.*, 2017, **15**, 5976–5982.
- 276 G. Gupta, B. S. Murray, P. J. Dyson and B. Therrien, *J. Organomet. Chem.*, 2014, **767**, 78–82.
- 277 G. Gupta, B. S. Murray, P. J. Dyson and B. Therrien, *Materials.*, 2013, **11**, 5352–5366.
- 278 M. D. Hall, K. A. Telma, K.-E. Chang, D. L. Tobie, J. P. Madigan, J. R. Lloyd, I. S. Goldlust, J. D. Hoeschele, J. D. Hoeschele and M. M. Gottesman, *Cancer Res.*, 2014, **74**, 3913–3922.

- 279 A. Weiss, R. H. Berndsen, M. Dubois, C. Muller, R. Schibli, A. W. Griffioen, P. J. Dyson and P. Nowak-Sillwiska, *Chem. Sci.*, 2014, **1019**, 4742–4748.
- 280 L. B. Josefsen and R. W. Boyle, *Theranostics*, 2012, **2**, 916–966.
- 281 R. R. Allison and C. H. Sibata, *Photodiagnosis Photodyn. Ther.*, 2010, **7**, 61–75.
- 282 S. Dasari and P. B. Tchounwou, *Eur. J. Pharmacol.*, 2014, **740**, 364–378.
- 283 F. Schmitt, P. Govindaswamy, O. Zava, G. Suss-Fink, L. Juillerat-Jeanneret and B. Therrien, *J. Biol. Inorg. Chem.*, 2009, **14**, 101–109.
- 284 S. Y. Yap, T. W. Price, H. Savoie, R. W. Boyle and G. J. Stasiuk, *Chem. Commun.*, 2018, **54**, 7952–7954.
- 285 F. Giuntini, F. Dumoulin, R. Daly, V. Ahsen, E. M. Scanlan, A. S. P. Lavado, J. W. Aylott, G. A. Rosser, A. Beeby and R. W. Boyle, *Nanoscale*, 2012, **4**, 2034–2045.
- 286 K. J. Kilpin, S. M. Cammack, C. M. Clavel and P. J. Dyson, *Dalt. Trans.*, 2013, **42**, 2008–2014.
- 287 T. Aoki, H. Sakai, K. Ohkubo, T. Sakanoue, T. Takenobu, S. Fukuzumi and T. Hasobe, *Chem. Sci.*, 2015, **6**, 1498–1509.
- 288 E. Göransson, J. Boixel, C. Monnereau, E. Blart, Y. Pellegrin, H. C. Becker, L. Hammarström and F. Odobel, *Inorg. Chem.*, 2010, **49**, 9823–9832.
- 289 F. Hammerer, F. Poyer, L. Fourmois, S. Chen, G. Garcia, M. P. Teulade-Fichou, P. Maillard and F. Mahuteau-Betzer, *Bioorganic Med. Chem.*, 2018, **26**, 107–118.
- 290 A. M. Odeh, J. D. Craik, R. Ezzeddine, A. Tovmasyan, I. Batinic-haberle and L. T. Benov, *PLoS One*, 2014, **9**, 1–9.
- 291 F. Ricchelli, L. Franchi, G. Miotto, L. Borsetto, S. Gobbo, P. Nikolov, J. C. Bommer and E. Reddi, *Int. J. Biochem. Cell Biol.*, 2005, **37**, 306–319.
- 292 T. M. Tsubone, W. K. Martins, C. Pavani, H. C. Junqueira, R. Itri and M. S. Baptista, *Sci. Rep.*, 2017, **7**, 1–19.
- 293 D. B. G. Williams and M. Lawton, *J. Org. Chem.*, 2010, **75**, 8351–8354.